



Dissertation presented to receive the degree Doctor of the
Rovira i Virgili University
European PhD

Biobased Thermosets from Vegetable Oils. Synthesis, Characterization, and Properties

GERARD LLIGADAS I PUIG



UNIVERSITAT ROVIRA I VIRGILI
Departament de Química Analítica i Química Orgànica
Tarragona, novembre de 2006

M'agradaria donar les gràcies a totes aquelles persones que han contribuït a la realització d'aquesta tesi i especialment:

Voldria expressar la meva més sincera gratitud a la Dra. Virginia Cádiz per haver-me donat l'oportunitat de realitzar aquesta tesi al seu grup de recerca i als meus directors, la Dra. Marina Galià i el Dr. Joan Carles Ronda, tant per la seva paciència, empenta i dedicació, com pels coneixements, consells, ànims i innumerables solucions que m'han aportat durant aquests anys. Ha estat important trobar sempre una porta oberta.

Els meus agraïments a la resta de doctors de l'àrea, i especialment a la Dra. Àngels Serra, la Dra. Ana Mantecón i al Dr. Toni Reina, per estar sempre disposats a ajudar.

I would like to express my gratitude to Prof. Jürgen O. Metzger, from the Carl Von Ossietzky University, Oldenburg, not only for accepting me in his group, but also for his scientific advice and encouragement. I would also like to thank all the members of his research group who made me feel at home with their hospitality, and especially to Francesco for his friendship.

Certament la companyia amb la qual es treballa resulta bàsica per gaudir d'allò que es fa. Moltes gràcies a tots els companys que han aconseguit crear un ambient distès i acollidor. Un especial reconeixement a l'Àlex, al Sergio, al Luis Adolfo, al Robert, al Miguel, a l'Omar i al David, per escoltar i compartir tantes alegries i preocupacions que ens han anat sorgint durant aquests anys, que no és poca cosa.

Voldria acabar donant les gràcies als meus pares, pels valors que m'heu sabut transmetre i per la il·lusió mostrada sempre en cadascun dels meus projectes i molt especialment a la Marta, gràcies per ser la meva font de felicitat. També gràcies per la teva inesgotable paciència i recolzament. T'estimo.

A tots vosaltres, moltes gràcies.

Table of Contents

1. INTRODUCTION AND SCOPE	1
1.1. Sustainable Development and Chemistry	3
1.2. Vegetable Oils: Composition and Chemistry	5
1.3. Vegetable Oils: Polymer Applications	9
1.4. Polymer Materials from Vegetable Oils	10
1.4.1. Direct Polymerization	11
1.4.2. Chemical Modification and Polymerization	13
1.5. Scope and Objectives of this Thesis	28
2. BIOBASED ORGANIC-INORGANIC HYBRID MATERIALS	31
2.1. Organic-Inorganic Hybrid Materials	33
2.2. Vegetable Oil-Based Hybrid Materials	38
2.3. Objectives	40
2.4. Experimental Procedures and Results	41
2.4.1. Novel Organic-Inorganic Hybrid Materials from Renewable Resources: Hydrosilylation of Fatty Acid Derivatives	43
2.4.2. Bionanocomposites from Renewable Resources: Epoxidized Linseed Oil-Polyhedral Oligomeric Silsesquioxanes (POSS) Hybrid Materials	63

3. BIOBASED FLAME-RETARDANT EPOXY RESINS	79
3.1. Biobased Epoxy Resins	81
3.2. Flame Retardants: Mechanism and Environmental Concerns	82
3.3. Objectives	88
3.4. Experimental Procedures and Results	89
3.4.1. Synthesis and Properties of Thermosetting Polymers from a Phosphorous-containing fatty acid derivative	91
3.4.2. Development of Novel Phosphorus-Containing Epoxy Resins from Renewable Resources	113
4. BIOBASED POLYOLS AND POLYURETHANES	129
4.1. Basic Chemistry of Polyurethanes	131
4.2. Vegetable Oil-Based Polyols and Polyurethanes	133
4.3. Objectives	140
4.4. Experimental Procedures and Results	141
4.4.1. Synthesis and Characterization of Polyurethanes from Epoxidized Methyl Oleate Based Polyether Polyols as Renewable Resources	143
4.4.2. Novel-Silicon Containing Polyurethanes from Vegetable Oils as Renewable Resources. Synthesis and Properties	161
4.4.3. Poly(ether urethane) Networks from Renewable Resources as Candidate Biomaterials. Synthesis and Characterization	181
5. CONCLUSIONS	201
Appendix A: List of Abbreviations	203
Appendix B: List of Papers	207

1

Introduction and Scope

Sustainable development over the next century requires the use of renewable substrates as alternatives to the earth's limited petroleum derivatives. Vegetable oils are expected to represent an ideal alternative chemical feedstock.

This chapter discusses the contribution of chemistry to sustainable development, presents an overview of recent developments in the chemistry of vegetable oil-based polymers, and explains the aims of this thesis.

-
- 1.1 Sustainable Development and Chemistry
 - 1.2 Vegetable Oils: Composition and Chemistry
 - 1.3 Vegetable Oils: Polymer Applications
 - 1.4 Polymer Materials from Vegetable Oils
 - 1.4.1 Direct Polymerization
 - 1.4.2 Chemical Modification and Polymerization
 - 1.5 Scope and Objectives of this Thesis
-

1.1

Sustainable Development and Chemistry

Sustainable development, which became a key idea during the 20th century, may be regarded as the progressive and balanced achievement of sustained economic development, and improved social equity and environmental quality.¹ Sustainable development comprises the three components of society, environment, and economy, and its goals can only be achieved if all three components can be satisfied simultaneously (Figure 1.1).

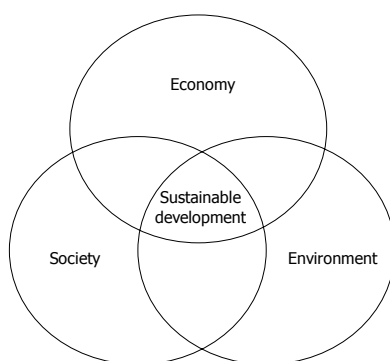


Figure 1.1 Three components of sustainable development.

The translation of this ideal into the real world of the 21st century will present chemists with some very demanding tasks. They must develop products that can be manufactured in environmentally acceptable ways involving the minimum consumption of energy and raw materials, whilst maintaining as favorable an ecological balance as possible. During and at the end of their lifetime these products must be useful to humans without harming them, and must not pollute the

1. Report of the United Nations Conference on Environment and Development, Rio de Janeiro, Brazil, June 3-14, 1992. <http://www.un.org/esa/sustdev>, accessed, September 18, 2006.

environment. Thus, chemistry will make important contributions to the ecological, economic, and social dimensions of sustainable development.²

The conservation and management of resources is especially important to this process.³ Since a large number of product lines are synthesized from a smaller number of base chemicals that are produced in large quantities, resource-saving production of the latter is especially important for sustainable development. During the last century the supply of raw materials for the chemical industry underwent radical changes. Whereas at the beginning of the 19th century the demand for basic chemicals was satisfied entirely by renewable raw materials, from about 1900 the chemical industry came to rely increasingly on coal. Mineral oil became increasingly important in the 1940s, and during the past 40 years it has remained by far the most important source of raw materials. The growing demand for petroleum-based products and the resulting negative impact on the environment, plus the scarcity of non-renewable resources, are some of the many factors that have encouraged the chemical industry to begin using renewable resources as raw materials (Figure 1.2).

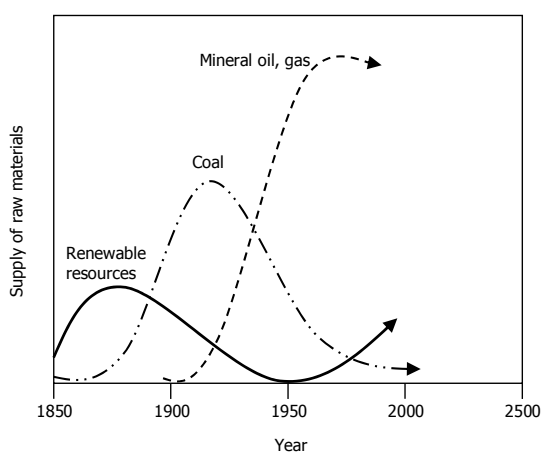


Figure 1.2 Changing sources of feedstock for the chemical industry.

2. Metzger, J. O. *Chemosphere* 2001, 43, 83.

3. Eissen, M.; Metzger, J. O.; Schmidt, E.; Schneidewind, U. *Angew Chem Int Ed Engl* 2002, 41, 414.

This situation has led to considerable attention being focused recently on the use of annually renewable agricultural feedstock to produce a wide range of base chemicals and other industrial products. According to Metzger and colleagues^{2,4} and other authors,⁵⁻⁸ the renewable raw materials that are most important to the chemical industry are natural oils and fats because of their high availability and versatile applications. Vegetable oils constitute about 80% of the global oil and fat production, with 20% (and declining) being of animal origin. The use of these materials offers an alternative approach that is both sustainable and, with the right application, far more environmentally benign than fossil sources. Although these materials dominate among the agricultural products, various other renewable resources have been used, such as starch, cellulose, sugars, and lignin.⁹⁻¹¹

1.2

Vegetable Oils: Composition and Chemistry

Vegetable oils and fats form part of a large family of chemical compounds known as lipids. Vegetable oils are predominantly made up of triglyceride molecules, which have the three-armed star structure shown in Figure 1.3. Triglycerides comprise of three fatty acids joined at a glycerol junction. Most of the common oils contain fatty acids that vary from 14 to 22 carbons in length, with 0 to 3 double bonds per fatty acid.

-
4. Biermann, U.; Friedt, W.; Lang, S.; Luhs, W.; Machmuller, G.; Metzger, J. O. *Angew Chem Int Ed Engl* 2000, 39, 2206.
 5. Warwel, S.; Brüse, F.; Demes, C.; Kunz, M.; Rühgen. Klaas, M. *Chemosphere* 2001, 43, 39.
 6. Nayak, P. L. *J Macrom Sci – Rev Macromol Chem Phys* 2000, 40, 1.
 7. Hill, K. *Pure Appl Chem* 2000, 72, 1255.
 8. Baumann, H.; Bühler, M.; Fochem, H.; Hirsinger, F.; Zoebelin, H.; Falbe, J. *Angew Chem Int Ed Engl* 1988, 27, 41.
 9. *Feedstocks for the future: Renewables for the Production of Chemicals and Materials*; Bozell, J. J.; Patel, M. Eds.; ACS Symposium Series 921; American Chemical Society: Washington, CD, 2006.
 10. *Natural Fibers, Biopolymers, and Biocomposites*; Mohanty, A. K.; Misra, M.; Drzal, L. T. Eds.; CRC Press Taylor & Francis Group: Boca Raton, FL, 2005.
 11. Yu, L.; Dean, K.; Li, L. *Prog Polym Sci* 2006, 31, 576.

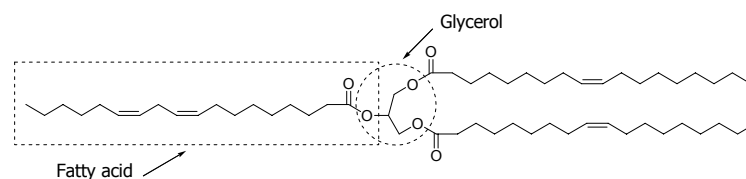


Figure 1.3 Triglyceride molecule, the major component of vegetable oils.

The number of known fatty acids is very large. Figure 1.4 lists fatty acids that are prevalent in common vegetable oils, and Table 1.1 lists their distribution in commercially significant vegetable oils.¹² It should be noted that there are also exotic oils composed of fatty acids with other types of functionalities, such as hydroxyl, epoxy, and furanoid groups.¹³

Table 1.1 Fatty acid percentage distribution in various plant oils

Fatty Acid	C:DB ^a	Canola	Corn	Cottonseed	Linseed	Olive	Palm	Soybean	Sunflower	High Oleic ^b
Myristic	14:0	0.1	0.1	0.7	0.0	0.0	1.0	0.1	0.0	0.0
Myristoleic	14:1	0.0	0.0	0.0	0.0	0.0	0.0	0.0	0.0	0.0
Palmitic	16:0	4.1	10.9	21.6	5.5	13.7	44.4	11.0	6.1	6.4
Palmitoleic	16:1	0.3	0.2	0.6	0.0	1.2	0.2	0.1	0.0	0.1
Margaric	17:0	0.1	0.1	0.1	0.0	0.0	0.1	0.0	0.0	0.0
Margaroleic	17:1	0.0	0.0	0.1	0.0	0.0	0.0	0.0	0.0	0.0
Stearic	18:0	1.8	2.0	2.6	3.5	2.5	4.1	4.0	3.9	3.1
Oleic	18:1	60.9	25.4	18.6	19.1	71.1	39.3	23.4	42.6	82.6
Linoleic	18:2	21.0	59.6	54.4	15.3	10.0	10.0	53.2	46.4	2.3
Linolenic	18:3	8.8	1.2	0.7	56.6	0.6	0.4	7.8	1.0	3.7
Arachidic	20:0	0.7	0.4	0.3	0.0	0.9	0.3	0.3	0.0	0.2
Gadoleic	20:1	1.0	0.0	0.0	0.0	0.0	0.0	0.0	0.0	0.4
Eicosadienoic	20:2	0.0	0.0	0.0	0.0	0.0	0.0	0.0	0.0	0.0
Behenic	22:1	0.3	0.1	0.2	0.0	0.0	0.1	0.1	0.0	0.3
Erucic	22:1	0.7	0.0	0.0	0.0	0.0	0.0	0.0	0.0	0.1
Lignoceric	24:0	0.2	0.0	0.0	0.0	0.0	0.0	0.0	0.0	0.0
DB/triglyceride		3.9	4.5	3.9	6.6	2.8	1.8	4.6	0.0	3.0

^a C, number of carbon atoms; DB, number of C=C double bonds.

^b Genetically engineered high oleic acid content soybean oil (DuPont).

12. Liu, K. *Soybeans: Chemistry, Technology, and Utilization*; Chapman and Hall Press: New York, 1997.

13. Gunstone, F. *Fatty Acid and Lipid Chemistry*; Blackie Academic and Professional: London, 1996.

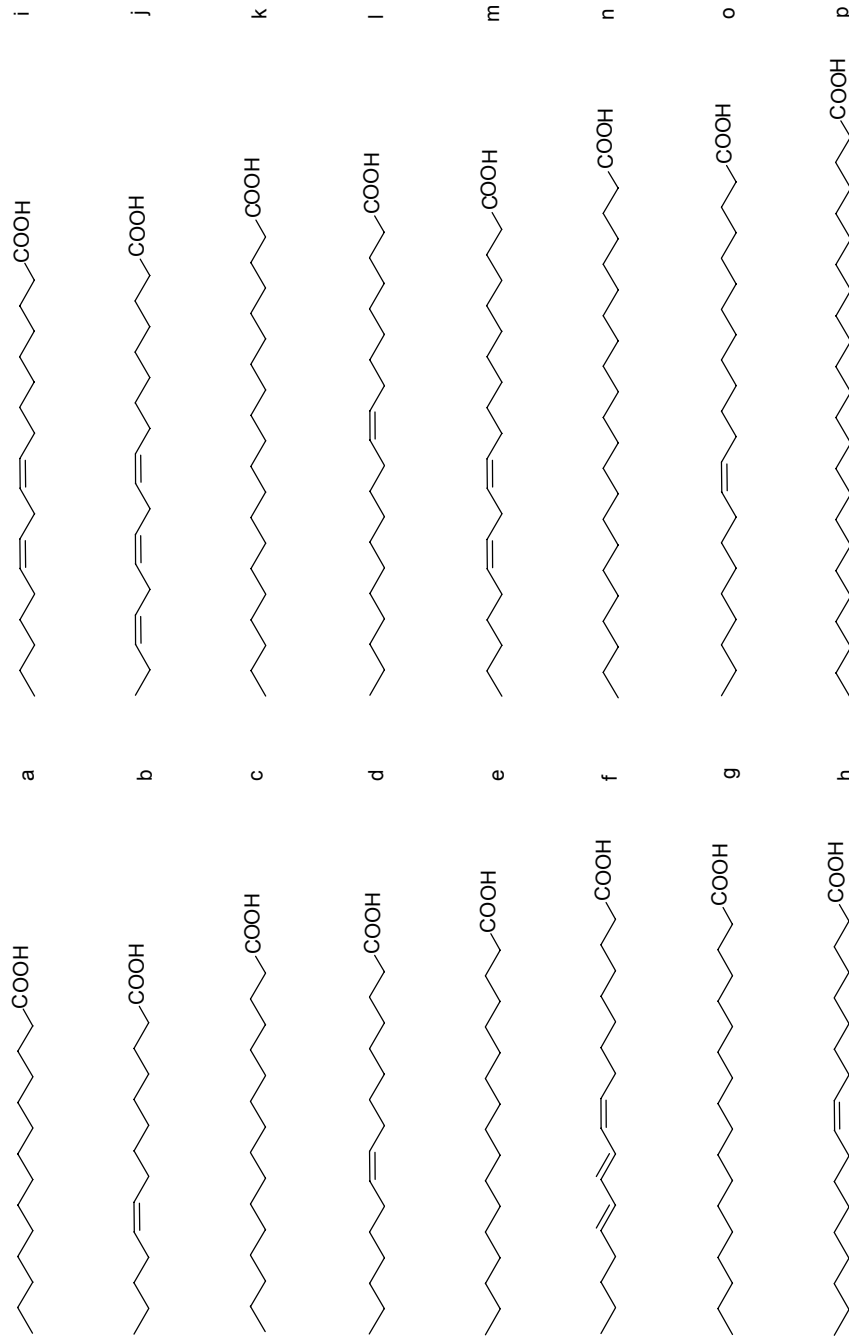


Figure 1.4 Structure of common fatty acids: (a) myristic, (b) myristoleic, (c) palmitic, (d) palmitoleic, (e) margaric, (f) margaroleic, (g) stearic, (h) oleic, (i) linoleic, (j) linoleic, (k) arachidic, (l) gadoleic, (m) eicosadienoic, (n) behenic, (o) erucic, and (p) lignoceric.

The presence of many types of fatty acid indicates that at the molecular level these oils are composed of many different types of triglycerides with diverse levels of saturation. Newly developed genetic engineering techniques are likely to make unique contributions to the expansion of raw materials available to the chemical industry, such as increasing the content of individual fatty acids or dramatically changing the oil quality by the introduction of a new fatty acid. Within this context, “high oleic” soybeans (82.6% oleic acid content) produced using techniques based on genetic engineering have been developed by DuPont (Table 1.1).

Triglycerides contain several reactive positions that can act as starting points in different reactions: ester groups (a in Figure 1.5), C=C double bonds (b), allylic positions (c), and the α -position of ester groups (d).

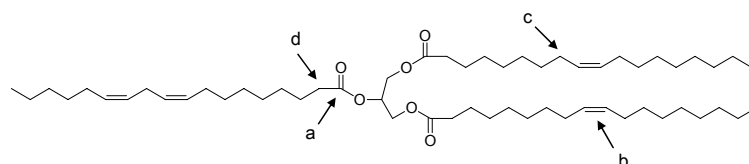


Figure 1.5 Reactive positions in triglycerides: ester groups (a), C=C double bonds (b), allylic positions (c), and the α -positions of ester groups (d).

After years of relative stagnation, the modification of oil-based fatty compounds has recently made important advances. Chemical modification of fatty compounds is an important route to obtaining useful products from renewable feedstocks. Industrial oleochemistry has concentrated on the carboxylic functionality of fatty acids:¹⁴ the basic oleochemicals are free fatty acids, methyl esters, fatty alcohols, and fatty amines, with glycerol as a by-product,¹⁵ although modern synthesis methods have been recently applied extensively to fatty compounds for the selective

14. Gunstone, F. D. *Eur J Lipid Sci Technol* 2001, 103, 307.

15. Gunstone, F. D. *Basic Oleochemicals, Oleochemical Products and New Industrial Oils*. In: *Oleochemical Manufacture and Applications*; Gunstone F. D.; Hamilton R. J. Eds.; Sheffield Academic Press: Sheffield, 2001.

fuctionalization of the alkyl chain.^{3,16-18} Moreover, enzymatic and microbial transformations constitute another vast branch of chemistry that still needs to be explored.^{4,19} Therefore, there is the potential to develop new, efficient, and environmentally friendly reaction pathways for new products or to find new applications for ones that already exist.

1.3

Vegetable Oils: Polymer Applications

Polymers are quantitatively the most important products of the chemical industry that are used in diverse applications in everyday life. Almost all current polymers are produced from fossil sources. The consumption of material and energy resources is not the only issue surrounding polymer material and products. Because of their widespread use and the dominant consumption patterns, in which materials and products are used only once and then discarded, polymers also make a significant contribution to the increasing amount of solid waste due to a very large percentage of the plastics produced from fossil-fuel feedstock being non-biodegradable. Moreover, efforts such as recycling and combustion in incinerating plants have to be considered carefully from economic and ecological perspectives.

Nowadays, there is a growing interest to produce vegetable oil-based biopolymers. These polymers have many advantages compared with polymers prepared from petroleum-based monomers. They are biodegradable and, in many cases cheaper than petroleum-based polymers. The life cycle of vegetable-oil-based polymers is shown in Figure 1.6.

-
16. Biermann, U.; Fürmeier, S.; Metzger, J. O. *New Chemistry of Oils and Fats*. In: *Oleochemical Manufacture and Applications*; Gunstone F. D.; Hamilton R. J. Eds.; Sheffield Academic Press: Sheffield, 2001.
 17. Biermann, U.; Metzger, J. O. *Topics in Catalysis* 2004, 27, 119.
 18. Biermann, U.; Fürmeier, S.; Metzger, J. O. *Fett/Lipid* 1998, 100, 236.
 19. Metzger, J. O.; Bornscheuer, U. *Appl Microbiol Biotechnol* 2006, 71, 13.

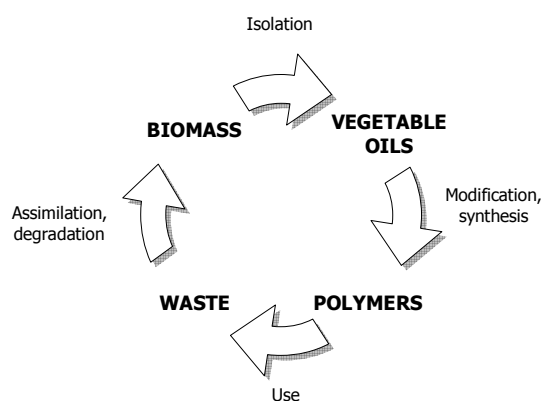


Figure 1.6 Life cycle of polymers based on vegetable oils.

The use of vegetable oils and fatty acids for polymer applications has a long tradition. One can differentiate between their use as polymer additives (e.g., epoxidized soybean oil as plasticizer), as building blocks for thermoplastic polymers (e.g., dicarboxylic acids such as azelaic, sebacic, and dimer acid for polyesters or polyamides), and as a basis for thermosets. In the last decade, a broad range of chemical routes has been developed for using natural or modified vegetable oils as a basis for polymers, adhesives, and composites with specific properties and applications.²⁰ The next section presents an overview of the different chemical pathways that have been reported.

1.4

Polymeric Materials from Vegetable Oils

Triglyceride molecules contain many active sites that are amenable to chemical reactions (Figure 1.5). These can be used to polymerize triglycerides directly (Section 1.4.1) or to modify the triglyceride structure with polymerizable groups

20. Güner, F. S.; Yagci, Y.; Erciyas, A. T. *Prog Polym Sci* 2006, 31, 633.

(Section 1.4.2) using the same synthesis techniques that have been applied in the synthesis of petroleum-based polymers.

1.4.1 Direct Polymerization

Triglyceride molecules contain C=C double bonds capable of being polymerized. As is well known,²¹ these double bonds can be polymerized through a free radical or a cationic mechanism. The free-radical polymerization of triglyceride double bonds has received little attention due to the presence of chain-transfer processes to the many allylic positions in the molecule; however, vegetable oils such as linseed and tung oils have been classically exploited as drying oils. The drying power of these oils is directly related to their highly unsaturated nature, which allows them to react with atmospheric oxygen that leads to the formation of a network. These oils are used mostly in paints and coatings, but also in inks and resins.

Cationic polymerization has been widely studied by Larock's group,²² who have focused on the direct cationic polymerization of the C=C double bonds of natural oils. They have reported the preparation of thermosetting polymers ranging from rubbers to hard plastics by the cationic polymerization of a variety of oils: fish, tung, and soybean oil with petroleum-based comonomers such as styrene, divinylbenzene, and dicyclopentadiene in the presence of boron trifluoride diethyl etherate as the initiator. The resulting thermosetting materials possess thermal and mechanical

-
21. Smith, M. B.; March, J. *March's Advanced Organic Chemistry: Reactions, Mechanism, and Structure* 5thed.; Wiley Interscience, John Wiley & Sons: Canada, 2001.
22. (a) Li, F.; Larock, R. C.; Otaigbe, J. U. *Polymer* 2000, 41, 4849; (b) Li, F.; Larock, R. C. *J Appl Polym Sci* 2000, 78, 1044; (c) Li, F.; Larock, R. C. *J Polym Sci: Part B, Polym Phys* 2000, 38, 2721; (d) Li, F.; Marks, D. W.; Larock, R. C.; Otaigbe, J. U. *Polymer* 2000, 41, 7925; (e) Li, F.; Hanson, M. V.; Larock, R. C. *Polymer* 2001, 42, 1567; (f) Li, F.; Larock, R. C. *J Appl Polym Sci* 2001, 80, 658; (g) Li, F.; Larock, R. C. *J Polym Sci Part B: Polym Phys* 2001, 39, 60; (h) Li, F.; Perounoud, A.; Larock, R. C. *Polymer* 2001, 42, 10133; (i) Li, F.; Larock, R. C. *Polym Adv Technol* 2002, 13, 436; (j) Li, F.; Larock, R. C. *J Appl Polym Sci* 2002, 84, 1533; (k) Andjelkovic, D. D.; Larock, R. C. *Biomacromolecules* 2006, 7, 927.

properties comparable to those of industrial plastics, as well as some other useful properties, including high damping and shape memory.

Some vegetable oils contain naturally occurring functional groups, such as hydroxyl and epoxide, which make them candidates for direct crosslinking with various hardeners to form polymer networks. Castor oil, extracted from castor beans, is basically the triglyceride of ricinoleic acid, which constitutes from 83.6% to 90.0% of all acid residues (a, Figure 1.7). Ricinoleic acid has 18 carbon atoms, a double bond ($C_9=C_{10}$), and a secondary hydroxyl group. Castor oil has been used in many polyurethane applications.²³⁻²⁵ Vernonia oil, which is obtained from the seeds of *Vernonia galamensis*, comprises triglycerides that contain about 70–80% vernolic acid (b, Figure 1.7), which contains a naturally occurring epoxide functional group. The triepoxide functionality of vernonia oil has been exploited to obtain crosslinked polymers with difunctional reagents, such as dibasic acids²⁶ and aromatic diamines.²⁷



Figure 1.7 Chemical structures of acids ricinoleic (a) and vernolic (b).

Moreover, castor and vernonia oils have also been used to produce interpenetrating polymer networks (IPNs). IPNs formed by triglycerides could increase the toughness and fracture resistance of conventional thermosetting polymers.^{28,29}

23. Athawale, V. D.; Kolekar, S. L. *J Appl Polym Sci* 2000, 75, 6.

24. Tran, N. B.; Vialle, J.; Pham, Q. T. *Polymer* 1997, 38, 2467.

25. Tran, N. B.; Pham, Q. T. *Polymer* 1997, 38, 3307.

26. Afolabi, O. A.; Aluko, M. E.; Wang, G. C.; Anderson, W. A.; Ayorinde, F. O. *J Am Oil Chem Soc* 1989, 66, 983.

27. Gringberg, S.; Kolot, V.; Mills, D. *Ind Crops Products* 3, 1994, 113.

28. Barret, L. W.; Sperling, L. H.; Murphy, C. J. *J Am Oil Chem Soc* 1993, 70, 523.

29. Sperling, L. H.; Manson, J. A. *J Am Oil Chem Soc* 1983, 60, 1887.

1.4.2 Chemical Modification and Polymerization

Since the internal double bonds in the triglyceride structure are not sufficiently reactive for any viable polymerization process (except for cationic polymerization), considerable efforts have recently been devoted to modifications that could facilitate a subsequent polymerization of the triglycerides to produce solid polymers. These modifications consist of:

- Introducing reactive groups into the aliphatic chains, which would exhibit a higher aptitude to polymerize (pathway A, Figure 1.8), and
- the reduction of the triglycerides to monoglycerides through a glycerolysis reaction³⁰ (pathway B).

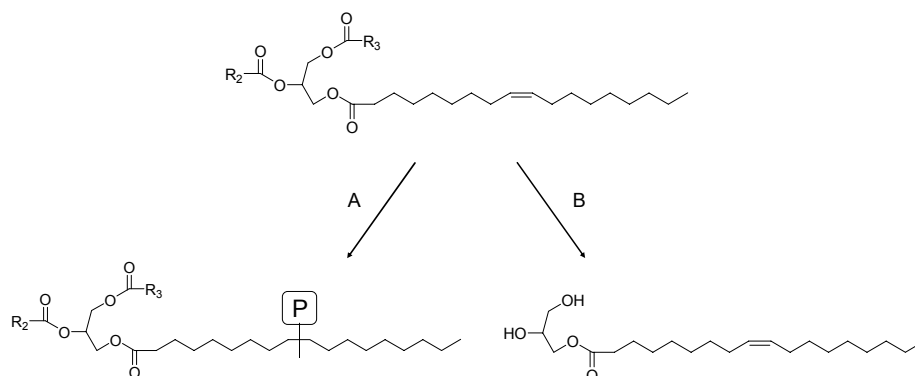


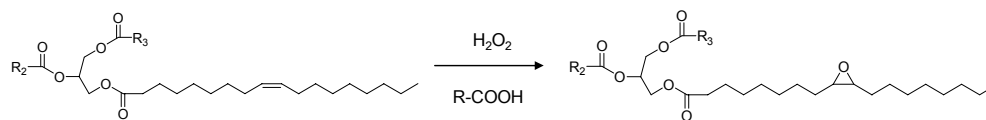
Figure 1.8 General modification pathways: introduction of polymerizable groups into the triglyceride (A) and reduction of the triglycerides to monoglycerides (B).

a. Pathway A: Introduction of Polymerizable Groups

Epoxidation is one of the most important functionalization reactions involving C=C double bonds. The chemistry of the Prileshajev epoxidation of unsaturated fatty

30. Sonntag, N. O. V. J Am Oil Chem Soc 1982, 59, 795.

compounds is well known.³¹ A short-chain peroxy acid, usually peracetic acid, is prepared from hydrogen peroxide and the corresponding acid either in a separate step or *in situ* (Scheme 1.1).



Scheme 1.1

For chemical synthesis on the laboratory scale, better results can be achieved with preformed peroxy acids such as *m*-chloroperbenzoic acid. Other epoxidation methods include the use of dioxiranes,³² the generation of peracids from aldehydes and molecular oxygen,³³ and the use of hydrogen peroxide and methyltrioctylammonium(diperoxotungsto)phosphate as a phase transfer catalyst.³⁴ A convenient method for the chemoenzymatic self-epoxidation of unsaturated fatty acids was developed.³⁵ This method is of considerable interest because it abolishes the undesirable ring-opening of the epoxide. The unsaturated acid or ester is initially converted into an unsaturated percarboxylic acid by a lipase-catalyzed reaction with H_2O_2 , and is then self-epoxidized in an essentially intermolecular reaction. A method for the enzymatic epoxidation of unsaturated fatty acids was reported recently by Uyama et al.³⁶

On an industrial scale, it is preferable for unsaturated fatty compounds to be epoxidized using the *in situ* performic acid procedure. Industrially, epoxidized

31. Findley, T. W.; Swern, D.; Scalan, J. T. *J Am Chem Soc* 1945, 67, 412.

32. Sonnet, P. E.; Lankin, M. E.; Mc Neill, G. P. *J Am Oil Chem Soc* 1995, 72, 199.

33. Kuo, M. C.; Chou, T. C. *Ind Eng Chem Res* 1987, 26, 277.

34. Crivello, J. V.; Narayan, R. *Chem Mater* 1992, 4, 692.

35. Rüschen Klaas, M.; Warwel, S. *J Mol Catal A Chem* 1997, 17, 311.

36. Uyama, H.; Kuwabara, M.; Tsujimoto, S.; Kobayashi, S. *Biomacromolecules* 2003, 4, 211.

vegetable oils are currently used as plasticizers for polyvinyl chloride,³⁷ reactive diluents,³⁸ IPNs³⁹ and toughening materials for commercial epoxy resins.^{40,41}

The epoxidation reaction makes triglycerides capable of reacting via ring-opening. The preparation of biobased epoxy resins from epoxidized vegetable oils has been the subject of many studies.^{34,42-46}

Ring-opening of epoxidized vegetable oils is an established method of introducing polymerizable groups into triglyceride. Several triglyceride-based polyols suitable for polyurethane synthesis were synthesized by reacting epoxidized vegetable oils with different chemical reagents. The conversion of epoxy groups to secondary hydroxyl groups was accomplished by (i) reacting with hydrochloric or hydrobromic acid, resulting in halogenated polyols (a and b, Figure 1.9), (ii) an acid-catalyzed ring-opening reaction with methanol, yielding a methoxylated polyol (c), or with water, forming vicinal hydroxyl groups (d), and (iii) catalytic hydrogenation (e).^{47,48}

37. Rösch, J.; Mülhaupt, R. *Polym Bull* 1993, 31, 1993.

38. Mustata, F. J. *J Polym Eng* 1997, 17, 491.

39. Qureshi, S.; Manson, J. A.; Sperling, L. H.; Murphy, C. J. *Polymer Applications of Renewable Resource Materials*; Carraher, C. E.; Sperling, L. H. Eds.; Plenum Press: New York, 1983.

40. Park, S. J.; Jin, F. L.; Lee, J. R. *Mater Sci Eng A* 2004, 374, 109.

41. Ratna, D.; Banthia, A. K. *J Adhesion Sci Technol* 2000, 14, 15.

42. Boquillon, N.; Fringant, C. *Polymer* 2000, 41, 8603.

43. Zhu, J.; Chandrashekhara, K.; Flanigan, V.; Kapila, S. J. *J Appl Polym Sci* 2004, 91, 3513.

44. Thames, S. F.; Yu, H. *Surf Coat Technol* 1999, 115, 208.

45. Park, S. J.; Jin, F. L.; Lee, J. R. *Macromol Rapid Commun* 2004, 25, 724.

46. Park, S. J.; Jin, F. L.; Lee, J. R.; Shin, J. S. *Eur Polym J* 2005, 41, 231.

47. Guo, A.; Cho, Y.; Petrovic, Z. S. *J Polym Sci Part A: Polym Chem* 2000, 38, 3900.

48. Zlatanovic, A.; Lava, C.; Zhang, W.; Petrovic, Z. S. *J Polym Sci Part B: Polym Phys* 2004, 42, 809.

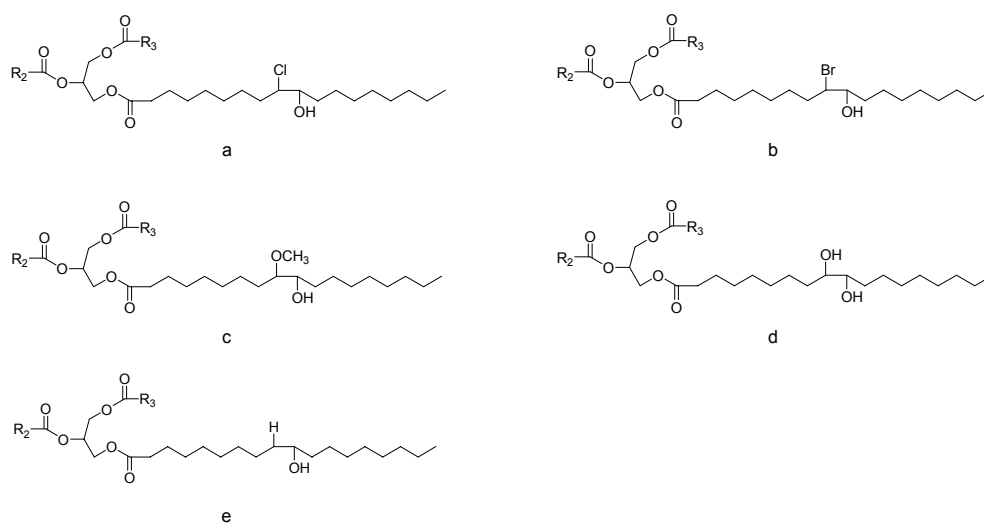
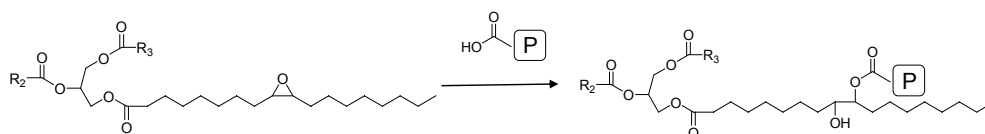


Figure 1.9 Chemical structures of polyols obtained by ring-opening with hydrochloric acid (a), hydrobromic acid (b), methanol (acid-catalyzed) (c), water (acid-catalyzed) (d), and catalytic hydrogenation (e) of epoxidized triglycerides.

Polymerizable groups can also be introduced directly into a triglyceride structure by utilizing the $-\text{COOH}$ reactivity of carboxylic acid-type reagents toward the oxirane ring (Scheme 1.2).



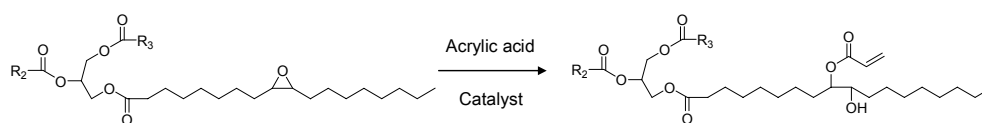
Scheme 1.2

Reacting the epoxy functional triglyceride with acrylic acid incorporates polymerizable acrylate moieties onto the triglyceride (Scheme 1.3). Although the reaction is partially catalyzed by acrylic acid, the additional catalysts *N,N*-dimethylaniline and triethylamine, are commonly used. Several epoxidized vegetable oils and fatty acids have been modified using acrylic acid.⁴⁹⁻⁵¹

49. Bunker, S. P.; Wool, R. P. *J Polym Sci Part A: Polym Chem* 2002, 40, 451.

50. La Scala, J. J.; Wool, R. P. *J Am Oil Chem Soc* 2002, 79, 59.

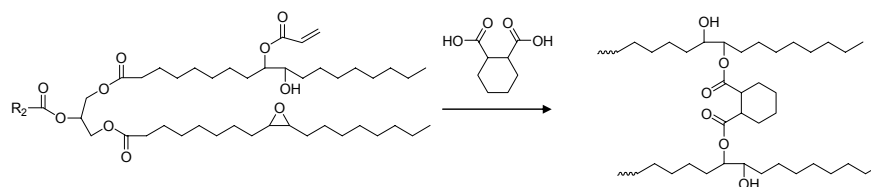
51. Kolot, V.; Gringberg, S. *J Appl Polym Sci* 2004, 91, 3835.



Scheme 1.3

Acrylated epoxidized soybean oil (AESO, commercialized by Aldrich Chemical) has been used extensively in surface coatings. Urethane and amine derivatives of AESO have also been developed for coating and ink applications.⁵²

Wool and coworkers have extensively studied the free-radical polymerization of AESO, and its blending with reactive diluents such as styrene to obtain solid polymer materials useful in structural applications.^{53,54} Pelletier et al.⁵⁵ have recently reported the polymerization of AESO with free-radical photoinitiators. A method for increasing the stiffness of AESO polymers has also been reported.^{54,56} Subsequent to the acrylation reaction, the triglyceride contains residual epoxy groups that are used to further modify the triglyceride by reacting with cyclohexane dicarboxylic anhydride, which contains cyclic groups conducive to stiffening the polymer (Scheme 1.4). The dynamic mechanical properties of the modified resins are better than those of the unmodified polymers, showing improvements in the storage modulus at room temperature and the glass-transition temperature (T_g).



Scheme 1.4

52. Trecker, D. J.; Borden, G. W.; Smith, O. W. U.S. Patent 3,979,270, 1976.

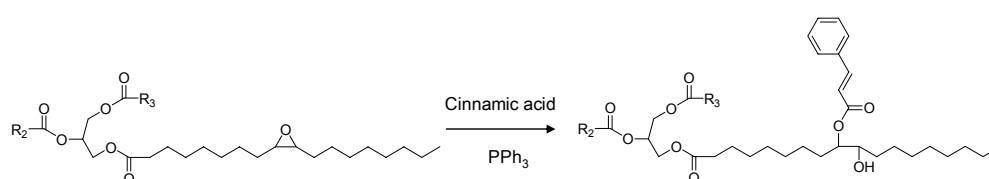
53. La Scala, J. J.; Wool, R. P. *Polymer* 2005, 46, 61.

54. Khot, S. N.; La Scala, J. J.; Can, E.; Morye, S. S.; Palmese, G. R.; Williams, G. I.; Kusefoglu, S. H.; Wool, R. P. *J Appl Polym Sci* 2001, 82, 703.

55. Pelletier, H.; Belgacem, N.; Gandini, A. *J Appl Polym Sci* 2006, 99, 3218.

56. Lu, J.; Wool, R. P. *J Appl Polym Sci* 2006, 99, 2481.

The ring-opening of epoxidized oils with other functionalized acids has also been reported. Cinnamic acid has been attached to epoxidized soybean oil using triphenyl phosphine (PPh_3) as a catalyst (Scheme 1.5).⁵⁷ In agreement with the generally correct view that 1,2-disubstituted alkenes are poor monomers, cinnamic acid does not free-radically homopolymerize to a high-molecular-weight polymer. However, it may readily undergo copolymerization with other alkene monomers, specially with those containing electron-deficient double bonds. The copolymerization of cinnamate ester of epoxidized soybean oil with 25% (w/w) styrene, vinyl acetate, and methyl methacrylate yields insoluble thermosetting materials.



Scheme 1.5

The monomer (a, Figure 1.10) resulting from reacting vernonia oil with a conventional phenolic antioxidant, DHTB [3-(3,5-di-tert-butyl-4-hydroxyphenyl)propionic acid], has been incorporated chemically into polystyrene and polyurethanes to form a macromolecular antioxidant.⁵⁸ Soybean phosphate ester polyol (b, Figure 1.10) has been synthesized by acid hydrolysis of epoxidized soybean oil in the presence of phosphoric acid, and has been used in the preparation of polyurethane formulations.⁵⁹

57. Esen, H.; Küseföglu, S. H. *J Appl Polym Sci* 2003, 89, 3882.

58. Laterre Dwan'lsa, J. P.; Mohanty, A. K.; Misra, M.; Drzal, L. T.; Kazemizadeh, M. *J Polym Environ* 2003, 11, 161.

59. Laterre Dwan'lsa, J. P.; Mohanty, A. K.; Misra, M.; Drzal, L. T.; Kazemizadeh, M. *J Mater Sci* 2004, 39, 1887.

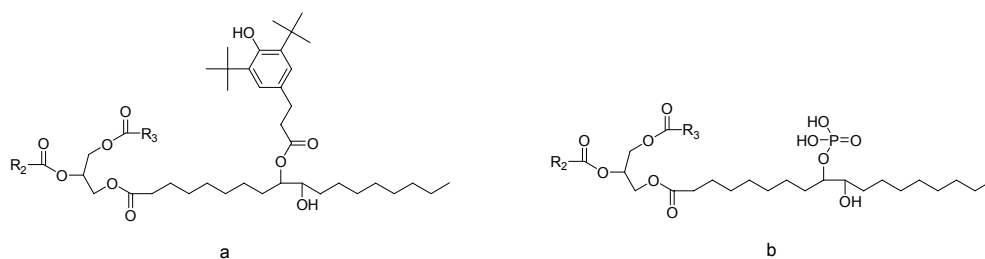
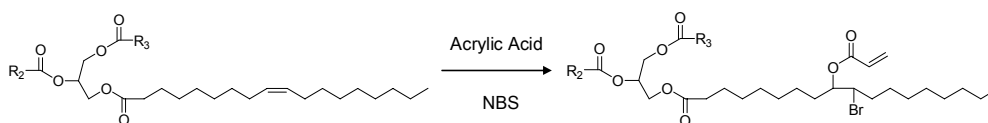


Figure 1.10 Chemical structure monomers resulting from reacting vernonia and soybean oils with DHTB (a) and phosphoric acid (b), respectively.

Other synthesis routes, which do not involve an epoxidation reaction, have been developed to introduce polymerizable groups into the aliphatic chain.

Acrylate moieties have also been attached to triglyceride structures by the one-step addition of bromide and acrylate groups to a C=C double bond. Soybean and sunflower oils have been bromoacrylated in the presence of acrylic acid and NBS (N-bromosuccinimide; Scheme 1.6).⁶⁰



Scheme 1.6

The free-radical homopolymerization of the bromoacrylated triglyceride products has been performed in the presence of methyl ethyl ketone peroxide and AIBN [2,2'-azobis(isobutylnitrile)]. Bromoacrylated soybean- and sunflower-based polymers showed good flame-retardant properties due to the presence of bromine in the structure.⁶¹ Acrylate and bromine have also been added simultaneously to the C=C double bonds of castor oil.⁶² Bromoacrylated castor oil was then reacted with toluene diisocyanate (TDI) forming polyurethane prepolymer containing acrylate

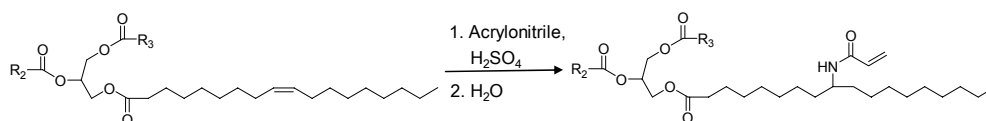
60. Eren, T.; Küseföglu, S. H. *J Appl Polym Sci* 2004, 91, 2700.

61. Ebdon, J. R.; Jones, M. S. *Flame retardants*. In: *Polymeric Materials Encyclopedia*; Salomone, J. C. Ed.; CRC Press: Boca Raton, 1996.

62. Eren, T.; Çolak, S.; Küseföglu, S. H. *J Appl Polym Sci* 2006, 100, 2947.

functional groups. The prepolymer was finally copolymerized with styrene, 2-hydroxyethyl methacrylate, and 3-(acryloxy)-2-hydroxypropyl methacrylate, leading to IPNs.

A very interesting acrylamide derivative of triglycerides was obtained by the Ritter reaction⁶³ between soybean and sunflower oils with acrylonitrile in the presence of sulfuric acid (Scheme 1.7).⁶⁴ Free-radical copolymerization of the resulting acrylamide derivatives with styrene produced semi-rigid polymers.



Scheme 1.7

As mentioned above, the preparation of polyols by epoxidation and subsequent ring-opening has been studied widely (Figure 1.9). However, several approaches that do not involve epoxy intermediate have also been successfully developed.

Hydroformylation, using either rhodium or cobalt as a catalyst, and subsequent hydrogenation by Raney nickel, have been used to convert the C=C double bonds of a vegetable oil to primary alcohols (a, Figure 1.11).⁶⁵ An ozonolysis reaction has also been applied to different vegetable oils (triolein, low-saturated canola oil, and soybean oil), yielding polyols with terminal primary hydroxyl groups and different functionalities (b, Figure 1.11).⁶⁶ Reacting soybean oil with paraformaldehyde in the presence of a Lewis acid catalyst has yielded a hydroxymethylated soybean oil derivative (c, Figure 1.11).⁶⁷ As mentioned above, hydroxylated triglycerides with vicinal diols can be obtained by reacting epoxidized triglyceride with water (d, Figure 1.9).

63. Ritter, J. J.; Minieri, P. P. *J Am Chem Soc* 1948, 70, 4045.

64. Eren, T.; Küseföglu, S. H. *J Appl Polym Sci* 2005, 97, 2264.

65. Guo, A.; Demydov, D.; Zhang, W.; Petrovic, Z. S. *J Polym Environ* 2002, 10, 49.

66. Petrovic, Z. S.; Zhang, W.; Javni, I. *Biomacromolecules* 2005, 6, 713.

67. Eren, T.; Küseföglu, S. H. *J Appl Polym Sci* 2004, 91, 4037.

Alternatively, since harsh reaction conditions are technically necessary for ring-opening of fatty epoxides,⁶⁸ hydroxylated oil (d, Figure 1.11) has also been synthesized directly from the unsaturated oil by reacting with hydrogen peroxide and formic acid.⁶⁹ Moreover, hydroxybrominated triglyceride derivatives (b, Figure 1.9) have also been synthesized in one step, using an NBS/acetone/H₂O mixture.⁷⁰

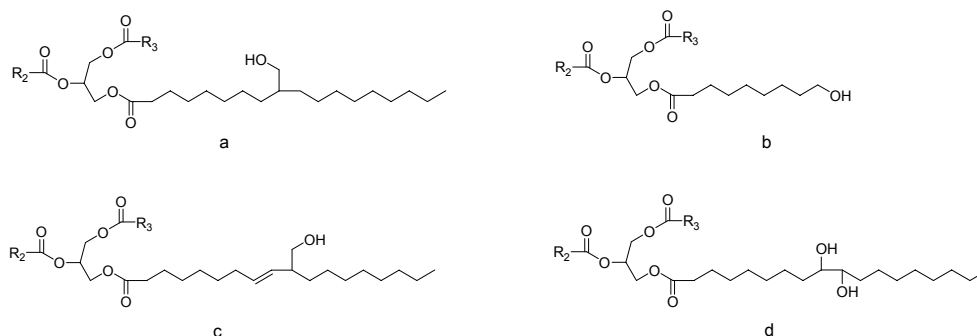


Figure 1.11 Chemical structure of polyols obtained by hydroformylation and subsequent hydrogenation (a), ozonolysis (b), hydroxymethylation (c), and hydroxylation of triglycerides (d).

Hydroxylated vegetable oils have been classically used in polyurethane formulations. However, they have also been modified by cyclic anhydrides, such as maleic anhydride, leading to triglycerides functionalized with maleate half-esters. Hydroxymethylated soybean oil derivative (c, Figure 1.11) has been functionalized with maleate half-esters by reacting with maleic anhydride.⁶⁷ The resulting maleinized triglyceride (a, Figure 1.12) was copolymerized with styrene to produce a rigid polymer. Another type of maleate half-ester derivative, maleinated hydroxylated soybean oil, has been synthesized by Wool's group.⁵⁴ Hydroxylated triglyceride (d, Figure 1.11) was reacted with maleic anhydride to functionalize the triglyceride with maleate half-esters (b, Figure 1.12). Once the maleinization reaction was finished, the monomer resin was radically polymerized and

68. Dahlke, B.; Hellbardt, S.; Paetow, M.; Zech, W. H. *J Am Oil Chem Soc* 1995, 72, 349.

69. Swern, D.; Billen, G. N.; Findley, T. W.; Scalan, J. T. *J Am Chem Soc* 1945, 67, 1786.

70. Eren, T.; Küseföglü, S. H. *Eur J Lipid Sci Technol* 2004, 106, 27.

copolymerized with styrene. The dynamic mechanical properties of the homopolymer were found to be better than those of the AESO polymers.

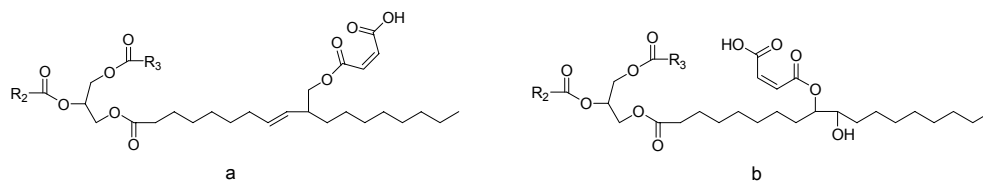
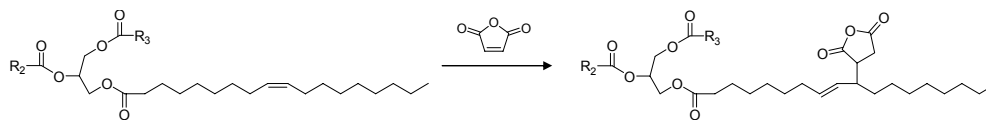


Figure 1.12 Chemical structures of maleinized hydroxymethylated (a) and hydroxylated (b) triglycerides.

Maleic anhydride can also be attached to unsaturated compounds. Maleinization of vegetable oils, which has been widely used, follows an “ene” reaction path and results in the addition of a succinic anhydride group to the allylic position of the fatty acid.^{71,72} Eren et al.⁷³ reported the conversion of soybean oil to succinic anhydride-modified soybean oil (Scheme 1.8) and subsequent polymerization with different alcohols. The polymers were soft and tacky, and hence could not be used as structural polymers. However, these new polymers may be suitable for applications such as adhesives, film formers, and textile and paper sizes.



Scheme 1.8

Maleinated oils have also been used as anhydride-functional curing agents of epoxy resins, such as bisphenol-A (BA)-diglycidyl ether and epoxidized vegetable oils.⁷⁴

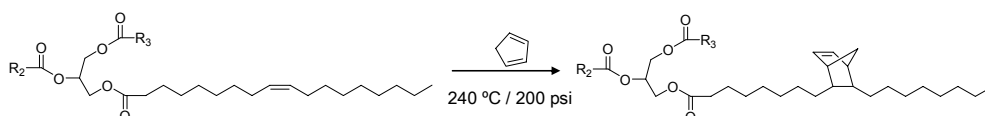
71. Bickford, G. W.; Fischer, G. J. *J Am Oil Chem Soc* 1948, 25, 254.

72. Metzger, J. O.; Biermann, U. *Fat Sci Technol* 1994, 96, 321.

73. Eren, T.; Küsefoğlu, S. H.; Wool, R. P. *J Appl Polym Sci* 2003, 90, 197.

74. Wartha, H.; Mülhaupt, R.; Hoffmann, B.; Lawson, S. *Angew Makromol Chem* 1997, 249, 79.

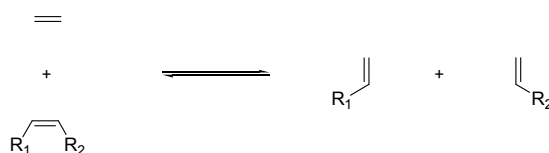
Vegetable oils, on the other hand, have been modified via the Diels-Alder reaction. Linseed oil was modified by reacting it with cyclopentadiene at high temperatures to form a partially norbornylized product (Dilulin®).⁷⁵ Dilulin® contains an average of only one norbornyl group per triglyceride molecule. Chen et al.⁷⁶ reported the synthesis of highly norbornylized linseed oil via a high-pressure, high-temperature Diels-Alder reaction (Scheme 1.9).



Scheme 1.9

This compound was further epoxidized and photopolymerized. It was found that the curing rate was higher for norbornyl epoxidized linseed oil than for epoxidized linseed oil. Additionally, norbornylized linseed oil was successfully used in the formulation of UV-curable hybrid films.⁷⁷

Triglycerides contain internal C=C double bonds, but ω -unsaturated fatty compounds are available by catalytic metathesis with ethylene.⁷⁸ In metathesis reactions, olefins are converted into new olefins via an exchange of alkylidene groups (Scheme 1.10).



Scheme 1.10

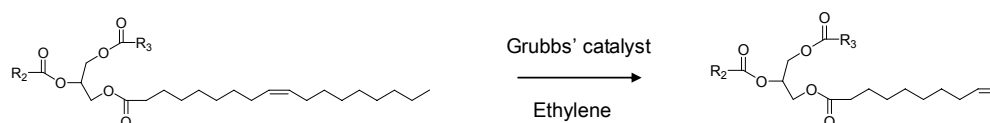
75. Dharma, R. U.S. Patent 5,288,805, 2000.

76. Chen, J.; Soucek, M. D.; Simonsick, W. J.; Celikay, R. W. *Polymer* 2002, 43, 5379.

77. Zoung, Z.; He, J.; Soucek, M. D. *Prog Org Coat* 2005, 53, 83.

78. Mol, J. C. *J Mol Catal* 1994, 90, 185.

ω -Unsaturated esters were obtained from unsaturated fatty acid methyl esters by metathesis with ethylene using heterogeneous rhenium or homogeneous ruthenium catalysts.^{5,79} Alternatively, ω -unsaturated fatty compounds are also available by pyrolysis. Pyrolysis of ricinoleic acid leads to 10-undecenoic acid.⁵ Bis(tricyclohexylphosphine) benzylidene ruthenium (IV) dichloride $[(C_6H_{11}P)_2Cl_2RuCHPh]$ (Grubbs' ruthenium catalyst^{80,81}) has been also used in the metathesis of vegetable oils. 9-undecenoyl triglyceride was obtained by reacting triolein with ethylene in the presence of Grubbs' catalyst (Scheme 1.11).⁸²



Scheme 1.11

Moreover, olefin metathesis has also been used as a polymerization reaction. Cross-metathesis has been applied to soybean oil leading to sticky to rubbery polymers.⁸³ Cross-metathesis polymerization of 10-undecenoyl triglyceride has also been studied.⁸⁴

The naturally occurring hydroxyl groups present in castor oil have also been used to attach polymerizable acrylic, styrenic, and glycidyl moieties by reacting castor oil with acryloyl chloride,^{85,86} 3-isopropenyl- α,α' -dimethylbenzylisocyanate,⁸⁵ and epichlorohydrin⁸⁷ (Figure 1.13). Castor oil glycidyl ether, commercialized by Aldrich Chemical, has been used in formulations of cationic UV-curable coatings.⁸⁸

79. Warwel, S.; Brüse, F.; Demes, C.; Kunz, M. *Ind Crops Prod* 2004, 20, 301.

80. Sanford, M. S.; Ullman, M.; Grubbs, R. H. *J Am Chem Soc* 2001, 123, 749.

81. Grubbs, R. H. *Angew Chem Int Ed Engl* 2006, 45, 3760.

82. Zlatanovic, A.; Petrovic, Z. S.; Dusek, K. *Biomacromolecules* 2002, 3, 1048.

83. Refvik, M. D.; Larock, R. C.; Tian, Q. *J Am Oil Chem Soc* 1999, 76, 93.

84. Callau, L.; Galià, M.; Cádiz, V. Unpublished Results.

85. Nelson, J. S.; Applewhite, T. H. *J Am Oil Chem Soc* 1966, 43, 542.

86. Pelletier, H.; Gandini, A. *Eur J Lipid Sci Technol* 2006, 108, 411.

87. Hicks, D. D.; Belanger, W. J. U.S. Patent 3,351,574, 1967.

88. Thames, S. F.; Yu, H.; Subramanian, R. *J Appl Polym Sci* 2000, 77, 8.

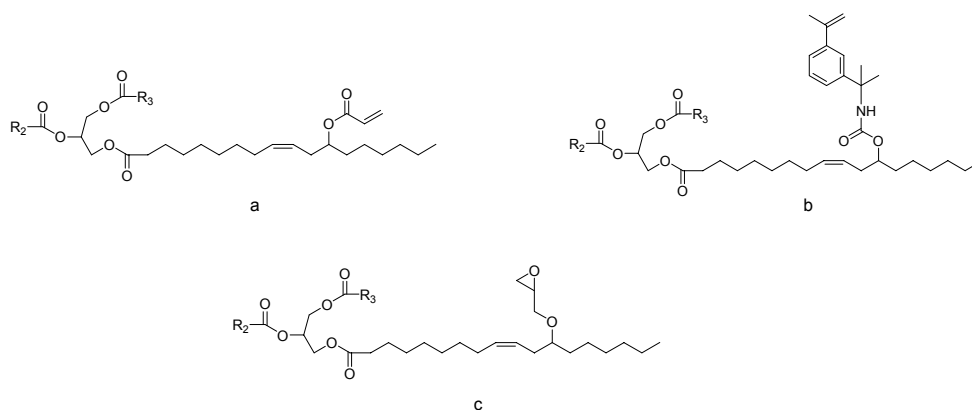
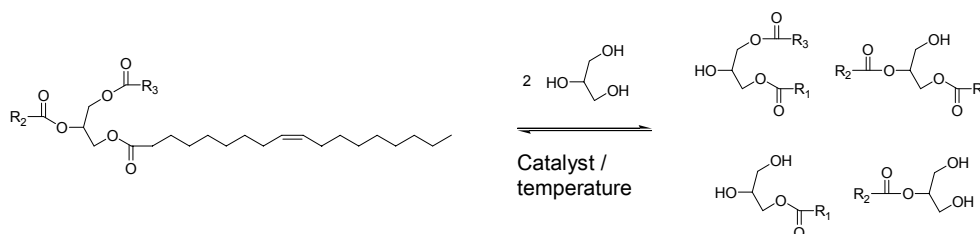


Figure 1.13 Chemical structures of castor oil modified with acryloyl chloride (a), 3-isopropenyl- α,α' -dimethylbenzylisocyanate (b), and epichlorohydrin (c).

b. Pathway B: Reduction of Triglycerides to Monoglycerides

The reduction of triglycerides to monoglycerides via a glycerolysis reaction is another established method for synthesizing monomers from triglycerides. This involves reacting triglycerides with glycerol, for which the product is generally a mixture of monoglycerides and diglycerides, as illustrated in Scheme 1.12.³⁰



Scheme 1.12

The manufacture of alkyd resins is based on the conversion of plant oil triglycerides to monoglycerides that are subsequently used as the diol component in polyesterification reactions with various diacids and anhydrides. Alkyd resins are one

of the oldest polymers from triglyceride oils, and have acquired a good reputation because of their economy and ease of application.⁸⁹

Friedman and Garti⁹⁰ synthesized monoesters of maleic acid using monoglycerides mixtures derived from tallow oil. These products were then sulfonated and used as wetting agents and surfactants, but the unsaturated reactive maleates were not used in radical-initiated polymerization. Wool's group have explored the synthesis and polymerization of soybean oil monoglyceride maleates (SOMGMA; a, Figure 1.14) to yield rigid thermosetting polymers.⁹¹ They subsequently maleinized mixtures of soybean oil monoglycerides, BA, and neopentyl glycol (NPG) under the same reaction conditions, and the resulting maleates [SOMGMA, BAMA (b, Figure 1.14), and NPGMA (c, Figure 1.14)] were then copolymerized with styrene.⁹²

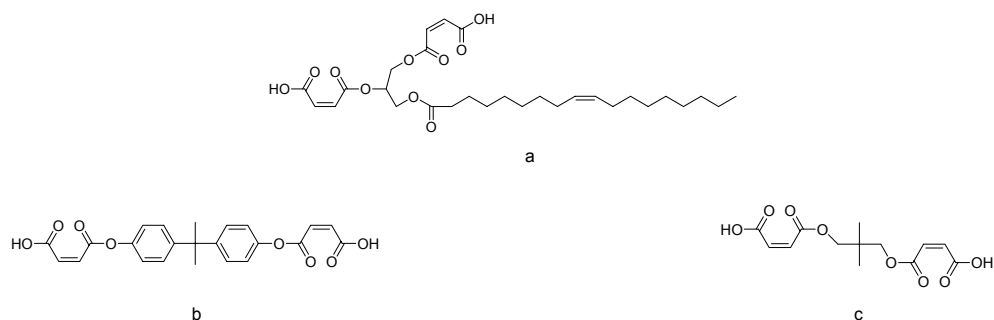


Figure 1.14 Chemical structures of SOMGMA (a), BAMA (b), and NPGMA (c).

The introduction of NPGMA to SOMGMA increased the T_g and modulus of the final polymer, while introducing BAMA had little effect on T_g and caused only a slight increase in the modulus.

89. Deligny, P.; Tuck, N. Alkyd and Polyesters. In: Resins for Surface Coatings, vol. II; Oldring P. K. T., Ed.; John Wiley & Sons, New York, 1996.

90. Friedman, M.; Garti, N. J Am Oil Chem Soc 1983, 60, 1134.

91. Can, E.; Küsefoğlu, S. H.; Wool, R. P. J Appl Polym Sci 2001, 81, 69.

92. Can, E.; Küsefoğlu, S. H.; Wool, R. P. J Appl Polym Sci 2002, 83, 972.

It should be noted that in SOMGMA monomers, part of the resulting network remains elastically inactive even when the functional groups are fully reacted. These elastically inactive regions are types of *dangling chains*, which act as plasticizers that do not participate in polymerization and decrease the modulus and T_g of the resulting polymers.

To reduce this plasticizing effect, castor oil has been recently used instead of soybean oil in alcoholysis reactions with several alcohols: glycerol, pentaerythritol, and BA propoxylate.⁹³ The resulting alcoholysis products were then reacted with maleic anhydride to form maleate half-esters (Figure 1.15). The resulting monomers were finally copolymerized with styrene. The polymers prepared from castor oil exhibit significantly improved modulus, strength, and T_g values compared with soybean oil-based polymers.⁹⁴

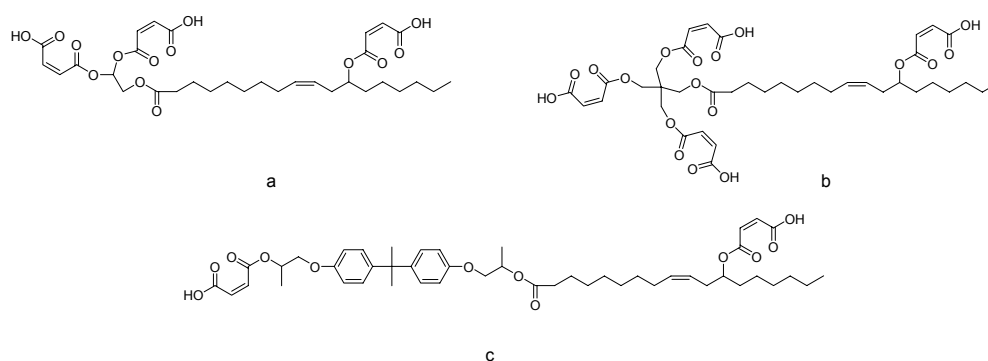


Figure 1.15 Chemical structures of castor oil monoglyceride (a), castor oil pentaerythritol glyceride (b), and castor oil BA propoxylate (c) maleates.

It should also be noted that this methodology combines the above-mentioned synthesis pathways: the introduction of reactive groups into the aliphatic chains (pathway A, Figure 1.8), and the reduction of the triglycerides to monoglycerides (pathway B).

93. Can, E.; Wool, R. P.; Küseföglu, S. H. *J Appl Polym Sci* 2006, 102, 2433.

94. Can, E.; Wool, R. P.; Küseföglu, S. H. *J Appl Polym Sci* 2006, 102, 1497.

To conclude, triglyceride oils derived from plants have been used to synthesize several different monomers that form polymers with diverse properties, with the results suggesting that these materials will prove useful as alternatives for current petroleum-based plastics in practical applications.

1.5

Scope and Purpose of this Thesis

Research into the industrial exploitation of products derived from renewable resources is currently of immense international importance. In particular, the development of polymer materials from renewable resources is receiving considerable attention since the availability of crude oil will become severely restricted within the foreseeable future. The replacement of crude oil by renewable raw materials is also consistent with the aim of global sustainability.

The purpose of the study reported in this thesis was to develop new biobased thermosetting polymers from vegetable oils as renewable resources. To achieve this goal, the experimental work focused on exploiting the reactivity of unsaturated fatty compounds.

Chapter 2 describes the preparation of two new types of organic-inorganic hybrid materials from vegetable oils. Hybrids with promising properties for optical applications were prepared by the hydrosilylation of alkenyl-terminated fatty acid derivatives with several hydrosilylating agents, and the first example of the preparation of biobased polyhedral oligomeric silsesquioxanes-nanocomposites from vegetable oil derivatives is reported.

Chapter 3 describes the synthesis of a new phosphorus-containing fatty acid derivative. This compound is used as a reactive flame-retardant in the preparation

of flame-retardant epoxy resins from terminal epoxy fatty acid derivatives. The incorporation of phosphorous into biobased epoxy resins yields polymers with good flame-retardant properties.

Finally, chapter 4 describes the preparation of a new family of epoxidized methyl oleate-based polyether polyols. These polyols are used in the synthesis of polyurethanes, some with specific applications: silicon-containing polyurethanes with enhanced flame-retardant properties, and polyurethane networks with potential applications in biomedicine.

2

Biobased Organic-Inorganic Hybrid Materials

Organic-inorganic hybrid materials are promising systems for a variety of applications due to the extraordinary properties that result from the combination of different building blocks. In particular, the development of vegetable oil-based hybrid materials shows great promise in the design of new materials for diverse applications.

With the aim of discovering new applications and uses of vegetable oils, this chapter describes work on the design, synthesis, and characterization of two new classes of silicon-containing biobased organic-inorganic hybrid materials.

-
- 2.1 Organic-Inorganic Hybrid Materials
 - 2.2 Vegetable Oil-Based Hybrid Materials
 - 2.3 Objectives
 - 2.4 Experimental Procedures and Results
 - 2.4.1 Novel Organic-Inorganic Hybrid Materials from Renewable Resources: Hydrosilylation of Fatty Acid Derivatives
 - 2.4.2 Bionanocomposites from Renewable Resources: Epoxidized Linseed Oil – Polyhedral Oligomeric Silsesquioxanes (POSS) Hybrid Materials
-

2.1

Organic-Inorganic Hybrid Materials

The major problems encountered in certain applications of polymers are their low stiffness, rigidity, and thermal and oxidative stabilities. These deficiencies can be reduced by fiber reinforcement, with most polymers composites containing strong fibers such as carbon, glass, or natural fibers embedded in a polymer matrix. The high strength and modulus of the embedded fibers increase the strength and rigidity of the material relative to that of the pure polymer.¹

Organic-inorganic polymers have become increasingly important in recent years due to their extraordinary properties that arise from the synergism between the properties of the components.² This concept has been considered potentially attractive for developing materials with properties intermediate between those of traditional organic polymer systems (i.e., processability, flexibility, toughness, and cost) and those of inorganic compounds (i.e., rigidity, and thermal and oxidative stabilities). Composites in which the inorganic phase is chemically attached to the polymeric phase can also be referred to as organic-inorganic hybrid polymers.³

Recent attention has focused on organic-inorganic hybrid materials consisting of inorganic components with sizes on the nanometer or tens-of-nanometer scale. Such materials are called nanocomposites, and they also have great potential for future applications.

There are several routes to the preparation of these materials, but probably the most prominent is incorporating inorganic building blocks into organic polymers.

-
1. McCrum, N. G.; Buckley, C. P.; Bucknall, C. B. *Principles of Polymer Engineering*; Oxford University Press: New York, 1997.
 2. Kikelbick, G. *Prog Polym Sci* 2003, 28, 83.
 3. *Hybrid Organic-Inorganic Composites*; Mark, J. E.; Lee, C. Y.-C.; Bianconi, P. A., Eds.; ACS Symposium Series 585; American Chemical Society: Washington, DC, 1995.

These materials differ remarkably from pure organic polymers, such as in their mechanical, thermal, electrical, and magnetic properties.⁴ The most commonly employed preparation procedures for these materials are as follows:

- a. Using the sol-gel process.
- b. Incorporating preformed inorganic structures in polymers.
- c. Intercalating polymers in clay-layered inorganic materials.

a. Using the Sol-gel Process

The sol-gel process starts with a mononuclear species that forms metal oxide frameworks by hydrolysis and condensation reactions⁵ (Figure 2.1). Molecular species such as certain organometallic compounds based on alkoxides of silicon, titanium, tin, aluminum, or zirconium act as precursors of this class of hybrids. Frequently used strategies for applying the sol-gel approach to the formation of hybrid materials are (i) mixing the precursor for the sol-gel process with the organic polymer followed by an inorganic polycondensation reaction, (ii) polymerization of an organic monomer in the inorganic gel, (iii) simultaneous formation of the inorganic and organic network, and (iv) dual-network materials in which the two networks are covalently linked to each other. In the conventional sol-gel route, the inorganic components - which are generally polydisperse and locally heterogeneous in chemical composition - lead to amorphous materials exhibiting a multitude of microstructures.⁴

4. Functional Hybrid Materials; Gómez-Romero, P.; Sanchez, C., Eds.; Wiley-VCH: Weinheim, 2004.

5. Brinker, C. J.; Scherer, G. W. Sol-Gel Science. The Physics and Chemistry of Sol-Gel Processing; Academic Press: Boston, 1990.

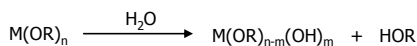
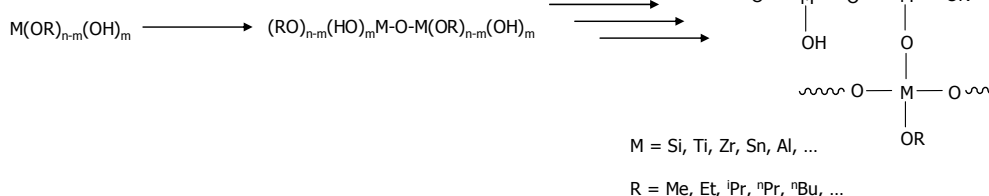
Hydrolysis:**Condensation:**

Figure 2.1 Hydrolysis and condensation mechanisms of the sol-gel process.

This strategy is simple and inexpensive, but the loss of volatile by-products formed in the hydrolysis and condensation reactions makes it difficult to control sample shrinkage during processing. Organopolysiloxane materials are the most important group of hybrids prepared by sol-gel methods. Tetraethoxysilane,⁶ tetramethoxysilane,⁷ functional silane coupling reagents such as 3-glycidyloxypropyltrimethoxysilane,⁸ 3-methacryloxypropyltrimethoxysilane,⁹ and monomers that contain an organic bridging group and two or more trialkoxysilyl groups⁴ have been used extensively in the sol-gel process.

b. Incorporating Preformed Inorganic Structures in Polymers

A suitable method for achieving better definition and control of the inorganic component in hybrid materials is using perfectly calibrated preformed particles that maintain their integrity in the final product.¹⁰ The most prominent representatives of cluster-like inorganic components are probably the polyhedral oligomeric

6. Liu, Y. L.; Lin, Y. L.; Chen, C. P.; Jeng, R. J. *J Appl Polym Sci* 2003, 90, 4047.

7. Ochi, M.; Takahashi, R.; Terauchi, A. *Polymer* 2001, 42, 5151.

8. Liu, Y. L.; Wu, C. S.; Chiu, Y. S.; Ho, W. H. *J Polym Sci Part A: Polym Chem* 2003, 41, 2354.

9. Abe, Y.; Honda, Y.; Gunji, T. *Appl Organometal Chem* 1998, 12, 749.

10. Sanchez, C.; Soler-Illia G. J. de A. A.; Ribot, F.; Lalot, T.; Mayer, C. R.; Cabuil, V. *Chem Mater* 2001, 13, 3061.

silsesquioxane (POSS) compounds, which possess unique cage-like structures and nanoscale dimensions.¹¹ POSS, $(\text{RSiO}_{1.5})_x$ with $x = 6, 8, 10, \dots$, can be incorporated into linear or thermosetting polymers.¹² Generally, a higher thermal stability, a better environmental durability in certain conditions (e.g., exposure to molecular oxygen or fire), and, in some cases, an improvement in mechanical properties (reinforcement) are exhibited by POSS-modified polymers.² Octahedral compounds (i.e., $x = 8$) are the most representative members of this family (Figure 2.2).

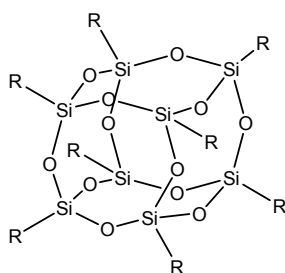


Figure 2.2 Generalized representation of POSS monomers.

Depending on the number of organic groups (i.e., R in Figure 2.2) bearing reactive functionalities, POSS can be classified as non-functional, monofunctional, or polyfunctional. Reactive POSS have been grafted or copolymerized in a variety of polymeric materials, including styrenics,¹³ acrylics,¹⁴ epoxides,¹⁵ polyolefins,¹⁶ polyurethanes,¹⁷ and polyimides.¹⁸

-
11. Phillips, S. H.; Haddad, T. S.; Tomczak, S. J. *Curr Opin Solid State Mater Sci* 2004, 8, 21.
 12. Lichtenhan, J. D. Silsesquioxane-Based Polymers. In: *Polymeric Material Encyclopedia: Synthesis, Properties and Applications*, vol. X; Salamone, J. C. Ed.; CRC Press: Boca Raton, FL, 1996.
 13. Lichtenhan, J. D.; Otonari, Y.A.; Carr, M. J. *Macromolecules* 1995, 28, 8435.
 14. Lee, A.; Lichtenhan, J. D. *Macromolecules* 1998, 31, 4970.
 15. Matejka, L.; Strachota, A.; Plestil, J.; Whelan, P.; Steinhart, M.; Slouf, M. *Macromolecules* 2004, 37, 9449.
 16. Leu, C. M.; Reddy, G. M.; Wie, K. H.; Shu, C. F. *Chem Mater* 2003, 15, 2261.
 17. Liu, H.; Heng, S. *Macromol Rapid Commun* 2005, 26, 196.
 18. Tamaki, R.; Choi, J.; Laine, R. M. *Chem Mater* 2003, 15, 793.

c. Intercalating Polymers in Clay-Layered Inorganic Materials

Polymer-clay nanocomposites are receiving increasing attention from both research and industrial quarters.¹⁹ Compared with conventional composites that contain high concentrations of the filler, clay nanocomposites exhibit substantially improved modulus,²⁰ strength,²¹ heat resistance,²² and fire resistance^{23,24} at very low clay contents (generally less than 5 wt %). The main reason for their improved properties is the strong interfacial interactions between the matrix and the layered silicate, which are not present in conventional composites.²⁵ Layered silicates generally have layer thicknesses on the order of 1 nm and very high aspect ratios (e.g., 10–1000). The polymer chains are generally intercalated into the silicate galleries by either (i) inserting suitable monomers into the silicate galleries and subsequent polymerization, or (ii) directly inserting polymer chains into the galleries from either a solution or a melt. Depending on the strength of the polymer-clay interaction, nanocomposites with two different structures are thermodynamically achievable (Figure 2.3): (i) intercalated nanocomposites, where the insertion of polymer chains into the silicate structure is crystallographically regular and with a repeat distance of a few nanometers, and (ii) exfoliated nanocomposites, in which the individual silicate layers are separated in the polymer matrix. Polymer-clay nanocomposites have been successfully developed from most conventional polymers by inserting polymer chains into silicate galleries.²⁶⁻³⁰

19. Sinha Ray, S.; Okamoto, M. *Prog Polym Sci* 2003, 28, 1539.

20. Weon, J. I.; Sue, H. J. *Polymer* 2005, 46, 6325.

21. Dai, X.; Xu, J.; Guo, X.; Lu, Y.; Shen, D.; Zhao, N.; Luo, X.; Zhang, X. *Macromolecules* 2004, 37, 5615.

22. Chen, G. X.; Yoon, J. S. *Polym Degrad Stab* 2005, 88, 206.

23. Gianelli, W.; Camino, G.; Tabuani, D.; Bortolon, V.; Savadori, T.; Monticelli, O. *Fire Mater* 2006, 30, 333.

24. Zanetti, M.; Lomakin, S.; Camino, G. *Macromol Mater Eng* 2000, 279, 1.

25. Chen, J. S.; Poliks, M. D.; Ober, C. K.; Zhang, Y.; Wiesner, U.; Giannelis, E. P. *Polymer* 2002, 43, 4895.

26. Li, C. P.; Huang, C. M.; Hsieh, M. T.; Wei, K. H. *J Polym Sci, Part A: Polym Chem* 2005, 43, 534.

27. Ray, S.; Galgali, G.; Lele, A.; Sivaram, S. *J Polym Sci Part A: Polym Chem* 2005, 43, 304.

28. Triantafyllidis, K. S.; LeBaron, P. C.; Park, I.; Pinnavaia, T. J. *Chem Mater* 2006, 18, 4393.

29. Lee, H. T.; Lin, L. H. *Macromolecules* 2006, 39, 6133.

30. Wheeler, P. A.; Wang, J.; Mathias, L. J. *Chem Mater* 2006, 18, 3937.

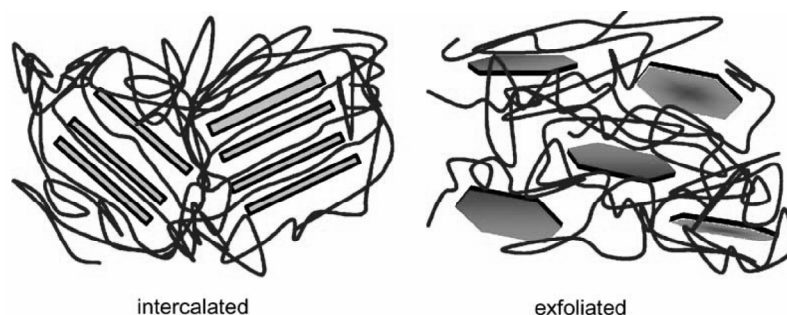


Figure 2.3 Schematics of the two types of thermodynamically achievable polymer-clay nanocomposites.

2.2

Vegetable Oil-Based Hybrid Materials

Vegetable oil-based materials can be reinforced with traditional fibers, such as carbon or glass.³¹⁻³³ However, the increasing demand for environmentally friendly materials and the desire to reduce the cost has led to interest in the use of natural fibers, such as flax, pulp, cellulose, jute, hemp, straw, and bamboo. These natural fibers are based on cellulose and are biodegradable, inexpensive, and have a low density. At the University of Delaware, the ACRES (affordable composites from renewable sources) group has been actively involved in developing biobased thermosetting resins from plant oils reinforced with natural fibers.³³⁻³⁵

As mentioned above, the enormous interest in organic-inorganic hybrid materials is due to the novel properties that derive from the unique contributions of each component.² Coatings based on vegetable oil-based hybrids that incorporate inorganic macromolecular sol-gel networks into organic polymer structures have

31. Lu, Y.; Larock, R. C. *J Appl Polym Sci* 2006, 102, 3345.

32. Music, S.; Javni, I.; Petrovic, Z. S. *Compos Sci Technol* 2005, 65, 19.

33. Khot, S. N.; La Scala, J. J.; Can, E.; Morye, S. S.; Palmese, G. R.; Williams, G. I.; Küsefoglul, S. H.; Wool, R. P. *J Appl Polym Sci* 2001, 82, 703.

34. Williams, G. I.; Wool, R. P. *Appl Composite Mater* 2000, 7, 421.

35. Wool, R. P.; Küsefoglul, S. H.; Palmese, G. R.; Zhao, R.; Khot, S. N. U.S. Patent 6,121,398 2000.

been widely studied by Soucek's group.³⁶⁻⁴¹ They have found that varying the amounts and types of sol-gel precursors allows coatings with diverse properties to be obtained.

The nanoreinforcements that are currently being used to modify petroleum-based resins are clay-layered silicates, single- and multi-walled nanotubes, carbon nanofibers, sol-gel precursors, and POSS nanostructured chemicals. Tsujimoto et al.⁴² reported that acid-catalyzed curing of epoxidized plant oils with 3-glycidyloxypropyltrimethoxysilane produced biodegradable nanocomposites with improved hardness and mechanical strength, and excellent transparency. Clay has also been widely used due its widespread availability and low cost, and the use of impure carbon nanotubes as a reinforcement has also been reported.⁴³ Wool et al.⁴⁴ prepared biobased nanocomposites by dispersing an organoclay in acrylated epoxidized soybean oil (AESO) and styrene, followed by free-radical polymerization. Kobayashi et al.^{45,46} and Mohanty et al.⁴⁷ have developed nanocomposites by acid-catalyzed curing and anhydride curing of epoxidized linseed oil and epoxidized soybean oil, respectively, in the presence of an organoclay. The mechanical properties,⁴⁴⁻⁴⁷ thermal stability,⁴⁴⁻⁴⁷ and barrier properties⁴⁵ of the resulting nanocomposites are superior to those of the pure polymer. Recently, Larock et al.⁴⁸ reported on the preparation of novel biobased nanocomposites by the cationic

-
36. Ballart, R. L.; Tuman, S. J.; Fouquette, D. J.; Stegmiller, W.; Soucek, M. D. *Chem Mater* 1999, 11, 726.
37. Wold, C. R.; Soucek, M. D. *Macromol Chem Phys* 2000, 201, 382.
38. Teng, G.; Soucek, M. D. *J Am Oil Chem Soc* 2000, 77, 381.
39. Zou, K.; Soucek, M. D. *Macromol Chem Phys* 2004, 205, 2032.
40. Soucek, M. D.; Jonson, A. J. *Polym Adv Technol* 2005, 16, 257.
41. Zong, Z.; He, J.; Soucek, M. D. *Prog Org Coat* 2005, 53, 83.
42. Tsujimoto, T.; Uyama, H.; Kobayashi, S. *Macromol Rapid Commun* 2003, 24, 711.
43. Thielemans, W.; McAninch, I. M.; Barron, V.; Blau, W. J.; Wool, R. P. *J Appl Polym Sci* 2005, 98, 1325.
44. Lu, J.; Hong, C. K.; Wool, R. P. *J Polym Sci Part B: Polym Phys* 2004, 42, 1441.
45. Uyama, H.; Kuwabara, M.; Tsujimoto, T.; Nakano, M.; Usuki, A.; Kobayashi, S. *Macromol Biosci* 2004, 4, 354.
46. Uyama, H.; Kuwabara, M.; Tsujimoto, T.; Nakano, M.; Usuki, A.; Kobayashi, S. *Chem Mater* 2003, 15, 2492.
47. Miyagawa, H.; Mohanty, A.; Drzal, L. T.; Misra, M. *Ind Eng Chem Res* 2004, 43, 7001.
48. Lu, Y.; Larock, R. C. *Biomacromolecules* 2006, 7, 2692.

polymerization of soybean oil with styrene and divinylbenzene, and reactive organomodified montmorillonite clay as a reinforcing phase.

To conclude, the incorporation of nanoscale inorganic species in vegetable oil-based polymers offers the possibility of developing new materials with novel applications. This highly interdisciplinary scientific area is ripe for new ideas from all disciplines, and therefore has a promising future.

2.3

Objectives

In an attempt to identify new applications and uses of triglycerides, which are constituents of vegetable oils, the main objective of the work described in this chapter was to synthesize and characterize new organic-inorganic hybrid materials from vegetable oils. This objective can be divided into two sub objectives:

1. To synthesize organic-inorganic hybrid networks by the hydrosilylation of two alkenyl-terminated fatty acid derivatives (Figure 2.4): 10-undecenoyl triglyceride (UDTG) and methyl 3,4,5-tris(10-undecenoyloxy)benzoate (UDBM).

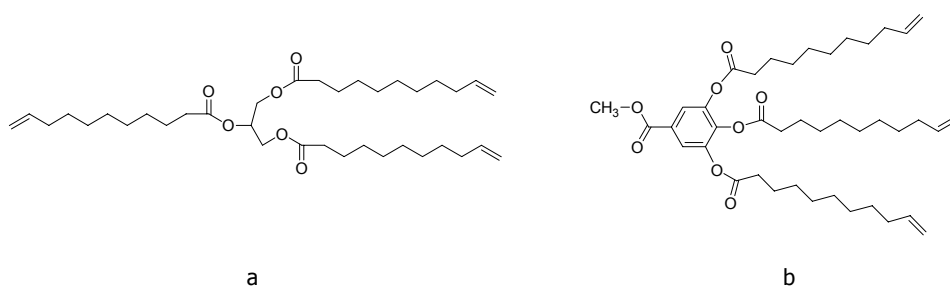


Figure 2.4 Chemical structures of UDTG (a) and UDBM (b) monomers.

2. To prepare and evaluate the properties of new bionanocomposites prepared from epoxidized linseed oil (ELO, Figure 2.5) and 3-glycidylpropylheptaisobutyl-T₈-polyhedral oligomeric silsesquioxane (G-POSS).

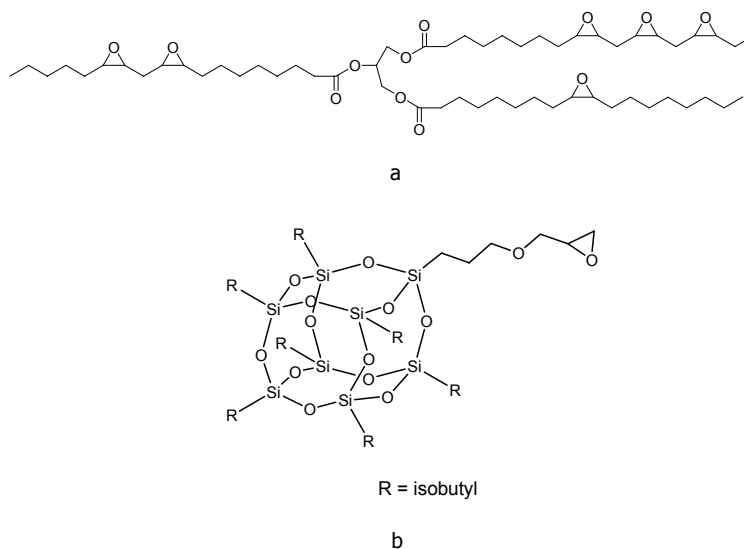


Figure 2.5 Chemical structures of ELO (a) and G-POSS (b) monomers.

2.4

Experimental Procedures and Results

The following experimental procedures and the results of the studies performed for this chapter have been published in different scientific journals, and so they are presented here in the journal format, as are the experimental procedures and the results presented in the following two chapters.

The work described in Section 2.4.1 has been published in the *Journal of Polymer Science Part A: Polymer Chemistry* (2005, 43, 6295), and includes the synthesis and

characterization of organic-inorganic hybrid networks prepared by the hydrosilylation of two alkenyl-terminated fatty acid derivatives: UDTG and UDBM. Several polyfunctional hydrosilylating agents were used as crosslinkers, and the hydrosilylation reaction was catalyzed using Karstedt's catalyst. The hydrosilylation of olefins has been widely studied,⁴⁹ but only a few studies of fatty acid esters have been reported,⁵⁰⁻⁵² and these have all involved adding a silane compound with a functionality of 1. Thus, the present study was the first to use a hydrosilylation reaction to synthesize organopolysiloxane networks from vegetable oils. The obtained materials exhibit good transparency and promising properties for optical applications.

The work described in Section 2.4.2 has been published in the journal *Biomacromolecules* (2006, in press), and includes the preparation and characterization of POSS-nanocomposites from ELO. In this study, ELO was copolymerized with G-POSS by cationic-initiated polymerization. The morphology of these nanocomposites was determined and the nanoscale-reinforcement effect of G-POSS was evaluated. POSS monomers have previously been copolymerized with several organic monomers via the formation of covalent bonds to afford a variety of polymer-POSS nanocomposites,¹³⁻¹⁸ but the present study was the first to prepare vegetable oil-based POSS nanocomposites.

49. Marcienic, B. *Comprehensive Handbook on Hydrosilylation*; Pergamon: London, 1992.

50. Saghian, N.; Gertner, D. *J Am Oil Chem Soc* 1974, 51, 363.

51. Behr, A.; Toslu, N. *Chem Eng Technol* 2000, 23, 122.

52. Delpéch, F.; Saadia, A.; Castel, A.; Rivière, P.; Rivière-Baudet, M.; Amin-Alami, A.; Manriquez, J. *Appl Organometal Chem* 2001, 15, 626.

2.4.1 Novel Organic-Inorganic Hybrid Materials
from Renewable Resources: Hydrosilylation of
Fatty Acid Derivatives

NOVEL ORGANIC-INORGANIC HYBRID MATERIALS FROM RENEWABLE RESOURCES: HYDROSILYLATION OF FATTY ACID DERIVATIVES

G. Lligadas, L. Callau, J.C. Ronda, M. Galià, V. Cádiz
Departament de Química Analítica i Química Orgànica, Universitat Rovira i Virgili,
Campus Sescelades, Marcel·lí Domingo s/n, 43007 Tarragona, Spain.

ABSTRACT: Novel hybrid organic-inorganic materials were prepared from 10-undecenoyl triglyceride and methyl 3,4,5-tris(10-undecenoyloxy)benzoate via hydrosilylation. 1,4-Bis(dimethylsilyl)benzene, tetrakis(dimethylsilyloxy)silane, and 2,4,6,8-tetramethylcyclotetrasiloxane were used as crosslinkers. The hydrosilylation reaction was catalyzed by Karstedt's catalyst [Pt(0)-divinyltetramethyldisiloxane complex]. The networks were structurally characterized by Fourier transform infrared spectroscopy, ^{13}C NMR, and ^{29}Si magic-angle-spinning NMR. The thermal properties of these hybrids were studied with differential scanning calorimetry, thermogravimetric analysis, and dynamic mechanical analysis. The obtained materials showed good transparency and promising properties for optical applications.

Keywords: crosslinking; heteroatom-containing polymers; renewable resources

INTRODUCTION

Sustainable development has become the key idea of the 21st century. In the search for sustainable chemistry, the use of renewable resources as alternatives to petroleum-derived ones is of considerable importance. Natural oils derived from both plant and animal sources make up a large proportion of the current consumption of renewable raw materials. Therefore, preparation of polymeric materials from renewable

resources is of great economic and ecological significance.^{1,2} Natural oils of plant and animal origins have excellent properties that can be used not only to produce valuable polymeric materials such as epoxy resins and polyurethanes but also in the agricultural and food industries.³

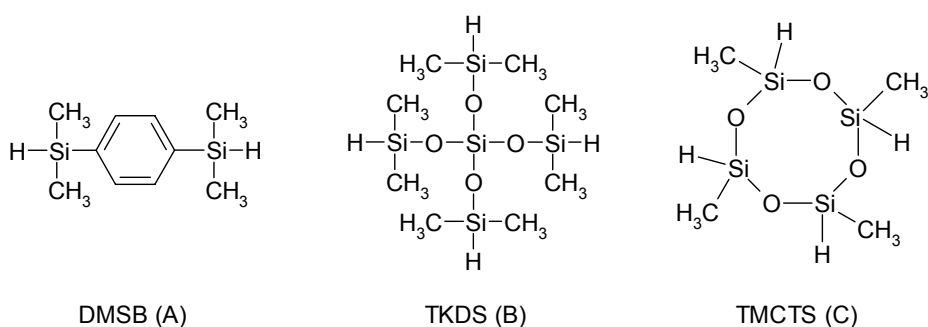
Vegetable oils are triglycerides of predominantly unsaturated fatty acids. The fatty acid composition of triglycerides varies not only from oil to oil

but also within the same oil, and there are considerable differences in the overall level of unsaturations, the number of double bonds per fatty acid residue, the position of the double bond within the fatty acid residue, and the length of the carbon chain of the carboxylic acid. Thus, a wide variety of monomers with different characteristics are potentially available from these materials.

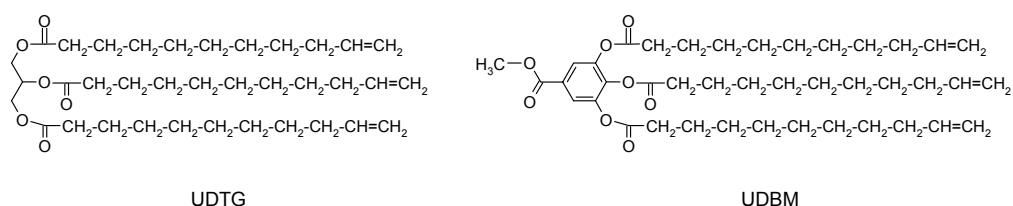
The radical polymerization of double bonds has been used in an attempt to convert vegetable oils to useful polymers⁴ because of its low cost and availability from a renewable nature resources and the possible biodegradability of these systems. The polymerization of free fatty acids as well as methyl esters of fatty acids of natural oils has also been initiated by boron trifluoride and boron trifluoride ether complexes, and the corresponding reports that have appeared in the literature have dealt with the production of viscous oils. Rigid, hard polymers have been produced by the cationic copolymerization of various natural oils with divinylbenzene.⁵

Vegetable oils are chemically relatively unreactive and can be functionalized to serve as components for polymeric materials. Several groups are usually introduced in the double-bond position to enhance their reactivity; for example, hydroxyl groups make it possible to prepare polyols for polyurethanes.^{6,7} Epoxidation is one of the most important addition reactions that can be applied to a triglyceride, and opening up the epoxide ring leads to a large number of products.⁸⁻¹⁰ As is well known, olefin metathesis is a bond rearrangement reaction catalyzed by certain transition-metal compounds¹¹ than can also be applied to unsaturated fatty acid esters to produce polymers and other useful chemical products.¹² Metathesis with ethene or pyrolysis of the triglycerides with internal double bonds enables triglycerides with terminal double bonds to be synthesized that have a broad range of applications.¹³

Recently, there has been great interest in organic-inorganic hybrid materials because the unique combinations of each component give them unexpected properties.¹⁴



Scheme 1



Scheme 2

As far as oil-based hybrid materials are concerned, composites with good mechanical properties have been prepared from acrylate-modified soybean oil and natural fibers.¹⁵ Organic-inorganic hybrid coatings have been developed with plant oils and metal (Ti and Zr) oxides.^{16,17} In addition, several hybrid polymeric membranes have been investigated.^{18,19}

In an attempt to find out new applications and uses for triglycerides, which are constituents of various oils, we have investigated the synthesis of new organic-inorganic hybrid materials via hydrosilylation. Although the hydrosilylation of olefins has been widely studied,²⁰ few studies have been made of fatty acid esters.²¹⁻²³ For the platinum-catalyzed hydrosilylation of the terminal and internal unsaturated fatty acid esters, mild conditions can be used to obtain moderate-to-good yields of up to 90%. The reactivity of terminal unsaturated fatty acid esters is higher than that of internal unsaturated ones.^{24,25}

The aim of this study was to obtain hybrid organic-inorganic materials from renewable resources. We first investigated the hydrosilylation reaction of terminal unsaturated fatty acid esters with several polyfunctional hydrosilylating agents-1,4-bis(dimethylsilyl)benzene

(DMSB; A), tetrakis(dimethylsilyloxy)silane (TKDS; B), and 2,4,6,8-tetramethylcyclotetrasiloxane (TMCTS; C; Scheme 1)-catalyzed by H_2PtCl_6 in a 2-propanol solution (Speier's catalyst)²⁶ and by a Pt(0)-divinyltetramethyldisiloxane complex (Karstedt catalyst).²⁷ In this study, we developed hybrid organic-inorganic materials from 10-undecenoyl triglyceride (UDTG), which can be obtained from castor oil, and methyl 3,4,5-tris(10-undecenoyloxy) benzoate (UDBM), a new aromatic fatty acid derivative compound (Scheme 2). The properties of the materials prepared were studied with differential scanning calorimetry (DSC), thermogravimetric analysis (TGA) and dynamic mechanical analysis (DMTA).

EXPERIMENTAL

Materials

UDTG (iodine value = 120) was supplied by Dow Chemical. The hexachloroplatinic acid, purchased from Fluka, was used as received. A platinum-divinyltetramethyldisiloxane complex with 3-3.5 wt % of platinum in xylene (Aldrich) was dissolved in toluene to give a 274 ppm platinum concentration. The Pt solution was stored at 4 °C. 10-Undecenoic acid, 10-undecenoyl chloride, and methyl 3,4,5-trihydroxy-

benzoate were purchased from Aldrich and used without any further purification. The following silanes were obtained from the sources indicated: DMSB (from ABCR), TKDS (from Aldrich), and TMCTS (from Aldrich). They were used as received. Toluene was distilled from sodium immediately before use. Other solvents were purified by standard procedures.

Synthesis of Methyl 10-Undecenoate (UDM)

To a 500-mL, round-bottom flask, 60 g (0.3 mol) of 10-undecenoic acid, 300 ml of methanol, and a few drops of concentrated sulfuric acid were added, and then the mixture was refluxed and mechanically stirred. The reaction was followed by thin-layer chromatography with the chloroform/methanol (9:1) system as the eluent and the fluorescein/Br₂ system as the dyeing agent. Once the reaction was completed, the crude was left to cool, and the methanol evaporated. The oily ester was distilled *in vacuo* (bp = 54.6–55.0 °C at 0.1 mmHg) and afforded a 99% yield.

¹H NMR [CDCl₃/tetramethylsilane (TMS), δ, ppm]: 1.3 (m, 10H), 1.6 (m, 2H), 2.0 (m, 2H, CH₂-CH=), 2.3 (t, 2H, *J* = 7.7 Hz, CH₂CO), 3.6 (s, 3H, CH₃O), 5.0 (d, 1H, *J*_{cis} = 10.2 Hz, CH=CH₂), 5.04 (d, 1H, *J*_{trans} = 17.2 Hz, CH=CH₂), 5.8 (m, 1H, CH=CH₂). ¹³C NMR (CDCl₃, δ, ppm): 24.91 (CH₂-CH₂-CO), 28.84, 29.05, 29.11, 29.22, 29.33 (-CH₂-), 33.78 (CH₂-CO), 34.02 (CH₂-CH=), 51.43 (OCH₃), 114.14 (CH₂=CH), 139.17 (CH=CH₂), 174.39 (C=O).

Synthesis of UDBM

A 500-mL, three-necked, round-bottom flask equipped with a cooler, a Teflon-coated magnetic bar, and a pressure-equalized dropping funnel was charged with 5.0 g (26.6 mmol) of methyl 3,4,5-trihydroxybenzoate, 8.0 mL of pyridine, and 200 mL of anhydrous dichloromethane under dry nitrogen atmosphere. To this solution 17.0 g (8.1 mmol) of 10-undecenoyl chloride was added dropwise with stirring at room temperature for 15 min. The temperature was raised and maintained under reflux for about 15 min. The progress of the reaction was monitored by thin-layer chromatography with hexane/ethyl acetate (3:1) as the eluent. The mixture was cooled to room temperature and filtered to remove the pyridinium salt, which was washed three times with dichloromethane.

The reaction mixture was placed in a separation funnel and washed with 200 mL of water, 200 mL of 2 N HCl, a sodium bicarbonate solution until a neutral pH, and 200 mL of a saturated sodium chloride solution. The organic phase was dried over anhydrous magnesium sulfate, and the excess dichloromethane was evaporated off. The yellow oil obtained was purified by flash chromatography with a silica gel column and hexane/ethyl acetate (10:1) as the eluent. When the solvent was removed, 17.0 g of pure UDBM (yield = 93%) was obtained as a viscous oil.

¹H NMR (CDCl₃/TMS, δ, ppm): 1.3 (m, 30H), 1.7 (m, 6H), 2.0 (m, 6H),

CH₂-CH=), 2.52 (t, 6H, $J = 7.2$ Hz, CH₂CO), 3.9 (s, 3H, CH₃O), 4.9 (d, 3H, $J_{cis} = 10.4$ Hz, CH=CH₂), 5.0 (d, 3H, $J_{trans} = 17.2$ Hz, CH=CH₂), 5.8 (m, 3H, CH=CH₂), 7.8 (s, 2H). ¹³C NMR (CDCl₃), δ , ppm): 24.94, 25.04 (CH₂-CH₂-CO), 29.00, 29.18, 29.20, 29.26, 29.34, 29.39, 29.40, 29.45 (-CH₂-), 33.85, 33.90 (-CH₂-CO), 34.09 (CH₂-CH=), 52.65 (OCH₃), 114.33, 114.37 (CH₂=CH), 122.22, 128.19, 138.80 (Ar), 139.11, 139.18 (CH=CH₂), 143.60 (Ar), 165.10 (-COCH₃), 169.34, 170.57 (C=O).

Procedure for the Hydrosilylation Reaction

The hydrosilylation of UDM was carried out with the Speier's catalyst (H₂PtCl₆ in 2-propanol solution) and Karstedt's catalyst (Pt(0)-divinyltetramethyldisiloxane complex) with Schlenk-type material purged with argon. The hydrosilylation agents were as follows (the functionality is given in parentheses): (1) DMSB (A, $f = 2$), (2) TKDS (B, $f = 4$) and (3) TMCTS (C, $f = 4$; Scheme 1). All silane and catalyst transfers were carried out under an inert argon atmosphere and for the liquid silane reagents via a syringe. A general procedure for the hydrosilylation reaction is described next.

In 10 mL of anhydrous toluene, 3 g (15 mmol) of UDM was dissolved. Then, the corresponding stoichiometric amount of the silane and the desired amount of the catalyst were added under an argon atmosphere, and the mixture was warmed up to 65 °C while stirring. To follow the reaction progress, several samples were taken

at different times and were analyzed by Fourier transform infrared (FTIR) spectroscopy. The intensity of the ν_{Si-H} (2168 cm⁻¹) and $\nu_{C=C}$ (1640 cm⁻¹) bands was monitored. Once the reaction was finished, the crude mixture was dissolved in CH₂Cl₂ and passed through a silica gel column to remove the Pt catalyst. The product was isolated after the solvent had been evaporated. Some experiments were carried out in bulk. In these cases, the procedure was the same, but the methyl ester was not previously dissolved in toluene.

UDM-DMSB

¹H NMR (CDCl₃/TMS, δ , ppm): 0.02 (s, 12H, CH₃Si), 0.70 (m, 4H, CH₂Si), 1.3 (m, 28H), 1.6 (m, 4H), 2.3 (t, 4H, $J = 7.2$ Hz, CH₂CO), 3.6 (s, 6H, CH₃O), 7.5 (s, 4H). ¹³C NMR (CDCl₃, δ , ppm): -2.85 (CH₃Si), 15.81 (CH₂Si), 24.05 (CH₂-CH₂-Si), 25.85 (CH₂-CH₂-CO), 29.20, 29.38, 29.43, 29.59, 29.68, 33.79 (-CH₂-), 34.27 (CH₂-CO), 51.38 (OCH₃), 133.00, 140.18 (Ar), 174.13 (C=O). ²⁹Si NMR (CDCl₃, δ , ppm): -1.5.

UDM-TKDS

¹H NMR (CDCl₃/TMS, δ , ppm): 0.06 (s, 24H, CH₃Si), 0.5 (m, 8H, CH₂Si), 1.3 (m, 56H), 1.6 (m, 8H), 2.3 (t, 8H, $J = 7.6$ Hz, CH₂CO), 3.6 (s, 12H, CH₃O). ¹³C NMR (CDCl₃, δ , ppm): 0.15 (CH₃Si), 18.41 (CH₂Si), 23.32 (CH₂-CH₂-Si), 25.14 (CH₂-CH₂-CO), 29.45, 29.51, 29.62, 29.78, 29.89, 33.70 (-CH₂-), 34.20 (CH₂-CO), 51.54 (OCH₃), 174.13 (C=O). ²⁹Si NMR (CDCl₃, δ , ppm): 8.5.

UDM-TMCTS

^1H NMR (CDCl_3/TMS , δ , ppm): 0.05 (s, 12H, CH_3Si), 0.5 (m, 8H, CH_2Si), 1.3 (m, 56H), 1.6 (m, 8H), 2.3 (t, 8H, $J=7.7$ Hz, CH_2CO), 3.6 (s, 12H, CH_3O). ^{13}C NMR (CDCl_3 , δ , ppm): -0.51 (CH_3Si), 17.02 (CH_2Si), 22.86 ($\text{CH}_2\text{-CH}_2\text{-Si}$), 24.87 ($\text{CH}_2\text{-CH}_2\text{-CO}$), 29.01, 29.12, 29.29, 29.46, 29.65, 33.08 ($-\text{CH}_2-$), 33.9 (CH_2CO), 51.23 (OCH_3), 174.23 (C=O). ^{29}Si NMR (CDCl_3 , δ , ppm): -20.1.

General Procedure for the Hybrid Organic-Inorganic Materials

UDTG and UDBM were cured with the three Si-H-containing crosslinking agents: DMSB (A), TKDS (B) and TMCTS (C).

UDTG

For A, 0.5 g of UDTG was mixed with 0.25 g of DMSB, and 10 μl of the platinum catalyst (Karstedt) was added. After stirring for 5 min, the mixture was cured via heating for 20 h at 85 $^\circ\text{C}$ and postcured for 4 h at 150 $^\circ\text{C}$. For B, the same procedure was used, but with 0.21 g of TKDS. For C, the same procedure was used, but with 0.15 g of TMCTS.

HNTGA (UDTG/DMSB). ^{13}C NMR [tetrachloroethane- d_2 (TCE), δ , ppm]: -3.10 (CH_3Si), 15.43 (CH_2Si), 23.67, 24.62, 29.10, 33.43, 33.80 ($-\text{CH}_2-$), 61.85 (CH_2O), 68.57 (CHO), 132.63, 139.77 (Ar), 173.15 (C=O). ^{29}Si magic-angle-spinning (MAS) NMR (δ , ppm): -1.0.

HNTGB (UDTG/TKDS). ^{13}C NMR (TCE- d_2 , δ , ppm): -0.26 (CH_3Si), 17.72 (CH_2Si), 22.95, 24.54, 28.81, 32.29, 33.74 ($-\text{CH}_2-$), 61.85 (CH_2O), 68.69

(CHO), 173.71 (C=O). ^{29}Si MAS NMR (δ , ppm): 10.9.

HNTGC (UDTG/TMCTS). ^{13}C NMR (TCE- d_2 , δ , ppm): -0.51 (CH_3Si), 17.11 (CH_2Si), 22.82, 25.44, 29.21, 33.06, 33.91 ($-\text{CH}_2-$), 62.02 (CH_2O), 68.73 (CHO), 174.21 (C=O). ^{29}Si MAS NMR (δ , ppm): -17.7.

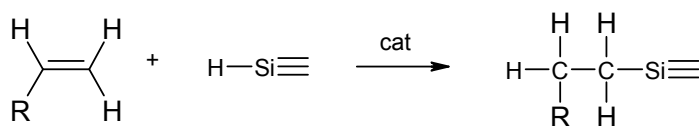
UDBM

For A, 0.57 g UDBM was mixed with 0.25 g of DMSB, and 10 μl of the platinum catalyst (Karstedt) was added. After stirring for 5 min, the mixture was cured via heating for 20 h at 85 $^\circ\text{C}$ and postcured for 4 h at 150 $^\circ\text{C}$. For B, the same procedure was used, but with 0.21 g of TKDS. For C, the same procedure was used, but with 0.15 g of TMCTS.

HNBMA (UDBM/DMSB). ^{13}C NMR (TCE- d_2 , δ , ppm): -3.18 (CH_3Si), 15.43 (CH_2Si), 23.68, 24.56, 29.00, 33.43 ($-\text{CH}_2-$), 52.48 (OCH_3), 121.83, 129.15, 132.63, 139.65, 143.27 (Ar), 164.70 (COCH_3), 170.48 (C=O). ^{29}Si MAS NMR (δ , ppm): -1.1.

HNBMB (UDBM/TKDS). ^{13}C NMR (TCE- d_2 , δ , ppm): -0.30 (CH_3Si), 17.75 (CH_2Si), 22.97, 24.48, 28.99, 32.22, 33.42 ($-\text{CH}_2-$), 51.61 (OCH_3), 122.31, 131.23, 133.18, 142.80 (Ar), 165.43 (COCH_3), 169.30 (C=O). ^{29}Si MAS NMR (δ , ppm): 10.7.

HNBMC (UDBM/TMCTS). ^{13}C NMR (TCE- d_2 , δ , ppm): -0.67 (CH_3Si), 17.87 (CH_2Si), 22.84, 24.68, 29.12, 32.29, 33.61 ($-\text{CH}_2-$), 52.50 (OCH_3), 121.84, 131.36, 133.04, 142.78 (Ar), 164.75



Scheme 3

(COCH₃), 170.35 (C=O). ²⁹Si MAS NMR (δ, ppm): -17.9.

Characterization

¹H and ¹³C NMR spectra were recorded on a Varian Gemini 400-MHz spectrometer (400 MHz for ¹H and 100.57 MHz for ¹³C). ²⁹Si NMR spectra were obtained with a Varian Gemini 300-MHz spectrometer (59.3 MHz for ²⁹Si, *d*_f = 20 s) with CDCl₃ as solvent and TMS as the internal standard. ¹³C NMR spectra of swollen networks were recorded at room temperature in TCE-d₂. ²⁹Si MAS NMR spectra were performed, with finely ground samples, on a Varian Gemini 400-MHz spectrometer at a 79-MHz resonance frequency, MAS being applied with a 20-s delay time.

The FTIR spectra were recorded on a Bomem Michelson MB 100 FTIR spectrophotometer with a resolution of 4 cm⁻¹ in the absorbance mode. An attenuated total reflection (ATR) accessory with thermal control and a diamond crystal (Golden Gate heated single-reflection diamond ATR accessory, Specac-Teknokroma) was used to determine FTIR spectra.

Calorimetric studies were carried out on a Mettler DSC822e thermal analyzer with N₂ as the purge gas. A heating rate of 20 °C/min was used.

Thermal stability studies were carried out on a Mettler TGA/SDTA851e/LF/1100 with N₂ as the purge gas at scanning rates of 10 °C/min.

The mechanical properties were measured with a TA DMA 2928 dynamic mechanical thermal analyzer. Specimens 2 mm thick x 5 mm wide x 10 mm long were tested in a three-point-bending configuration. The various thermal transitions were studied between -100 and 40 or 100 °C at a heating rate of 5 °C/min and at a fixed frequency of 1 Hz.

RESULTS AND DISCUSSION

Although the hydrosilylation of olefins has been widely studied,^{20,28} recently only a few studies on fatty acid esters and oils have been reported.²²⁻²⁴ They all involved adding a silane compound with a functionality of 1 to the double bond and introducing a certain silicon reagent to the ester or oil. The reaction known as hydrosilylation proceeds when, after certain hydrosilanes have been activated, they undergo addition across the carbon-carbon multiple bonds. This reaction usually requires a catalyst; the most commonly used are the transition-metal complexes [Co(I), Rh(I), Pd(0), and Pt(0)]. It is well

Table 1. Reaction Conditions and Results for the Hydrosilylation of Methyl 10-undecenoate (UDM) with DMSB, TKDS, and TMCTS (Si-H:C=C 1:1 molar ratio, T = 65 °C)

Silane	Catalyst	Catalyst/CH=CH ₂ mol ratio	Reaction time (hours)	-CH=CH ₂ conversion ^a
DMSB	Speier	1.2 10 ⁻⁵ /1	9	88
DMSB	Karstedt	3.5 10 ⁻⁵ /1	0.5	100
TKDS	Speier	1.2 10 ⁻⁵ /1	14	87
TKDS	Karstedt	3.5 10 ⁻⁵ /1	1	100
TMCTS	Speier	1.2 10 ⁻⁵ /1	10	95
TMCTS	Karstedt	3.5 10 ⁻⁵ /1	1	100

^a Determined by ¹H NMR spectroscopy.

documented^{26,28} that the hydrosilylation of 1-alkenes is catalyzed by these metals and proceeds with anti-Markovnikov selectivity (β addition), leading to 1-silylalkanes (see Scheme 3).

It is difficult to investigate the hydrosilylation reaction of triglyceride compounds with multifunctional silanes in detail because gelation occurs easily. Therefore, the compound from the reaction is partially insoluble for NMR measurements. For this reason, we used UDM, previously synthesized as a model compound, to study the hydrosilylation reaction with various silicon reagents (Scheme 1): DMSB (A), TKDS (B), and TMCTS (C). Gelation does not occur, and the reaction can be investigated easily. The catalysts chosen to carry out the hydrosilylation reaction were chloroplatinic acid (H₂PtCl₆), frequently used as a solution in 2-propanol and known as Speier's catalyst, and a 1,3-divinyltetramethyl-disiloxane-platinum complex known as Karstedt's catalyst. Speier's catalyst is by far the most common catalyst for

the hydrosilylation of a variety of olefinic substrates.²⁸ Only a very small quantity is necessary; usually, the amount is in the region of 10⁻⁵ mol/mol of hydrosilane, but in some cases, 10⁻⁸ mol/mol of reactant has been used successfully.²⁶

Several reaction conditions were tested (temperature, C=C/Si-H ratio, and C=C/catalyst ratio), and the results were best for the conditions collected in Table 1. ¹H and ¹³C NMR analysis of the products showed the presence of the expected dimer (UDM/DMSB) and tetramers (UDM/TKDS and UDM/TMCTS) as major products. With Speier's catalyst, moderate terminal double-bond conversion (determined by the integration of olefinic protons in the ¹H NMR spectrum) was obtained. In all cases, double-bond isomerization to internal positions (signal at 5.4 ppm) was observed to a low extent. Furthermore, monotransesterification of methyl ester with 2-propanol occurred. Using Karstedt's catalyst, we obtained the expected products in

higher $-\text{CH}=\text{CH}_2$ conversions and shorter reaction times than when we used Speier's catalyst, as can be seen in Table 1. In this case, traces of double-bond migration were also observed by ^1H NMR. All these results lead us to conclude that an isomerization process takes place alongside the hydrosilylation.

Because of these results, UDTG (Scheme 2) was chosen as the organic component and DMSB, TKDS and TMCTS were chosen as the inorganic components of the novel hybrid polymeric networks. The unique feature of UDTG's molecular architecture is the terminal $\text{C}=\text{C}$ group on each of the three acyl glyceride segments. Three hybrid organic-inorganic networks-HNTGA, HNTGB, and HNTGC-were

prepared by means of platinum-catalyzed hydrosilylation of UDTG with DMSB (A), TKDS (B), and TMCTS (C), respectively. Two reactive Si-H groups are enough to connect all the fatty acid chains and to cure the polymer completely, but four silane groups will lead to a more densely crosslinked system, although spatial hindrance makes it unlikely that all Si-H bonds will react. All these reactions were carried out with a 1:1 Si-H/ $\text{CH}=\text{CH}_2$ molar ratio. To crosslink UDTG, and in view of the model reaction results (Table 1), only Karstedt's catalyst was employed.

The crosslinking reaction was monitored by FTIR spectroscopy. Figure 1 shows FTIR spectra before and after the curing of the hybrid HNTGA.

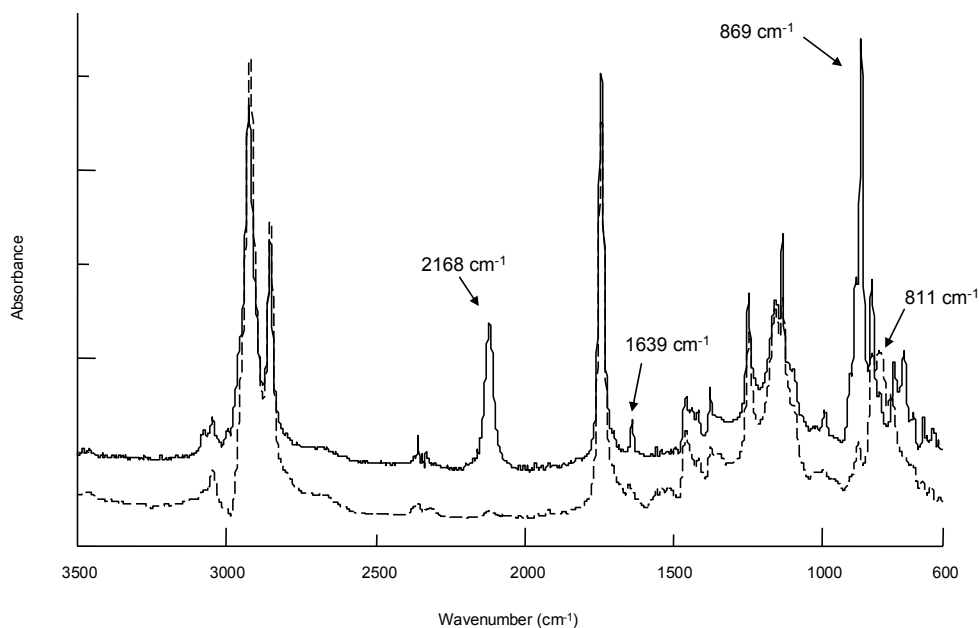


Figure 1. FTIR spectra of HNTGA (—) before and (- -) after crosslinking.

The starting mixture shows a characteristic peak at 2168 cm^{-1} ascribed to Si-H stretching of the crosslinking agent. After curing, a significant decrease in this peak was observed. The reaction's progress was also observed by changes in the peaks at 1639 and 869 cm^{-1} , which are ascribed to C=C stretching and Si-H bending, respectively.

Furthermore, a peak at 811 cm^{-1} , which is due to Si-C stretching of the resulting hydrosilylation group (Si-CH₂), appears. In conclusion, FTIR analysis allowed us to monitor the crosslinking reaction and confirm the presence of residual silane and C=C groups that were not incorporated into the network structure.

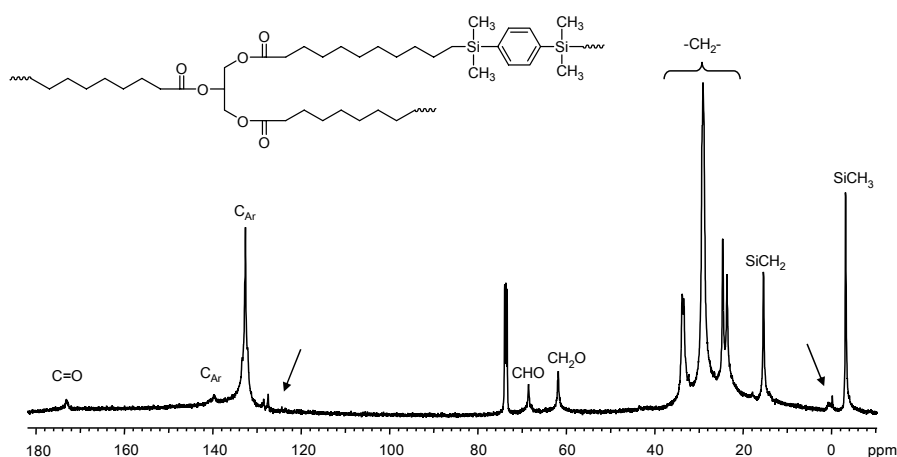


Figure 2. ^{13}C NMR spectrum of HNTGA (TCE- d_2 , 400 MHz)

The presence of unreacted groups was also observed by ^{13}C NMR analysis. The ^{13}C NMR spectrum of the swollen HNTGA with the all assignments is shown in Figure 2. The signal at 0.1 ppm could be assigned to methyl groups of residual Ph-(CH₃)₂Si-H units. The ^{13}C -NMR spectrum of HNTGA reveals the absence of signals corresponding to unreacted terminal C=C groups from triglyceride at approximately 114 and 139 ppm . The small signals at 124 and 128 ppm could be attributed to the internal double bond formed by isomerization of terminal double bonds. These results

are fully consistent with those of the model reaction.

^{29}Si MAS NMR was used for the molecular structural characterization of the hybrids because it can distinguish between different structural siloxane units. The ^{29}Si MAS NMR spectra of HNTGA, HNTGB, and HNTGC are shown in Figure 3. One major absorption peak at about -1.0 , 10.9 , and -17.7 ppm , corresponding to Si-CH₂ units¹⁸ produced by hydrosilylation, was observed for HNTGA, HNTGB, and HNTGC, respectively. Weak signals at -15.0 , -3.6 , and -32.6 ppm , assigned to unreacted Si-H, were also observed.

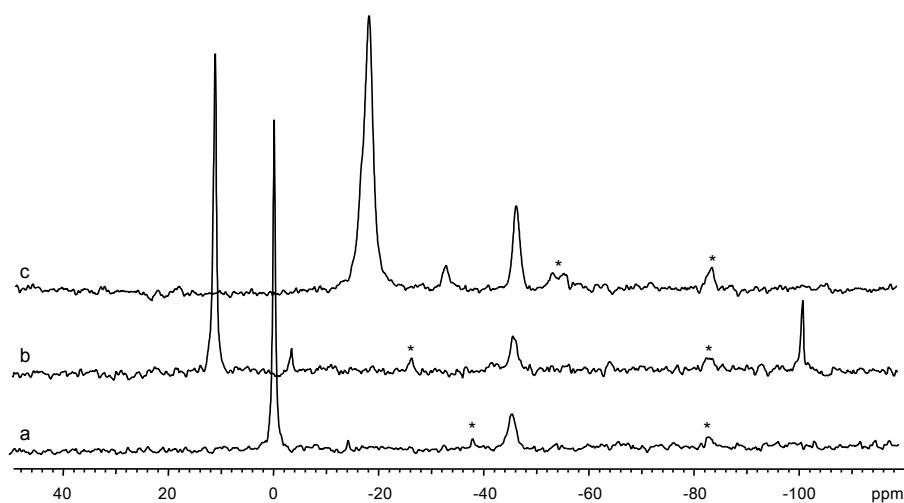


Figure 3. ^{29}Si MAS NMR spectra of UDTG-based hybrid networks: (a) HNTGA, (b) HNTGB, and (c) HNTGC (79 MHz). The spinning bands are marked with asterisks.

Furthermore, for HNTGB, a peak at -101.8 ppm, due to the absorption of the $\text{Si}(\text{-O})_4$ unit, was observed. The peak at -46 ppm is due to absorption of the NMR rotor from Si_3N_4 . The relatively small integration of the residual Si-H absorption peak demonstrated that hydrosilylation is a highly efficient crosslinking reaction. These results confirmed the presence of unreacted functional groups in these materials as observed in the ^{13}C NMR and FTIR analysis. The residual groups were not incorporated into the network structure by hydrosilylation, mainly because of the increase in the steric hindrance around them during the network formation and the Pt-catalyzed isomerization of terminal double bonds. The resulting cured hybrid networks showed good transparency (Figure 4), which meant that the organic and inorganic components were miscible.

Triglycerides are made up of aliphatic chains, and consequently, triglyceride-

based materials are not strong or rigid enough for some applications. To improve the properties of triglyceride-based materials, and to incorporate into a polymer network such chemical moieties as aromatic or cyclic structures, which are known to impart stiffness, a new aromatic fatty acid derived compound was prepared: UDBM (Scheme 2).



Figure 4. Photograph of HNTGC showing good transparency.

This compound can be synthesized from commercially available 10-undecenoyl chloride and methyl 3,4,5-trihydroxybenzoate by esterification.

UDBM was obtained in a good yield and characterized by spectroscopic techniques. The FTIR spectrum shows bands at 1640 (C=C), 1780 and 1730 (C=O stretching vibration), 1595 cm^{-1} (C=C aromatic). Figure 5 shows the ^1H and ^{13}C NMR spectra with all the assignments corresponding to the expected signals.

As described previously for UDTG, three organic-inorganic networks-HNBMA, HNBMB, and HNBMC-were prepared by the mixing of UDBM with DMSB, TKDS, and TMCTS, respectively. All these reactions were carried out with a 1:1 Si-H/CH=CH₂ molar ratio. UDBM hybrid materials were also characterized with FTIR spectroscopy, ^{13}C NMR, and ^{29}Si MAS NMR, and they showed the same trends that were observed for UDTG networks.

The thermal behavior of the obtained materials was investigated with DSC. The glass-transition temperatures (T_g 's) of the cured hybrid materials are listed in Table 2. As can be seen, elastomeric materials are obtained in all cases. UDBM-based hybrid materials have higher T_g 's than UDTG-based hybrid materials, as expected from the aromatic nature of starting monomer. The obtained values also depend on the functionality and structure of the curing agent. UDTG-based hybrid materials have low T_g 's that increase with the functionality of the crosslinker. Therefore, T_g of the HNTGA (UDTG/DMSB; $f = 2$) hybrid is lower than that of the material crosslinked with TMCTS ($f = 4$) but is similar to that of the material crosslinked with TKDS ($f = 4$).

Table 2. Glass-Transition Temperatures (T_g) of UDTG and UDBM-based Hybrid Networks from DSC and DMTA

	Hybrid composition	T_g ($^{\circ}\text{C}$)		
		$1/2 \Delta C_p^a$	$E''_{\text{max}}{}^{b,c}$	$\text{Tan } \delta_{\text{max}}{}^{b,d}$
HNTGA	UDTG/DMSB	-29	-30	-22
HNTGB	UDTG/TKDS	-30	-37	-30
HNTGC	UDTG/TMCTS	-10	-22	-15
HNBMA	UDBM/DMSB	-4	-3	3
HNBMB	UDBM/TKDS	-4	-7	1
HNBMC	UDBM/TMCTS	25	16	24

^a From the second heating scan of DSC measurements (20 $^{\circ}\text{C}/\text{min}$).

^b Samples for DMA experiments were prepared as described in the Experimental part.

^c Temperature of the maximum of the loss modulus-temperature curve from DMTA.

^d Maximum value of the $\text{tan } \delta$ -temperature curve from DMTA.

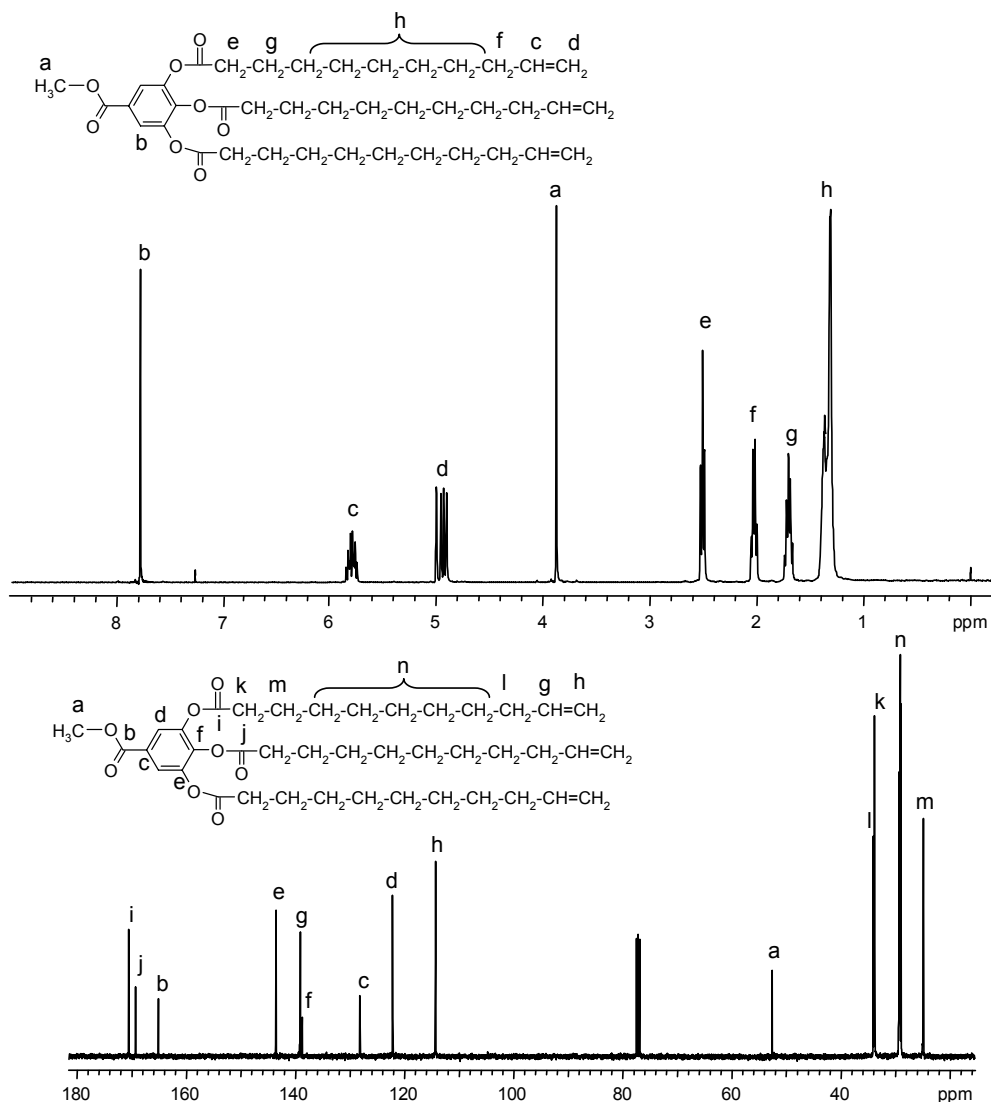


Figure 5. ^1H and ^{13}C NMR spectra of UDBM (CDCl_3 , 400 and 100 MHz, respectively).

This can be understood if it is taken into account that the aromatic structure of DMSB restricts the mobility of the network and consequently increases its T_g . For the material crosslinked with TMCTS, T_g is higher than that of the material derived from

TKDS, although the two curing agents have the same functionality. This may be because of the cyclic structure of TMCTS, which imparts stiffness to the polymer network and consequently increases its T_g . Similar trends can be observed for UDBM-based networks.

Table 3. Thermogravimetric Data of UDTG and UDBM-based Hybrid Networks

	Hybrid composition	TGA (N ₂ Atmosphere)			TGA (Air Atmosphere)		
		T _{5% loss} (°C)	T _{max} (°C)	Yield _{800°C} (%)	T _{5% loss} (°C)	T _{max} (°C)	Yield _{800°C} (%)
HNTGA	UDTG/DMSB	393	432	2	262	359	9
HNTGB	UDTG/TKDS	396	438	9	247	355	20
HNTGC	UDTG/TMCTS	415	450	9	278	369	28
HNBMA	UDBM/DMSB	361	382	19	302	343	11
HNBMB	UDBM/TKDS	361	365	36	307	340	20
HNBMC	UDBM/TMCTS	384	427	38	305	341	23

The thermal stability of the hybrid thermosets was evaluated by TGA under nitrogen and air atmospheres, and the corresponding weight-loss data are listed in Table 3. The thermogravimetric plots under nitrogen (Figure 6) showed that all the materials have good thermal stabilities, with initial temperatures of weight loss above 350 °C, regardless of the starting monomer or the curing agent. UDBM hybrids seem to decompose at slightly lower temperatures than UDTG derivatives for the same crosslinking agent. The shape of the derivative TGA plots shows that the degradation takes place in a broad temperature range. For analogous systems,¹⁹ it has been reported that the degradation is initiated by the cleavage of Si-CH₃, Si-CH₂, and C-C bonds and rearrangements of the main network structure up to the mineralization of material and consequent formation of silicon oxycarbide as the major product. The thermal stability in air is lower than in nitrogen, and it is higher for the UDBM derivatives. Thermo-

oxidative degradation takes place at temperatures higher than 500 °C.

Detailed information may be obtained by the measurements of the dynamic mechanical behavior of samples as a function of temperature. The dynamic mechanical properties of the hybrids were obtained from the glassy state, through T_g, and well into the rubbery plateau of each material. The effects of temperature on the storage modulus (*E'*) for the UDTG and UDBM hybrid materials are shown in Figures 7 and 8, respectively. DMTA enables T_g of the crosslinked materials to be determined. It is detected as the maximum of the loss modulus (*E''*), which corresponds to the initial drop from the glassy state into the transition. Moreover, the α -relaxation peak of the loss factor ($\tan \delta$) is associated with T_g and corresponds to the transition midpoint of the log of the *E'* curve. The T_g values from both measurements are shown in Table 2. As expected, T_g as $\tan \delta$ peak is higher than the *E'* peak.

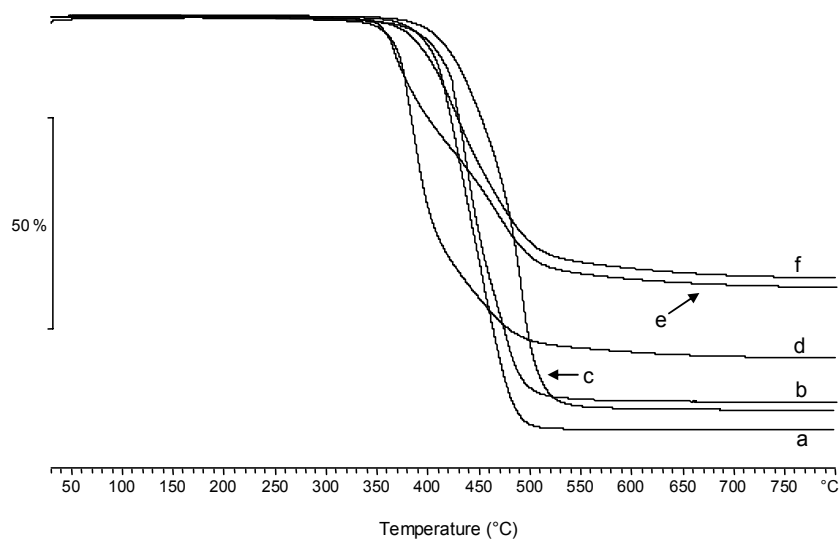


Figure 6. TGA thermograms of hybrid networks under nitrogen: (a) HNTGA, (b) HNTGB, (c) HNTGC, (d) HNBMA, (e) HNBMB, and (f) HNBMC.

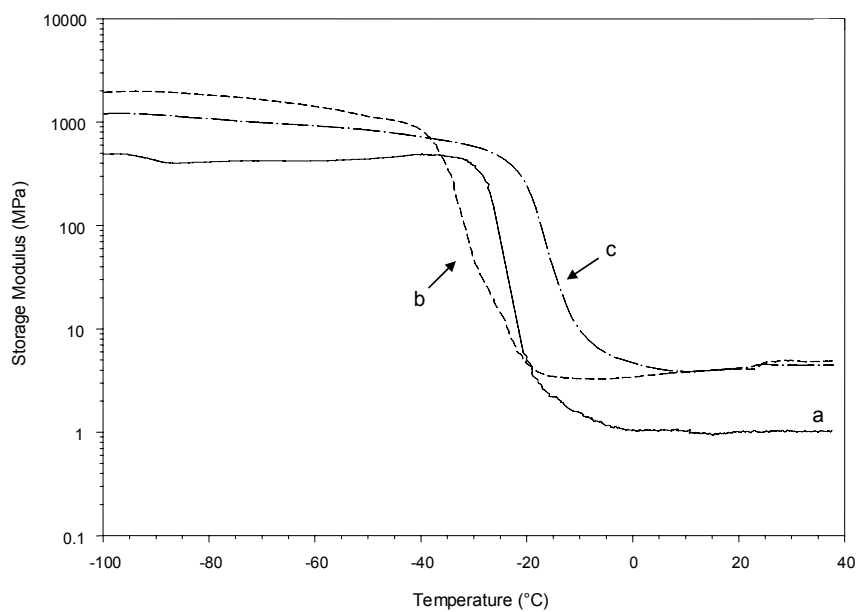


Figure 7. E' of UGTG-based hybrid networks: (a) HNTGA, (b) HNTGB, and (c) HNTGC as a function of temperature.

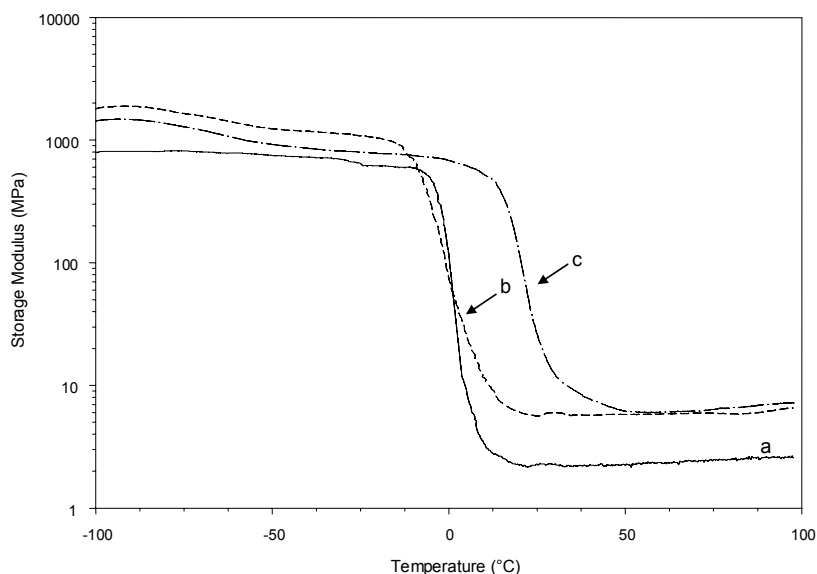


Figure 8. E' of UDBM-based hybrid networks: (a) HNBMA, (b) HNBMB, and (c) HNBMC as a function of temperature.

From the DMTA curves, the plateau of the elastic modulus in the rubbery state can be used to make qualitative comparisons of the level of crosslinking among the different hybrids. Figure 7 and 8 show that E' of DMSB-cured hybrids is lower in the rubbery plateau than that of TKDS and TMCTS hybrids. This may be attributed to the lower functionality of DMSB ($f = 2$) in comparison with that of TKDS and TMCTS ($f = 4$). The crosslinking density can also be estimated by the height of the $\tan \delta$ peak. As expected, the height of the $\tan \delta$ peak is lower when the functionality of the crosslinking agent is higher, and this indicates a higher crosslinking density.

CONCLUSIONS

Hybrid organic-inorganic networks were developed by the hydrosilylation of alkenyl-terminated fatty acid derivatives. The high efficiency of the hydrosilylation as a crosslinking reaction was demonstrated by ^{29}Si MAS NMR spectroscopy. Elastomeric materials with good thermal stabilities were obtained in all cases. The resulting cured hybrid networks showed good transparency according to the good miscibility of the organic and inorganic components.

Acknowledgements

The authors gratefully acknowledge the Comisión Interministerial de Ciencia y Tecnología (MAT2002-00223) and the Comissió Interdepartamental de Recerca i Innovació Tecnològica (2001SGR00318) for financial support

for this work. We would like to thank R. Guerrero for ^{29}Si MAS NMR analysis.

REFERENCES AND NOTES

- Baumann, H.; Bühler, M.; Fochem, H.; Hirsinger, F.; Zobelein, H.; Falbe, J. *Angew Chem Int Ed Engl* 1988, 27, 41.
- Biermann, U.; Friedt, W.; Lang, S.; Lühs, W.; Machmüller, G.; Metzger, J. O.; Klaas, M.R.; Schäfer, J.; Schneider, M.P. *Angew Chem Int Ed Engl* 2000, 39, 2206.
- Li, F.; Larock, R.C. *J Polym Environ* 2002, 10, 59.
- Harrison, S. A.; Tolberg, W. E. *J Am Oil Chem Soc* 1953, 30, 114.
- Li, F.; Larock, R. C. *Polym Adv Technol* 2002, 13, 436.
- Guo, A.; Cho, Y.; Petrovic, Z. *J Polym Sci Part A: Polym Chem* 2000, 38, 3900.
- Zlatanic, A.; Petrovic, Z. S.; Dusek, K. *Biomacromolecules* 2002, 3, 1048.
- Khot, S. N.; La Scala, J. J.; Can, E.; Morye, S. S.; Palmese, G. R.; Kusefoglu, S. H.; Wool, R. P. *J Appl Polym Sci* 2001, 82, 703.
- Esen, H.; Küsefoglu, S. H. *J Appl Polym Sci* 2003, 89, 3882.
- Guo, A.; Javni, I.; Petrovic, Z. S. *J Appl Polym Sci* 2000, 77, 467.
- Ivin, K. J.; Mol, J. C. *Olefin Metathesis and Metathesis Polymerization*; Academic Press: San Diego, CA, 1997.
- Mol, J. C. *J Mol Catal* 1994, 90, 185.
- Warwel, S.; Brüse, F.; Demes, C.; Kunz, M.; Klaas, M. R. *Chemosphere* 2001, 43, 39.
- Uyama, H.; Kuwabara, M.; Tsujimoto, T.; Nakano, M.; Usuki, A.; Kobayashi, S. *Chem Mater* 2003, 15, 2492.
- Williams, G. I.; Wool, R. P. *Appl Composite Mater* 2000, 7, 421.
- Wold, C. R.; Soucek, M. D. *Macromol Chem Phys* 2000, 201, 382.
- Deffar, D.; Teng, G.; Soucek, M. D. *Macromol Mater Eng* 2001, 286, 204.
- Redondo, S. U. A.; Radovanovic, E.; Torriani, I. L.; Yoshida, I. V. P. *Polymer* 2001, 42, 1319.
- Pinho, R. O.; Radovanovic, E.; Torriani, I. L.; Yoshida, I. V. P. *Eur Polym J* 2004, 40, 615.
- Marcienic, B. *Comprehensive Handbook on Hydrosilylation*, Pergamon Press, UK 1992.
- Saghian, N.; Gertner, D. *J Am Oil Chem Soc* 1974, 51, 363.
- Berh, A.; Toslu, N. *Chem Eng Technol* 2000, 23, 122.
- Delpech, F.; Saadia, A.; Castel, A.; Rivière, P.; Rivière-Baudet, M.; Amin-Alami, A.; Manriquez, J. *Appl Organometal Chem* 2001, 15, 626.
- Behr, A.; Naendrup, F.; Obst, D. *Adv Synth Catal* 2002, 344, 1142.
- Behr, A.; Naendrup, F.; Obst, D. *Eur J Lipid Sci Technol* 2002, 104, 161.
- Speier, J. L.; Webster, J. A.; Barnes, G. H. *J Am Chem Soc* 1957, 79, 974.
- Karstedt, B. D. U.S. Patent 3,775,452, 1973.
- (a) Ojima, I. In: *The Chemistry of Organic Silicon Compounds*; Patai, S.; Rappoport, Z., Eds.; Wiley: New York, 1989; Part 1, Vol. 2, Chapter 25; (b) *The Chemistry of Organic Silicon Compounds*; Rappoport, Z.; Apeloig, Y., Eds.; Wiley: New York, 1998; Part 2, Vol. 1-3.

2.4.2 Bionanocomposites from Renewable Resources: Epoxidized Linseed Oil–Polyhedral Oligomeric Silsesquioxanes (POSS) Hybrid Materials

BIONANOCOMPOSITES FROM RENEWABLE RESOURCES: EPOXIDIZED LINSEED OIL – POLYHEDRAL OLIGOMERIC SILSESQUIOXANES (POSS) HYBRID MATERIALS

G. Lligadas, J.C. Ronda, M. Galià, V. Cádiz
Departament de Química Analítica i Química Orgànica, Universitat Rovira i Virgili,
Campus Sescelades, Marcel·lí Domingo s/n, 43007 Tarragona, Spain.

ABSTRACT: This study concerns with the preparation and properties of a new class of bionanocomposites from renewable resources. Epoxidized linseed oil and 3-glycidylpropylheptaisobutyl-T₈-polyhedral oligomeric silsesquioxane (G-POSS) (2, 5, and 10 wt.-%) were crosslinked, and Fourier transform infrared spectroscopy, dynamic mechanical thermal analysis, thermogravimetric analysis and scanning electron microscopy (SEM) were employed to characterize the POSS reinforced oil based polymer networks. No POSS aggregates were observed for the 2 wt.-% G-POSS nanocomposite by SEM. POSS-rich particles with diameters of several nanometers were observed in the nanocomposites with 5 and 10 wt.-% G-POSS. Enhanced glass transition temperatures, and storage moduli of the networks in the glassy state and rubber plateau were observed to be higher than that of the POSS-free oil based polymer network, due to the reinforcement effect of POSS cages.

Keywords: epoxidized plant oils; nanocomposites; polyhedral oligomeric silsesquioxanes; renewable resources

INTRODUCTION

Growing interest in the exploitation of renewable resources in the areas of energy and materials has been one of the major scientific and technological issues of these past few decades. Vegetable oils represent one of the cheapest and most abundant biological feedstocks available in large quantities,

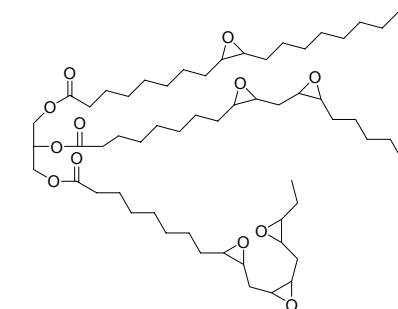
and their use as starting materials offers numerous advantages, such as low toxicity and inherent biodegradability.¹ Although they possess double bonds, which are used as reactive sites in coatings, they can also be functionalized by epoxidation. Epoxidized vegetable oils show excellent promise as inexpensive, renewable materials for industrial applications.² In recent years,

extensive work has been done to develop polymers from epoxidized triglycerides or fatty acids.³ The cationic polymerization of epoxidized vegetable oils has been investigated using photoinitiated⁴ and thermal⁵ latent cationic catalysts to produce biobased epoxy resins with promising properties. Latent initiators show no activity under normal conditions, but form active species to initiate polymerization only with external stimuli such as heating or photoirradiation.⁶

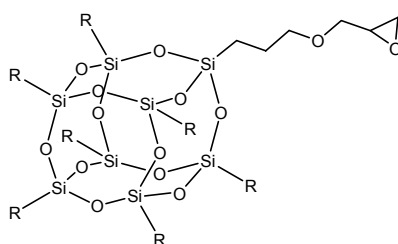
Triglycerides are made up of aliphatic chains and consequently, the triglyceride based materials are incapable of the necessary rigidity and strength required for some applications.⁷ There has been great interest in organic-inorganic hybrid materials because of their unusual properties, derived from unique combinations of each component.⁸ Specifically, the physical, mechanical and thermal properties may be greatly improved. Regarding vegetable oil-based hybrid materials, composites with good mechanical properties have been prepared from acrylate-modified soybean oil and natural fibers,⁹ organic-inorganic hybrid coatings have been developed using plant oils and metal (Ti and Zr) oxides,¹⁰ organic-inorganic hybrid networks with good transparency were developed by hydrosilylation of alkenyl terminated fatty acid derivatives,¹¹ and carbon nanotubes have been used as reinforcements for acrylated epoxidized soy oil-based resins.¹² In addition, a new class of green hybrid materials incorporating clay¹³⁻¹⁵ or a silica network¹⁶ into vegetable oil polymer matrix has been reported.

Polymers reinforced with well-defined nanosized inorganic clusters have attracted a tremendous amount of interest because of their versatility; among these systems polyhedral oligomeric silsesquioxane (POSS) compounds, which possess a unique cage-like structure and nanoscale dimensions, are of particular interest. POSS compounds are 1-3 nm in diameter and their inorganic cage framework is made up of a fixed proportion of silicon and oxygen: $(\text{SiO}_{1.5})_n$, where $n=8, 10, \text{ or } 12$. A different polymerizable POSS macromers have been employed to copolymerize with organic monomers, via the formation of covalent bonds, to afford a variety of polymer/POSS nanocomposites.¹⁷ Epoxy resins/POSS nanocomposites are the most studied of these nanocomposites, and various mono-^{18,19} or polyepoxide²⁰ POSS monomers have been used to modify epoxy networks. The incorporation of POSS derivatives into polymeric materials can lead to substantial improvements in polymer properties including increases in use temperature²¹ and mechanical properties,²² as well as reductions in flammability,²³ heat evolution²⁴ and viscosity²⁵ during processing. These property improvements have encouraged academic and industrial research, that were critical in both reducing the prices and increasing production of POSS feedstocks.

To the best of our knowledge, this is the first example the preparation of biobased POSS-nanocomposites from plant oil derivatives. In this study, 3-glycidylpropylheptaisobutyl- T_8 -polyhedral oligomeric silsesquioxane (G-POSS, Chart 1) was incorporated into an epoxidized linseed oil (ELO, Chart 1)

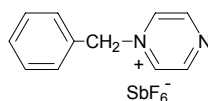
Chart 1. Chemical Structures of ELO, G-POSS, and BPH

ELO



R = isobutyl

G-POSS



BPH

crosslinked network, by cationic-initiated polymerization. The cationic latent initiator used in this study was N-benzylpyrazinium hexafluoroantimonate (BPH, Chart 1). Chemical incorporation of G-POSS into the network was studied by solvent extraction and Fourier transform infrared (FTIR) analysis; the morphology of these nanocomposites were determined by X-ray diffraction (XRD) and scanning electron microscopy (SEM); and the nanoscale reinforcement effect of POSS on the prepared epoxy biobased nano-

composites were evaluated using differential scanning calorimetry (DSC), dynamic mechanical thermal analysis (DMTA) and thermogravimetric analysis (TGA).

EXPERIMENTAL

Materials

The linseed oil and 3-glycidylpropylhepta-isobutyl- T_8 -polyhedral oligomeric silsesquioxane (G-POSS, Chart 1) used in

this study were supplied by Aldrich and were used as received. The following chemicals were obtained from the sources indicated: formic acid (Scharlau), hydrogen peroxide 50 % w/v (Aldrich), sodium hexafluoroantimonate (Aldrich), pyrazine (Aldrich), benzyl bromide (Fluka) and all were used without further purification. All solvents were purified by standard procedures.

N-benzylpyrazinium hexafluoroantimonate (BPH) was synthesized in our laboratory according to the published procedure.⁶

Epoxidation of Linseed Oil

A solution of linseed oil (20.1 g, 67.0 mmol) and formic acid (1.0 mL, 26.2 mmol) was stirred at 45 °C, and H₂O₂ 50% w/v (38 mL, 659.0 mmol) was added dropwise. After H₂O₂ addition was complete, the temperature was raised to 70 °C and the flask contents were stirred vigorously for 6 h. The mixture was then cooled and transferred to a separating funnel containing ethyl acetate (75 mL). The organic fraction was washed with approximately 100 mL of distilled water, and 100 mL saturated sodium bicarbonate solution (aqueous). These washings were continued until the pH reached 7. The ethyl acetate solution was then dried over anhydrous magnesium sulphate, filtered and concentrated in vacuo to give the product as clear oil with a yield of 96%.

FTIR (ν , cm⁻¹): 2957, 2860 (ν , C-H), 1743 (ν , C=O), 825 (ν , C-O oxirane ring). ¹H NMR [CDCl₃/TMS, δ , ppm]: 0.8-1.1 (-CH₃ of fatty acids), 1.2-1.8 (-CH₂- of fatty acids), 2.3 (-CH₂C=O-),

2.8-3.2 (-CH-O-CH-), 4.1-4.3 (CH₂-O-C=O), 5.2 (-CH-O-C=O). ¹³C NMR (CDCl₃/TMS, δ , ppm): 10.6, 14.2 (-CH₃ of fatty acids), 21.2-34.8 (-CH₂- of fatty acids), 54.1-58.0 (-CH-O-CH-), 62.2 (-CH₂-O-C=O), 68.9 (CH-O-C=O), 172.4, 172.7, 172.8 (C=O).

General Preparation of ELO/G-POSS Bionanocomposites

To prepare the bionanocomposites containing POSS (2, 5, and 10 wt.-%), the desired amount of G-POSS was dissolved in a minimum of acetone, and this solution was added to pre-weighed ELO. On formation of a homogeneous solution, 1 wt.-% of the latent catalyst (BPH) was added. The mixture was stirred for 2 h and the solvent was removed under vacuum. The mixture was cast and cured in a mold at 140 °C for 1 h, 170 °C for 2 h and 190 °C for 1 h, in air using an oven. The curing conditions were determined from the DSC data. ELO homopolymer was prepared under the same curing conditions for comparison. Ground to powder samples (~1.0 g) of every nanocomposite were immersed into a large excess of tetrahydrofuran or chloroform and refluxed for 12 h to determine if any soluble material could be extracted by the solvent.

Characterization

The Fourier transform infrared (FTIR) spectra were recorded on a Bomem Michelson MB 100 FTIR spectrophotometer with a resolution of 4 cm⁻¹ in the absorbance mode. An attenuated-total-reflection (ATR) accessory with thermal control and a diamond crystal (Golden Gate heated single-reflection

diamond ATR, Specac-Teknokroma) was used to determine FTIR spectra.

The NMR spectra were recorded on a Varian Gemini 400 MHz spectrometer (400 MHz for ^1H , 100.57 MHz for ^{13}C). The samples were dissolved in deuterated chloroform, and spectra were obtained at room temperature using TMS as an internal standard.

Calorimetric studies were carried out on a Mettler DSC822e thermal analyzer in a dry nitrogen atmosphere. All the samples (about 10 mg in weight) were heated from -80 to 150 °C at a rate of 20 °C/min.

Thermal stability studies were carried out on a Mettler TGA/SDTA851e/LF/1100. The samples (about 10 mg) were heated, under nitrogen or air atmospheres, from ambient temperature to 800 °C and a rate of 10 °C/min.

Dynamic mechanical properties were measured with a dynamic mechanical thermal analyzer (DMTA) (TA DMA 2928). Specimens with dimensions 2 mm \times 5 mm \times 10 mm were tested in a three point bending configuration. The various thermal transitions were studied between -80 and 90 °C at a heating rate of 5 °C/min and at a fixed frequency of 1 Hz.

WAXD measurements were made using a Siemens D5000 diffractometer (Bragg-Brentano parafocusing geometry and vertical θ - θ goniometer) fitted with a curved graphite diffracted-beam monochromator, incident and diffracted-beam Soller slits, a 0.06 ° receiving slit and scintillation counter as a detector. The angular 2θ diffraction range was between 1 and 40 °. Samples were

dusted onto a low background Si(510) sample holder. The data were collected with an angular step of 0.05 ° at 3 s per step. CuK_α radiation was obtained from a copper X-ray tube operated at 40 kV and 30 mA.

The surfaces of different biobased nanocomposites were observed with SEM. A gold coating, which is a few nanometers thick, was made on the fracture surfaces to be observed. A JEOL JSM 6400 SEM with a field emission filament and an accelerating voltage of 10 kV was used to collect SEM images for all samples. For the atomic mapping, an Oxford INCA Energy Dispersive X-Ray Micro Analyzer was used.

RESULTS AND DISCUSSION

In this study, epoxidized linseed oil (ELO, Chart 1) and 3-glycidylpropylheptaisobutyl- T_8 -polyhedral oligomeric silsesquioxane (G-POSS, Chart 1) were used as organic monomers and inorganic nanoparticles, respectively. Naturally linseed oil contains triglycerides consisting of a mixture of linolenic (57%), oleic (19%), linoleic (15%), palmitic (5%) and stearic (4%) fatty acids. ELO was prepared by the reaction of linseed oil with formic acid and hydrogen peroxide at 70 °C for 6 h. The chemistry of the Prileshajev epoxidation of unsaturated fatty compounds is well known:²⁶ a short-chain peroxy-acid is prepared from hydrogen peroxide and the corresponding acid, either in a separate step or *in situ*.²⁷ The structure of ELO was confirmed by its FTIR, ^1H and ^{13}C NMR spectra. The epoxy group number of ELO per molecule, deter-

mined by ^1H NMR spectroscopy, was 5.6.

The bionanocomposites were synthesized by curing the epoxidized linseed oil and the designated amount of G-POSS, using 1 wt.-% of N-benzylpyrazinium hexafluoroantimonate (BPH, Chart 1) as a thermally-latent cationic catalyst on the basis of published results.⁵ The C-N bond in BPH is thermally cleaved to generate benzyl cationic reactive specie, which catalyzes the cationic polymerization of the epoxides.⁶ ELO nanocomposites containing 2, 5, 10 wt.-% of G-POSS and neat ELO polymer were prepared by thermal curing at 140 °C for 1 h, 170 °C for 2 h and 190 °C for 1 h (conditions determined by DSC).

All the cured nanocomposites were homogeneous and transparent, implying that no phase separation had occurred, at least on the scale greater than the wavelength of visible light. All samples were refluxed in chloroform or tetrahydrofuran for 12 h to dissolve and extract any soluble components present. No soluble fractions were detected in the solvent residues, suggesting that the crosslinking reaction had occurred between the two components and showing that all the cured composites were no longer soluble. FTIR spectra of the above POSS-containing nanocomposites allowed examination of the degree of curing after the introduction of POSS into the network. Shown in Figure 1 are the FTIR spectra of ELO, the ELO polymer and the hybrid composites containing 2, 5 and 10 wt.-% POSS. ELO is characterized by the stretching vibration of the epoxide moieties at 825 cm^{-1}

(C-O-C), and completion of the curing reaction was confirmed by its complete disappearance (see curves b-e). New bands were also observed at 1075 and 3500 cm^{-1} , and assigned to the aliphatic ether and terminal hydroxyl groups produced during oxirane ring-opening. The absorption at 1109 cm^{-1} , assigned to Si-O-Si of the POSS, is present in all the composites and indicates a silsesquioxane structure; its intensity increasing with POSS concentration.

The morphology of the POSS bionanocomposites was further investigated by WAXD, EDX Si-mapping and SEM. The WAXD patterns of the nanocomposites are shown in Figure 2; for comparison, the X-ray patterns of G-POSS and the neat ELO polymer are also shown. The diffractogram of the G-POSS shows a main reflection at 2θ of 7.4° and a series of smaller peaks at 2θ 's of 8.1° , 8.7° , 9.3° , etc. This complicated diffractogram and the presence of two well-defined melting peaks, at 112 and 132 °C, in the DSC thermogram may indicate the coexistence of two different crystalline phases. The WAXD patterns of all the ELO nanocomposites are similar to that of the neat ELO polymer, displaying a broad peak with 2θ around 20° , corresponding to an amorphous halo. Therefore, the WAXD data give no indication of the presence of crystalline POSS aggregate in the synthesized nanocomposites. However, because of the limited sensitivity of WAXD, the occurrence of some clustering of POSS units or phase-separated small-sized inorganic domains can not be ruled out.

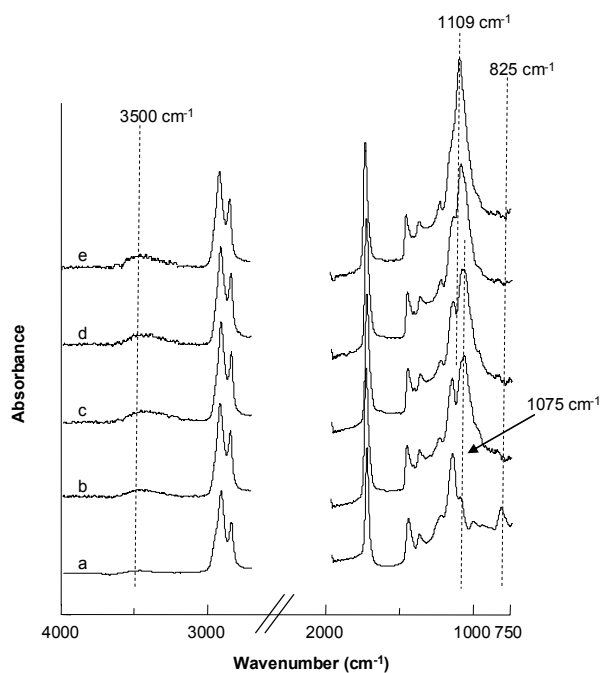


Figure 1. FTIR of ELO (a), ELO polymer (b), and ELO nanocomposites containing G-POSS: 2 (c), 5 (d), and 10 wt.-% (e).

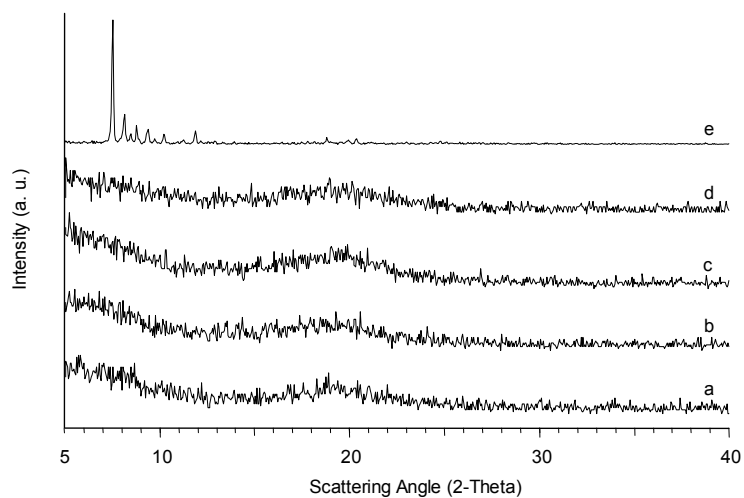


Figure 2. WAXD data of ELO polymer (a), and ELO nanocomposites containing G-POSS: 2 (b), 5 (c), 10 wt.-% (d), and G-POSS (e).

The homogeneity of the POSS nanoparticles dispersion was further examined with SEM. As a first approach, EDX Si-mapping of all the composites showed that the particles were uniformly dispersed in the cross-sectional surfaces observed (Figure 3). The white points in the image denote POSS-enriched regions.



Figure 3. SEM-EDX Si-mapping of cross-section of ELO 5 wt.-% G-POSS nanocomposite.

The Figure 4 displays the SEM cross-sectional images of ELO/G-POSS composites having different POSS contents. The SEM micrograph of the composite containing 2 wt.-% G-POSS exhibits a

featureless morphology, with no discernable phase separation, suggesting that POSS nanoparticles are homogeneously dispersed throughout the matrix. When the concentration of POSS was 5 wt.-%, the SEM micrograph reveals aggregation, showing many spherical particles (40-50 nm in diameter) uniformly dispersed. More serious aggregation (80-150 nm in diameter) occurs in 10 wt.-% containing composite. This behaviour can be explained assuming that the reactivity of epoxy POSS is likely to be lower compared to that of ELO due to steric hindrance, phase separation of G-POSS rich domains could occur at low conversions, before a significant advance in the copolymerization with ELO occurs. G-POSS, which is initially soluble in the monomer mixture, phase separates because its solubility in the organic medium becomes lower during the polymerization and this phase separation occurs at lower conversions when increasing G-POSS content. These particles may contain ELO segments chemically bonded, in agreement with the reduced crystallinity.

Table 1. Thermal Properties of ELO/G-POSS Nanocomposites

Entry	ELO/G-POSS wt.-%	T _g ^a (DSC)	T _g ^b (DMTA)	TGA (Nitrogen)		TGA (Air)	
				T _{5% loss} (°C) ^c	R _{800°C} (%) ^d	T _{5% loss} (°C) ^c	R _{800°C} (%) ^d
1	100:0	29	44	357	3	327	0
2	98:2	35	49	355	4	338	2
3	95:5	39	52	356	5	334	4
4	90:10	30	42	355	5	327	7

^a Rough estimation from a broad transition.

^b Maximum of tan δ .

^c Temperature of 5 % of weight loss.

^d Char yield at 800 °C.

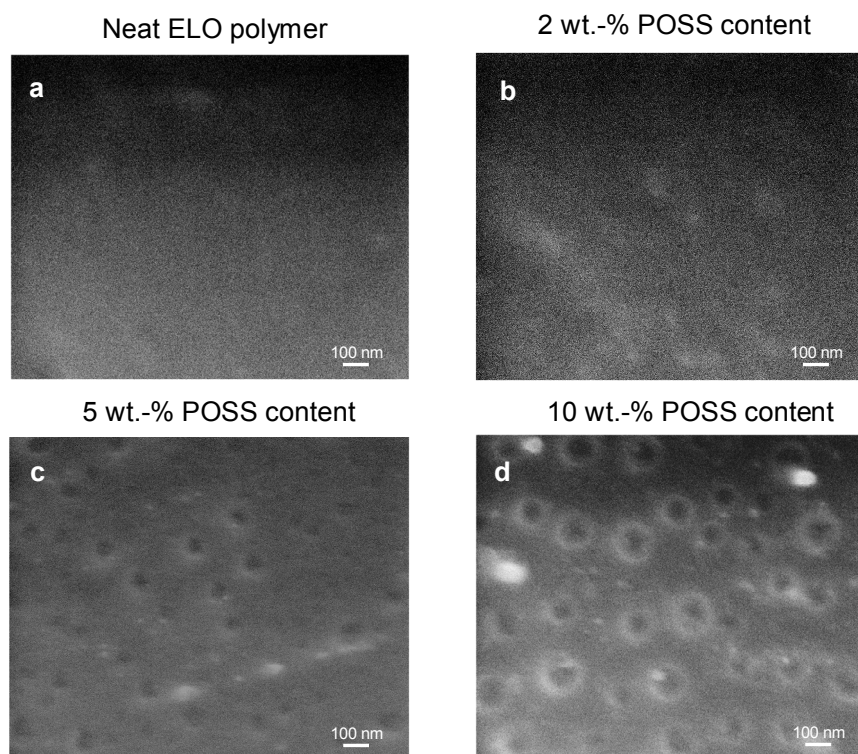


Figure 4. SEM cross-sectional micrographs of (a) ELO polymer and ELO nanocomposites containing G-POSS: (b) 2, (c) 5, and (d) 10 wt.-%.

The thermal behaviour of ELO/POSS bionanocomposites was investigated by DSC and DMTA. All the DSC thermograms display single glass transition temperatures (T_g s) in the experimental temperature range, attributed to the ELO matrices. Although SEM micrograph of 10 wt.-% G-POSS containing composite showed a heterogeneous morphological structure, no separated T_g values were detected. The approximate T_g values, determined by DSC, are listed in Table 1. The transition was broad, therefore greater accuracy was not possible. Using DMTA, it was possible to determine with far greater accuracy the T_g of the crosslinked materials: it is measured at the maximum

intensity of the $\tan \delta$ curves, which reflects the viscous-elastic characteristic of a polymeric material. Shown in Figure 5 a) are the DMTA plots of $\tan \delta$ as a function of temperature for the ELO polymer and its nanocomposites. The neat ELO polymer exhibits a well-defined α relaxation peak centered at 44 °C, which corresponds to the glass transition of the polymer. The ELO/POSS nanocomposites that contain 2, 5, and 10 wt.-% of G-POSS also clearly exhibit a single transition at 49, 52 and 42 °C, respectively. The glass transition behaviour of the nanocomposite systems is dependent on the morphology of the hybrid composites. The T_g of the nanocomposites slightly increased and the

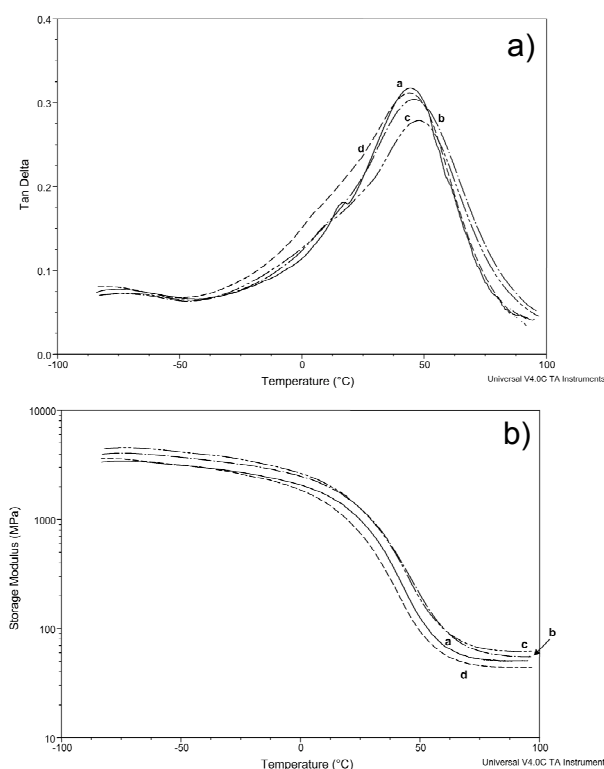


Figure 5. a) Loss factor ($\tan \delta$) and b) dynamic storage moduli as a function of temperature for the (a) neat ELO polymer, and ELO nanocomposites containing G-POSS: (b) 2, (c) 5, and (d) 10 wt.-%.

intensity of the α transition decreased with an increasing POSS content up to 5 wt.-%. This observation is ascribed to the nanoreinforcement effect of the POSS cages on oil based polyether networks.¹⁹ The bulky POSS cages may restrict the motion of the macromolecular chains and thus higher temperatures are required to provide the requisite thermal energy to cause a glass transition in hybrid materials. However, the T_g of the composite that contains 10 wt.-% G-POSS doesn't follow the same trend. The decreased T_g for this phase separated composite could be attributed to the incomplete curing reaction due to the inclusion of

bulky POSS cages. Infrared spectroscopy (Figure 1) showed the disappearance of the epoxide band at 825 cm^{-1} , suggesting that the curing reaction occurred to completion. The glass transition behaviour cannot be explained solely on the basis of the nanoreinforcement effect. The depression of T_g could be ascribed to the increase in free volume of the system due to the inclusion of bulky POSS cages and the lower crosslinking density in the composite. The $\tan \delta$ plots for all samples displayed a β relaxation at approximately $-60\text{ }^\circ\text{C}$. This β transition, which is generally observed in fatty acid containing thermosets, may

be related to the rotational motions of short units in the fatty acid chain.²⁸

Figure 5 b) shows the dynamic storage moduli (E') as a function of temperature for neat ELO polymer and all its composites. All materials exhibit E' curves with the typical behaviour of crosslinked polymeric networks. At low temperature, there is a glassy state with E' staying at a high moduli plateau and a rubbery state with a lower E' for temperatures higher than T_g . As can be seen in Figure 5 b), at -80 °C the E' of the hybrids is slightly higher than E' of the neat ELO polymer, therefore the introduction of small amounts of POSS cages gave rise to an small increase in E' in the glassy state. It is also worth noticing that the E' at the rubbery plateau for POSS-containing polymers was close to or higher than that of the neat ELO polymer. Only at the higher concentration of G-POSS the storage modulus in the rubbery plateau was lower than that of the neat ELO polymer. This behaviour has been observed by other authors²⁹ and can be related to the nanoreinforcement effect of the POSS cages on the networks that will give an increase in E' in the glassy and the rubbery states. The inclusion of POSS could give a decrease in the densities of the materials ascribed to an increase in the free volume of the nanocomposites that can come from the increase in the free volume caused by the interaction of POSS cages and polymer chains, and also from the nanoporosity of the POSS core. The crosslinking density per unit volume will decrease with increasing concentration of the POSS in the hybrids, which will result in a decrease in E' of the nanocomposites. Nonetheless, it can be seen

that the storage moduli of the hybrids with less than 10 wt.-% of G-POSS are higher than the neat oil network. This implies significant nano-reinforcement by the POSS cages, which counteracts the effect of decreased densities on the storage moduli. Only at higher POSS contents could the effect of the reduced density to dominate on the nanoreinforcement effect.³⁰

Thermogravimetric analysis (TGA) was used to evaluate the thermal stability of these composites as function of the POSS content. Table 1 collects the TGA data determined under nitrogen and air atmospheres and Figure 6 a) shows the TGA curves for all samples under nitrogen atmosphere at 10 °C/min. For the all samples, there is only a single degradation process under nitrogen, which is due to the degradation of crosslinked polymer network, suggesting that the presence of POSS does not significantly alter the degradation mechanism of the ELO polymers. For the POSS-containing polymers the char yields at 800 °C slightly increased with the POSS content. The TGA experiments were also carried out in the presence of air as the carrier gas. Under air, a second step in the weight loss rate appears at higher temperature, above 450 °C, corresponding to the thermooxidative degradation. Figure 6 b) shows that under air atmosphere hybrids with POSS content up to 5 wt.-% are more thermally stable than the neat ELO polymer. It has been proposed that the tethering of the structure of the POSS cage to the organic polymer was crucial to improve the thermal stabilities of POSS-containing nanocomposites.³¹ The temperature of 5% of weight loss ($T_{5\%loss}$) is slightly increased because of

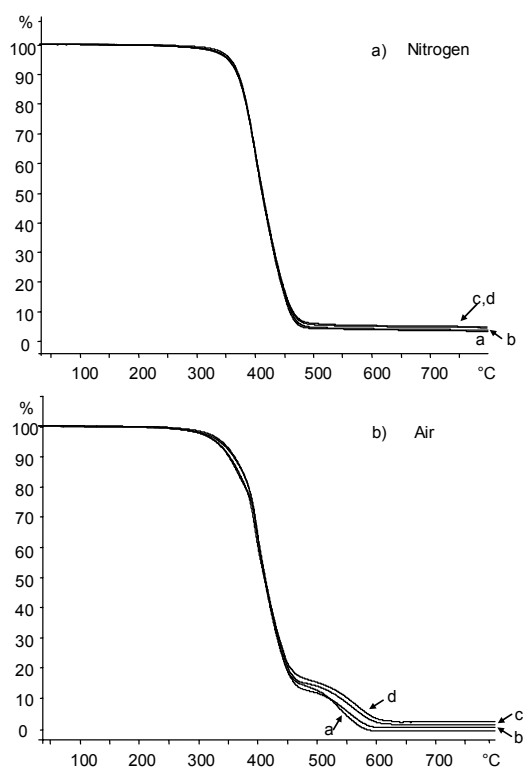


Figure 6. TGA thermograms for the (a) neat ELO polymer and ELO nanocomposites containing G-POSS: (b) 2, (c) 5, and (d) 10 wt.-% under nitrogen and air atmospheres.

the POSS cages retards the movement of the molecular chains at high temperature (see Table 1). The aggregated structure when POSS content is at 10 wt.-%, reduces its overall effectiveness in hindering polymer movement and its T_d value. It is noted that the char residues under air atmosphere increases with POSS content and are in good agreement with the added POSS which would be converted into inorganic silica at high temperatures. High char yields correspond to reduced amount of volatile and combustible compounds evolving from the thermal degradation processes and improved flammability.

CONCLUSIONS

In conclusion, new biobased nanocomposites have been developed from plant oils as renewable resources. The bionanocomposites were obtained from epoxidized linseed oil and 3-glycidylpropylheptaisobutyl- T_8 -polyhedral oligomeric silsesquioxane. Most of the resulting POSS-containing networks displayed slightly enhanced glass transition temperatures. The storage moduli of the networks at the glassy and the rubbery plateau were observed to be somewhat higher than that of POSS-free network. These results can be ascribed to the nanoscale reinforce-

ment effect of POSS cages on the crosslinked matrix.

Acknowledgements

The authors gratefully acknowledge the Comisión Interministerial de Ciencia y Tecnología (MAT2005-01593) for financial support for this work and the Departament d'Universitats, Recerca i Societat de la Informació and Fons Social Europeu for G. Lligadas' predoctoral (2003FI00765) grant. We would like to thank F. Guirado for XRD and M. Moncusí for SEM analysis.

REFERENCES AND NOTES

1. (a) Baumann, H.; Bühler, M.; Fochem, H.; Hirsinger, F.; Zoeblein, H.; Falbe, J. *Angew Chem Int Ed Engl* 1988, 27, 41; (b) Biermann, U.; Friedt, W.; Lang, S.; Lühs, W.; Machmüller, G.; Metzger, J. O.; Klaas, M. R.; Schäfer, H. J.; Schneiderüs, M. P. *Angew Chem Int Ed Engl* 2000, 39, 2206; (c) Eissen, M.; Metzger, J.O.; Schmidt, E. Schneidewind, U. *Angew Chem Int Ed Engl* 2002, 41, 414.
2. Kaplan, D. L. *Biopolymers from Renewable Resources*, Springer, Berlin 1998, p. 267.
3. (a) Lligadas, G.; Ronda, J. C.; Galià, M.; Cádiz, V. *Biomacromolecules* 2006, 7, 2420; (b) Lligadas, G.; Ronda, J. C.; Galià, M.; Biermann, U.; Metzger, J. O. *J Polym Sci Part A: Polym Chem* 2006, 44, 634; (c) Pelletier, H.; Belgacem, N.; Gandini, A. *J Appl Polym Sci* 2006, 99, 3218; (d) Uyama, H.; Kuwabara, M.; Tsujimoto, T.; Kobayashi, S. *Biomacromolecules* 2003, 4, 211; (e) Esen, H.; Kusefoglul, S. H. *J Appl Polym Sci* 2003, 89, 3882; (f) Bunker, S. P.; Wool, R. P. *J Polym Sci Part A: Polym Chem* 2002, 40, 451; (g) Petrovic, Z.; Guo, A.; Zhang, W. *J Polym Sci Part A: Polym Chem* 2000, 38, 4062; (h) Petrovic, Z.; Guo, A.; Javni, I. U.S. Patent 2000, 6, 107, 433.
4. Crivello, J. V.; Narayan, R. *Chem Mater* 1992, 4, 692.
5. (a) Park, S. J.; Jin, F. L.; Lee, J. R.; Shin, J. S. *Eur Polym J* 2005, 41, 231; (b) Park, S. J.; Jin, F. L.; Lee, J. R. *Macromol Rapid Commun* 2004, 25, 724.
6. Kim, M. S.; Lee, K. W.; Endo, T.; Lee, S. B. *Macromolecules* 2004, 37, 5830.
7. Khot, S. N.; La Scala, J. J.; Can, E.; Morye, S. S.; Williams, G. I.; Palmese, G. R.; Kusefoglul, S. H.; Wool, R. P. *J Appl Polym Sci* 2001, 82, 703.
8. Sanchez, C.; Soler-Illia, G. J. de A. A.; Robot, F.; Lalot, T.; Mayer, C. R.; Cabuil, V. *Chem Mater* 2001, 13, 3061.
9. Williams, G. I.; Wool, R. P. *Appl Composite Mater* 2000, 7, 421.
10. (a) Wold, C. R.; Soucek, M. D. *Macromol Chem Phys* 2000, 201, 382; (b) Deffar, D.; Teng, G.; Soucek, M. D. *Macromol Mater Eng* 2001, 286, 204.
11. Lligadas, G.; Callau, L.; Ronda, J. C.; Galià, M.; Cádiz, V. *J Polym Sci Part A: Polym Chem* 2005, 43, 6295.
12. Thielemans, W.; McAninch, I. M.; Barron, V.; Blau, W. J.; Wool, R. P. *J Appl Polym Sci* 2005, 98, 1325.
13. Uyama, H.; Kuwabara, M.; Tsujimoto, T.; Nakano, M.; Usuki, A.; Kobayashi, S. *Chem Mater* 2003, 15, 2492.
14. Uyama, H.; Kuwabara, M.; Tsujimoto, T.; Nakano, M.; Usuki, A.; Kobayashi, S. *Macromol Biosci* 2004, 4, 354.
15. Lu, J.; Hong, C. K.; Wool, R. P. *J Polym Sci Part B: Polym Phys* 2004, 42, 1441.
16. (a) Tsujimoto, T.; Uyama, H.; Kobayashi, S. *Macromol Rapid Commun* 2003, 24, 12; (b) Ballard, R. L.; Tuman, S. J.; Fouquette, D. J.; Stegmiller, W.; Soucek, M. D. *Chem Mater* 1999, 11, 726.
17. (a) Vizet, S.; Galy, J.; Gérard, J-F. *Macromolecules* 2006, 39, 2574; (b) Castelvetro, V.; Ciardelli, F.; De Vita,

- C.; Puppo, A.; *Macromol Rapid Commun* 2006, 27, 619; (c) Lin, H. C.; Kuo, S. W.; Huang, C. F.; Chang, F. C. *Macromol Rapid Commun* 2006, 27, 537; (d) Lee, Y. J.; Huang, J. M.; Kuo, S. W.; Chen, J. K.; Chang, F. C. *Polymer* 2005, 46, 2320; (e) Chen, Q.; Xu, R.; Zhang, J.; Yu, D. *Macromol Rapid Commun* 2005, 26, 1878; (f) Phillips, S. H.; Haddad, T. S.; Tomczak, S. *J Curr Opin Solid State Mater Sci* 2004, 8, 21; (g) Zheng, L.; Kasi, R. M.; Farris, R. J.; Coughlin, E. B. *J Polym Sci Part A: Polym Chem* 2002, 40, 885; (h) Pittman, C. U.; Ni, H.; Wang, L.; Li, G. *J Inorg Organomet Polym* 2001, 11, 123; (i) Pyun, J.; Matyjaszewski, K. *Macromolecules* 2000, 33, 217; (j) Bharadwaj, B. K.; Berry, R. J.; Farmer, B. L. *Polymer* 2000, 41, 7209.
18. (a) Matejka, L.; Strachota, A.; Pledtil, J.; Whelan, P.; Steinhart, M.; Slouf, M. *Macromolecules* 2004, 37, 9449; (b) Abad, M. J.; Barral, L.; Fasce, D. P.; Williams, R. J. *Macromolecules* 2003, 36, 3128.
19. Lee, A.; Lichtenhan, J. D. *Macromolecules* 1998, 31, 4970.
20. (a) Liu, Y. L.; Chang, G. P.; Hsu, K. Y.; Chang, F. C. *J Polym Sci Part A: Polym Chem* 2006, 44, 3825; (b) Liu, Y.; Zheng, S.; Nie, K. *Polymer* 2005, 46, 12016.
21. Xu, H. Y.; Kuo, S. W.; Lee, J. Y.; Chang, F. C. *Polymer* 2002, 43, 5117.
22. Pellice, S. A.; Fasce, D. P.; Williams, R. J. *J Polym Sci Part B: Polym Phys* 2003, 41, 1451.
23. Phillips, S. H.; Gonzalez, R. I.; Chaffee, K. P.; Haddad, T. S.; Hoflund, G. B.; Hsiao, B. S.; Fu, B. X. *SAMPE* 2000, 45, 1921.
24. Huang, J. C.; He, C. B.; Xiao, Y.; Mya, K. Y.; Dai, J.; Siow, Y. P. *Polymer* 2003, 44, 4491.
25. Fu, B. X.; Namani, M.; Lee, A. *Polymer* 2003, 44, 7739.
26. Findley, T. W.; Swern, D.; Scalan, J. T. *J Am Chem Soc* 1945, 67, 412.
27. Rangarajan, B.; Havey, A.; Grulke, E. A.; Culnan, P. D. *J Am Oil Chem Soc* 1995, 72, 1161.
28. Petrovic, Z.; Zhang, W.; Javni, I. *Bio-macromolecules* 2005, 6, 713.
29. Li, G. Z.; Cho, H.; Wang, L.; Toghiani, H.; Pittman C. U. *J Polym Sci Part A: Polym Chem* 2005, 43, 355.
30. Liu, H.; Zheng, S. *Macromol Rapid Commun* 2005, 26, 196.
31. (a) Choi, J.; Harcup, J.; Yee, A. F.; Zhu, Q.; Laine, R. M. *J Am Chem Soc* 2001, 123, 11420; (b) Choi, J.; Kim, S. G.; Laine, R. M. *Macromolecules* 2004, 37, 99.

3

Biobased Flame-Retardant Epoxy Resins

Epoxy resins exhibit excellent properties and are used in many technological applications. Most of the epoxy resins used industrially are derived from petroleum-based chemicals, but epoxidized vegetable oils are extremely promising as inexpensive, renewable materials for industrial applications. However, the flammability of the epoxy resins is a shortcoming in some applications.

This chapter describes the synthesis of a new phosphorous-containing fatty acid derivative and its use in the synthesis of biobased flame-retardant epoxy resins.

-
- 3.1 Biobased Epoxy Resins
 - 3.2 Flame Retardants: Mechanism and Environmental Concerns
 - 3.3 Objectives
 - 3.4 Experimental Procedures and Results
 - 3.4.1 Synthesis and Properties of Thermosetting Polymers from a Phosphorous – Containing Fatty Acid Derivative
 - 3.4.2 Development of Novel Phosphorus-Containing Epoxy Resins from Renewable Resources
-

3.1

Biobased Epoxy Resins

As important industrial materials, epoxy resins exhibit the attractive characteristics of excellent moisture, solvent, and chemical resistance, low shrinkage on cure, superior electrical and mechanical properties, and good adhesion to many substrates.¹ Most of the epoxy resins used industrially are derived from petroleum-based chemicals. However, the depletion of the earth's limited petroleum reserves has heightened interest in using renewable resources as replacement materials for epoxy resins.

The preparation of biobased epoxy resins from epoxidized vegetable oils has been the subject of many studies. Cyclic acid anhydride hardeners and tertiary amine and imidazole catalysts that are usually used for the crosslinking of industrial epoxy prepolymers have been employed to cure epoxidized linseed oil.² Curing reactions of epoxidized soybean oil with diverse diamine reagents have also been investigated,^{3,4} although the amide that can form when using polyamine hardeners results in cured products of poor quality.⁵

Common epoxy/amine systems are often subject to problems associated with the toxicity of the amine, low heat resistance, and the deterioration of electrical properties. The thermal and photoinitiated cationic polymerizations of epoxy resins have been intensively investigated using various latent cationic catalysts, such as iodonium, ammonium, pyridinium, and sulfonium salts.^{6,7} The use of latent catalysts improves the storage stability and handling properties of the resin. Focusing on

-
1. Epoxy Resins : Chemistry and Technology; May, C. A. Ed.; Marcel Decker, Inc.: New York, 1998.
 2. Boquillon, N.; Fringant, C. *Polymer* 2000, 41, 8603.
 3. Zhu, J.; Chandrashekhara, K.; Flanigan, V.; Kapila, S. J. *J Appl Polym Sci* 2004, 91, 3513.
 4. Juangvanich, N.; Stoffer, J. *Polym Prep (Am Chem Soc Div Polym Chem)* 2002, 43, 22.
 5. *Handbook of Epoxy Resins*; Lee, H.; Neville, K. Eds.; McGraw Hill: New York, 1982.
 6. Lee, S. D.; Takata, T.; Endo, T. *Macromolecules* 1996, 29, 3317.
 7. Park, S. J.; Kim, T. J.; Lee, J. R. *J Polym Sci Part B: Polym Phys* 1996, 29, 3317.

vegetable oil-based epoxy resins, Crivello and Narayan⁸ examined the use of a wide variety of epoxidized triglyceride oils as renewable monomers in photoinitiated cationic polymerization. The oils were photopolymerized as thin films using soluble diaryliodonium and triarylsulfonium salt photoinitiators bearing long-chain alkoxy substituents. Characterization of the photopolymerized polymer networks both thermally and mechanically showed that they may represent excellent inexpensive raw materials for thin-film applications. Thames and Yu evaluated the application of vernonia oil and epoxidized soybean oil as UV-curable coatings.⁹ Latent cationic catalysts can also be stimulated by heat. The cationic polymerization of epoxidized castor oil and epoxidized soybean oil initiated by N-benzylpyrazinium hexafluoroantimonate and N-benzylquinoxalinium hexafluoroantimonate as thermally latent catalysts has also been studied.^{10,11}

There is a very strong demand for flame-retardant epoxy resins because of their widespread applications in electronics and transportation. However, commonly used epoxy systems are unsuitable for applications that require flame resistance. It is therefore essential to develop new polymer materials with flame retardants so as to reduce the combustibility of the polymers and their smoke or toxic fume production.

3.2

Flame Retardants: Mechanism and Environmental Concerns

A flame retardant is a substance or treatment incorporated in or applied to a material that suppresses or delays its combustion under specified conditions.¹²

8. Crivello, J. V.; Narayan, R. *Chem Mater* 1992, 4, 692.

9. Thames, S. F.; Yu, H. *Surf Coat Technol* 1999, 115, 208.

10. Park, S. J.; Jin, F. L.; Lee, J. R. *Macromol Rapid Commun* 2004, 25, 724.

11. Park, S. J.; Jin, F. L.; Lee, J. R.; Shin, J. S. *Eur Polym J* 2005, 41, 231.

12. Ebdon, J. R.; Jones, M. S. *Flame retardants*. In: *Polymeric Materials Encyclopedia*; Salomone, J. C. Ed.; CRC Press: Boca Raton, FL, 1996.

In order to understand how flame retardants work, it is necessary to first consider the processes of ignition and burning. The combustion of a polymer material is a highly complex process involving a series of independent and/or interrelated stages occurring in the condensed and gas phases, and at the interphase between them. The most important step in the burning of a polymer is fuel production, in which an external heat source causes an increase in temperature that results in the dissociation of chemical bonds and the evolution of volatile fragments. These fragments diffuse into the surrounding air to create a flammable mixture, and combustion is initiated when this mixture reaches its ignition temperature. Flaming combustion proceeds if the exothermic gas-phase combustion reactions generate sufficient energy in the form of heat transferred back to the condensed phase to decompose the polymer further, thus producing more fuel and so maintaining the combustion cycle. A simple schematic of a self-sustaining polymer combustion cycle is shown in Figure 3.1.

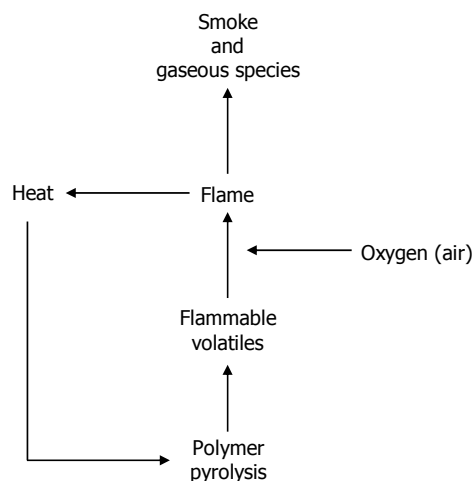


Figure 3.1 Representation of polymer combustion processes.

Successful strategies to reduce the flammability of a polymer material involve interrupting the complex stages of the combustion process at one or more points so to reduce the rate of and/ or change the mechanism.¹² A flame retardant interferes

in one or more stages of the combustion cycle by acting physically or chemically in the solid or gas phase, as follows:

- Interferes with free-radical reactions that occur during combustion (gas-phase reactions).
- Insulates the underlying material from temperature increases using char formation (solid-phase reactions) and provides a protective layer or coating.
- Lowers the temperature by endothermic reactions.
- Slows the spread of fire by diluting oxygen with non-combustible gases.

The complex nature and poor reproducibility of fire has resulted in many techniques being used to estimate the flammability of polymer materials, depending upon the importance of different fire properties¹³ such as easy of ignition, flame spread, rate of heat release, fire endurance, easy of extinction, smoke release, and toxic gas evolution.

The most widely used laboratory test is the limiting oxygen index (LOI) (ASTM-D-2683) technique, which is a very convenient test that yields reproducible data. The LOI value is the minimum amount of oxygen in a mixture of oxygen and nitrogen that will support flaming combustion of a top-ignited specimen, with a higher LOI value indicating a less-flammable material. A disadvantage of the LOI test is that the high concentration of oxygen employed is not representative of a real fire. Several techniques have been developed for measuring a range of properties that correlates well with those obtained from full-scale tests. The most common one is the use of a cone calorimeter (ASTM E1354), which reveals an accurate pyrolysis profile of a polymer material.

13. Pitts, J. J. *Flame Retardancy of Polymeric Materials*, vol. I; Kurya, W. C.; Papa, A. J. Ed.; Marcel Dekker Inc.: New York, 1973.

Several techniques have been employed to improve the flame retardance of epoxy resins. The most common approach is to include halogen (bromine or chlorine) atoms in the epoxy resins. Most organic halogen compounds are primarily gas-phase retardants that decompose to yield HBr or HCl, which quenches the propagation of free-radical reactions in the flame.¹³ Combining antimony trioxide (Sb_2O_3) or antimony pentoxide (Sb_2O_5) with organic halogen compounds result in a gas-phase free-radical inhibitor that is even more effective than halogen.

Recent research into the safety of flame retardants has revealed disadvantages of currently used halogen-based flame retardants: they increase the amounts of smoke and toxic decomposition products, such as halogenated dibenzodioxins and dibenzofurans evolved during polymer combustion. The use of halogenated compounds also gives rise to the additional hazard of the liberation of strongly acidic gases upon heating, such as HCl and HBr. These drawbacks have increased the amount of research into the development of innovative, and environmentally friendly halogen-free flame-retardant epoxy resins. Phosphorylation has recently been considered one of the most efficient methods of conferring flame retardance on epoxy resins.¹²⁻¹⁴ Organophosphorus compounds are both non-toxic and very effective.¹⁵ Phosphorus-containing flame retardants affect the reactions taking place in the condensed phase, during which phosphorus acids (e.g., phosphoric acid or polyphosphoric acid) are thermally liberated from the flame retardant. These acids act as dehydrating agents that alter the thermal degradation of the polymer, promoting char formation at the expense of flammable volatiles. The non-volatile, polymeric phosphoric acids inhibit further pyrolysis reactions by simultaneously forming a carbonaceous layer with a glassy coating that is resistant to high temperatures and shields the underlying polymer from attack by oxygen and radiant heat. Some phosphorus flame retardants, such as triphenylphosphine oxide can also

14. Von Gentzow, W.; Huber, J.; Kapitza, H.; Rogler, W.; *J Vinyl & Additive Technology* 1997, 3, 175.

15. Wang, C. S.; Shieh, J. Y. *Polymer* 1998, 39, 5819.

act in the gas phase by reducing the energy of the flame, but this mechanism is less common.¹⁶

Organophosphorus compounds can be directly introduced into a thermosetting epoxy resin by utilizing the P-OH reactivity of dialkyl (or diaryl) phosphates toward the oxirane ring. However, epoxy resins with the highest flame retardancy has been achieved using phosphorus-containing oxirane compounds or curing agents.^{17,18} There is an extremely wide range of phosphorus-containing flame retardants since the element exists in several oxidation states. Several phosphine oxide-based and phosphate-based epoxides and curing agents described in the literature are shown in Figure 3.2.

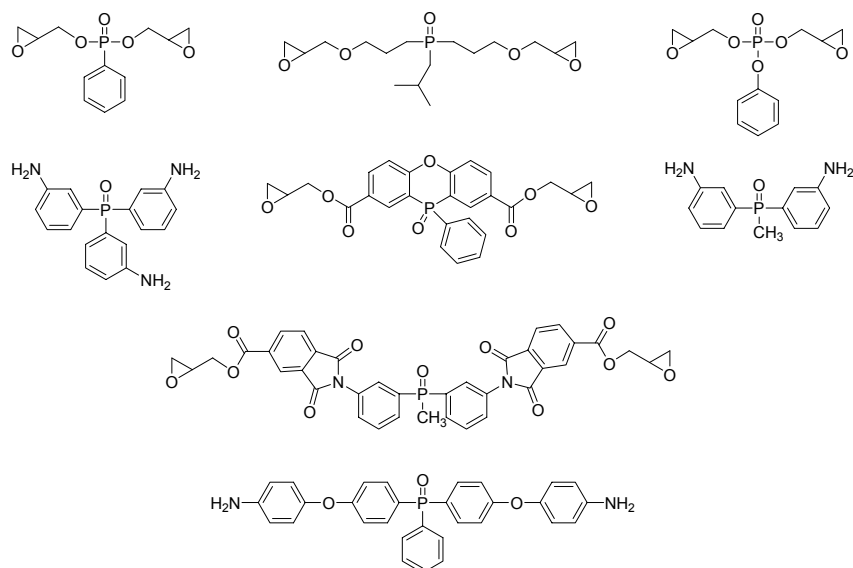


Figure 3.2 Chemical structures of several phosphorus-containing epoxides and curing agents.

16. Hörold, S. *Polym Degrad Stab* 1999, 64, 427.

17. Levchik, S. V.; Piotrowski, A.; Weil, E. D.; Yao, Q. *Polym Degrad Stab* 2005, 88, 57.

18. Levchik, S. V.; Weil, E. D. *Polym Int* 2004, 53, 1901.

There are many reports of the use of a rigid and bulky phosphonate derivative, 9,10-dihydro-9-oxa-10-phosphaphenanthrene-10-oxide (DOPO) and its derivatives, in the formulation of epoxy resins.¹⁸⁻²⁰ This group contains a P-O-C bond whose thermal stability is unusually high, which can be attributed to the O=P-O group being protected by phenylene groups. Several oxirane and amine derivatives have been prepared from DOPO (Figure 3.3).

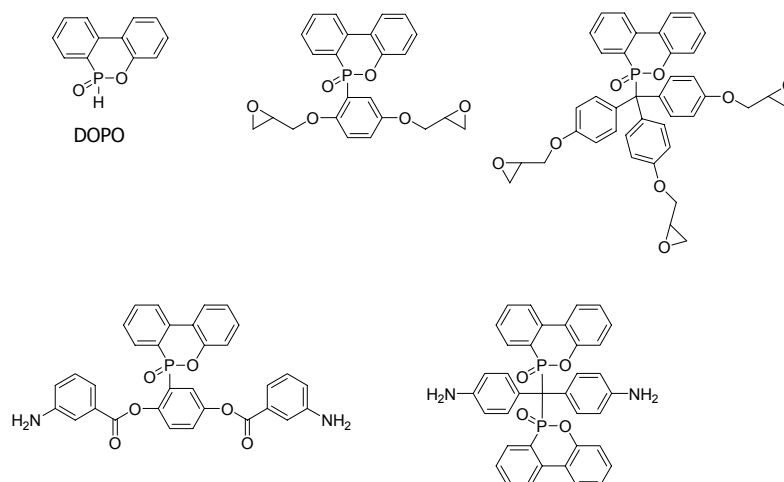


Figure 3.3 Chemical structures of several DOPO based epoxides and curing agents.

The incorporation of phosphorus into biobased epoxy resins may represent an alternative to the current petroleum-based flame retardant epoxy resins, and may provide the important advantage of being more environmentally sustainable. Moreover, it is more environmentally friendly to use phosphorous than halogens in flame-retardant epoxy resins.

19. Lin, C. H.; Cai, S. X.; Lin, C. H. *J Polym Sci Part A: Polym Chem* 2005, 43, 5971.

20. Lu, S. Y.; Hamerton, I. *Prog Polym Sci* 2002, 27, 1661.

3.3

Objectives

In recent years there has been a considerable focus on the synthesis of biobased epoxy monomers and epoxy resins, but little attention has been paid to improving their flame retardancy.

The main objective of the work described in this chapter was to develop new biobased flame-retardant epoxy resins. This objective can be divided into two sub objectives:

1. To synthesize and evaluate the properties of thermosetting polymers obtained from a new phosphorous-containing fatty acid diepoxide, 10-(2',5'-bis(9-oxiranyl-nonanoyloxy)-phenyl)-9,10-dihydro-9-oxa-10-phosphaphenanthrene-10-oxide (DOPO-III, Figure 3.4).

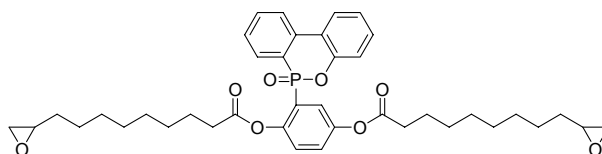


Figure 3.4 Chemical structure of DOPO-III epoxide monomer.

2. To evaluate the effects on the thermal, mechanical, and flame-retardant properties of incorporating DOPO-III into epoxidized 10-undecenyl triglyceride (UDTGE, Figure 3.5) and epoxidized methyl 3,4,5-tris(10-undecenoyloxy)benzoate (UDBME)-based epoxy resins as a reactive flame-retardant.

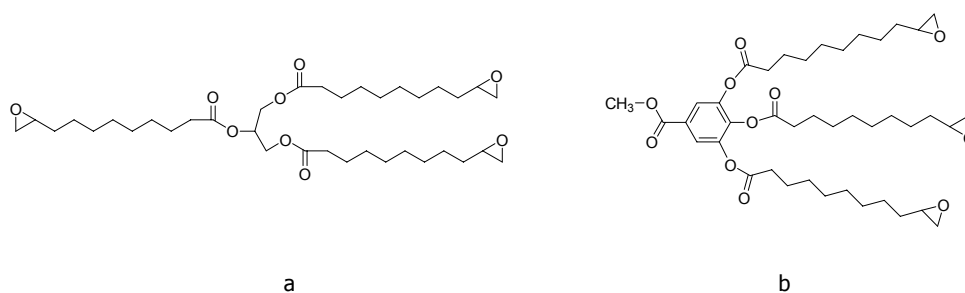


Figure 3.5 Chemical structures of UDTGE (a) and UDBME (b) epoxy monomers.

3.4

Experimental Procedures and Results

The following two works includes the experimental procedures and the results of the studies performed for this chapter.

The work described in Section 3.4.1 has been published in the *Journal of Polymer Science Part A: Polymer Chemistry* (2006, 44, 5630), and includes the synthesis and characterization of DOPO-III, and its crosslinking with amine reagents. The thermal, mechanical, and flame-retardant properties of the obtained thermosetting materials, as well as their thermal and thermooxidative degradation mechanisms were studied.

The development of novel biobased epoxy resins from UDTGE and UDBME, and the improvement of the flame retardance of these resins by adding DOPO-III and by crosslinking with a phosphorous-containing curing agent are discussed in Section 3.4.2. The thermal, mechanical properties of the obtained thermosetting materials were also evaluated. This work has also been published in the *Journal of Polymer Science Part A: Polymer Chemistry* (2006, in press).

3.4.1 Synthesis and Properties of Thermosetting
Polymers from a Phosphorous-Containing
Fatty Acid Derivative

SYNTHESIS AND PROPERTIES OF THERMOSETTING POLYMERS FROM A PHOSPHOROUS-CONTAINING FATTY ACID DERIVATIVE

G. Lligadas, J.C. Ronda, M. Galià, V. Cádiz

Departament de Química Analítica i Química Orgànica, Universitat Rovira i Virgili, Campus Sescelades, Marcel·lí Domingo s/n, 43007 Tarragona, Spain.

ABSTRACT: A new phosphorous-containing fatty acid diepoxide was obtained from 10-undecenoyl chloride and 10-(2',5'-dihydroxyphenyl)-9,10-dihydro-9-oxa-10-phosphaphenanthrene-10-oxide and crosslinked with 4,4'-diaminodiphenylmethane and bis(*m*-aminophenyl)methylphosphine oxide. The properties of the thermosetting materials were evaluated by differential scanning calorimetry, dynamic mechanical thermal analysis, thermogravimetric analysis, and limiting oxygen index (LOI). Thermal and thermooxidative degradation was studied by gas chromatography/mass spectrometry, FTIR, ^{31}P magic angle spinning NMR spectroscopy, and scanning electron microscopy. LOI values indicate good flame-retardant properties that are related to the formation of a protective phosphorous-rich layer that slowed down the degradation and prevented it from being total.

Keywords: crosslinking; curing; epoxy resins; flame-retardancy; renewable resources

INTRODUCTION

With the depletion of the earth's limited petroleum reserves, the use of renewable resources as replacement materials for industrial products is attracting great interest. These resources have various potential applications, which petrochemical sources have difficulty in satisfying.¹ Triglyceride vegetable oils are a major class of such resources and are now being used in an increasing number of industrial applications, in

addition to being a food source for human beings. Recently, there have been many attempts to convert vegetable oils and fatty acids to useful polymers.²⁻⁴

The main components of these triglyceride oils are saturated and unsaturated fatty acids. Although they possess double bonds, which are used as reactive sites in coatings, they cannot be converted easily to high molecular weight products without the introduc-

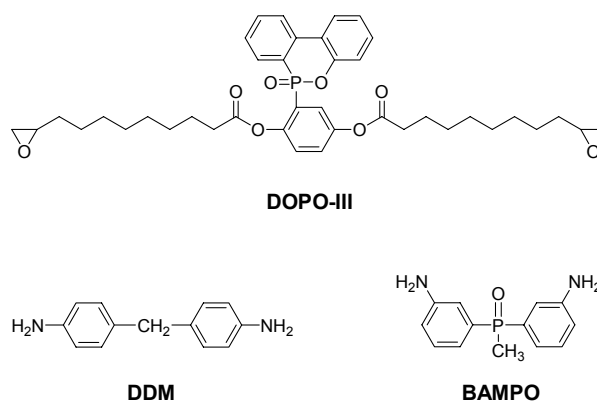
tion of more reactive functional groups, such as hydroxyl, epoxy, or carboxyl groups. Various chemical pathways for functionalizing triglycerides and fatty acids have been studied.³ Epoxidation is one of the most important functionalization reactions of C-C double bonds and opening up the epoxide ring leads to numerous products.^{3,5,6} Recently, there have been attempts to find new uses for these epoxy resources.⁷

Triglycerides are made up of aliphatic chains and, consequently, triglyceride-based materials do not have the rigidity and strength required for some applications. Moreover, like other organic polymeric materials, the flammability of these materials is a shortcoming in some applications. Most of the flame-retardant resins used in industry come from petroleum-based chemicals. Eren and Kusefoglu reported the synthesis and characterization of flame-retardant polymers from bromoacrylated plant oil triglycerides.⁸ However, the flame-retardant resins that contain bromine release hydrogen bromide during combustion, which causes corrosion and toxicity. The concept of sustainable development requires fire retardant technologies to be developed, which have minimum impact on health and the environment throughout the life cycle of the fire-retardant material: that is to say, its synthesis, fabrication, use, recycling and disposal. These considerations mean that the search is now on new environmentally friendly flame-retardant polymeric materials. Phosphorous-containing polymers are well recognized for their flame retardant properties,⁹ and they are

increasingly becoming more popular than their halogen counterparts, as they generally give off nontoxic combustion products. Therefore, the incorporation of organophosphorous functionality in the polymeric structure is recognized as one of the most efficient ways of obtaining an environmentally friendly flame-retardant system. Phosphorous compounds influence the reaction via a solid-state fire-protection mechanism¹⁰ and can also act in the gas state as a catalyst radical scavenger, when degradation produces volatile P-containing moieties.

Since 1972,¹¹ the cyclic organic phosphorous compound, 9,10-dihydro-9-oxa-10-phosphaphenanthrene-10-oxide (DOPO), and its derivatives have been used to make many synthetic resins flame retardant: for example epoxy,¹² polyurethanes,¹³ polyesters,¹⁴ and novolac resins.¹⁵ This rigid and bulky group contain an unusually high thermally stable P-O-C bond, which can be attributed to the O=P-O group being protected by phenylene groups.

In an attempt to find new fatty acid-derived compounds that could find applications in flame retardant materials, in this work a new dioxirane compound was synthesized from 10-undecenoyl chloride, an ω -unsaturated fatty acid derivative, which can be easily obtained from natural castor oil, and a DOPO derivative. The structure of the synthesized dioxirane fatty compound 10-(2',5'-bis(9-oxiranylnonyloxy) phenyl)-9,10-dihydro-9-oxa-10-phosphaphenanthrene-10-oxide (DOPO-III) (Scheme 1) was confirmed

**Scheme 1**

by elemental analysis, FTIR, ^1H NMR, ^{13}C NMR, and ^{31}P NMR. DOPO-III was cured with 4,4'-diaminodiphenylmethane (DDM) and bis(*m*-aminophenyl) methylphosphine oxide (BAMPO) (Scheme 1). The properties of the materials prepared were evaluated by using differential scanning calorimetry (DSC), dynamic mechanical thermal analysis (DMTA), and the limiting oxygen index (LOI). It is of crucial importance to understand the thermal decomposition of a polymer for practical applications; therefore, thermal degradation mechanisms of these DOPO-containing resins have been studied by thermogravimetric analysis (TGA), gas chromatography (GC)/mass spectrometry (MS), FTIR, ^{31}P magic angle spinning (MAS) NMR spectroscopies, and scanning electron microscopy (SEM).

EXPERIMENTAL

Materials

DOPO (9,10-Dihydro-9-oxa-10-phosphaphenanthrene-10-oxide) was a gift from

Aismalibar S.A. *m*-Chloroperbenzoic acid (MCPBA; from Fluka), *p*-benzoquinone (from Aldrich), and 10-undecenoyl chloride (from Fluka) were used without further purification. 4,4'-Diaminodiphenylmethane (DDM) and methylphenyl-phosphine oxide (both from Aldrich) were used as received. 3-*tert*-Butyl-4-hydroxy-5-methylphenyl-sulphide, hydrazine mono-hydrate, and boron trifluoride-ethylamine complex ($\text{BF}_3 \cdot \text{MEA}$) were obtained from Aldrich. Sulfuric and nitric acids were purchased from Prolabo. Tetrahydrofuran (THF) was distilled from sodium/benzophenone immediately before use. Other solvents were purified by standard procedures.

10-(2',5'-Dihydroxyphenyl)-9,10-dihydro-9-oxa-10-phosphaphenanthrene-10-oxide (DOPO-I) was synthesized in our laboratory according to the published procedure.¹⁶ Bis(*m*-aminophenyl)methylphosphine oxide (BAMPO) was synthesized as described elsewhere.¹⁷

Synthesis of 10-(2',5'-bis(10-undecenoyloxy)phenyl)-9,10-dihydro-9-oxa-10-phosphaphenanthrene-10-oxide (DOPO-II) (Scheme 2)

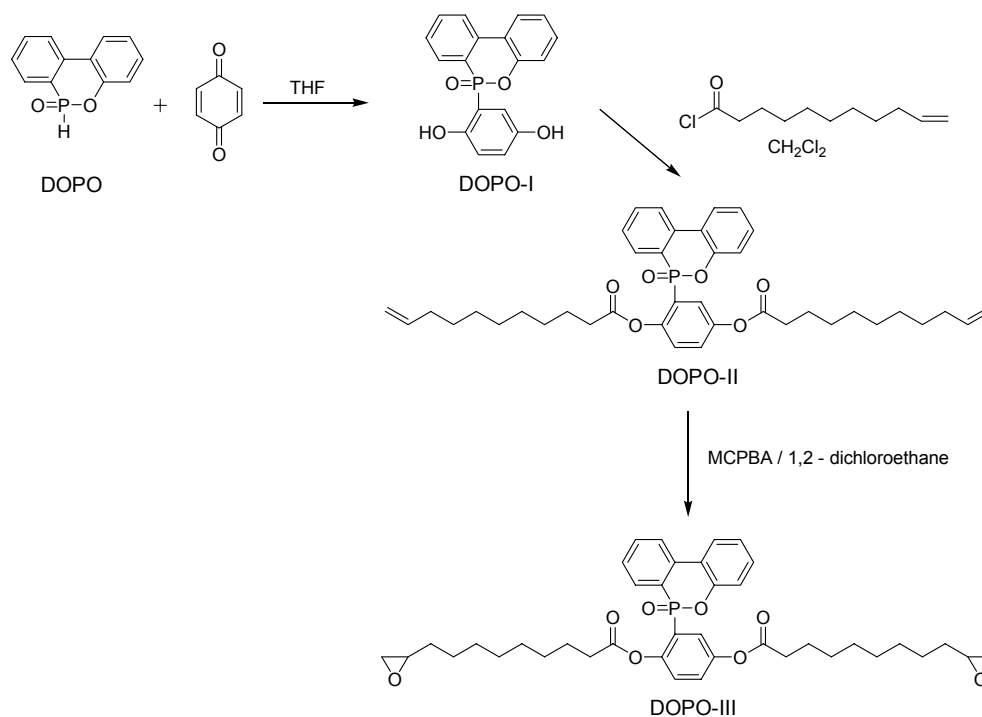
The esterification was carried out by mixing 5.0 g (15.4 mmol) of 10-(2',5'-dihydroxyphenyl)-9,10-dihydro-9-oxa-10-phosphaphenanthrene-10-oxide (DOPO-I), 4 mL of pyridine, and 125 mL of anhydrous dichloromethane under dry argon atmosphere. To this solution, 6.5 g (32.0 mmol) of 10-undecenoyl chloride were added dropwise while stirring at room temperature for 15 min. The temperature was raised to reflux temperature for 15 min. The progress of the reaction was monitored by thin layer chromatography using hexane/ethyl acetate (1:1) as eluent. After the reaction had finished, the crude was placed in a separation funnel, and washed with water, 2 N HCl aqueous solution, a 5% NaHCO₃ solution, and brine. DOPO-II was obtained after drying the dichloromethane solution with anhydrous magnesium sulphate and eliminating the solvent at reduced pressure. The product was purified by silica gel column using hexane/ethyl acetate (5/2) as eluent to give 9.5 g of DOPO-II (yield 94%).

ELEM. ANAL. for C₄₀H₄₉O₆P (656): Calcd. %: C, 73.15; H, 7.52; P, 4.72. Found %: C, 73.05; H, 7.69; P, 4.58. ¹H NMR (CDCl₃/TMS, δ (ppm)): 1.01 (m, 2H), 1.04 (m, 2H), 1.10-1.26 (m, 6H), 1.30-1.43 (m, 12H), 1.69 (dt, 2H), 1.76 (m, 2H), 2.04 (m, 4H), 2.58 (t, 2H), 4.94 (d, 2H), 5.01 (d, 2H), 5.81 (m, 2H), 7.16 (m, 1H), 7.26 (m, 2H), 7.41 (m, 3H), 7.58 (m, 1H), 7.69 (t,

1H), 7.95-8.08 (m, 3H). ¹³C NMR (CDCl₃, δ (ppm)): 24.17 (t), 24.98 (t), 28.92 (t), 28.98 (t), 29.03 (t), 29.14 (t), 29.21 (t), 29.32 (t), 29.35 (t), 29.42 (t), 33.32 (t), 33.94 (t), 34.37 (t), 114.33 (t), 114.38 (t), 120.85 (dd, J_{C-P} = 6.1 Hz), 121.21 (d, J_{C-P} = 12.9 Hz), 123.52 (d, J_{C-P} = 145.6 Hz), 123.29 (dd, J_{C-P} = 11.0 Hz), 124.69 (d, J_{C-P} = 132.5 Hz), 124.74 (d), 124.82 (d), 124.90 (d), 128.25 (dd, J_{C-P} = 8.4 Hz), 128.36 (d), 128.87 (dd, J_{C-P} = 14.6 Hz), 130.82 (d), 130.94 (dd, J_{C-P} = 13.1 Hz), 133.30 (d), 135.25 (d, J_{C-P} = 5.3 Hz), 139.25 (d), 139.32 (d), 147.95 (d, J_{C-P} = 16.8 Hz), 149.42 (d, J_{C-P} = 8.4 Hz), 149.82 (s), 171.01 (s), 172.07 (s). ³¹P NMR (CDCl₃/H₃PO₄), δ (ppm): 18.08 (s).

Synthesis of 10-(2',5'-bis(9-oxiranonyloxy)phenyl)-9,10-dihydro-9-oxa-10-phosphaphenanthrene-10-oxide (DOPO-III) (Scheme 2)

The epoxidation reaction was carried out by dissolving 9.2 g (37.3 mmol) of dry MCPBA (70%), 9.5 g of DOPO-II, and 0.1 g (0.27 mmol) of 3-*tert*-butyl-4-hydroxy-5-methylphenylsulphide into 250 mL of 1,2-dichloroethane.¹⁸ The mixture was maintained at reflux temperature for 1 h. After the reaction had finished, the reaction crude was washed with 5% Na₂S₂O₅, 5% NaHCO₃ solution, and brine. The organic phase was dried over anhydrous magnesium sulphate, and 1,2-dichloroethane was evaporated off. The oil obtained was purified with a silica gel column and hexane/ethyl acetate (5:4) as the eluent.



Scheme 2

When the solvent was removed, 9.4 g of pure DOPO-III (yield 88%) was obtained as a white solid.

ELEM. ANAL for C₄₀H₄₉O₈P (688): Calcd. %: C, 69.75; H, 7.17; P, 4.50. Found %: C, 69.88; H, 7.30; P, 4.38. ¹H NMR (CDCl₃/TMS, δ (ppm)): 1.01 (m, 2H), 1.07 (m, 2H), 1.19 (m, 4H), 1.27 (m, 2H), 1.35-1.56 (m, 16H), 1.69 (dt, 2H), 1.76 (m, 2H), 2.46 (m, 2H), 2.58 (t, 2H), 2.74 (t, 2H), 2.90 (m, 2H), 7.16 (m, 1H), 7.26 (m, 2H), 7.41 (m, 3H), 7.58 (m, 1H), 7.69 (t, 1H), 7.95-8.08 (m, 3H). ¹³C NMR (CDCl₃, δ (ppm)): 24.10 (t), 24.89 (t), 26.03 (t), 28.83 (t), 29.01 (t), 29.10 (t), 29.21 (t), 29.30 (t), 29.37 (t), 29.39 (t), 29.43 (t), 32.55 (t), 33.25 (t), 34.28 (t), 47.18 (t), 47.21 (t), 52.44 (d), 52.47 (d), 120.75 (dd, J_{C-P} = 6.9 Hz),

121.16 (d, J_{C-P} = 11.5 Hz), 122.77 (d, J_{C-P} = 144.9 Hz), 123.26 (dd, J_{C-P} = 9.9 Hz), 124.62 (d, J_{C-P} = 132.6 Hz), 124.69 (d), 124.76 (d), 124.87 (d), 128.14 (dd, J_{C-P} = 8.4 Hz), 128.27 (d), 128.64 (dd, J_{C-P} = 15.2 Hz), 130.74 (d), 130.85 (dd, J_{C-P} = 12.9 Hz), 133.27 (d), 135.19 (d, J_{C-P} = 6.0 Hz), 147.88 (d, J_{C-P} = 17.5 Hz), 149.35 (d, J_{C-P} = 8.3 Hz), 149.76 (s), 170.92 (s), 171.95 (s). ³¹P NMR (CDCl₃/H₃PO₄), δ (ppm): 18.03 (s).

Preparation of polymers

DDM and BAMPO were used as curing agents. Stoichiometric amounts of epoxy compound and curing agent were polymerized using 1% mol

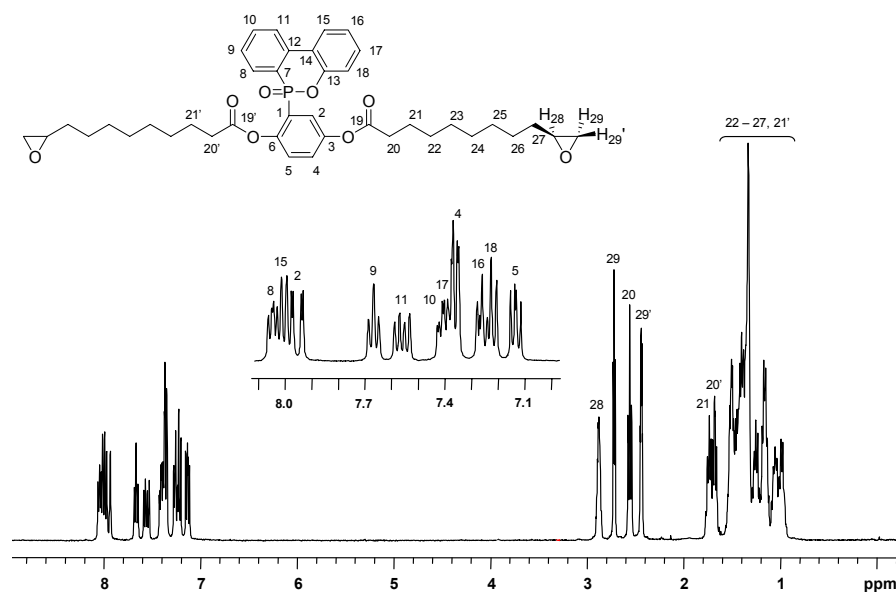


Figure 1. ^1H NMR spectrum of DOPO-III (CDCl_3 , 400 MHz).

$\text{BF}_3 \cdot \text{MEA}$ as accelerator. Sample bars for dynamomechanical analysis, TGA, and burn tests were cured in aluminum moulds by heating. The curing cycles were determined from the DSC data of the respective epoxy/curing agent composition.

Degradation studies

The polymers were degraded at 350 °C for 3 h in an oven with nitrogen or air as the purge gas. Solid residues were collected and analyzed by FTIR and ^{31}P MAS NMR spectroscopies. Volatile products were collected in a trap cooled by liquid nitrogen and examined by gas chromatography–mass spectrometry (GC–MS). Under nitrogen, the DOPO-III/DDM and DOPO-III/BAMPO samples lost 41 and 36% in weight, respectively, and under air, the weight loss was 18 and 19%.

Characterization

Elemental analyses were performed by a Perkin-Elmer 2400 CHN micro-analyzer. Quantitative P analyses were carried out by inductively coupled plasma spectroscopy. The NMR spectra were recorded on a Varian Gemini 400-MHz spectrometer (400 MHz for ^1H , 100.57 MHz for ^{13}C , and 161.9 MHz for ^{31}P). The samples were dissolved in deuterated chloroform, and ^1H NMR, ^{13}C NMR, and ^{31}P NMR spectra were obtained at room temperature using TMS and H_3PO_4 as the internal standard. ^{31}P MAS NMR spectra were performed on a Varian Gemini 400 MHz spectrometer at a 161.9 MHz resonate frequency, with the MAS technique. The samples were ground into fine powder. The FTIR spectra were recorded on a Bomem Michelson MB 100 FTIR spectrophotometer with a resolution of 4 cm^{-1} in the absorbance mode. An attenuated-total-reflection

(ATR) accessory with thermal control and a diamond crystal (Golden Gate heated single-reflection diamond ATR, Specac-Teknokroma) was used to determine FTIR spectra.

Calorimetric studies were carried out on a Mettler DSC821e thermal analyzer with N₂ as the purge gas. The heating rate was 10 °C/min. Thermal stability studies were carried out on a Mettler TGA/SDTA851e/LF/1100 with N₂ as the purge gas at scanning rates of 10°C/min.

Mechanical properties were measured with a dynamic mechanical thermal analyzer (DMTA) (TA DMA 2928). Specimens with dimensions of 2 mm x 5 mm x 10 mm were tested in a three point bending configuration. The various thermal transitions were studied between -100 and 150 °C at a heating rate of 5 °C/min and at a fixed frequency of 1 Hz.

LOI values were measured on a Stanton Redcroft, provided with an Oxygen Analyzer, on polymer bars that measured 100 x 6 x 4 mm³ and which were prepared by molding. The char produced by the samples was characterized by ³¹P MAS NMR spectroscopy.

Degradation studies were carried out in a Carbolite TZF 12/38/400 oven connected to a condenser cooled by liquid nitrogen. GC-MS measurements were carried out using an HP 6890 gas chromatograph with an Ultra 2 capillary column (crosslinked 5% PH ME siloxane) and an HP 5973 mass detector.

Scanning electron microscopy (SEM) was performed on a JEOL JSM 6400 scanning electron microscope, at an activation voltage of 10 kV. For the atomic mapping, an Oxford INCA Energy Dispersive X-Ray Micro Analyzer was used.

RESULTS AND DISCUSSION

DOPO-I was synthesized from DOPO and *p*-benzoquinone in THF by a method described in the literature (Scheme 2).¹⁶ The chemical structure of DOPO-I was confirmed by FTIR, ¹H, ¹³C and ³¹P NMR spectroscopies.

DOPO-III was synthesized in two steps (Scheme 2). The hydroxyl groups of DOPO-I were esterified with 10-undecenoyl chloride to obtain DOPO-II. The chemical structure of DOPO-II was confirmed with spectroscopic techniques (FTIR, ¹H NMR, ¹³C NMR, and ³¹P NMR) and elemental analysis. The ¹H NMR and ¹³C NMR spectra were assigned by bidimensional NMR experiments (gHSQC, gCOSY, and gHMBC). In the subsequent step, DOPO-II was epoxidized with MCPBA in the presence of a small amount of a radical inhibitor (3-*tert*-butyl-4-hydroxy-5-methylphenylsulphide), which prevents the peracid from thermally decomposing.¹⁸ DOPO-III was obtained in a good yield and characterized by spectroscopic techniques. DOPO-III shows characteristic bands in the FTIR spectrum. The absorption peak at 832 cm⁻¹ confirms the existence of the oxirane ring in the compound. Furthermore, peaks at 1120 cm⁻¹ (P-O-Ph), 1594 cm⁻¹ (P-Ph), 1210 cm⁻¹ (P=O), 1766 cm⁻¹ (C=O), 2926 and 2854 cm⁻¹ (-CH₂-) appear.

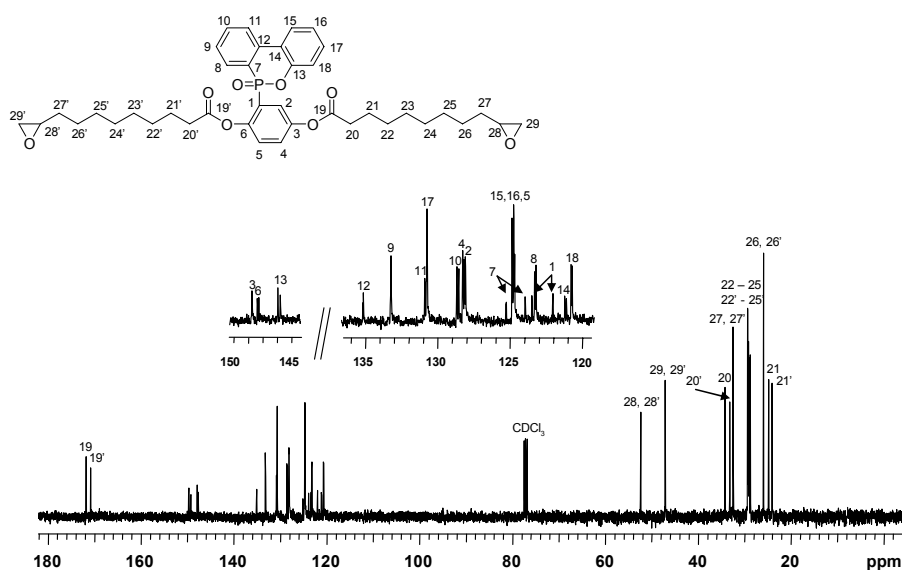


Figure 2. ^{13}C NMR spectrum of DOPO-III (CDCl_3 , 100.57 MHz).

Figures 1 and 2 show ^1H and ^{13}C NMR spectra with all the assignments corresponding to the expected signals. In the ^1H NMR spectrum, aromatic protons appeared at 7.1–8.1 ppm. The $\text{H}_{29'}$, H_{29} and H_{28} of the oxirane ring were assigned at 2.46 ppm (1H, m), 2.74 ppm (1H, t), and 2.90 ppm (1H, m), respectively. As can be seen in Figure 1, the chemical shift of $-\text{CH}_2-\text{CH}_2-\text{C}(\text{O})-$ protons of two side groups are quite different. One possible reason for these unusual chemical shifts is the ring current effect that arises when protons $\text{H}_{20'}$ and $\text{H}_{21'}$ are positioned below the pendent aryl phosphinate group.¹⁹ The resonance lines in the ^{13}C NMR spectrum fall into three main regions: 24.1–54.3 ppm for the aliphatic carbons, 120.8–149.8 ppm for the aromatic carbons, and approximately 170 ppm for the carbonyl carbons of the ester groups.

In this study, the DOPO-III was crosslinked with DDM and BAMPO as hardeners and borontrifluoride-ethylamine complex ($\text{BF}_3 \cdot \text{MEA}$) as accelerator. First, the curing reaction between DOPO-III and DDM in the absence of $\text{BF}_3 \cdot \text{MEA}$ was studied by dynamic DSC. The DSC plot shows two exothermic peaks at about 170 and 300 °C, which indicates that there are at least two reactions [Fig. 3(a)]. The higher temperature DSC peak is associated with the addition reaction of the primary and secondary amines to the epoxy groups, while the peak at about 180 °C is associated with the amidation reaction. This reaction takes place by nucleophilic attack of the amine curing agent on the ester carbonyl group, leading to the fatty amide and the phenol derivative. The DSC plot was similar in the curing of DOPO-III with BAMPO [Fig. 3(b)].

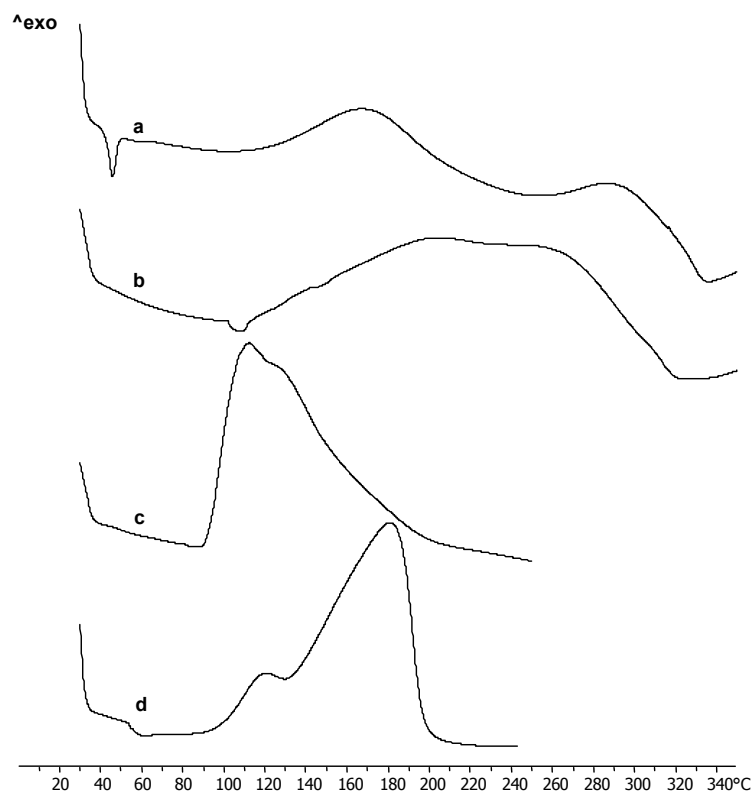


Figure 3. DSC plots (10 °C/min) of DOPO-III cured with DDM (a), BAMPO (b), DDM (1 mol % $\text{BF}_3 \cdot \text{MEA}$) (c), and BAMPO (1 mol % $\text{BF}_3 \cdot \text{MEA}$) (d).

Figure 4 shows the FTIR spectra of the final products after DSC treatment. The FTIR spectra of the products obtained in the absence of $\text{BF}_3 \cdot \text{MEA}$ [Figs. 4 (a,b)] show absorptions at 1688 and 1543 cm^{-1} , which were assigned to the amide group. ^{13}C NMR analysis of the soluble product after it had been heated to 250 °C showed a new carbonyl signal attributable to the amide moiety at 172.3 ppm. The appearance of the signal corresponding to the phenol in the ^1H NMR spectra also supports this evidence.

To prevent the amidation reaction, lower reaction temperatures would be desirable. The addition of $\text{BF}_3 \cdot \text{MEA}$ is known to have a strong accelerating effect on the amine epoxy reaction.²⁰⁻²² The mechanism of catalysis by $\text{BF}_3 \cdot \text{MEA}$ and related compounds on epoxy curing is still not fully understood. The DSC curing behaviors of DOPO-III/DDM and DOPO-III/BAMPO systems cured in the presence of 1 mol % $\text{BF}_3 \cdot \text{MEA}$ show that the exotherm shifts to lower temperature [Fig. 3(c,d)] and the temperatures of the maximum heat release rate are 112 and 181 °C, respectively. DDM, which has a lower

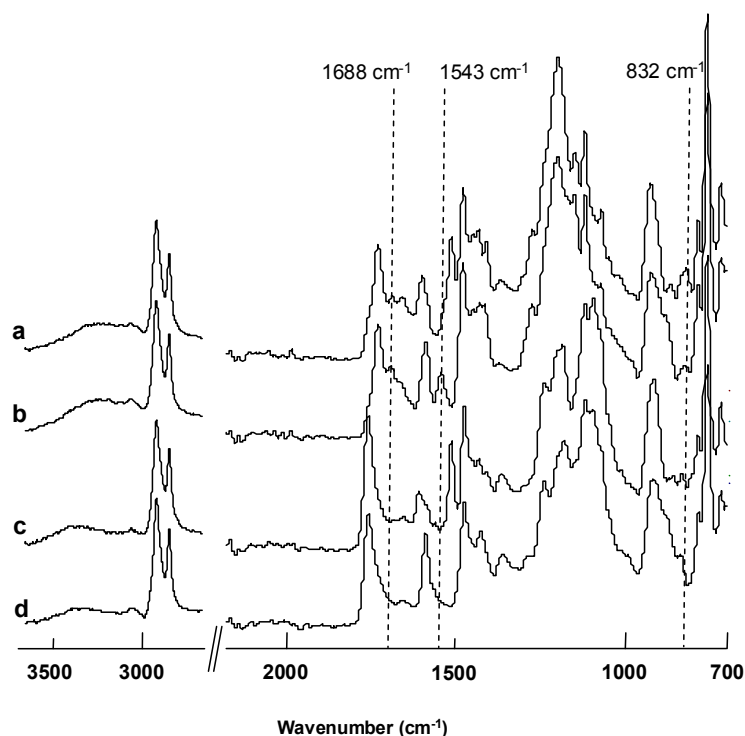


Figure 4. FTIR spectra of DOPO-III cured with DDM (a), BAMPO (b), DDM (1 mol % $\text{BF}_3 \cdot \text{MEA}$) (c), and BAMPO (1 mol % $\text{BF}_3 \cdot \text{MEA}$) (d) after DSC treatment (10 °C/min).

peak exothermic temperature under the same set of curing conditions, is more reactive toward the DOPO-III monomer. The fact that BAMPO is less reactive to DOPO-III than DDM is probably due to electronic effects. In the case of BAMPO, the electron-withdrawing group ($\text{P}=\text{O}$) reduced the electron density of the amine nitrogen and subsequently reduced its nucleophilicity.²³

As can be seen in Figure 4(c,d), when $\text{BF}_3 \cdot \text{MEA}$ is used as the accelerator, the FTIR spectra of the resulting products show that the absorption at 832 cm^{-1} , corresponding to the oxirane ring, completely disappeared, so the

desired reaction between the amino group and the oxirane ring takes place. The amidation process seems not to take place because the absorption corresponding to the amide group does not appear.

According to DSC data, the network from DOPO-III/DDM was prepared by curing at 100 °C for 90 min and postcuring at 150 °C for 60 min. The thermoset from DOPO-III/BAMPO was obtained by curing at 150 °C for 90 min and postcuring at 180 °C for 60 min.

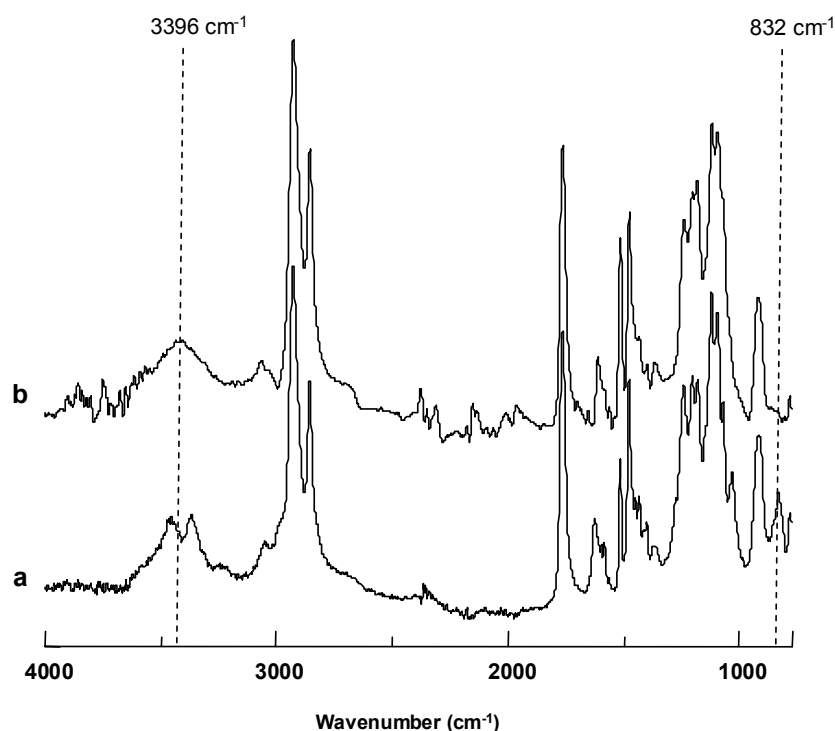


Figure 5. FTIR of DOPO-III thermoset before (a) and after (b) isothermal crosslinking. Curing at 100 °C for 90 min and postcuring at 150 °C for 60 min.

The isothermal crosslinking reaction was monitored by FTIR spectroscopy. Figure 5 shows the FTIR spectra before (a) and after (b) the curing of the DOPO-III/DDM thermoset. The initial mixture had a characteristic band at 832 cm^{-1} ascribed to C-O-C stretching of the oxirane moiety. After curing, this band completely disappeared. The crosslinking reaction could also be seen because the bands associated to the N-H bond (3400-3500 cm^{-1}) of the amine group disappeared. Furthermore, a band appeared at 3396 cm^{-1} because of -OH stretching of the resulting crosslinked moiety. As has been previously described,²⁴ epoxides are susceptible to homopolymerization in the presence of cationic initiators

such as $\text{BF}_3 \cdot \text{MEA}$ and form a polyether backbone. FTIR spectra show that etherification does not take place because the absorption around 1100 cm^{-1} (ether backbone) does not change significantly.

Table 1. Thermal Properties of the Cured Thermosets

	T_{max} (°C) ^a	T_g (°C)		
		$1/2 \Delta C_p$	E''_{max}	$\tan \delta_{\text{max}}$
DOPO-III/DDM	112	98	88	108
DOPO-III/BAMPO	181	91	78	95

^a Temperature of the maximum of the crosslinking exotherm (10 °C/min).

The thermal behavior of the materials obtained was investigated by DSC. The glass transition temperatures (T_g s) of

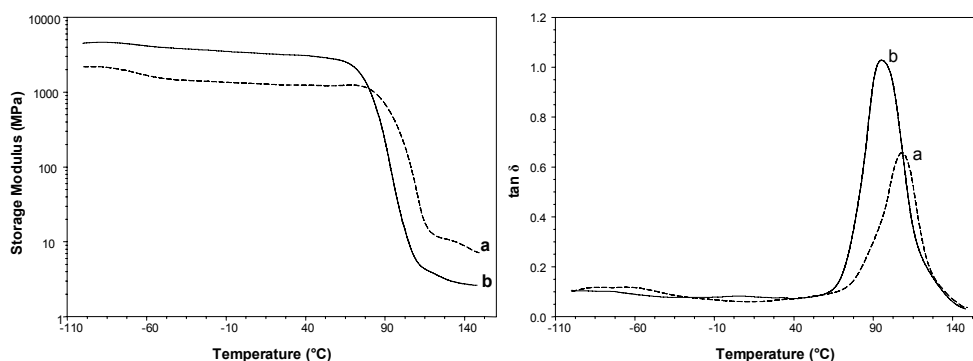


Figure 6. Storage modulus and loss factor ($\tan \delta$) for DOPO-III/DDM (a) and DOPO-III/BAMPO (b) as a function of temperature.

the cured materials are listed in Table 1.

The dynamic mechanical behaviour of the prepared materials was obtained as a function of the temperature beginning in the glassy state to the rubbery plateau of each material. Figure 6 shows how the storage (E') modulus changes with temperature for the DOPO-III materials. The crosslinking density can be estimated from the equilibrium storage (E') modulus using the theory of rubber elasticity.²⁵ Although this theory is strictly valid only for rubbers with light crosslinks, it can still be used to provide an approximate measure of the level of crosslinking in highly crosslinked materials. As can be seen, the crosslink density was lower when BAMPO was used as the hardener, which may be because of its lower reactivity. DMTA also makes it possible to determine the T_g of the crosslinked materials. It is detected as the maximum of the loss factor, $\tan \delta$. Figure 6 shows the $\tan \delta$ plots of the DOPO-III/DDM and DOPO-III/BAMPO materials and Table 1 shows the T_g values determined by DMTA. As expected, the T_g values from

$\tan \delta$ are higher than from DSC and as can be seen T_g values from DMTA follow the trend mentioned earlier. Moreover, the analysis of the height and width of the α relaxation peak shows trends in the crosslinking densities and network homogeneities. The lower height of the $\tan \delta$ peak for the DOPO-III/DDM thermoset is indicative of lower segmental mobility and a more crosslinked network. The width of the $\tan \delta$ peaks reflects the structural homogeneity of the crosslinked networks. The broadening of the glass transition region in the DOPO-III/BAMPO network could be due to an increasing number of branching modes and a wider distribution of structures. The $\tan \delta$ plots displayed a β relaxation at approximately -60 °C. This β transition, which is generally observed in amine-crosslinking epoxy resins, can be assigned to the motion of $[-CH_2-CH(OH)-CH_2-]$ aliphatic segments from the ring opening of the epoxide.²⁶

To determine the thermal stability and decomposition behaviour, TGA was carried out under nitrogen and air atmospheres. Figure 7 shows TGA

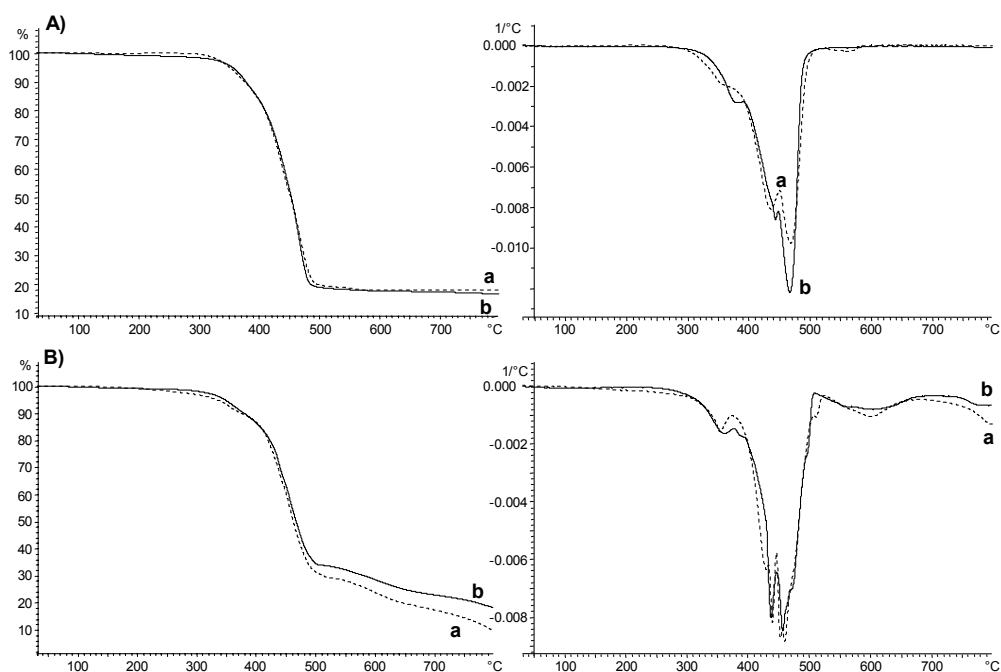


Figure 7. TGA plots (10 °C/min) and first derivative curves of crosslinked polymers DOPO-III/DDM (a) and DOPO-III/BAMPO (b) under nitrogen (A) and air (B) atmospheres.

curves and the first derivative curves. Table 2 summarizes the TGA data for weight loss with temperature for both epoxy compositions. As can be seen, the temperature of 10% weight loss does not change significantly with both amines. The shape of the derivative curves shows that the degradation takes place in a broad temperature

range and three degradation steps can be observed. The phosphorous content seems to have no influence on the degradation. Under air, a fourth step in the weight loss rate appears at higher temperatures, above 500 °C, corresponding to the thermooxidative degradation.

Table 2. Thermogravimetric Data and LOI Values for the Cured Thermosets

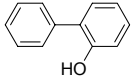
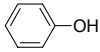
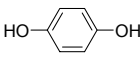
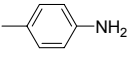
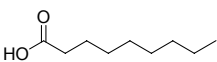
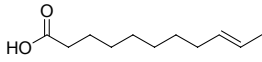
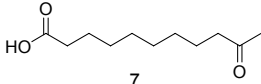
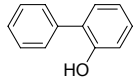
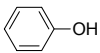
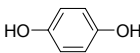
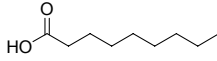
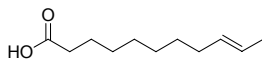
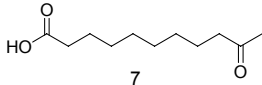
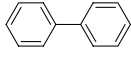
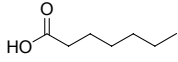
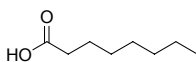
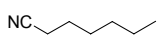
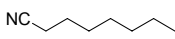
	P(%)	TGA (N ₂ Atmosphere)			TGA (Air Atmosphere)			LOI
		T _{10% loss} (°C) ^a	T _{max} (°C) ^b	Yield _{800°C} (%) ^c	T _{10% loss} (°C) ^a	T _{max} (°C) ^b	Yield _{800°C} (%) ^c	
DOPO-III/DDM	3.9	375	468, 435	18	374	458, 439	10	31
DOPO-III/BAMPO	5.7	377	467, 440	16	378	455, 435	18	32

^a Temperature of 10% of weight loss.

^b Temperature of the maximum weight loss rate.

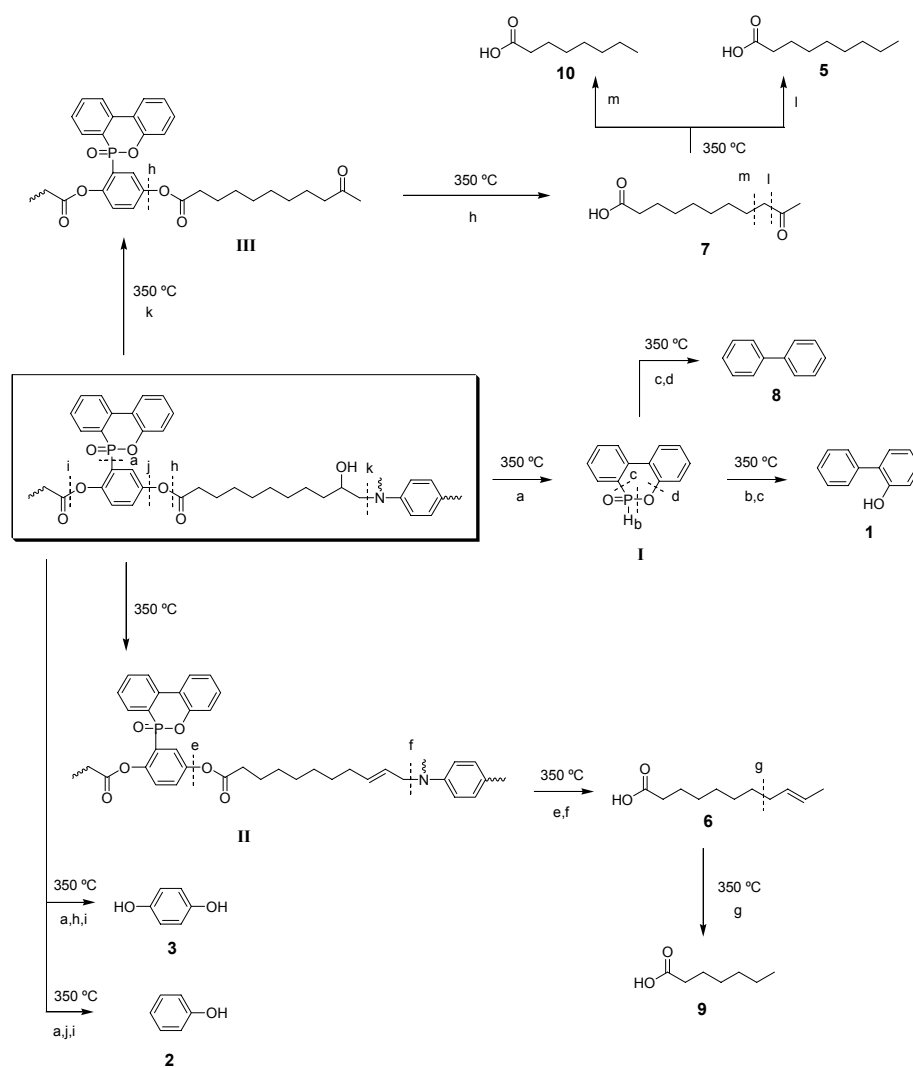
^c Char yield at 800 °C.

Table 3. Gaseous Products of Polymers DOPO-III/DDM and DOPO-III/BAMPO in Degradation-GC/MS at 350 °C

Polymer	Compound			
DOPO-III/DDM				
	1	2	3	4
				
	5	6		
				
	7			
DOPO-III/BAMPO				
	1	2	3	
				
	5	6		
				
	7	8		
				
	9	10		
				
	11	12		

Char yields for both resins are not significantly different under nitrogen. Under air, the char yield increases with the phosphorous content.

To further investigate the thermal degradation mechanism, samples were heated in an oven at 350 °C for 3 h with nitrogen or air as the purge gas.



Scheme 3

The degradation temperature was selected from dynamical TGA data and the time at which no weight loss was detected at 350 °C in an isothermal TGA experiment was selected as the degradation time. Volatile products were trapped at the liquid nitrogen temperature and subsequently analysed by GC/MS.

Table 3 lists the gaseous degradation products that have been identified for polymers DOPO-III/DDM and DOPO-III/BAMPO. It can be seen that these gaseous fragments mainly come from the cleavage of $-\text{CH}_2-\text{CH}(\text{OH})-\text{CH}_2-\text{N}$, ester linkages, and DOPO degradation. On the basis of these results, the proposed degradation mechanisms of

DOPO-III/DDM and DOPO-III/BAMPO are presented in Scheme 3. The release of 2-phenylphenol (1) and biphenyl (8) at 350 °C indicates the degradation at the pendant DOPO groups. These results are consistent with literature studies that show that DOPO derivatives undergo P-C cleavage (a) to give DOPO (I), which further degrade (cleavages b and c) to form 2-phenylphenol (1). Biphenyl (8) can also evolve from DOPO by P-C and O-C cleavage bonds (c and d).²⁷

The thermal decomposition of epoxy resins starts when secondary alcohols dehydrate to form allyl amines (II) with C-N bonds that are thermally less stable than the original C-N bonds and chain scission mostly occurs at this position (f).¹² If a homolytic scission of C-N bonds takes place, followed by termination of the radicals by hydrogen abstraction, compound 6 is formed. Product 6 can continue to degrade by allylic chain scission (g) to form 9. As was shown in the literature,¹² the dehydration of secondary alcohol groups is the source of the water that is the major gas evolved when epoxy formulations are heated. This water attacks polymer chains, which leads to the hydrolysis of ester linkages and a splitting of the molecular chain, which in turn produces a carboxylic acid and a phenol group for each bond broken. The hydrolysis of the ester linkage (h,i) gave 4-hydroxyphenol (3), although the formation of phenol (2) suggested that homolytic scission of the C-O bond (j) also occurred. If C-N bond scission (k) occurred before the secondary alcohols dehydrated, III is formed. The cleavage of ester linkages (h) gave 7, which was further thermally

degraded to yield 1-nonanoic (5) and 1-octanoic acids (10) by losing ketene (l) or acetone (m). The presence of nitrile derivatives (11 and 12, Table 3) was only observed in the degradation products of the DOPO-III/BAMPO polymer. The formation of these nitrile derivatives could be explained by the appearance of ammonia in the thermal degradation of BAMPO-cured epoxy resins.²⁸ Moreover, *p*-toluidine (4, Table 3) was observed in the degradation products of the DOPO-III/DDM polymer.

The solid residues of pyrolyzed polymers were characterized by FTIR spectroscopy. FTIR spectra of the solid residues of DOPO-III/DDM under air or nitrogen showed no significant differences. The disappearance of bands due to OH stretching (3402 cm^{-1}) and C-OH (1095 cm^{-1}) corroborates the dehydration process. As a result of the ester bond cleavage, the band at 1760 cm^{-1} also disappeared. The fact that there are considerably fewer aliphatic groups is evident from the decrease in the intensity of the bands at $2980\text{--}2850\text{ cm}^{-1}$, and the increase in the concentration of the aromatic structures. Moreover, the disappearance of the band at 1118 cm^{-1} attributed to the P-O-Ph bond confirms the degradation of the DOPO moiety. The presence of P in the residue can be seen from the bands at 1473 and 1198 cm^{-1} , corresponding to the P-Ph and P=O bonds, respectively. FTIR spectra of residues from BAMPO show no significant differences, which means that the degradation of this resin is similar to the degradation of DOPO-III/DDM.

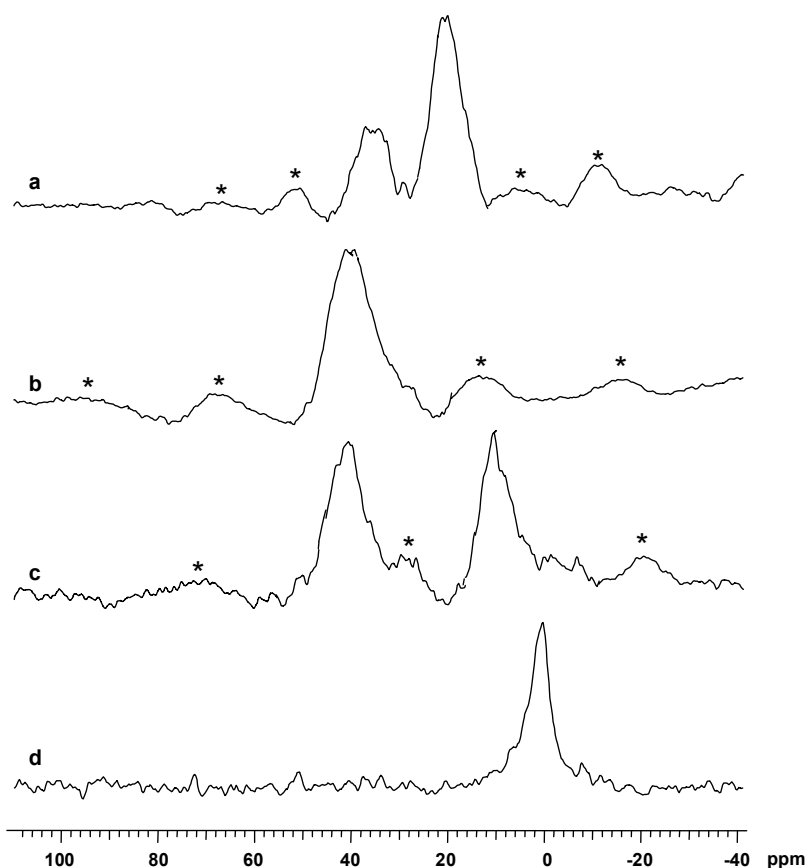


Figure 8. ^{31}P MAS NMR spectra of initial DOPO-III/BAMPO thermostet (a), solid products collected after degradation in an oven at 350 °C for 3 h under nitrogen (b) and air (c) as the purge gas and char after LOI test (d). Spinning bands are marked with *.

The solid residues of pyrolyzed polymers were also characterized by ^{31}P MAS NMR spectroscopy (Fig. 8). The spectrum of the initial DOPO-III/BAMPO resin shows two peaks at 35 and 20 ppm, which can be attributed to P atoms in the BAMPO²⁸ and DOPO structures, respectively [Fig. 8(a)]. The spectra of residues after being thermally treated under nitrogen [Fig. 8(b)] show a broad peak which is centred at 40 ppm and attributed to P-C bonds. However, under air atmosphere

[Fig. 8(c)] a second peak of similar intensity appears at 10 ppm, which indicates the existence of P-O bonds. Moreover, the presence of phosphoric acid is shown by peak tailing at 0 ppm.

We used the LOI to test the flame retardancy of the synthesized materials. LOI measures the ease of extinction of materials, and is the minimum percentage of oxygen in an oxygen/nitrogen atmosphere that will just sustain combustion in a candle-like configuration

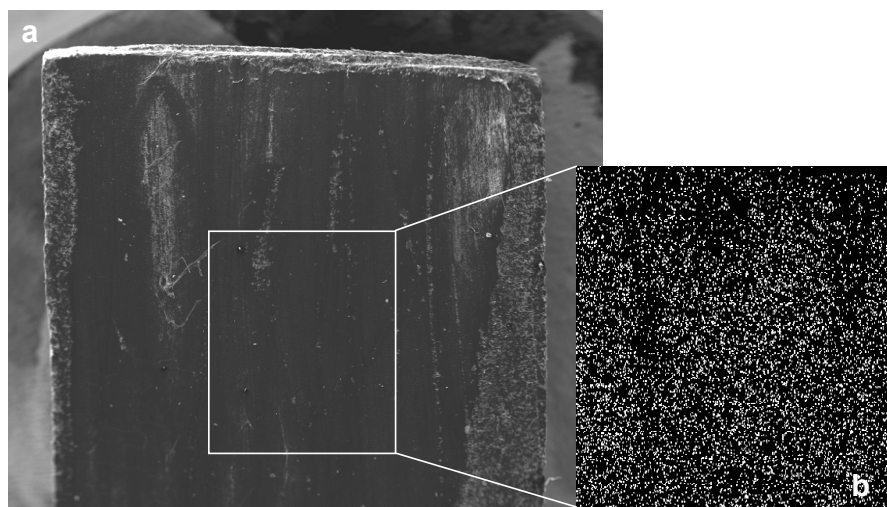


Figure 9. SEM (a) and SEM-EDX P mapping (b) micrographs of DOPO-III/BAMPO specimen before LOI test.

of a top-ignited vertical test specimen. LOI values of 31 and 32 were found for DOPO-III/DDM and DOPO-III/BAMPO thermosets, which indicated good flame-retardant properties.

To better understand the role of phosphorous in the flame-retardant properties of the polymer, element mapping was performed with energy-dispersive X-ray spectroscopy (EDX) on the surfaces of the initial samples and of the samples after the LOI test.

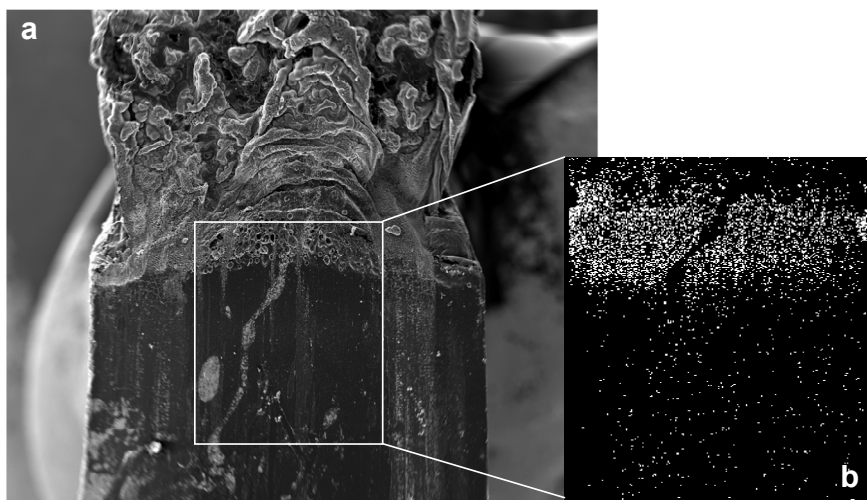


Figure 10. SEM (a) and SEM-EDX P mapping (b) micrographs of DOPO-III/BAMPO specimen after LOI test.

P mapping of the DOPO-III/BAMPO initial sample indicated a homogeneous distribution of this element, as can be observed in the micrograph (Fig. 9). The white points in the figure denote P atoms. After burning, the presence of phosphorous in the char was confirmed by ^{31}P MAS NMR spectroscopy. Figure 8 d) shows a broad peak at 0 ppm typical of phosphoric acid. Figure 10 a) is the SEM micrograph of the top surface view of the DOPO-III/BAMPO specimen after the LOI test. The burned zone has the appearance of a black charred material with small cavities. The P distribution [Fig. 10(b)] shows that the phosphorous density increased towards the top burned surface and that a phosphorous-rich layer formed. When they are heated, phosphorous compounds can form glass-like polyphosphoric acid, which protects the burning surface, or they can form inflammable phosphorous-carbon char by reacting with organic components. This protective layer is resistant to even higher temperatures and shields the underlying polymer from attack by oxygen and radiant heat as well as prevents the combustible gases from transferring to the surface of the materials and feed the flame, thus improving the fire resistance.

Acknowledgements

The authors gratefully acknowledge the CICYT (Comisión Interministerial de Ciencia y Tecnología) (MAT2005-01593) for financial support for this work and the DURSI (Departament d'Universitats, Recerca i Societat de la Informació) and Fons Social Europeu for G. Lligadas' predoctoral (2003FI00765)

grant. We would like to thank R. Guerrero for ^{31}P MAS NMR analysis, C. Crespo for GC-MS measurements and M. Moncusí for SEM analysis.

REFERENCES AND NOTES

1. (a) Baumann, H.; Bühler, M.; Fochem, H.; Hirsinger, F.; Zoblein, H.; Falbe, J. *Angew Chem, Int Ed Engl* 1988, 27, 41; (b) Biermann, U.; Friedt, W.; Lang, S.; Lühs, W.; Machmüller, G.; Metzger, J. O.; Klaas, M. R.; Schäfer, H. J.; Schneiderüs, M. P. *Angew Chem Int Ed* 2000, 39, 2206.
2. Tsujimoto, T.; Uyama, H.; Kobayashi, S. *Macromolecules* 2004, 37, 177.
3. Khot, S. N.; LaScala, J. J.; Can, E.; Morye, S. S.; Williams, G. I.; Palmese, G. R.; Küseföglu, S. H.; Wool, R. P. *J Appl Polym Sci* 2001, 82, 703.
4. Andjelkovic, D. D.; Valverde, M.; Henna, P.; Li, F.; Larock, R.C. *Polymer* 2005, 46, 9674.
5. Esen, H.; Küseföglu, S. H. *J Appl Polym Sci* 2003, 89, 3882.
6. Guo, A.; Javni, I.; Petrovic, Z. S. *J Appl Polym Sci* 2000, 77, 467.
7. (a) Lligadas, G.; Ronda, J. C.; Galià, M.; Biermann, U.; Metzger, J. O. *J Polym Sci Part A: Polym Chem* 2006, 44, 634; (b) Tsujimoto, T.; Uyama, H.; Kobayashi, S. *Macromol Rapid Commun* 2003, 24, 12; (c) Bunker, S. P.; Wool, R. P. *J Polym Sci Part A: Polym Chem* 2002, 40, 451; (d) Warwel, S.; Rüschen, Klaas, M.; Schier, H.; Brüse, F.; Wiege, B. *Eur J Lipid Sci Technol* 2001, 103, 645.
8. Eren, T.; Küseföglu, S. H. *J Appl Polym Sci* 2004, 91, 2700.
9. Jain, P.; Choudhary, V.; Varma, I. K. *J Macromol Sci Polym Rev* 2002, 42, 139.
10. Hörold, S. *Polym Deg Stab* 1999, 64, 427.
11. Saito, T. U.S. Patent 3, 702,878, 1972.

12. Levchik, S. V.; Weil, E. D. *Polym Int* 2004, 53, 1901.
13. Wu, C. S.; Liu, Y. L.; Chiu, Y. S. *J Appl Polym Sci* 2002, 5, 2254.
14. Shan, W. C.; Hsuan, L. C. *Polymer* 1999, 40, 4387.
15. Espinosa, M. A.; Cádiz, V.; Galià, M. J. *J Polym Sci Part A: Polym Chem* 2004, 42, 279.
16. Chin, W. K.; Hsueh, M. D.; Tsai, W. C. *J Polym Sci Part A: Polym Chem* 1995, 33, 373.
17. Varma, I. K.; Gupta, U. J. *Macromol Sci A: Chem* 1986, 23, 19.
18. Kishi, Y.; Aratani, M.; Tanino, H.; Fukuyama, T.; Goto, T.; Inoue, S.; Sugiura, S.; Kakoi, H. *J Chem Soc, Chem Commun* 64, 1972.
19. Cho, C. S.; Chen, L. W.; Fu, S. C.; Wu, T.-R. *J Polym Res* 1998, 5, 59.
20. Morgan, R. J.; Walkup, C. M.; Hoheisel, T. H. *J Appl Polym Sci* 1985, 30, 289.
21. Jagadeesh and Siddaramaiah, K. S. *J Appl Polym Sci* 1991, 43, 1459.
22. Juangvanich, N.; Stoffer, J. *Polym Prepr (Am Chem Soc Div Polym Chem)* 2002, 43, 22.
23. Mercado, L. A.; Ribera, G.; Galià, M.; Cádiz, V. *J Polym Sci Part A: Polym Chem* 2006, 44, 1676.
24. May, C. A. *Epoxy Resins: Chemistry and Technology*; Marcel Dekker, Inc., New York, 1998.
25. Tobolsky, A. V.; Carlson, D. W.; Inductor, N. J. *J Polym Sci* 1961, 54, 2156.
26. Heux, L.; Halary, J. L.; Lauprêtre, F.; Monnerie, L. *Polymer*, 1997, 38, 1767.
27. Guo, W.; Leu, W. T.; Hsiao, S. H.; Liou, G. S. *Polym Degrad Stab* 2006, 91, 21.
28. Levchik, S. V.; Camino, G.; Luda, M. P.; Costa, L.; Muller, G.; Costes, B. *Polym Deg Stab* 1998, 60, 169.

3.4.2 Development of Novel Phosphorus-Containing Epoxy Resins from Renewable Resources

DEVELOPMENT OF NOVEL PHOSPHORUS-CONTAINING EPOXY RESINS FROM RENEWABLE RESOURCES

G. Lligadas, J.C. Ronda, M. Galià, V. Cádiz
Departament de Química Analítica i Química Orgànica, Universitat Rovira i Virgili,
Campus Sescelades, Marcel·lí Domingo s/n, 43007 Tarragona, Spain.

ABSTRACT: Novel biobased epoxy resins were prepared from two fatty acid derivatives; epoxidized 10-undecenoyl triglyceride and epoxidized methyl 3,4,5-tris(10-undecenoyloxy)benzoate, with 4,4'-diaminodiphenylmethane as a crosslinking agent. The flame retardancy of these epoxy resins was improved by the addition of 10-[2',5'-bis(9-oxiranyl-nonanoyloxy)phenyl]-9,10-dihydro-9-oxa-10-phosphaphenanthrene-10-oxide and by crosslinking with a phosphorus-containing curing agent, bis(*m*-aminophenyl) methylphosphine oxide. The thermal, thermomechanical, and flame-retardant properties of the cured materials were measured with differential scanning calorimetry, thermogravimetric analysis, dynamic mechanical thermal analysis, and limiting oxygen index.

Keywords: epoxidized vegetable oils; epoxy resins; flame retardance; renewable resources

INTRODUCTION

Polymeric materials from renewable resources have attracted considerable interest in recent years.¹ The growing demand for petroleum-based products and the resulting negative impact on the environment, plus the scarcity of nonrenewable resources, are just a few of the many factors that have encouraged the scientific community to find more sustainable and environmentally responsible solutions for these problems. Furthermore, polymers based on biore-

newable resources have often been shown to possess properties comparable to or better than those of widely used industrial polymers. As such, they show promise as replacements for petroleum-based plastics, thus reducing waste and preserving petroleum reserves.

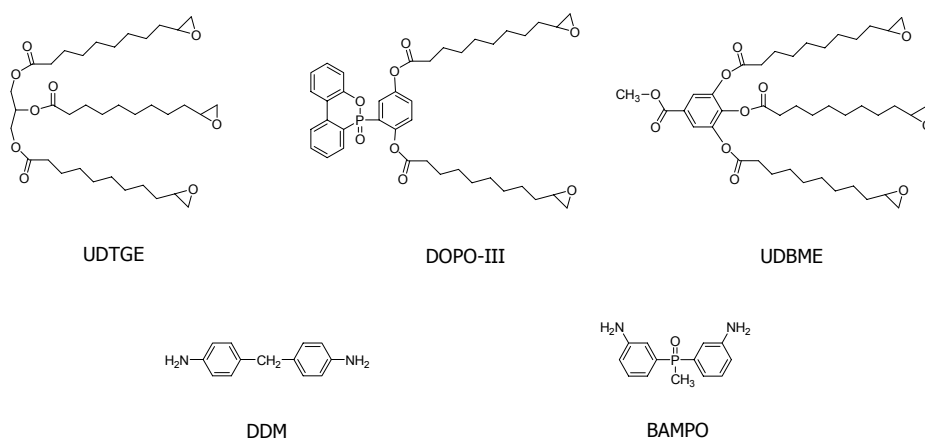
Triglyceride vegetable oils are a major class of such resources and are now being used in an increasing number of industrial applications, in addition to being a food source for human beings.²

The main components of these triglyceride oils are saturated and unsaturated fatty acids. Although they have double bonds, which are used as reactive sites in coatings, they cannot be converted easily to high-molecular-weight products without the introduction of more reactive functional groups, such as hydroxyl, epoxy, or carboxyl groups. Various chemical pathways for functionalizing triglycerides and fatty acids have been studied.³ Epoxidation is one of the most important functionalization reactions of C-C double bonds, and opening up the epoxide ring leads to numerous products.³⁻⁵ Epoxidized vegetable oils are extremely promising as inexpensive, renewable materials for industrial applications. Recently,⁶ there have been attempts to find new uses for these epoxy resources, which share many of the characteristics of conventional epoxy thermosets. Among them, terminal epoxy fatty acid derivatives provide good reactivity with amines. Materials based on epoxidized 10-undecenoyl triglyceride, which have possible applications to composites, adhesives, and coatings, have shown tensile moduli and elongations similar to those of diglycidyl ether of bisphenol A/amine systems and excellent UV stability.

Triglycerides are made up of aliphatic chains; triglyceride-based materials do not have the rigidity and strength required for some applications.³ Moreover, like other organic polymeric materials, the flammability of these materials is a shortcoming in some applications. Although the synthesis of flame-retardant epoxy resins has been widely studied, few studies have been conducted with vegetable oils and fatty

acids as starting materials. Castor oil and brominated castor oil have been added as reinforcing agents to epoxy resins, leading to good toughness and flame retardancy of the cured epoxy resins.⁷ Moreover, Eren and Küseföglü reported the synthesis and characterization of flame-retardant polymers from bromoacrylated plant oil triglycerides.⁸ Halogen-containing resins are not well received nowadays because they release highly toxic and corrosive fumes during combustion. The concept of sustainable development requires the development of fire-retardant technologies that have minimum impact on health and the environment throughout the life cycle of the fire-retardant material, that is, its synthesis, fabrication, use, recycling, and disposal.

Phosphorus-containing polymers are well recognized for their flame-retardant properties,⁹ and they are becoming more popular than their halogen counterparts, as they generally give off nontoxic combustion products. They can form a carbonaceous char during combustion, which acts as a physical barrier to insulate heat from the flame and to prevent the diffusion of combustible gases.¹⁰ In the search for new environmentally friendly flame-retardant polymeric materials, we recently reported the synthesis and characterization of biobased epoxy resins from a new diepoxy fatty compound 10-[2',5'-bis(9-oxiranyl-nonanoyloxy)phenyl]-9,10-dihydro-9-oxa-10-phosphaphenanthrene-10-oxide (DOPO-III; Scheme 1).¹¹ The crosslinking of DOPO-III with 4,4'-diaminodiphenylmethane (DDM) and bis(*m*-aminophenyl)methylphosphine oxide (BAMPO)



Scheme 1

led to materials with increased limiting oxygen indices (LOIs) of 31 and 32, respectively.

In an attempt to find new biobased epoxy resins, we report the synthesis and characterization of epoxidized 10-undecenoyl triglyceride (UDTGE) and epoxidized methyl 3,4,5-tris(10-undecenoyloxy)benzoate (UDBME; Scheme 1) and their crosslinking with DDM. This article also presents research that seeks to improve the flame-retardant properties of these biobased resins either by addition of DOPO-III as reactive flame retardant or by crosslinking with a phosphorus-containing curing agent (BAMPO). The properties of the prepared materials were evaluated with differential scanning calorimetry (DSC), thermogravimetric analysis (TGA), dynamic mechanical analysis (DMTA) and LOI.

EXPERIMENTAL

Materials

The 10-undecenoyl triglyceride (UDTG; iodine value = 120) and 9,10-dihydro-9-oxa-10-phosphaphenanthrene-10-oxide (DOPO) were supplied by Dow Chemical and Aismalibar S.A., respectively. The following chemicals were obtained from the sources indicated; *m*-chloroperbenzoic acid, 10-undecenoyl chloride, methyl trioctylammonium chloride (from Fluka); tungstic acid, hydrogen peroxide (32%), hydrazine monohydrate, boron trifluoride/ethylamine complex (BF₃·MEA), methyl 3,4,5-trihydroxybenzoate, *p*-benzoquinone, DDM, methyldiphenylphosphine oxide, 3-*tert*-butyl-4-hydroxy-5-methylphenyl sulphide (from Aldrich); and orthophosphoric acid (84%), sulfuric and nitric acids (from Prolabo).

Tetrahydrofuran was distilled from sodium/benzophenone immediately before use. Other solvents were purified with standard procedures.

Methyl 3,4,5-tris(10-undecenoxy)benzoate (UDBM) was prepared by a procedure described previously.¹² DOPO-III was synthesized in our laboratory according to published procedure.¹¹ BAMPO was synthesized as described elsewhere.¹³

Synthesis of Quaternary Ammonium Tetrakis(diperoxotungsto) Phosphate (3-)¹⁴



A suspension of tungstic acid (2.5 g, 10 mmol) in 7 mL of 32% aqueous H₂O₂ was stirred and heated to 60 °C until a colorless solution was obtained. To this solution, filtered and cooled to room temperature, 40% (w/v) H₃PO₄ (0.62 mL, 2.5 mmol) was added, and the whole was diluted to 30 mL with water. To the resultant solution, 2.09 g of methyl trioctylammonium chloride (97% pure, equivalent to 2.027 g, 5 mmol) in dichloromethane (40 mL) was added dropwise with stirring over about 2 min. Stirring was continued for an additional 15 min. The organic phase was then separated, dried over anhydrous magnesium sulphate, filtered, and dichloromethane was evaporated off to give 3.5 g (93% based on the quaternary ammonium salt charged) of colorless syrup.

Fourier transform infrared (FTIR; ν , cm⁻¹): 1088, 1066, and 1035 (P-O), 966 (W=O), 856 and 845 (O-O), 586

and 522 (W-O-O, asymmetric and symmetric).

Synthesis of UDTGE (Scheme 1)

UDTG (10 g, 16.9 mmol) and the epoxidation catalyst [quaternary ammonium tetrakis(diperoxotungsto) phosphate(3-); 0.2 g, 0.08 mmol] were placed in a 250-mL, three-necked flask equipped with a thermometer, dropping funnel, condenser, and magnetic stirrer. The temperature of the mixture was gradually brought to 60 °C, and 20 g of 16% hydrogen peroxide (47.2 mmol) was added dropwise. The resulting biphasic mixture was vigorously stirred for 23 h. The viscous organic layer, diluted with ethyl acetate, was washed with warm water to remove catalyst residues and traces of hydrogen peroxide. The organic phase was dried over anhydrous magnesium sulphate, and ethyl acetate was evaporated off. The obtained oil was purified with a silica gel column and with hexane/ethyl acetate (9:5) as the eluent. When the solvent was removed, 9.8 g of pure UDTGE (yield = 88%) was obtained as a viscous oil.

¹H NMR [CDCl₃/tetramethylsilane (TMS), δ , ppm]: 1.3-1.6 (m, 42H), 2.3 (t, 6H), 2.44 (m, 3H), 2.72 (t, 3H), 2.88 (m, 3H), 4.10-4.29 (m, 4H), 5.24 (m, 1H). ¹³C NMR (CDCl₃/TMS, δ , ppm): 24.94 (t), 24.98 (t), 26.09 (t), 29.15 (t), 29.18 (t), 29.28 (t), 29.30 (t), 29.48 (t), 29.50(t), 32.61 (t), 34.14 (t), 34.30 (t), 47.26 (t), 52.52 (d), 62.23 (t), 68.99 (d), 172.99 (s), 173.40 (s).

Table 1. Epoxy Resin Compositions and Curing Data

Sample	Epoxy Monomer	Molar Ratio	Curing Agent	% P	T _{max} ^a	Curing Temperature (°C) ^b	Postcuring Temperature (°C) ^c
1	UDTGE	-	DDM	0	107/117	100	140
2	UDTGE/DOPO-III	1/1	DDM	1.8	106/126	100	140
3	UDBME	-	DDM	0	108/121	90	160
4	UDBME/DOPO-III	1/1	DDM	1.9	110/122	90	160
5	UDBME	-	BAMPO	2.5	117/171	150	180

^a Temperature of the maximum of the crosslinking exotherm (10 °C/min).

^b Curing time = 90 min.

^c Postcuring time = 60 min.

Synthesis of UDBME (Scheme 1)

UDBME was obtained from UDBM by the procedure described previously and purified with silica gel column and hexane/ethyl acetate (2:1) as the eluent. When the solvent was removed, 9.8 g of pure UDBME (yield = 92%) was obtained as viscous oil.

¹H NMR (CDCl₃/TMS, δ, ppm): 1.31-1.53 (m, 36H), 1.68 (m, 6H), 2.44 (m, 3H), 2.49 (t, 6H), 2.72 (t, 3H), 2.88 (m, 3H), 3.90 (s, 3H), 7.75 (s, 2H). ¹³C NMR (CDCl₃/TMS, δ, ppm): 24.89 (t), 25.01 (t), 26.06 (t), 26.09 (t), 29.14 (t), 29.20 (t), 29.26 (t), 29.31 (t), 29.43 (t), 29.46 (t), 32.57 (t), 33.81 (t), 34.05 (t), 47.18 (t), 47.20 (t), 52.43 (d), 52.46 (d), 52.65 (q), 122.20 (d), 128.18 (s), 138.76 (s), 143.58 (d), 165.09 (s), 169.33 (s), 170.55 (s).

Curing procedure of epoxy resins

DDM and BAMPO were used as curing agents. Stoichiometric amounts of the epoxy compounds and curing agent were polymerized with 1 mol % BF₃·MEA as the accelerator. Sample bars for DMTA, TGA, and burn tests

were cured in aluminum molds via heating. The prepared epoxy/curing-agent compositions and the curing cycles determined from the DSC data are listed in Table 1.

Characterization

The NMR spectra were recorded on a Varian Gemini 400-MHz spectrometer (400 MHz for ¹H, 100.57 MHz for ¹³C and 161.9 MHz for ³¹P). The samples were dissolved in deuterated chloroform, and ¹H, ¹³C, and ³¹P NMR spectra were obtained at room temperature using TMS and H₃PO₄ as the internal standard. The FTIR spectra were recorded on a Bomem Michelson MB 100 FTIR spectrophotometer with a resolution of 4 cm⁻¹ in the absorbance mode. An attenuated-total-reflection (ATR) accessory with thermal control and a diamond crystal (Golden Gate heated, single-reflection, diamond ATR, Specac-Teknokroma) was used to determine the FTIR spectra.

Calorimetric studies were carried out on a Mettler DSC821e thermal analyzer with N₂ as the purge gas. The heating

rate was 10 °C/min. Thermal stability studies were carried out on a Mettler TGA/SDTA851e/LF/1100 with N₂ as the purge gas at scanning rates of 10 °C/min.

The mechanical properties were measured with a TA DMA 2928 dynamic mechanical thermal analyzer. Specimens with dimensions of 2 mm x 5 mm x 10 mm were tested in a three-point-bending configuration. The various thermal transitions were studied between -100 and 150 °C at a heating rate of 5 °C/min and a fixed frequency of 1 Hz.

LOI values were measured on a Stanton Redcroft, provided with an oxygen analyzer, on polymer bars that measured 100 x 6 x 4 mm³ and that were prepared by molding.

RESULTS AND DISCUSSION

The use of epoxy resins has grown steadily since they were first commercialised in the late 1940s. With the depletion of the earth's limited petroleum reserves, vegetable oils and fatty acids constitute a potentially diverse and inexpensive class of renewable substrates for synthesizing epoxidized monomers and preparing cured epoxy resins. The synthesized epoxy monomers; UDTGE and UDBME were obtained by the epoxidation of UDTG and UDBM, respectively. UDTG can be obtained from naturally occurring castor oil, and UDBM can be synthesized by a method described in the literature with gallic acid as a renewable feedstock.¹² The chemical structure of UDBM was confirmed by FTIR and ¹H and ¹³C NMR.

Epoxidation is one of the most important functionalization reactions of the C-C double bond. The chemistry of the Prileshajev epoxidation of unsaturated fatty compounds is well known.¹⁵ A short-chain peroxy acid, preferably peracetic acid, is prepared from hydrogen peroxide and the corresponding acid either in a separate step or *in situ*.¹⁶ Peracids are excellent epoxidation reagents, and the reaction does not require catalysts.¹⁷ However, it does require at least stoichiometric amounts of peracid, which results in the production of the large amounts of acid waste. Another problem of this method is the side reactions, such as epoxy ring-opening reactions. Venturello and D'Aloisio reported¹⁴ a very efficient epoxidation catalyst, quaternary ammonium tetrakis(diperoxotungsto) phosphate (3-). The epoxidation reaction using this catalyst in conjunction with hydrogen peroxide as the primary oxidant in an aqueous/organic biphasic system is an extremely attractive method for two reasons: no organic solvent is needed, so it is an advantageous process from an environmental viewpoint, and side reactions (especially ring openings) are negligible.

In this study, UDTGE and UDBME were synthesized with hydrogen peroxide as the epoxidation reagent and quaternary ammonium tetrakis(diperoxotungsto) phosphate (3-) as the epoxidation catalyst. The products were obtained in good yields and characterized with spectroscopic techniques. Figures 1 and 2 show ¹H and ¹³C NMR spectra of UDTGE with all the assignments corresponding to the expected signals. In the ¹H NMR spectrum, the signals of the oxirane ring were assigned at

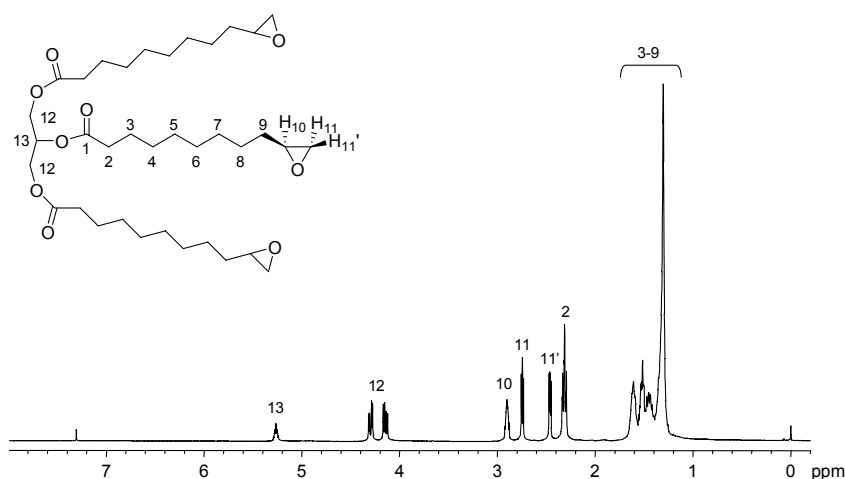


Figure 1. ^1H NMR spectrum of UDTGE (CDCl_3 , 400 MHz).

2.44 (m, 3H), 2.72 (t, 3H), and 2.88 ppm (m, 3H). The resonance lines in the ^{13}C NMR spectrum fall into four main regions: 24.8–34.3 ppm for the fatty acid chain carbons, 47.2 and 52.5 ppm for the oxirane carbons, 62.2 and 68.9 ppm for the glycerol unit carbons, and approximately 173 ppm for the carbonyl

carbons of the ester groups. DOPO-III was obtained as previously described.¹¹ The synthesized compounds (UDTGE, UDBME, and DOPO-III) were used as monomers for preparing cured epoxy resins.

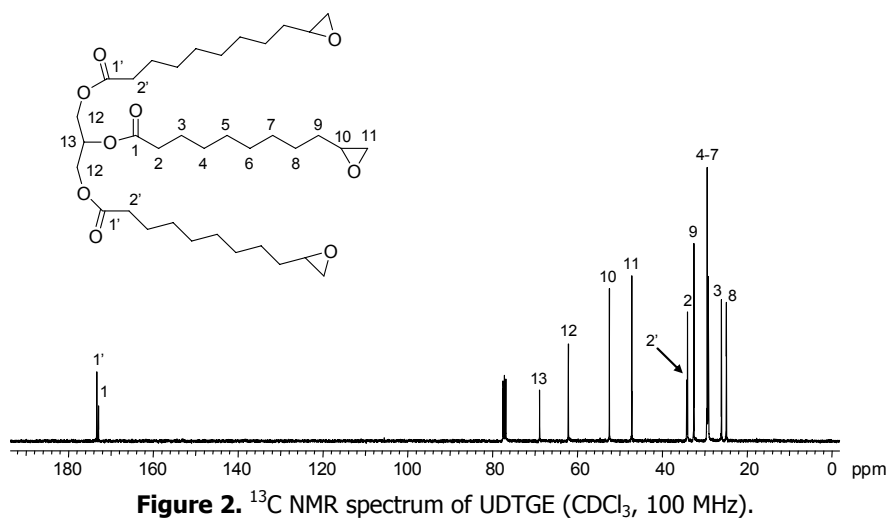


Figure 2. ^{13}C NMR spectrum of UDTGE (CDCl_3 , 100 MHz).

First, UDTGE or UDBME was crosslinked with DDM as a hardener. To further improve the flame-retardant properties of these biobased resins by the introduction of phosphorus, the addition of DOPO-III or crosslinking with a phosphorus-containing curing agent (BAMPO) was studied. DOPO-III contains a rigid and bulky DOPO unit with an unusually highly thermally stable P-O-C bond because the O=P-O group is protected by phenylene groups. The thermal and flame-retardant properties of the new phosphorus-containing and phosphorus-free epoxy were evaluated by the preparation of five polymers; UDTGE/DDM (sample 1), UDTGE/DOPO-III/DDM (sample 2), UDBME/DDM (sample 3), UDBME/DOPO-III/DDM (sample 4) and UDBME/BAMPO (sample 5; see Table 1). We could not prepare a sample of UDTGE/BAMPO because of miscibility problems between the two components.

The amine-epoxy curing reaction has been widely studied.¹⁸ The addition of the $\text{BF}_3 \cdot \text{MEA}$ is known to have a strong accelerating effect on the amine-epoxy reaction.¹⁹ In a previous study,¹¹ DOPO-III was crosslinked with DDM and BAMPO as hardeners and $\text{BF}_3 \cdot \text{MEA}$ as an accelerator, and we showed how the addition of $\text{BF}_3 \cdot \text{MEA}$ prevented the amidation reaction that could take place in the curing reaction of epoxidized fatty acid compounds with polyamine hardeners.²⁰ In accordance with these previous results, all the networks were prepared using 1 mol % $\text{BF}_3 \cdot \text{MEA}$ as the accelerator. The crosslinking reaction of all the compositions was studied with dynamic DSC. Figure 3 shows the dynamic DSC plots (10 °C/min) for UDBME-containing mix-

tures (samples 3-5). As can be seen, the DSC scans show multiple peaks that are symptomatic of complex reactions. The mechanism of catalysis by $\text{BF}_3 \cdot \text{MEA}$ and related compounds in epoxy curing is still not fully understood, but the lower temperature DSC peak is caused by the thermal conversion of $\text{BF}_3 \cdot \text{MEA}$ to HBF_4 ,²¹ whereas the peak at higher temperature can be attributed to the catalyzed addition reaction of the primary and secondary amines to the epoxy groups. The temperature of the exothermic peak of this reaction can be taken to be indicative of the reactivity of the compositions under curing. As can be seen from the crosslinking exotherms, the maximum of the crosslinking is around 120 °C when DDM is used as the hardener, whereas for BAMPO it is around 170 °C. The fact that BAMPO is less reactive than DDM under the same set of curing conditions is probably due to electronic effects. In the case of BAMPO, the electron-withdrawing group, P=O, reduces the electronic density of the amine nitrogen and subsequently reduces its nucleophilicity.²²

The operation conditions for thermal curing were determined from dynamic and isothermal DSC experiments and are listed in Table 1. The isothermal crosslinking reactions were monitored with FTIR/ATR spectroscopy. FTIR/ATR experiments showed how the vibrations associated with the oxirane ring at 830 cm^{-1} and with N-H bonds between 3400 and 3500 cm^{-1} disappeared completely, thus indicating that the amine-epoxy reaction took place.

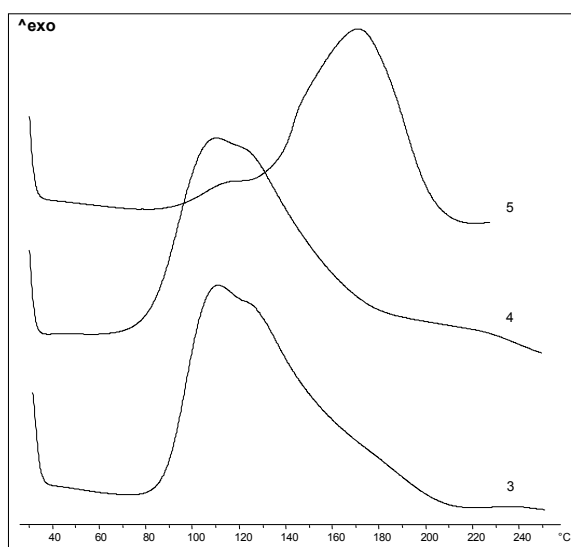


Figure 3. DSC plots (10 °C/min) of (3) UDBME/DDM, (4) UDBME/DOPO-III/DDM, and (5) UDBME/BAMPO curing reactions.

Furthermore, a band appeared at 3396 cm^{-1} because of -OH stretching of the resulting crosslinked moiety. Moreover, the final materials proved to be insoluble in common solvents as crosslinked materials.

The thermal behavior of the obtained materials was investigated with DSC. The glass-transition temperatures (T_g 's) of the cured materials are listed in Table 2.

Table 2. T_g Values of the Cured Epoxy Resins from DSC and DMTA

Sample	Epoxy Monomers	Curing Agent	T_g (°C)		
			$\frac{1}{2} \Delta C_p^a$	$E''_{\max}{}^{b,c}$	$\tan \delta_{\max}{}^{b,d}$
1	UDTGE	DDM	56	63	66
2	UDTGE/DOPO-III	DDM	75	77	83
3	UDBME	DDM	85	74	89
4	UDBME/DOPO-III	DDM	80	76	88
5	UDBME	BAMPO	88	72	85

^a T_g from the second heating scan of DSC measurements at 20 °C/min as the temperature of the halfway point of jump in the heat capacity.

^b Samples for the DMTA experiments were prepared as described in the Experimental section.

^c Temperature of the maximum of the loss-modulus temperature curve from DMTA.

^d Maximum value of the $\tan \delta$ temperature curve from DMTA.

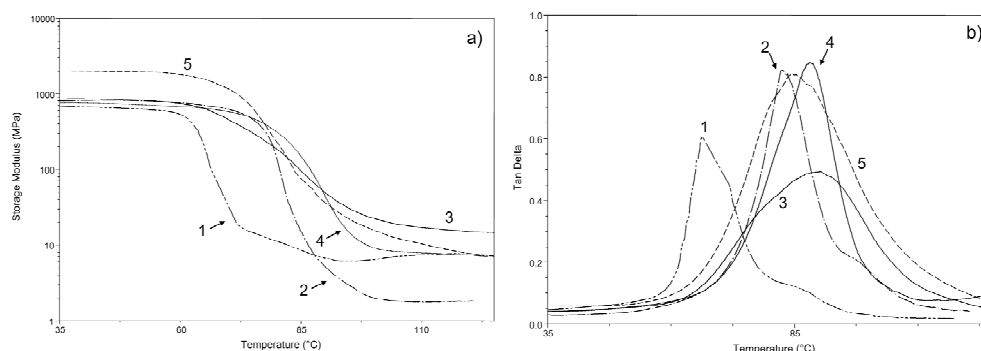


Figure 4. (a) E' and (b) $\tan \delta$ for (1) UDTGE/DDM, (2) UDTGE/DOPO-III/DDM, (3) UDBME/DDM, (4) UDBME/DOPO-III/DDM, and (5) UDBME/BAMPO as functions of temperature.

Several competitive factors affect the glass transition of these biobased epoxy resins. On the one hand, the presence of aromatic moieties will increase the T_g . Therefore, UDBME-based materials have higher T_g 's than UDTGE-based ones (samples 1 and 3). On the other hand, the inclusion of DOPO-III in the system can reduce the crosslinking densities of the materials because its functionality is lower. However, the presence of a bulky aromatic DOPO moiety with a strong polar group ($P=O$) would increase T_g values. Samples 3 and 4 had similar T_g values, and this seems to indicate that this last factor counteracts the effect of decreased densities. We observed a similar effect when comparing the T_g values of samples 3 and 5. On the one hand, a lower crosslinking density that arises from the BAMPO's lower reactivity can be inferred.¹¹ On the other hand, the polar $P=O$ group in BAMPO would increase T_g values.

The dynamic mechanical behavior of the epoxy resins was obtained as a function of the temperature. The dy-

amic mechanical properties of the networks were obtained from the glassy state, through T_g , and well into the rubbery plateau of each material. Figure 4 a) shows how the storage (E') modulus changes with temperature for all the networks. The crosslinking density of a lightly crosslinked polymer can be estimated from the plateau of the elastic modulus in the rubbery state.²³ In this article, it can be used to make qualitative comparisons of the level of crosslinking among the various polymers. As can be seen in Figure 4 a), the crosslinking density is higher for UDBME networks than for UDTGE-based ones. As far as the chemical structures of the monomers are concerned, this behavior can be related not only to the crosslinking density but also to the aromatic core of UDBME, which appears to be more able to resist segmental motion; therefore, the UDBME-containing networks are more able to store elastic energy. The result is a higher modulus. Figure 4 a) also shows that the introduction of DOPO-III into UDTGE and UDBME networks leads to

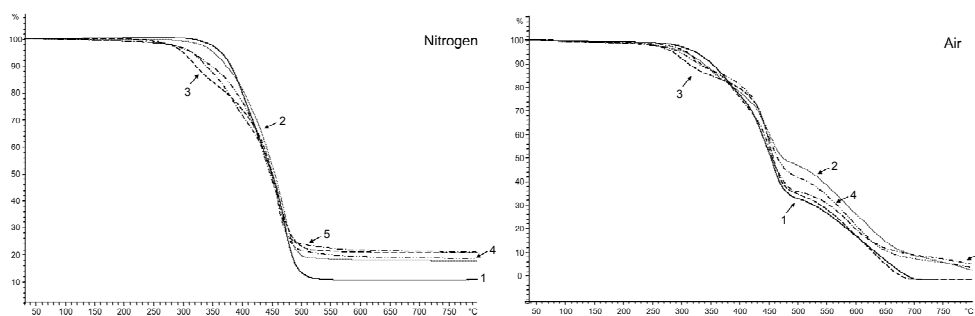


Figure 5. TGA plots (10 °C/min) of the cured epoxy resins: (1) UDTGE/DDM, (2) UDTGE/DOPO-III/DDM, (3) UDBME/DDM, (4) UDBME/DOPO-III/DDM, and (5) UDBME/BAMPO under nitrogen and air atmospheres.

a lower crosslinking density. This may be because the functionality of DOPO-III ($f=2$) is lower than that of UDTGE and UDBME ($f=3$). Moreover, the crosslinking density of the UBME/BAMPO network is lower than that of UDBME/DDM, and this may be because of the lower reactivity of the BAMPO hardener. DMTA also makes it possible to determine the T_g of the crosslinked materials. It is detected as the maximum of the loss modulus (E''), which corresponds to the initial drop from the glassy state into the transition. Moreover, the α -relaxation peak of the loss factor ($\tan \delta$) is associated with T_g and corresponds to the transition midpoint of the logarithm of the E' curve. Figure 4(b) shows the $\tan \delta$ plots for the networks, and Table 2 shows the T_g values from both measurements. As expected, T_g as the $\tan \delta$ peak is higher than that as the E'' peak, and the values follow the same trend mentioned for the DSC measurements. The analysis of the width of the α -relaxation peak shows trends in the network homogeneities. The peak width at half-height seems to be broader for UDBME-containing networks, thus indicating an increasing number of branching modes and a

wider distribution of structures. In DMTA experiments from -100 °C, β transitions occurred around -60 °C, and this may have been due to the motions of $-\text{CH}_2-\text{CH}(\text{OH})-\text{CH}_2-$ aliphatic segments from the ring opening of the epoxide.²⁴

To examine the effect of phosphorus on the thermal stability of the cured epoxy resins, TGA was carried out under nitrogen and air. Figure 5 shows the effects of temperature on the weight loss behavior for all the networks. Table 3 summarizes the TGA data. For comparison, previously published TGA data for DOPO-III/DDM and DOPO-III/BAMPO networks are also shown.¹¹ The thermogravimetric plots under nitrogen show that all the materials have good thermal stabilities, with initial temperatures of weight loss above 300 °C, regardless of the starting monomer or curing agent. UDBME networks seem to decompose at lower temperatures than UDTGE derivatives for the same composition. This may be related to the degradation of the methyl ester moiety in UDBME. The shape of the TGA plots shows that the degradation takes place in a broad temperature range and the phosphorus

Table 3. TGA Data and LOI Values for the Cured Epoxy Resins

Sample	Epoxy Monomers	Curing Agent	P(%)	TGA (N ₂ Atmosphere)			TGA (Air Atmosphere)			LOI
				T _{5% loss} (°C) ^b	T _{max} (°C) ^c	Yield _{800°C} (%) ^d	T _{5% loss} (°C) ^b	T _{max} (°C) ^c	Yield _{800°C} (%) ^d	
1	UDTGE	DDM	0	363	400/468	11	321	379/456/ 625	0	21.9
2	UDTGE/DOPO-III	DDM	1.8	350	359/469	17	302	349/449/ 620	2	27.7
3	UDBME	DDM	0	299	316/457	20	283	300/450/ 615	0	23.5
4	UDBME/DOPO-III	DDM	1.9	313	324/461	18	294	318/441/ 600	4	28.5
5	UDBME	BAMPO	2.5	313	330/459	20	306	324/452/ 595	5	30.2
6 ^a	DOPO-III	DDM	3.9	350	435/468	18	333	439/458/ 602	10	31
7 ^a	DOPO-III	BAMPO	5.7	354	440/467	16	346	435/455/ 600	18	32

^a For comparison, previously published¹¹ TGA data and LOI values for DOPO-III/DDM and DOPO-III/BAMPO are also shown.

^b Temperature of 5% of weight loss.

^c Temperature of the maximum weight-loss rate.

^d Char yield at 800 °C.

content seems to have no influence on the degradation. Under an air atmosphere, a new step in the weight-loss rate appeared at temperatures greater than 550 °C because of the thermooxidative degradation. The char yields at 800 °C are listed in Table 3. In this case, the experimental char yields under nitrogen for the phosphorus-containing and phosphorus-free epoxy resins were not significantly different. Under air, however, significant differences were observed. Although the char yields for the phosphorus-free resins were nonexistent, the char yields for the phosphorus-containing resins increased with the phosphorus content (Figure 6). The phosphorus, therefore, plays a role in char formation, and because the char yield has been correlated to the flame retardancy,²⁵ these resins were expected to have enhanced flame-retardant properties. The high char yield limited the production of combustion gases, decreased the exothermicity of the pyrolysis reactions, and inhibited

the thermal conductivity of the burning material.

We tested the flame retardancy of the cured polymers by measuring LOI values (see Table 3), which can be taken as an indicators for evaluating the polymer's flame retardancy. The LOI values increased from 21.9 to 27.7 and from 23.5 to 28.5 when the phosphorous content increased from 0 to 1.8% and 0 to 1.9%, respectively. Similar LOI increases have been described for diglycidyl ether of bisphenol A epoxy resins when DOPO derivatives are used as reactive flame retardants.²⁶ To get more information about the effect of phosphorus on the flame retardancy, the relationships between the phosphorous content and the LOI or the residue at 800 °C are plotted in Figure 6. The presence of phosphorus linearly increases the char yield at 800 °C under an air atmosphere. On the other hand, the LOI value increases as the phosphorous content increases and reaches a plateau value around 30.

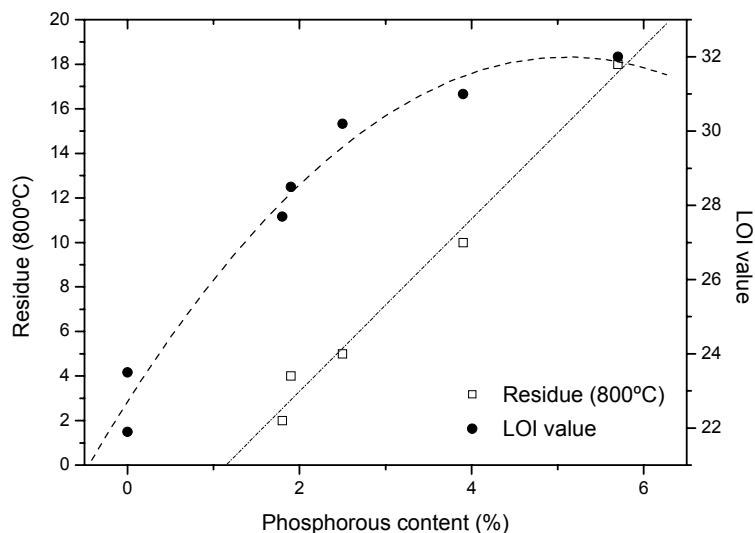


Figure 6. (□) Residue at 800 °C under an air atmosphere and (●) LOI values versus the phosphorous weight contents of the cured epoxy resins.

CONCLUSIONS

In this study, UDTGE and UDBME were synthesized from their corresponding alkenyl-terminated fatty acid compounds by epoxidation using quaternary ammonium tetrakis(diperoxotungsto) phosphate (3-) as epoxidation catalyst. UDTGE, UDBME, and DOPO-III were used as epoxy monomers for preparing phosphorus-containing, biobased epoxy resins from renewable resources with DDM and BAMPO as hardeners. Thermal, dynamic mechanical, and flame-retardant properties were evaluated. Thermosetting materials with moderate T_g 's and good thermal stabilities were obtained in all cases. The presence of phosphorus increased the LOI values, leading to polymers with enhanced flammability. These results demonstrate the efficiency of DOPO-III as a reactive flame retardant and show that it is possible to exploit renewable re-

sources to manufacture original and useful materials.

Acknowledgements

The authors gratefully acknowledge the Comisión Interministerial de Ciencia y Tecnología (MAT2005-01593) for its financial support of this work and the Departament d'Universitats, Recerca i Societat de la Informació and Fons Social Europeu for G. Lligada's predoctoral grant (2003FI00765).

REFERENCES AND NOTES

1. Bozell, J. J. *Chemicals and Materials from Renewable Resources*; ACS Symposium Series 784; American Chemical Society: Washington, DC, 2001.
2. (a) Baumann, H.; Bühler, M.; Fochem, H.; Hirsinger, F.; Zoblein, H.; Falbe, J. *Angew Chem, Int Ed Engl* 1988, 27, 41; (b) Biermann, U.; Friedt, W.; Lang,

- S.; Lühs, W.; Machmüller, G.; Metzger, J. O.; Klaas, M. R.; Schäfer, H. J.; Schneiderüsch, M. P. *Angew Chem Int Ed* 2000, 39, 2206.
3. Khot, S. N.; LaScala, J. J.; Can, E.; Morye, S. S.; Williams, G. I.; Palmese, G. R.; Küseföglu, S. H.; Wool, R. P. *J Appl Polym Sci* 2001, 82, 703.
 4. Esen, H.; Küseföglu, S. H. *J Appl Polym Sci* 2003, 89, 3882.
 5. Guo, A.; Javni, I.; Petrovic, Z. S. *J Appl Polym Sci* 2000, 77, 467.
 6. (a) Lligadas, G.; Ronda, J. C.; Galià, M.; Cádiz, V. *Biomacromolecules* 2006, 7, 2420; (b) Lligadas, G.; Ronda, J. C.; Galià, M.; Biermann, U.; Metzger, J. O. *J Polym Sci Part A: Polym Chem* 2006, 44, 634; (c) Tsujimoto, T.; Uyama, H.; Kobayashi, S. *Macromol Rapid Commun* 2003, 24, 12; (d) Bunker, S. P.; Wool, R. P. *J Polym Sci Part A: Polym Chem* 2002, 40, 451; (e) Warwel, S.; Rüschen, Klaas, M.; Schier, H.; Brüse, F.; Wiege, B. *Eur J Lipid Sci Technol* 2001, 103, 645.
 7. (a) Takahashi, E.; Sanda, F.; Endo, T. *J Polym Sci Part A: Polym Chem* 2002, 40, 1037; (b) Park, S. J.; Kim, H. C. *J Polym Sci Part B: Polym Phys* 2001, 39, 121.
 8. Eren, T.; Küseföglu, S. H. *J Appl Polym Sci* 2004, 91, 2700.
 9. Jain, P.; Choudhary, V.; Varma, I. K. *J Macromol Sci Polym Rev* 2002, 42, 139.
 10. Hörold, S. *Polym Deg Stab* 1999, 64, 427.
 11. Lligadas, G.; Ronda, J. C.; Galià, M.; Cádiz, V. *J Polym Sci Part A: Polym Chem* 2006, 44, 5630.
 12. Lligadas, G.; Callau, L.; Ronda, J. C.; Galià, M.; Cádiz, V. *J Polym Sci Part A: Polym Chem* 2005, 43, 6295.
 13. Varma, I. K.; Gupta, U. *J Macromol Sci A: Chem* 1986, 23, 19.
 14. Venturello, C.; D'Aloisio, R. *J Org Chem* 1988, 53, 1553.
 15. Findley, T. W.; Swern, D.; Scalan, J. T. *J Am Chem Soc* 1945, 67, 412.
 16. Rangarajan, B.; Havey, A.; Grulke, E. A.; Culnan, P. D. *J Am Oil Chem Soc* 1995, 72, 1161.
 17. Swern, D. *Organic Peroxides*, Vol. 2, D. Swern, Ed., John Wiley and Sons, New York 1971.
 18. May, C.A. *Epoxy Resins: Chemistry and Technology*; Marcel Dekker, Inc., New York, 1998.
 19. (a) Morgan, R. J.; Walkup, C. M.; Hoheisel, T. H. *J Appl Polym Sci* 1985, 30, 289; (b) Jagadeesh and Siddaramaiah, K. S. *J Appl Polym Sci* 1991, 43, 1459; (c) Juangvanich, N.; Stoffer, J. *Polym Prep. (Am Chem Soc Div Polym Chem)* 2002, 43, 22.
 20. Lee, H.; Neville, K. *Handbook of Epoxy Resins*. New York: Mc Graw Hill, 1982.
 21. (a) Smith, R. E.; Larsen, F. N.; Long, C. L. *J Appl Polym Sci* 1984, 29, 3697; (b) Smith, R. E.; Smith, C. H. *J Appl Polym Sci* 1986, 31, 929.
 22. Mercado, L. A.; Ribera, G.; Galià, M.; Cádiz, V. *J Polym Sci Part A: Polym Chem* 2006, 44, 1676.
 23. Tobolsky, A. V.; Carlson, D. W.; Indictor, N. J. *J Polym Sci* 1961, 54, 175.
 24. Heux, L.; Halary, J. L.; Lauprêtre, F.; Monnerie, L. *Polymer*, 1997, 38, 1767.
 25. Van Krevelen D. W. *Polymer* 1975, 16, 615.
 26. Levchik, S.V.; Weil, E.D. *Polym Int* 2004, 53, 1901.

4

Biobased Polyols and Polyurethanes

Polyurethanes are one of the most widespread classes of polymers, and their use covers practically all polymer applications. Polyols derived from vegetable oils are new raw materials that when combined with isocyanates produce polyurethanes whose properties compete with many of the polyurethanes produced from petrochemical polyols.

This chapter describes the design, synthesis, and characterization of a new class of polyether polyols from epoxidized methyl oleate, and their use in developing polyurethanes for different applications.

-
- 4.1 Basic Chemistry of Polyurethanes
 - 4.2 Vegetable Oil-Based Polyols and Polyurethanes
 - 4.3 Objectives
 - 4.4 Experimental Procedures and Results
 - 4.4.1 Synthesis and Characterization of Polyurethanes from Epoxidized Methyl Oleate Based Polyether Polyols as Renewable Resources
 - 4.4.2 Novel Silicon-Containing Polyurethanes from Vegetable Oils as Renewable Resources. Synthesis and Properties
 - 4.4.3 Poly(ether urethane) Networks from Renewable Resources as Candidate Biomaterials. Synthesis and Characterization
-

4.1

Basic Chemistry of Polyurethanes

Polyurethanes are a class of polymers that have found many important applications such as elastomers, coatings, and flexible and rigid foams.¹ The exothermic reaction between isocyanates and alcohols - the most important reaction in polyurethane synthesis - leads to the production of urethane [-NH-COO-] linkages. This reaction is catalyzed by tertiary amines with low steric hindrance, such as triethylenediamine and N,N-dimethyl cyclohexylamine, and certain tin, lead, and mercury compounds like stannous octoate (tin 2-ethylhexanoate).

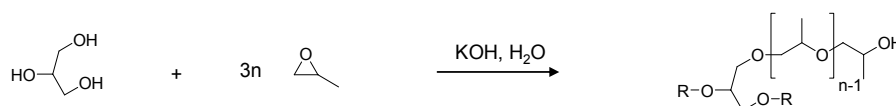
Whilst the highly reactive isocyanate group is the principal feature of polyurethane technology, it is the polyol that largely determines the properties of the final polyurethane polymer. The term polyol describes compounds with hydroxyl (OH) groups that react with isocyanates to produce polyurethane polymers. Polyols are divided into two groups based on their structure. The first group comprises low-molecular-weight polyols that have a unitary and concrete molecular weight, such as propylene glycol, ethylene glycol, diethylene glycol, and neopentyl glycol. These polyols are currently used in the synthesis of polyurethanes as chain extenders (diols) or as crosslinkers (e.g., triols and tetraols). The second group of polyols comprises low-molecular-weight polymers (oligopolyols) with molecular weights of 300-10000 Da and with a functionality of 2-8 OH groups/molecule. Nowadays, polyether polyols account for 80% of the total worldwide consumption of oligopolyols.

The use of polyether polyols of low functionality (2-3 OH groups/molecule) and a molecular weight of 2000-10000 Da leads to low-crosslinked and flexible

1. Polyurethane Handbook, 2nd ed.; Oertel, G. Ed.; Carl Hanser Publishers: Munich, 1993.

polyurethanes, whereas polyether polyols of 300-1000 Da with a high functionality (3-8 OH groups/molecule) lead to rigid crosslinked materials.²

The synthesis of polyether polyols can be generalized as the stepwise addition of an alkylene oxide to an active-hydrogen compound or initiator with the aid of a catalyst (Scheme 4.1), being potassium hydroxide the most widely used. The three most commonly used cyclic ethers are ethylene oxide, propylene oxide and tetrahydrofuran, of which propylene oxide is the most significant, whilst the use of ethylene oxide is limited to the production of copolymers with propylene oxide. Tetrahydrofuran is used for the manufacture of a range of specialty polyols. The active-hydrogen compound is usually an alcohol, polyalcohol, or amine. Propylene glycol, glycerol, and trimethylolpropane are widely used, although products for rigid polyurethane foams may be initiated with a variety of compounds of higher functionality, such as sorbitol, sucrose, ethylenediamine, and diethylenetriamine.



Scheme 4.1

Irrespective of the chemical structure of the oligomeric chain, the most important chemical property of oligopolyols is the OH content (HV). The HV is a measure of the concentration of OH groups in a polyol, expressed as the milligrams of potassium hydroxide equivalent to the OH groups in one gram of the polyol (units of mg KOH/g). The most important analytical method for determining HV is the reaction of the OH groups with organic anhydrides (acetic anhydride or phthalic anhydride). Other key parameters are molecular weight, equivalent weight, water content, viscosity, and color.

2. Dietrich, D.; Uhlig, K. Polyurethanes. In: Ullmann's Encyclopedia of Industrial Chemistry, vol. A21; Elvers, B.; Hawkins, S.; Schulz, G. Eds.; VCH Verlagsgesellschaft: Weinheim, Germany, 1992.

Isocyanate is the other essential component in the preparation of any polyurethane product. The most used isocyanates, covering the majority of polyurethane applications are aromatic isocyanates: 4,4'-methylenebis(phenyl isocyanate) (MDI) and toluene diisocyanate (TDI). Aliphatic isocyanates such as hexamethylene diisocyanate (HDI), isophorone diisocyanate (IPDI), or 4,4'-methylenebis(cyclohexyl diisocyanate) (HMDI) are used to a much lesser extent, and only for special applications. The industrial route to the manufacture of diisocyanates is based on first synthesizing the required molecular structure, but with amine functional groups instead of isocyanate groups, followed by transformation of the amine to isocyanate groups.³

4.2

Vegetable Oil-Based Polyols and Polyurethanes

The petrochemicals that are used intensively in the worldwide chemical industry are a limited resources that will be depleted within the foreseeable future,⁴ which has fueled efforts to find alternatives.

In the polyurethane industry, conventional polyether polyols are mostly produced from petroleum-based alkylene oxides. Due to uncertainty about the future cost of petroleum, as well as the desire to move toward more environmentally friendly feedstocks, many recent efforts have focused on replacing all or part of the conventional petroleum-based polyols with those made from renewable resources such as vegetable oils. However, it is a challenge to synthesize suitable diisocyanates via diamino compounds derived from vegetable oils, making possible to produce polyurethanes completely from renewables.⁵

3. *The Polyurethane Book*; Randall, D.; Lee, S. Eds.; John Wiley & Sons, LTD: New York, 2002.

4. Azapagic, A.; Emsley, A.; Hamerton, I. *Polymers, the Environment and Sustainable Development*; Hamerton, I. Ed.; John Wiley & Sons: Chichester, 2003.

5. Metzger, J. O.; Bornscheuer, U. *Appl Microbiol Biotechnol* 2006, 71, 13.

The history of the polyurethane industry is strongly linked to renewable resources. For example, glycerol - the most important starter for the synthesis of polyether polyols - can be produced by the hydrolysis of natural triglycerides. Tetrahydrofuran - the cyclic monomer used for the synthesis of polytetramethyleneglycols - was produced in the early stages of this technology from furfural, which results from the acid hydrolysis of the pentosanes present in many agricultural waste products. Moreover, castor oil played an especially important role in the infancy of the polyurethane industry, before synthetic polyols were available.

Polyols derived from vegetable oils are new raw materials derived from renewable resources. Polyurethanes prepared from vegetable oils exhibit a number of excellent properties that are attributable to the hydrophobic nature of triglycerides.⁶ Two different ways of preparing vegetable oil-based polyols have been developed:

1. By a combined reaction at the C=C double bond and subsequent reduction of the carboxyl group.
2. Using reactions involving only the C=C double bonds.

1. Synthesis of Vegetable Oil-Based Polyols by a Combined Reaction at the C=C Double Bond and Subsequent Reduction of the Carboxyl Group

Dimerization of unsaturated fatty acids is an interesting procedure for the synthesis of high-molecular-weight dicarboxylic acids.⁷ The high-pressure hydrogenation of carboxylate groups is a convenient way to use these dicarboxylic acids for polyurethane applications as a long-chain diols. Oleic or linoleic acids can be dimerized to form a complex mixture known as dimer acid. Dimer diol, that can be prepared from dimer acid by hydrogenation, is used as a building block for the soft segment in thermoplastic polyurethanes. Dimer diol oligoethers are industrially

6. Chemistry and Tehnology of Polyols for Polyurethanes; Ionescu, M. Ed.; Rapra Technology Limited: Shawbury, UK, 2005.

7. Heidbreder, A.; Hofer, R.; Grutzmacher, R.; Westfechtel, A; Blewett, C. W. Fett/Lipid 1999, 101, 418.

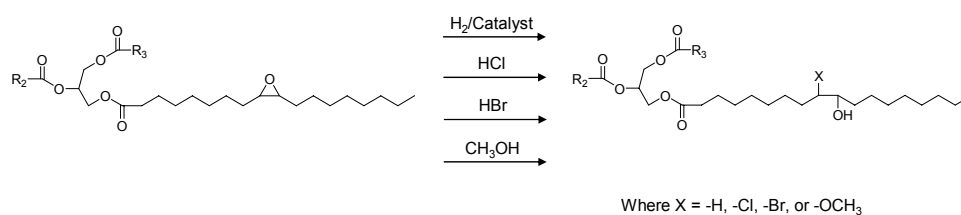
manufactured by acid-catalyzed dehydration of dimer diol. By transesterification with dimethyl carbonate, dimer diol can also be oligomerized via carbonate bridges instead of ether linkages. Polyurethanes based on dimer diol oligoethers exhibit improved hydrolysis and saponification resistance.⁷

2. Synthesis of Vegetable Oil-Based Polyols Using Reactions Involving only the C=C Double Bonds

Epoxidation is one of the most important functionalization reactions of the C=C double bonds, and ring-opening of epoxidized vegetable oils is an established method of introducing OH groups into a triglyceride structure. Several polyols have been synthesized from various vegetable oils and derivatives (i.e., sunflower, canola, soybean, midoleic, corn, linseed, triolein, and metathesized triolein) using a two-step process: epoxidation followed by ring-opening with monohydric alcohols.⁸⁻¹¹ Although alcohols such as ethanol, n-propanol, n-butanol, and n-pentanol, or branched isomers have been used, methanol is preferred due to its lower cost and the favorable results obtained.

There has been considerable interest in the development of polyols from epoxidized soybean oil due to its very low price and abundant supply. The epoxy groups of epoxidized soybean oil have been converted to OH groups by (i) catalytic hydrogenation, (ii) reaction with hydrochloric or hydrobromic acid, and (iii) the above-mentioned methanolysis reaction (Scheme 4.2).¹² The reactions took place at moderate temperature (40-50 °C) and gave high yields (94-100%). The resulting soybean oil-based polyols have an HV of around 170-200 mg KOH/g and a functionality of 3.5-4.1 OH groups/molecule.

-
8. Zlatanic, A.; Lava, C.; Zhang, W.; Petrovic, Z. *J Polym Sci Part B: Polym Phys* 2004, 42, 809.
 9. Zlatanic, A.; Petrovic, Z.; Dusek, K. *Biomacromolecules* 2002, 3, 1048.
 10. Hofer, R.; Meffert, A.; Gruetzmacher, R. U.S. Patent 4,826,944, 1989.
 11. Kluth, H.; Gruber, B.; Meffert, A.; Huebner, W. U.S. Patent 4,742,087, 1988.
 12. Guo, A.; Cho, Y.; Petrovic, Z. *J Polym Sci Part A: Polym Chem* 2000, 38, 3900.

**Scheme 4.2**

These four polyols (Scheme 4.2) were reacted with two commercial isocyanates: PAPI 2901 (crude MDI) and 2143L (a liquid MDI prepolymer containing carbodiimide bonds).¹³ The two isocyanates produced polyurethanes with comparable properties. Polyurethanes produced from brominated and chlorinated polyols exhibited comparable glass-transition temperatures (T_g) and strengths, being somewhat higher than the values for the methoxy-containing polyol-based polyurethane. Polyurethane produced from the hydrogenated polyol had a lower T_g and mechanical properties. The thermal stability of the brominated polyurethane was the lowest, followed by that of the chlorinated polyurethane, while the methoxy-containing and hydrogenated polyols-based polyurethanes had the highest stability.

Viscosity is an important characteristic of polyols.⁶ Halogenated and hydrogenated soybean polyols are waxes, whereas methoxy-containing polyol is liquid at room temperature. This is an important technological advantage, because the high-molecular-weight polyurethane polymers are obtained using only low- or medium-viscosity liquid intermediates. The viscosity gives an indication of the processability of a polyol. Methoxy-containing soybean oil polyols have been widely used to produce polyurethanes that can compete in many aspects with polyurethanes obtained from petrochemical polyols.^{14,15} The thermal and oxidative stabilities of methoxylated soybean oil-based polyurethanes are higher than those of

13. Petrovic, Z.; Guo, A.; Zhang, W. *J Polym Sci Part A: Polym Chem* 2000, 38, 4062.

14. Guo, A.; Javni, I.; Petrovic, Z. *J Appl Polym Sci* 2000, 77, 467.

15. Pechar, T. W.; Sohn, S.; Wilkes, G. L.; Ghosh, S.; Frazier, C. E.; Fornof, A.; Long, T. E. *J Appl Polym Sci* 2006, 101, 1432.

polypropylene oxide-based polyurethanes.¹⁶ This polyol has a functionality of 3.5-4 OH groups/molecule and a molecular weight of about 1000 Da, and its approximate structure is shown in Figure 4.1. Secondary OH groups are located on 9th or 10th and 12th or 13th carbon atoms in the fatty acid chain. Thus, when crosslinking is completed, a portion of the chains (e.g., from the 10th to the 18th carbon) is not included in the network. The dangling ends act as plasticizers that reduce polymer rigidity. In addition, soybean oil comprises about 15% saturated fatty acids, which are also dangling chains.

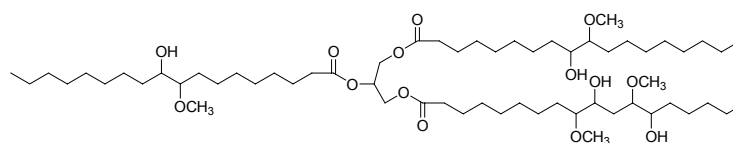


Figure 4.1 Chemical structure of methoxy-containing soybean oil polyols.

Methoxy-containing soybean oil polyols have recently been used as soft segments in the preparation of segmented polyurethanes.¹⁷ Segmented polyurethanes are block copolymers that are usually characterized by a microphase-separated structure consisting of soft and hard phases.¹⁸ In these polymers, the soft phase usually consists of polyether or polyester diol, whereas the hard segment consists of the diisocyanate component and a low-molecular-weight diol (chain extender) (Figure 4.2).

16. Javni, I.; Petrovic, Z.; Guo, A.; Fuller, R. *J Appl Polym Sci* 2000, 77, 1723.

17. Petrovic, Z.; Cevallos, M. J.; Javni, I.; Schafer, D. W.; Justice, R. *J Polym Sci Part B: Polym Phys* 2005, 43, 3178.

18. Petrovic, Z. *Polyurethanes*. In: *Handbook of Polymer Synthesis*; Kricheldorf, H. R.; Nuyken, O.; Swift, G., Eds.; Marcel Dekker: New York, 2005.

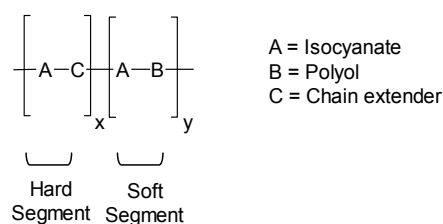


Figure 4.2 Generalized structure of segmented polyurethanes.

Hard phases play the role of physical crosslinks and act as a high-modulus filler, whereas the soft phase provides extensibility.¹⁹ Normally segmented polyurethanes are thermoplastic elastomers, but the introduction of crosslinking results in a polymer system with a rubber-like elasticity and swelling ability.

The reactivity of polyols toward isocyanates is a very important practical characteristic in polyurethane fabrication. The reactivity of primary OH groups is 3- to 3.3-times higher than that of secondary OH groups in the uncatalyzed reactions with isocyanates. Epoxidation and further oxirane ring-opening leads to polyols with secondary OH groups. Two different ways of preparing vegetable oil-based polyols with primary OH groups have been successfully developed.

The first and very efficient method is to directly transform an unsaturated triglyceride in polyols having primary OH groups, which involves the hydroformylation reaction and subsequent reduction of aldehyde groups (Figure 4.3). Soybean oil has been used as a starting material. In the first step the C=C double bonds are transformed to aldehyde groups (at a high yield) by the hydroformylation reaction with syngas (a mixture of hydrogen:carbon monoxide at 1:1) at 70-130 °C in the presence of rhodium or cobalt catalysts.^{20,21} In the second step, the resulting aldehyde groups are hydrogenated to a polyol comprising only

19. Petrovic, Z.; Ferguson, J. *Prog Polym Sci* 1991, 16, 695.

20. Kandamarachchi, P.; Guo, A.; Petrovic, Z. *J Mol Catal A: Chem* 2002, 184, 65.

21. Kandamarachchi, P.; Guo, A.; Demydov, D.; Petrovic, Z. *J Am Oil Chem Soc* 2002, 79, 1221.

primary OH groups, with HV of between 160 and 230 mg KOH/g depending on the hydroformylation catalyst used.²²

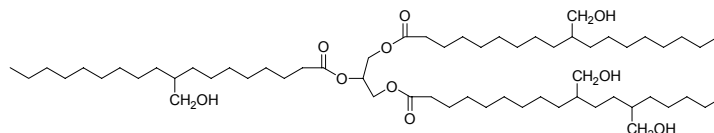


Figure 4.3 Chemical structure of hydroformylated hydrogenated soybean oil polyol.

The second method used to obtain vegetable oil-based polyols with primary OH groups (Figure 4.4) is the ozonolysis reaction²³. In the first step of ozonolysis produces aldehydes that are then reduced to primary alcohols. Ozonolysis has been successfully applied to soybean oil, low-saturation canola oil, and triolein.

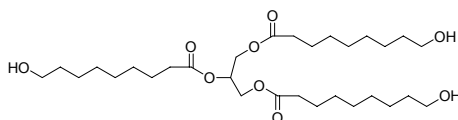


Figure 4.4 Chemical structure of triol obtained by the ozonolysis of triolein.

It should be noticed that the polyols produced by ozonolysis do not contain dangling chains, except for a small percentage of saturated fatty acid chains. Polyurethanes derived from these polyols displayed excellent mechanical properties and a higher T_g compared to polyurethanes from epoxidized and hydroformylated polyols of the same functionality, presumably due to the absence (or lower content) of dangling chains.

To conclude, the development of polyols for polyurethane applications from vegetable oils is a very promising future technology. In contrast to petrochemical

22. Guo, A.; Demydov, D.; Zhang, W.; Petrovic, Z. *J Polym Environ* 2002, 10, 49.

23. Petrovic, Z.; Zhang, W.; Javni, I. *Biomacromolecules* 2005, 6, 713.

resources, the availability of these renewable natural raw materials is practically unlimited.

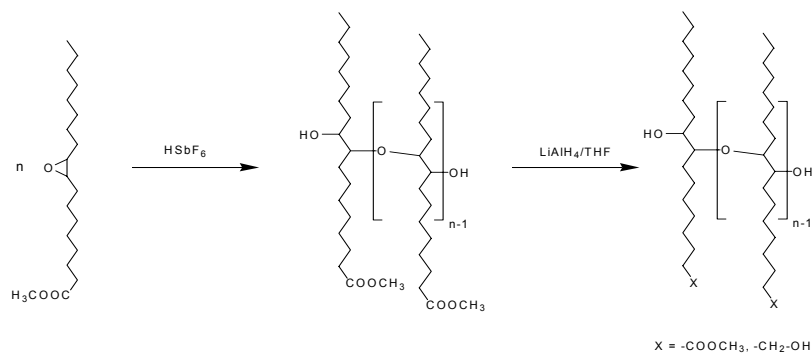
4.3

Objectives

In recent years there has been a considerable focus on the preparation of polyols and polyurethanes from fatty acids and oils, but limited attention has been paid to the preparation of polyether polyols from these compounds.

The main objective of the work described in this chapter was to develop and apply a new family of polyether polyols derived from epoxidized methyl oleate (EMO) in the synthesis of polyurethanes for use in specific applications. This main objective can be divided into two sub objectives:

1. To synthesize and characterize oligomeric polyether polyols through the acid-catalyzed ring-opening polymerization of EMO and the subsequent partial reduction of the ester groups (Scheme 4.3).



Scheme 4.3

2. To apply these new polyols to the synthesis of polyurethanes, some with specific applications: silicon-containing polyurethanes with enhanced flame retardancy and poly(ether urethane) elastomers with potential applications in biomedicine.

4.4

Experimental Procedures and Results

The following three works includes the experimental procedures and the results of the studies performed for this chapter.

The work described in the Section 4.4.1 has been published in the Journal of Polymer Science Part A: Polymer Chemistry (2006, 44, 634), and includes the synthesis of novel oligomeric polyether polyols through the acid-catalyzed ring-opening polymerization of EMO and the subsequent partial reduction of the ester groups to yield primary alcohols. The degree of reduction influenced the HV of the obtained polyols. These polyols were reacted with MDI to yield polyurethanes. The thermal and mechanical properties of the obtained thermosetting materials were studied.

The synthesis and characterization of a new silicon-containing triol (PSi194, Figure 4.5), which was prepared by hydrosilylation of methyl 10-undecenoate, which can be easily obtained from natural ricinoleic acid, with phenyl tris(dimethylsiloxy)silane followed by a reduction of carboxylate groups, is presented in Section 4.4.2.

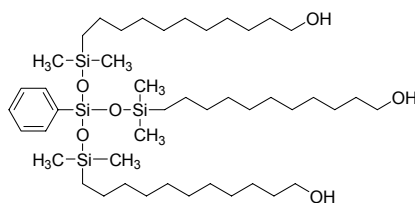


Figure 4.5 Chemical structure of the silicon-containing triol PSi194.

Silicon-containing biobased polyurethanes for applications that require flame resistance were prepared from an EMO-based polyether polyol with an HV of 184 mg KOH/g, PSi194, and MDI. The thermal, mechanical, and flame-retardant properties of these materials were examined. This work has been published in the journal *Biomacromolecules* (2006, 7, 2420).

The work described in Section 4.4.3 has been submitted for publication in the journal *Biomacromolecules*, and involves the synthesis and characterization of polyurethane networks with potential applications in biomedicine. Polyurethanes were synthesized from an EMO-based polyether polyol with an HV of 184 mg KOH/g as a soft segment, 1,3-propanediol as a chain extender, and L-lysine diisocyanate (LDI) as a non-toxic coupling agent. The thermal and mechanical properties of these materials were examined. In view of the future applications of the synthesized polyurethanes in biomedicine, water uptake and in vitro degradation studies were also performed.

4.4.1 Synthesis and Characterization of Polyurethanes from Epoxidized Methyl Oleate Based Polyether Polyols as Renewable Resources

SYNTHESIS AND CHARACTERIZATION OF POLYURETHANES FROM EPOXIDIZED METHYL OLEATE BASED POLYETHER POLYOLS AS RENEWABLE RESOURCES

G. Lligadas,¹ J.C. Ronda,¹ M. Galià,¹ U. Biermann,² J. O. Metzger²

¹Departament de Química Analítica i Química Orgànica, Universitat Rovira i Virgili, Campus Sescelades, Marcel·lí Domingo s/n, 43007 Tarragona, Spain.

²Institute of Pure and Applied Chemistry, University of Oldenburg, 26111 Oldenburg, Germany

ABSTRACT: Oligomeric polyether polyols were obtained through the acid-catalyzed ring-opening polymerization of epoxidized methyl oleate and subsequent partial reduction of ester groups to give primary alcohols. The oligomers were characterized with titration, spectroscopic techniques (Fourier transform infrared and nuclear magnetic resonance), matrix-assisted laser desorption/ionization time-of-flight mass spectrometry, size exclusion chromatography, and differential scanning calorimetry. Depending on the degree of reduction, polyols of different hydroxyl content values were obtained and were reacted with 4,4'-methylenebis(phenyl isocyanate) to yield polyurethanes. These materials, which were characterized by differential scanning calorimetry, thermogravimetric analysis, and dynamic mechanical thermal analysis, could behave as hard rubbers or rigid plastics.

Keywords: polyether; polyurethanes; renewable

INTRODUCTION

Sustainable development had become the key ideal of the 21st century. In the search for sustainable chemistry, considerable importance is being attached to renewable raw materials, which exploit the synthetic capabilities of nature and may eventually substitute

for fossil, depleting feedstocks.¹ The encouragement of environmentally sound and sustainable use of renewable natural resources is an important aim of Agenda 21.² Oils and fats of vegetable and animal origin make up the greatest proportion of the current consumption of renewable raw materials in the chemical industry

because they offer to chemistry a large number of possibilities for applications that can be rarely met by petrochemistry. Vegetable oils containing unsaturated fatty acids can be used in polymerizations to make biobased polymers.³⁻⁵ Numerous fatty acids are now available in a purity that makes them attractive for synthesis and as raw materials for the chemical industry.⁶

There have been many studies on the synthesis and characterization of a wide variety of polymers based on vegetable oils.^{7,8} Although they possess double bonds, which are used as reactive sites in coatings, they cannot be converted easily to high-molecular-weight products without the introduction of more reactive functional groups, such as hydroxyl, epoxy, or carboxyl groups. Various chemical pathways for the functionalization of triglycerides and fatty acids have been studied.⁹ Epoxidation is one of the most important functionalization reactions of C-C double bond. The chemistry of the Prileshajev epoxidation of unsaturated fatty compounds is well known.¹⁰ A short-chain peroxy acid, preferably peracetic acid, is prepared from hydrogen peroxide and the corresponding acid either in a separate step or *in situ*.¹¹ For chemical synthesis on the laboratory scale, better results can be achieved with preformed peroxy acids such as *m*-chloroperbenzoic acid. Other methods for the epoxidation include the use of dioxiranes¹², the generation of peracids from aldehydes and molecular oxygen,¹³ and the use of alkylhydroperoxides with transition metal catalysts.¹⁴ Recently, a convenient method for the chemoenzymatic self-epoxidation of unsaturated fatty acids

was developed.¹⁵ Unsaturated fatty compounds are preferably epoxidized on an industrial scale by the *in situ* performic acid procedure.¹⁶ Epoxidized fatty acids are monomers suited for ring opening polymerizations.¹⁷

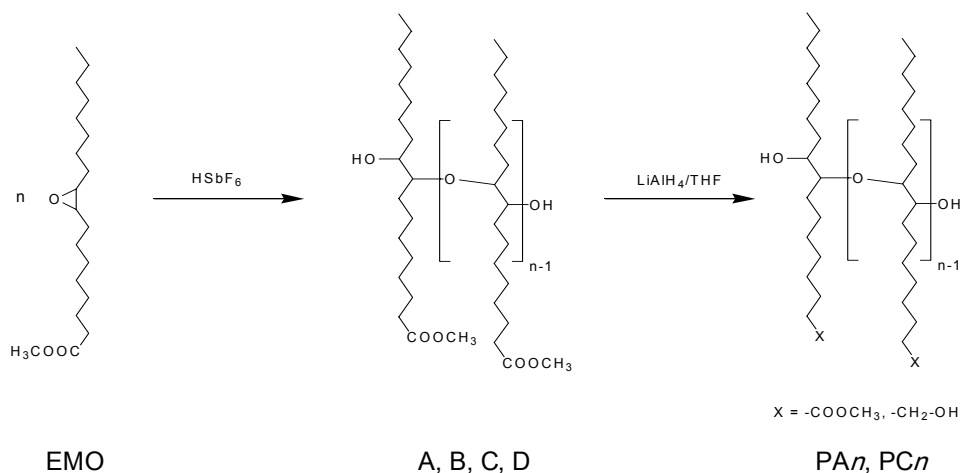
The preparation of polyols from fatty acids and oils for general polyurethane use has been the subject of many studies,¹⁸⁻²⁰ but limited attention has been paid to the preparation of polyether polyols from this kind of compound. Polyether polyols are important building blocks for polyurethane applications with molecular weights of 200-10000 g/mol.²¹ Polyols with molecular weights of about 3000 or more are used to produce flexible polyurethanes, and polyols of about 200 to 1200 g/mol are used for rigid polyurethanes. Polyether polyols are usually produced by the anionic ring-opening polymerization of alkylene oxides, such as ethylene oxide or propylene oxide.

Industrial polyether polyols mainly from ethylene oxide and propylene oxide, are produced for application in polyurethane foams. Longer chain oxiranes or functionalized epoxides show lower reactivity because of a higher sterical hindrance and side reactions, and high-molecular-weight polymers cannot be obtained with anionic or cationic catalysts.²² Coordinative ring-opening polymerization has been described for functionalized epoxides as phenyl glycidyl ether derivatives²³ or ω -epoxy alkanates.²⁴ As has been mentioned previously, polyether polyols of about 200-1200 g/mol are used to obtain rigid polyurethanes. These low-molecular-

weight polyethers can be synthesized by cationic ring-opening polymerization, which requires an acid catalyst. Several classes of cationic initiators have been developed, such as photosensitive onium salt initiators, which are inactive under ambient conditions and can release the acid initiator by UV radiation or heat¹⁷ and have been applied to epoxidized fatty compounds.²⁵⁻²⁷

In this article, we report the synthesis and characterization of polyether polyols from epoxidized methyl oleate (EMO; Scheme 1). Polyols (PA n and PC n ; Scheme 1) were prepared through the combination of the cationic polymerization of EMO oligomers (A-D, Scheme 1), and the controlled reduction of the carboxylate groups to hydroxyl moieties with lithium

aluminum hydride (LiAlH₄) as reducing agent. Polyols were characterized by chemical methods, spectroscopic techniques [Fourier transform infrared (FTIR) and nuclear magnetic resonance (NMR)], matrix-assisted laser desorption/ionization time-of-flight mass spectrometry (MALDI-TOF MS), and thermal techniques [differential scanning calorimetry (DSC)]. They were reacted with 4,4'-methylenebis(phenyl isocyanate) (MDI) to obtain polyurethanes. The properties of the prepared polyurethanes were studied with DSC, thermogravimetric analysis (TGA), and dynamic mechanical thermal analysis (DMTA).



Scheme 1

EXPERIMENTAL

Materials

The methyl oleate used in this study was supplied by Cognis (Düsseldorf, Germany). EMO was synthesized with a literature procedure.²⁸ The following chemicals were obtained from the sources indicated: formic acid (Scharlau), hydrogen peroxide, 50% (w/v; Aldrich), fluoroantimonic acid (HSbF₆; Aldrich), LiAlH₄ [1.0 M in tetrahydrofuran (THF); Aldrich], and MDI. They were used as received. THF was distilled from sodium immediately before use. Other solvents were purified by standard procedures.

Oligomerization of EMO

HSbF₆ (0.05 g; 0.5 wt %) was added to 10 g EMO. The mixture was stirred at room temperature for 1 h. The reaction was quenched by the addition of 1.5 mL of water followed by 100 mL of diethyl ether. The organic solution was washed with a sodium bicarbonate solution, dried over anhydrous magnesium sulfate, and filtered. Finally, the solvent was evaporated off under *in vacuo*, and this yielded oligomer A as a viscous oil. A similar procedure was followed to obtain oligomers B-D with the addition of 10, 20 and 50 mol % water to the oligomerization mixture.

¹H NMR [CDCl₃/tetramethylsilane (TMS), δ, ppm]: 3.63 (s, -OCH₃), 3.62-3.16 (m, polyether backbone), 2.27 (t, -CH₂COO-), 1.70-1.10 (m, -CH₂-aliphatic backbone), 0.85 (t, CH₃).

Representative Procedure for the Reduction of Oligomers A and C

Oligomer A (6 g, 3.2 mmol) was dissolved in 60 mL of anhydrous THF under nitrogen. A 1 M solution (6 mL) of LiAlH₄ in THF (6 mmol of LiAlH₄) was added slowly with stirring. After the LiAlH₄ addition was complete, the mixture was stirred vigorously at room temperature. After 30 min, excess LiAlH₄ was decomposed by the addition of 20 mL of ethyl acetate dropwise, then a saturated 10% H₂SO₄ solution (aqueous) was added, the phases were separated, and the aqueous layer was extracted with ethyl acetate. The combined organic phase was washed with a saturated aqueous NaCl solution, dried over anhydrous magnesium sulfate, and filtered, and the solvent was removed *in vacuo* at 50 °C.

¹H NMR (CDCl₃/TMS, δ, ppm): 3.63 (s, -OCH₃), 3.55 (t, -CH₂OH), 3.62-3.16 (m, polyether backbone), 2.27 (t, -CH₂COO-), 1.70-1.10 (m, -CH₂-aliphatic backbone), 0.85 (t, CH₃).

Representative Procedure for the Synthesis of Polyurethanes (PUAn and PUCn)

Polyurethanes were synthesized by the reaction of the polyols with MDI with a 2% molar excess of isocyanate (MDI). The samples were prepared through the mixing of a proper amount of polyol and MDI at 60 °C. Curing was carried out at 60 °C for 2 h and 110 °C overnight.

Characterization

NMR spectra were recorded on a Bruker AM 300 spectrometer. The samples were dissolved in deuteriochloroform, and ^1H NMR and ^{13}C NMR spectra were obtained at room temperature with TMS as an internal standard. The IR spectra were recorded on a Bomem Michelson MB 100 FTIR spectrophotometer with a resolution of 4 cm^{-1} in the absorbance mode. An attenuated total reflection (ATR) accessory with thermal control and a diamond crystal (Golden Gate heated single-reflection diamond ATR, Specac-Teknokroma) was used to determine FTIR spectra.

MALDI-TOF MS measurements were performed with a Voyager DE-RP mass spectrometer (Applied Biosystems, Framingham, MA) equipped with a nitrogen laser delivering 3-ns laser pulses at 337 nm. 2,5-Dihydroxybenzoic acid (DHB) was used as a matrix, and silver trifluoroacetate was used as a dopant. Size exclusion chromatography (SEC) analysis was carried out with a Waters 510 pump system equipped with a Shimadzu RID-6A refractive-index detector. THF was used as an eluent at a flow rate of 1.0 mL/min. The calibration curves for SEC analysis were obtained with polystyrene standards.

Calorimetric studies were carried with a Mettler DSC822e thermal analyzer with N_2 as the purge gas. A heating rate of $20\text{ }^\circ\text{C}/\text{min}$ was used. Thermal stability studies were carried out with a Mettler TGA/SDTA851e/LF/1100 with N_2 as the purge gas at a scanning rate of $10\text{ }^\circ\text{C}/\text{min}$.

The mechanical properties were measured with a TA DMA 2928 dynamic mechanical thermal analyzer. Specimens 1.2 mm thick, 5 mm wide, and 10 mm long were tested in a three-point-bending configuration. The various thermal transitions were studied between -100 and $140\text{ }^\circ\text{C}$ at a heating rate of $5\text{ }^\circ\text{C}/\text{min}$ and at a fixed frequency of 1 Hz.

General Procedure for Unilever Method Hydroxyl Value Determination²⁹

For an expected hydroxyl value (see ref. 29), an accurately measured volume of acetic acid anhydride was added to a known amount of a sample weighed into a round-bottom flask. After mixing, the flask was placed in an oil bath at $95\text{--}100\text{ }^\circ\text{C}$. After 1 h, the flask was cooled, and 1 mL of distilled water was added. After shaking, heating was continued for 10 min to convert acetic acid anhydride into acetic acid. After the mixture was cooled again, 5 mL of 95 % ethanol was added and the contents were titrated with a 0.5 M ethanolic potassium hydroxide solution with phenolphthalein as an indicator. A blank determination was carried out with a similar procedure.

RESULTS AND DISCUSSION

Oligomerization of EMO

EMO was prepared by the reaction of methyl oleate with formic acid and hydrogen peroxide. Precipitation with acetone was applied to purify the product. Gas chromatography analysis

showed that EMO was obtained in a purity of 96%.

EMO was cationically oligomerized. We tested several acids as catalysts: HSbF_6 , hexafluorophosphoric acid (HPF_6), and trifluoromethanesulfonic acid (HSO_3CF_3). Among these, only HSbF_6 predominantly produced oligoether species, as could be observed from MALDI-TOF MS analysis. The oligomerization was carried out with different amounts of HSbF_6 at room temperature (0.1, 0.5, 1.0, and 1.5 wt %). NMR analysis of the oligomer obtained with 0.1 wt % initiator revealed the presence of non reacted epoxide, whereas higher amounts of the initiator gave complete oligomerization. Therefore, the cationic polymerization of EMO was carried out in the presence of 0.5 wt % HSbF_6 at room temperature for 1 h. The catalyst was completely soluble in EMO at room temperature, and the oligomerization was performed homogeneously in the absence of a solvent, thus being an advantageous process from an environmental viewpoint.¹ The oligomerization reaction was monitored by FTIR spectroscopy, which showed a decrease

in the absorption centered at 836 cm^{-1} , corresponding to an oxirane ring, and a slight increase in the absorption at 1075 cm^{-1} (C-O-C ether) and in the broad band around 3500 cm^{-1} (O-H hydroxyl group). This indicated that oxirane ring opening took place to form ether linkages and hydroxyl-terminated polymer.

The cationic oligomerization of EMO resulted in a clear, yellow, viscous oil, and the results are summarized in Table 1 (oligomer A).

The ^1H NMR spectrum of oligomer A is given in Figure 1. ^1H NMR showed that no epoxy groups (2.8 ppm) remained after the polymerization, in accordance with FTIR results, thus showing that the epoxy group of the methyl ester is reactive enough to polymerize under the set conditions. A new broad peak due to the oligoether backbone was observed between 3.1 and 3.6 ppm. Signals in the ^1H NMR spectrum at 3.6 (-OCH₃), 2.3 (-CH₂-COO-), 1.1-1.7 (-CH₂- aliphatic backbone), and 0.8 ppm (-CH₃) confirmed the oligomer structure.

Table 1. General Properties of the Oligomers Obtained by the Cationic Ring-Opening Polymerization of EMO^a

Oligomer	Water (mol %)	HV (mg of KOH/g)	EW (g/equiv) ^b	M_n (SEC; g/mol)	M_w/M_n (SEC)	Functionality ^c
A	-	52	1079	1235	1.59	1.1
B	10	74	758	1076	1.48	1.4
C	20	89	630	1025	1.47	1.6
D	50	108	519	961	1.45	1.8

^a Polymerization conditions: 0.5 wt % HSbF_6 , 1 h, and room temperature.

^b Equivalent weight calculated from the HV.

^c Obtained by the division of the experimental molecular weight (M_n) by the EW.

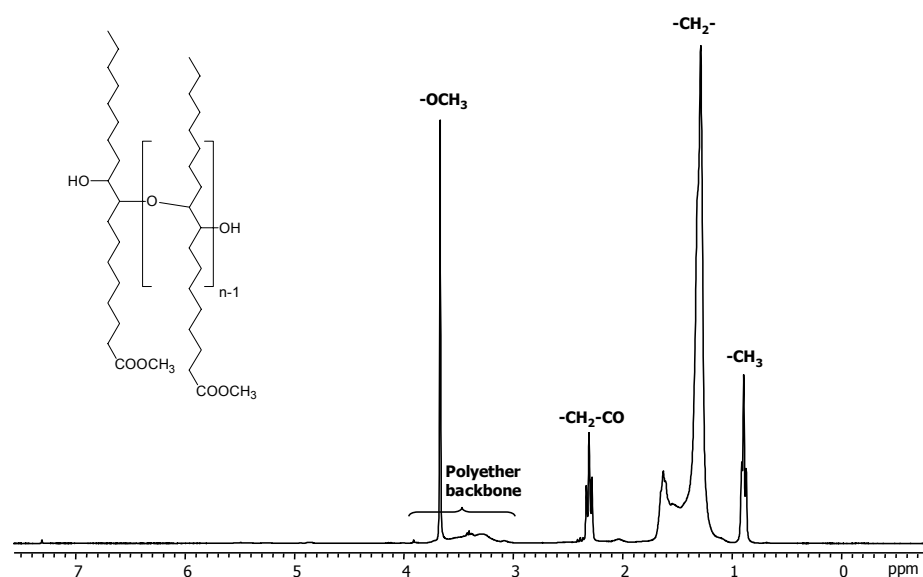


Figure 1. ^1H NMR spectrum (CDCl_3 , 300 MHz) of oligomer A.

Traces of ketones, formed by the acid catalyzed isomerization of the oxirane ring, were observed in the product of oligomerization initiated by HSbF_6 by ^1H NMR at 2.4 ppm. In contrast, we observed the formation of higher amounts of corresponding ketones when using HSO_3CF_3 as an initiator.

MALDI-TOF MS was used to analyze oligomer distribution. Figure 2 shows the MALDI-TOF MS spectrum of oligomer A which is dominated by a series of peaks ranging from a mass of 750 Da to a mass of 2630 Da, corresponding to linear hydroxyl terminated oligomers doped with Ag^+ ions of type $\text{H}[\text{O}-\text{C}_{19}\text{H}_{36}\text{O}_2]_n\text{-OH-Ag}^+$ (mass = $312n + 18 + \text{Ag}^+$); n values varying from 2 to 8 were detected (Scheme 1). The three most intense peaks belonging to this series corresponds to oligomers with n values of 3-5. The spectrum also displays other peaks of lower intensity with

masses of $312n + \text{Ag}^+$, corresponding to cyclic structures formed by back-biting (Scheme 2), and peaks with general formula $\text{CH}_3[\text{O}-\text{C}_{19}\text{H}_{36}\text{O}_2]_n\text{-OH-Ag}^+$ (mass = $312n + 32 + \text{Ag}^+$), corresponding to oligomers terminated by OH on one end and OCH_3 on the other (Scheme 2). These last peaks can appear in the spectrum because of the presence of traces of methanol, generated by transesterification of ester groups or as impurities in the monomer, which reacted during polymerization and formed chain ends. Therefore, MALDI-TOF MS confirmed the presence of a mixture of linear and cyclic oligomers.

As is well known, the cationic polymerization of epoxides produces macrocycles and hydroxy-terminated open chain oligomers. For disubstituted epoxides under photoinitiated cationic polymerization, Warwel²⁷ reported obtaining macrocycles, linear oligomers,

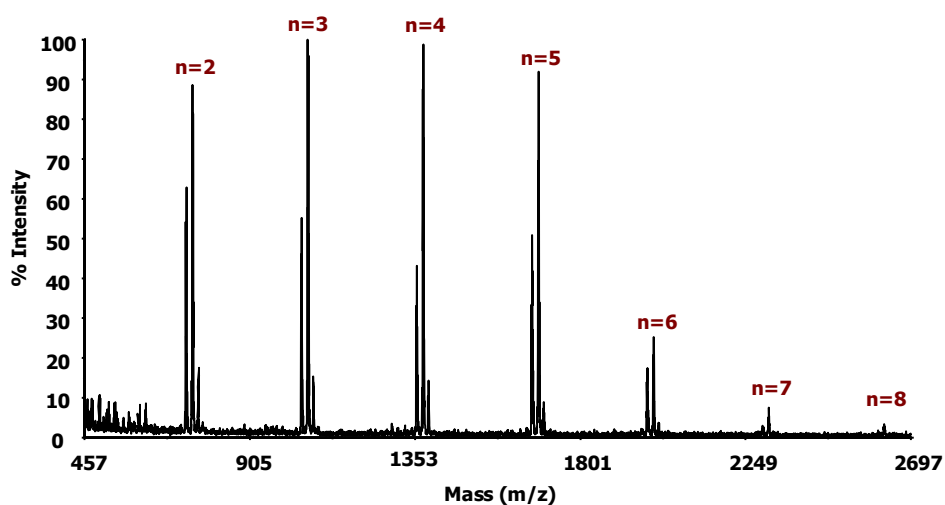
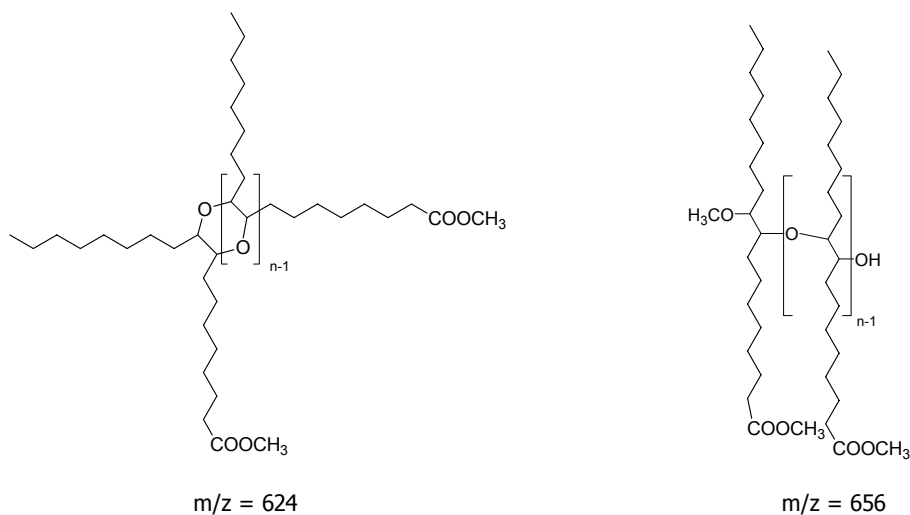


Figure 2. MALDI-TOF MS spectrum of oligomer A doped with silver trifluoroacetate, showing the ion series $\text{H}[\text{O}-\text{C}_{19}\text{H}_{36}\text{O}_2]_n\text{-OH-Ag}^+$ (mass = $312n + 18 + \text{Ag}^+$), $[\text{O}-\text{C}_{19}\text{H}_{36}\text{O}_2]_n\text{Ag}^+$ (mass = $312n + \text{Ag}^+$) and $\text{CH}_3\text{-}[\text{O}-\text{C}_{19}\text{H}_{36}\text{O}_2]_n\text{-OH-Ag}^+$ (mass = $312n + 32 + \text{Ag}^+$; see Schemes 1 and 2).

and ketones formed by the rearrangement of the monomer. By the addition of water, macrocyclisation was completely suppressed, and linear oligomers of different molecular

weights were obtained; this showed that the nucleophilic attack of water competes with the intramolecular attack, and the proportion of linear species increases.



Scheme 2

Polyols of industrial importance are usually required to have a low viscosity and a high hydroxyl content value (HV). To increase the proportion of linear oligomeric structures, to reduce their molecular weight, and to increase their hydroxyl content, water was added to the oligomerization system. The oligomerization of EMO was carried out in the presence of 10, 20, and 50 mol % water to give oligomers B, C, and D (Table 1). MALDI-TOF spectra show that the highest intensity signals corresponds to a lower molecular weight ($n = 2$ or 3). Moreover, from MALDI-TOF analysis, a decrease in the signal intensity corresponding to the cyclic oligomers was observed, and for the product obtained with 50%, this signal was almost negligible. These results are in accordance with the ones previously described.²⁷

¹H NMR spectra of the oligomers B-D did not show significant differences between them and sample A obtained in absence of water. FTIR spectra showed a significant increase in the hydroxyl absorption at 3500 cm^{-1} , which indicates that the presence of water causes an increase in the HV.

The HV of the oligomers was determined according to the Unilever method.²⁹ This method uses a solution of acetic anhydride in pyridine, and the HV is defined as the number of potassium hydroxide required to neutralize the amount of acetic acid capable of combining by acetylation with 1 g of the sample. The results are summarized in Table 1; as can be seen, the HV increases as the water content in the polymerization system increases, and SEC analysis has shown that the

molecular weight decreases as the HV increases, according to the MALDI-TOF results. The compounds obtained so far are polyether diols with secondary alcohol functionality and side products containing only one or no hydroxyl group. These products are not suited for synthesizing polyurethanes. In addition, primary hydroxyl groups are more reactive and much better suited for the synthesis of polyurethanes. Therefore, to obtain a broad range of polyol structures that may have different properties and may impart different properties to the final product when converted to polyurethanes, we carried out a partial reduction of the carboxylate groups to yield primary hydroxyl moieties.

Partial Reduction of Ester Groups of Oligomers A and C

Oligomers A and C were used as starting materials for the partial reduction of the ester groups to synthesize polyols having primary hydroxyl moieties. The reduction of these oligomers was carried out with different amounts of LiAlH_4 as reducing agent, giving polyols PA1, PA2, and PA3 (Table 2). Figure 3 shows the ¹H NMR spectra of oligomer A and the corresponding polyols. A new signal appears at $\delta = 3.6$ ppm due to the protons of the $\text{CH}_2\text{-OH}$ moiety. As the reduction degree increases, the intensity of this signal increases, whereas the intensity of the peak at $\delta = 2.3$ ppm decreases. The same trend can be observed for polyol C.

Table 2. General Properties of the Obtained Polyols

Polyol	Starting Oligomer	mmol of LiAlH ₄ /g of oligomer	HV (mg KOH/g)	EW ^a (g/equiv)	M _n (SEC)	Functionality ^b
PA1	A	0.5	94	597	1220	2.0
PA2	A	1.0	184	305	1187	3.8
PA3	A	1.5	260	216	1149	5.3
PC1	C	0.5	127	442	1010	2.3
PC2	C	1.0	216	260	980	3.7
PC3	C	1.5	298	188	935	4.9

^a Equivalent weight calculated from the HV.

^b Obtained by the division of the experimental molecular weight (M_n) by the EW.

The FTIR spectra of the polyols are presented in Figure 4. In comparison with the spectrum of A, there was an increase in the hydroxyl group peak (3500 cm⁻¹), whereas a decrease in the aliphatic ester carbonyl peak (1750 cm⁻¹)

was observed. We determined the HV of the polyols according to the Unilever method (Table 2). As the amount of LiAlH₄ increases, the hydroxyl value increases, as expected.

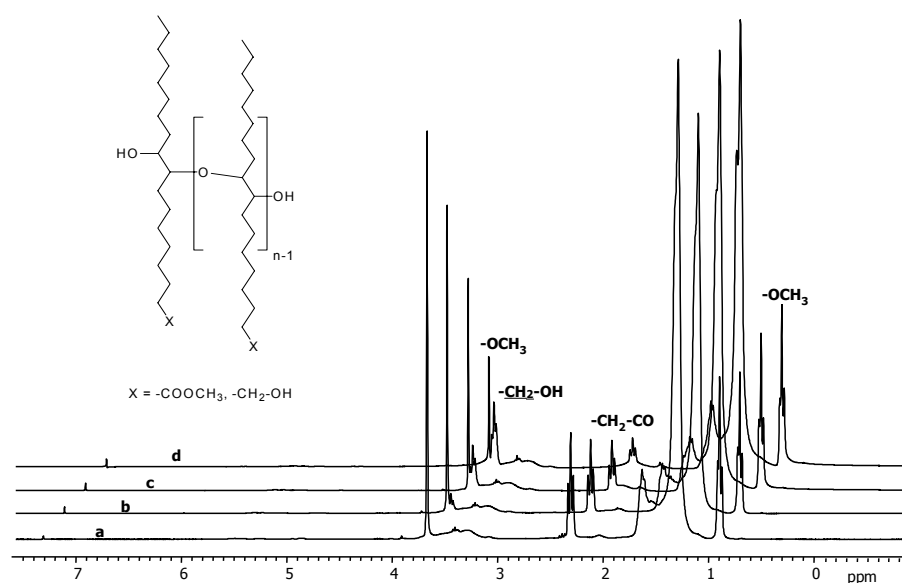


Figure 3. ¹H NMR spectra (CDCl₃, 300 MHz) of (a) oligomer A, (b) polyol PA1, (c) polyol PA2, and (d) polyol PA3.

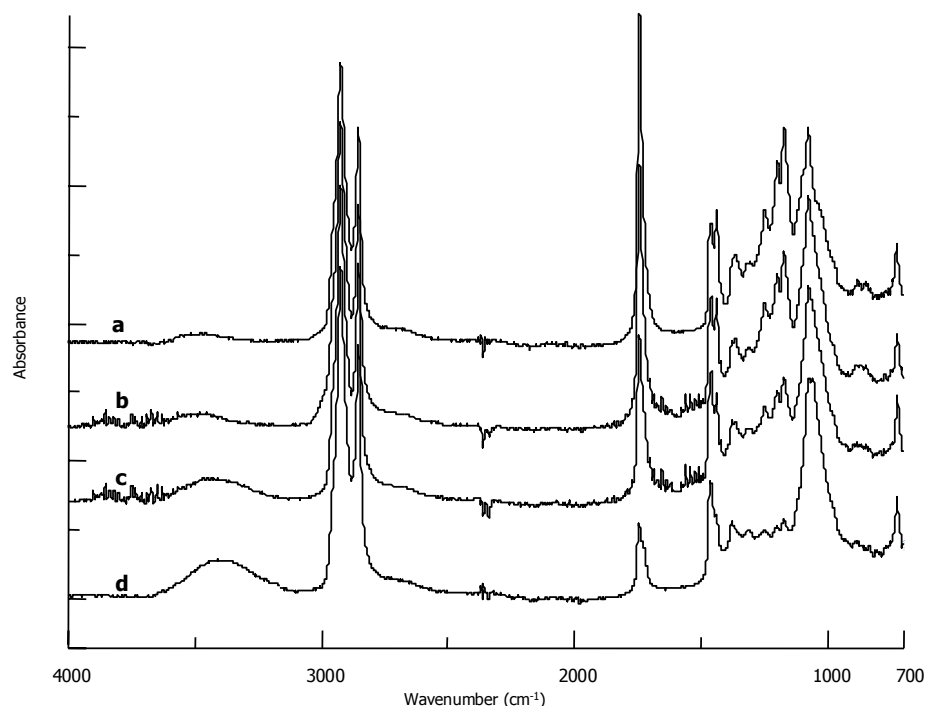


Figure 4. FTIR spectra of (a) oligomer A, (b) polyol PA1, (c) polyol PA2, and (d) polyol PA3.

In this way, polyols with a broad range of functionalities have been obtained, and they range from clear liquids to white, waxy solids at room temperature. DSC traces for A and its polyol derivatives are collected in Figure 5. As can be seen, A exhibits a broad melting peak centered at $-7\text{ }^{\circ}\text{C}$, which shifts to higher temperatures when the HV increases. Moreover, a second melting endotherm can be observed at $42\text{ }^{\circ}\text{C}$ for PA2 and PA3, with the highest functionality. Multiple peaks in these polyols should be ascribed to different crystalline forms.

Synthesis of Polyurethanes

The six polyols PA1-PA3 and PC1-PC3 were reacted with MDI at $60\text{ }^{\circ}\text{C}$ to give

polyurethanes PUA1, PUA2, PUA3, PUC1, PUC2, and PUC3. All the polyols had primary OH groups and gelled quickly at the mixing temperature. The crosslinking reaction was monitored by FTIR spectroscopy. Figure 6 shows FTIR spectra before and after the curing of polyurethane PUA2. The starting mixture showed a characteristic peak at 2240 cm^{-1} ascribed to $-\text{N}=\text{C}=\text{O}$ stretching of the isocyanate moiety. After the curing, this peak significantly decreased. The crosslinking reaction was also monitored by the appearance of the characteristic absorbances of the urethane link.

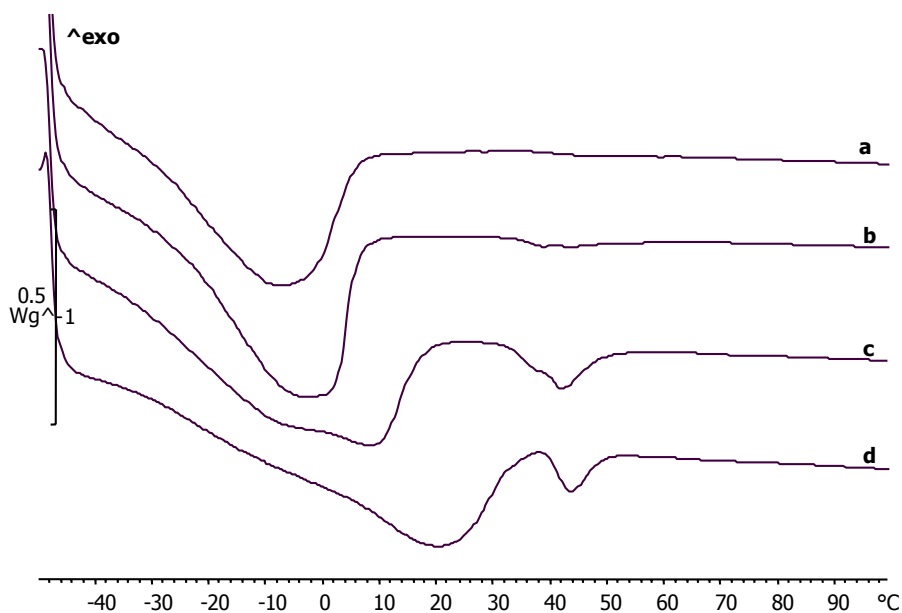


Figure 5. DSC curves of (a) oligomer A, (b) polyol PA1, (c) polyol PA2, and (d) polyol PA3.

The band due to the carbonyl stretching vibration of polyurethane occurred at 1723 cm^{-1} , and a combination of N-H deformation and C-N stretching vibrations occurred at 1533 and 1233 cm^{-1} , respectively. The peak appearing at 1309 cm^{-1} was due to $-\text{CONH}$ asymmetric stretching vibrations. Moreover, the broad band centered at 3500 cm^{-1} , corresponding to the O-H stretching, shifted to lower frequencies and showed a maximum at 3350 cm^{-1} , characteristic of N-H stretching.

Thermal behavior of the polyurethanes was investigated with DSC. The glass-transition temperature (T_g) could be observed by this technique. The T_g values determined by DSC are shown in Table 3. The data given show clearly for both series of polyurethanes the

expected trend, that T_g was higher when the functionality of the polyol used was higher, which indicates a higher degree of crosslinking.

TGA is the most favored technique for the evaluation of the thermal stability of polymers. Polyurethanes have relatively low thermal stability, mainly because of the presence of urethane bonds. The thermal stability of the obtained polyurethanes was studied with TGA (10 °C/min) in a nitrogen atmosphere, and the obtained data are shown in Table 3. The shapes of the weight-loss curves of all the polyurethanes are almost identical, and the differences in the thermal stability appear to be small. The decomposition of the polyurethanes in a nitrogen atmosphere does not take place below 300 °C .

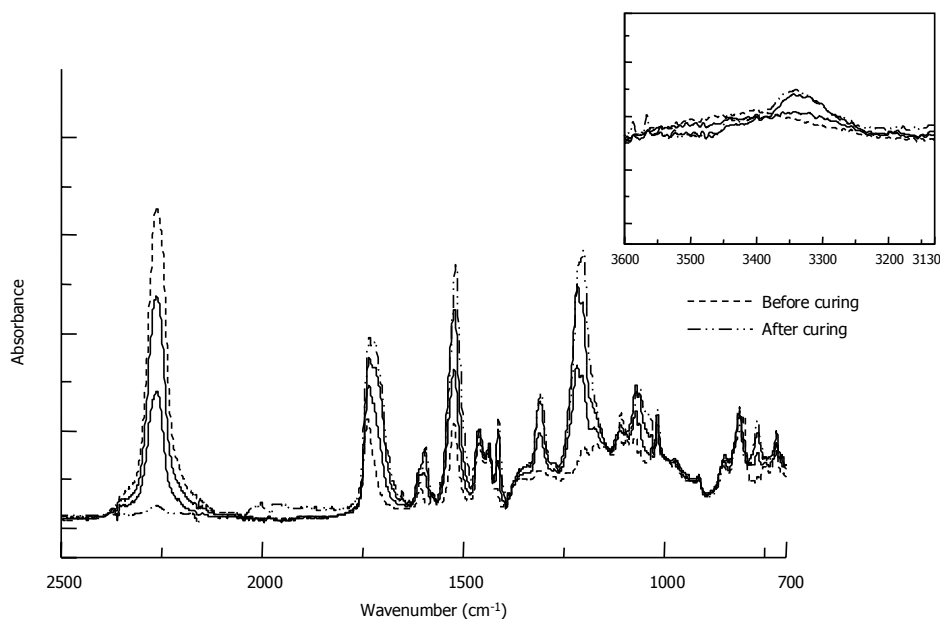


Figure 6. FTIR spectra of the crosslinking of polyether polyol PA2 with MDI to give polyurethane PUA2 at different curing times (0, 30, and 60 min at 60 °C and 110 °C overnight).

Table 3. Thermal Properties of the Polyurethanes

Polyurethane	Starting Polyol	T_g (°C)		TGA (N_2 Atmosphere)	
		$1/2 \Delta C_p^a$	$\tan \delta_{max}^b$	$T_{5\% loss}^c$	Yield $_{800^\circ C}$ (%) ^d
PUA1	PA1	-15	-	307	2
PUA2	PA2	39	63	310	3
PUA3	PA3	80	93	316	5
PUC1	PC1	0	-	309	2
PUC2	PC2	37	62	303	4
PUC3	PC3	52	76	313	4

^a Glass-transition temperature obtained by DSC.

^b Glass-transition temperature obtained by DMTA.

^c Temperature of 5% of weight loss.

The dynamic mechanical properties of the polyurethanes were obtained as a function of temperature beginning in the glassy state, through the T_g , and well into the rubbery plateau of each material. Figure 7(a,b) shows the temperature dependence of the storage modulus and loss factor ($\tan \delta$) of the polyurethanes. From the DMTA curves, the plateau of the elastic modulus in the rubbery state can be used to make qualitative comparisons of the level of crosslinking among the various polymers. Figure 7 a) shows that the value of the storage modulus in the rubber plateau decreased as the HV of the starting polyol decreased. DMTA also made it possible to determine the T_g of the crosslinked materials. It was detected as the maximum of $\tan \delta$. The T_g values determined by DMTA are shown in Table 3. As expected, the T_g values, like $\tan \delta$, are higher than the $1/2\Delta C_p$

values from DSC and increase as the HV of starting polyol increases [Figure 7(b)]. This is caused by the higher crosslinking degree, which increases the stiffness of the network structure. A weak β transition at about 0 °C can be observed. The origin of this peak is not known, but it may be related to the rotational motions of short units in the fatty acid chains.³⁰

CONCLUSIONS

Polyether polyols were synthesized by the cationic oxirane ring-opening oligomerization of EMO followed by partial reduction of the ester groups to primary alcohols. The corresponding polyurethane networks were prepared by the reaction of the polyols with MDI. This showed that plant oils as renewable resources can be used to make hard rubbers or rigid plastics.

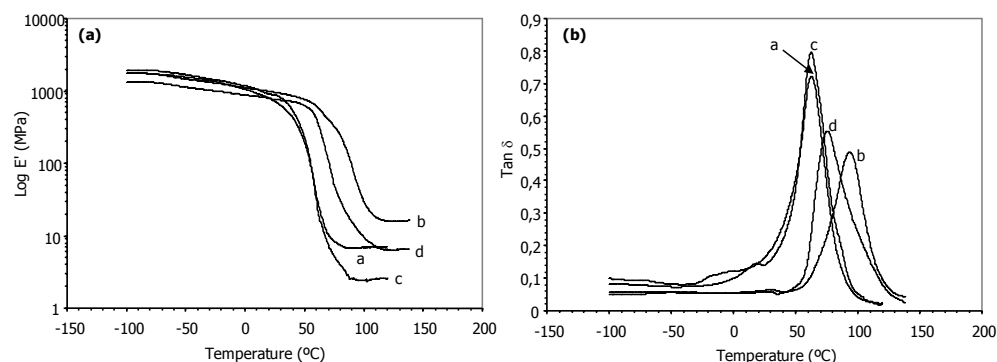


Figure 7. (a) Storage modulus (E')/temperature curves of (a) PUA2, (b) PUA3, (c) PUC2, and (d) PUC3 and (b) $\tan \delta$ /temperature curves of (a) PUA2, (b) PUA3, (c) PUC2, and (d) PUC3.

Acknowledgements

The authors gratefully acknowledge the Comisión Interministerial de Ciencia y Tecnología (MAT2002-00223) and the

Comissió Interdepartamental de Recerca i Innovació Tecnològica (2001SGR00318) for their financial support of this work and for G. Lligadas's predoctoral (2003FI00765)

and mobility (2004BV200032) grants. We would like to thank F. Fabbretti for matrix-assisted laser desorption/ionization time-of-flight mass spectrometry analysis and D. Töpken for the synthesis of epoxidized methyl oleate.

REFERENCES AND NOTES

- (a) Eissen, M.; Metzger, J. O.; Schmidt, E.; Schneidewind, U. *Angew Chem Int Ed Engl* 2002, 41, 414; (b) Metzger, J. O.; Eissen, M. C. R. *Chemie* 2004, 7, 569.
- Report of the United Nations Conference on Environment and Development, Rio de Janeiro, 3-14 June 1992; <http://www.un.org/esa/sustdev>, accessed, November 3, 2005.
- Li, F. K.; Larock, R. C. *J Polym Environ* 2002, 10, 59.
- Uyama, H.; Kuwabara, M.; Tsujimoto, T.; Kobayashi, S. *Biomacromolecules* 2003, 4, 211.
- Tsujimoto, T.; Uyama, H.; Kobayashi, S. *Macromolecules* 2004, 37, 1777.
- Biermann, U.; Friedt, W.; Lang, S.; Lühs, W.; Machmüller, G.; Metzger, J. O.; Klaas gen. Rüscher, M.; Schäfer, H. J.; Schneider, M. P. *Angew Chem Int Ed Engl* 2000, 39, 2206.
- Li, F.; Larock, R.C. *J Appl Polym Sci* 2002, 1533, 84.
- Eren, T.; Kusefoglu, S. H. *J Appl Polym Sci* 2004, 91, 2700.
- Khot, S. N.; LaScala, J. J.; Can, E.; Morye, S. S.; Williams, G. I.; Palmese, G. R.; Kusefoglu, S. H.; Wool, R. P. *J Appl Polym Sci* 2001, 82, 703.
- Findley, T. W.; Swern, D.; Scalan, J. T. *J Am Chem Soc* 1945, 67, 412.
- Rangarajan, B.; Havey, A.; Grulke, E. A.; Culnan, P. D. *J Am Oil Chem Soc* 1995, 72, 1161.
- Sonnet, P. E.; Lankin, M. E.; McNeill, G. P. *J Am Oil Chem Soc* 1995, 72, 199.
- Kuo, M. C.; Chou, T. C. *Ind Eng Chem Res* 1987, 26, 277.
- Ucciani, E.; Debal, A.; Rafaralahitsimba, J. *Fat Sci Technol* 1993, 95, 236.
- Rüscher, M.; Warwell, S. *Ind Crops and Prod* 1999, 9, 125.
- Baumann, H.; Bühler, M.; Fochem, H.; Hirsinger, F.; Zoblein, H.; Falbe, J. *Angew Chem Int Ed Engl* 1988, 27, 41.
- Crivello, J. V.; Narayan, R. *Chem Mater* 1992, 4, 692.
- Guo, A.; Demydov, D.; Zhang, W.; Petrovic, Z. S. *J Polym Environ* 2002, 10, 49.
- Guo, A.; Javni, I.; Petrovic, Z. *J Appl Polym Sci* 2000, 77, 467.
- Petrovic, Z.; Guo, A.; Javni, I. U.S. Patent 6,107,433, 2000.
- Dietrich, D.; Uhlig, K. In *Ullmann's Encyclopedia of Industrial Chemistry*; Elvers, B.; Hawkins, S.; Schulz, G., Eds.; VCH: Weinheim, 1992; p 665.
- Inoue, S.; Aida, T. *Handbook of Polymer Synthesis*; Marcel Dekker: New York, 1991; Part A.
- Ronda, J. C.; Serra, A.; Cadiz, V. *Macromol Chem Phys* 1999, 200, 221.
- Muggee, J.; Vogl, O. *J Polym Sci Polym Chem Ed* 1985, 23, 649.
- Chakrapani, S.; Crivello, J. V. *J Macromol Sci Pure Appl Chem* 1998, 35, 1.
- Crivello, J. V.; Carlson, K. D. *J Macromol Sci Pure Appl Chem* 1996, 33, 251.
- Warwel, S.; Fehling, E.; Kunz, M. *Eur J Lipid Sci Technol* 2001, 103, 133.
- Pages, X.; Alfos, C. *Oleagineux Corps Gras Lipides* 2001, 8, 122.
- Handbuch der Lebensmittelchemie*; Springer-Verlag: Berlin, 1965; Vol. IV.
- Petrovic, Z.; Zhang, W.; Javni, I. *Biomacromolecules* 2005, 6, 713.

4.4.2 Novel Silicon-Containing Polyurethanes from Vegetable Oils as Renewable Resources. Synthesis and Properties

NOVEL SILICON-CONTAINING POLYURETHANES FROM VEGETABLE OILS AS RENEWABLE RESOURCES. SYNTHESIS AND PROPERTIES

G. Lligadas, J.C. Ronda, M. Galià, V. Cádiz
Departament de Química Analítica i Química Orgànica, Universitat Rovira i Virgili,
Campus Sescelades, Marcel·lí Domingo s/n, 43007 Tarragona, Spain.

ABSTRACT: Hydrosilylation of methyl 10-undecenoate (UDM) with phenyl tris(dimethylsiloxy) silane (PTDS) followed by a reduction of carboxylate groups was used to obtain a silicon-containing polyol with terminal primary hydroxyl groups (PSi194). Biobased silicon-containing polyurethanes, with a silicon content between 1.7% and 9.0%, were prepared from epoxidized methyl oleate-based polyether polyol (P184), PSi194, and 4,4'-methylenebis(phenyl isocyanate) (MDI). The thermal, mechanical, and flame-retardant properties of these materials were examined. The most notable change resulting from the incorporation of PSi194 is the appearance of melting endotherms of variable enthalpy and position and a downward shift in the T_g . The incorporation of silicon does not change the thermal stability but enhances the stability of the char under air atmosphere. Polyurethanes with higher silicon content no longer burn in ambient air without complementary oxygen, which suggests that these biobased materials are very interesting for applications that require fire resistance.

Keywords: biopolymers; polyurethanes; renewable resources; vegetable oils

INTRODUCTION

Biomaterials, chemicals, and energy from renewable resources have been the object of considerable interest in recent years.¹ In the search for sustainable chemistry, considerable importance is being attached to polymers prepared from biological sources, and interest has focused on the use of cheap, biodegradable, and annually

renewable starting materials such as starch, cellulose, carbohydrates, proteins, and vegetable oils for synthesizing a wide range of bioplastics.² The aim of this research is to reduce petroleum dependence, reduce the negative impact on the environment, and add value to existing agricultural products so that farming and industry can benefit. Vegetable oils are one of the cheapest and most abundant biological

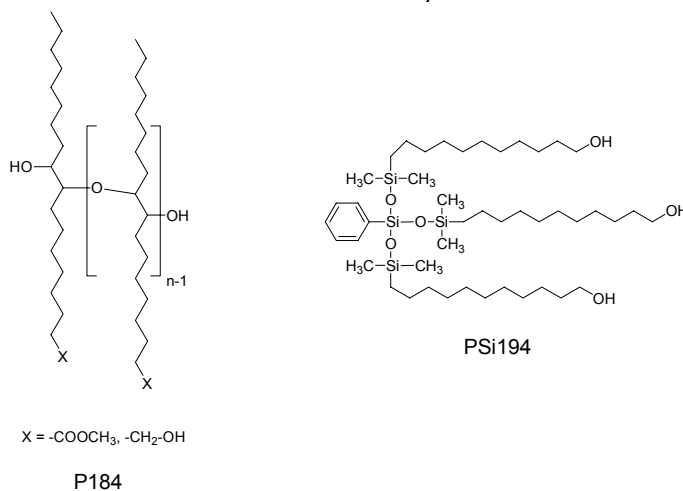
sources available in large quantities, and their use as starting materials has numerous advantages, for example, low toxicity, inherent biodegradability, and high purity.³ They are considered to be one of the most important classes of renewable resources for the production of biobased thermosets.⁴

Polyols derived from vegetable oils are new raw materials from renewable resources and are essential in the preparation of any polyurethane product. For natural oils to be used as raw materials for polyol production, multiple hydroxyl functionality is required. Two different ways of preparing vegetable oil-based polyols have been successfully developed. In the first, polyols are formed by reaction at the double bond of the unsaturated fatty oil. For example, the epoxidation and further oxirane ring opening leads to polyols with secondary hydroxyl groups,⁵⁻⁷ while the hydroformylation and the ozonolysis lead to polyols with primary hydroxyl groups.^{8,9} In the second, a combined reaction at the double bonds and subsequent reduction of the carboxyl group yields the hydroxyl moieties.¹⁰

Polyurethane polymers are a versatile class of polymers which are used in a wide range of applications, and their structure can be tailored to specific requirements.¹¹ Depending on the hydroxyl value and other characteristics of the polyol, it can be applied in the development of adhesives, coatings, and flexible or rigid foams. In combination with isocyanates, vegetable oil-based polyols produce polyurethanes that can compete in many ways with polyurethanes derived from petrochemical polyols, and their preparation

for general polyurethane use has been the subject of many studies.^{5-10,12-15} Moreover, due to the hydrophobic nature of triglycerides, vegetable oils produce polyurethanes which have such excellent chemical and physical properties as enhanced hydrolytic and thermal stability.^{16,17} Nowadays, it is a challenge to synthesize suitable diisocyanates via diamino compounds derived from vegetable oils, making it possible to produce polyurethanes completely from renewables. Like other organic polymeric materials, the flammability of these materials is a shortcoming in some applications. Major progress in the area of flame-retardant polyurethanes in recent years has been made in the field of phosphorous- or silicon-containing products.¹⁸

Some papers have appeared in recent years about the synthesis of siloxane-based polyurethanes with improved biostability and good mechanical properties.¹⁹ Linear polyhedral oligomeric silsesquioxane (POSS)-containing polyurethanes have been reported for application as surface coatings.^{20,21} Polyurethane networks incorporating POSS with enhanced glass transition temperatures, improved thermal stabilities, and flame retardance have been also reported.²² Besides the interest in investigating the structural properties of the new silicon-containing polyurethanes, we believe that many of their features (for example, improved thermal stability, biostability, and biocompatibility, good mechanical properties, and fire resistance) can be exploited in the field of polyurethanes for specialized applications.

Chart 1. Chemical Structures of Polyols P184 and PSi194

To further extend the applications of these renewable resources, our group has focused on converting vegetable oils into useful biopolymers. In a previous study, we described the synthesis of polyether polyols through the combination of cationic polymerization of epoxidized methyl oleate (EMO) and the reduction of carboxylate groups to hydroxyl moieties.¹⁰ Polyols with different hydroxyl contents were obtained and reacted with MDI to yield polyurethanes that behave like hard rubbers or rigid plastics. We have also investigated the synthesis of new organic-inorganic hybrid materials via the hydrosilylation reaction in an attempt to find new applications for unsaturated fatty compounds. There has been considerable interest in these materials because of their unexpected properties.²³ After our efforts to functionalize vegetable oils so that they could act as components for biopolymeric materials, we investigated the synthesis of a silicon-containing polyol and its application in the synthesis of silicon-containing poly-

urethanes with enhanced flame retardance.

The present study aims to develop novel, biobased silicon-containing polyurethanes from vegetable oils. We first investigated the hydrosilylation reaction of methyl 10-undecenoate (UDM), an ω -unsaturated fatty acid methyl ester which can be easily obtained from natural ricinoleic acid, with a trifunctional hydrosilylating agent, phenyltris(dimethylsiloxy)silane (PTDS), and the subsequent reduction of carboxylate groups to obtain a silicon-containing polyol (PSi194) with terminal primary hydroxyl groups. Silicon-containing polyurethanes were obtained from an EMO-based polyether polyol (P184), a silicon-containing polyol (PSi194) (Chart 1) and 4,4'-methylenebis(phenyl isocyanate) (MDI) as a crosslinking agent. The thermal properties of the polyurethanes prepared were studied by using differential scanning calorimetry (DSC), thermogravimetric analysis (TGA), and dynamomechanical analysis (DMTA),

and the flame retardance was assessed by the limiting oxygen index (LOI) test.

EXPERIMENTAL

Materials

The following chemicals were obtained from the sources indicated: phenyltris(dimethylsiloxy)silane, PTDS (95%, from ABCR), lithium aluminum hydride, LiAlH_4 (97%, from SDS), and 4,4'-methylenebis(phenyl isocyanate) (MDI, from Aldrich). They were all used as received. A platinumdivinyltetramethylsiloxane complex with 3–3.5 wt % platinum in xylene (Aldrich) was dissolved in toluene to give a 274 ppm platinum concentration. The Pt solution was stored at 4 °C. Toluene and tetrahydrofuran (THF) were distilled from sodium immediately before use. Other solvents were purified by standard procedures.

Synthesis of Polyether Polyol P184

Epoxidized methyl oleate-based polyether polyol (P184) with OH number of 184 mg KOH/g was synthesized in our laboratory using the procedure described earlier.¹⁰ This OH number corresponds to the equivalent weight of the polyol, 305, functionality, 3.8, and molecular weight, 1187. Methyl 10-undecenoate (UDM) was synthesized as previously described.²³

Synthesis of Polyol PSi194

Silicon-containing polyol was synthesized in two steps: hydrosilylation of methyl 10-undecenoate (UDM) with phenyl tris(dimethylsiloxy)silane (PTDS)

to obtain PTDS-UDM followed by a reduction of carboxylate groups to give primary hydroxyl groups in PSi194 (Scheme 1).

Hydrosilylation of UDM

Methyl 10-undecenoate (UDM) (16 g, 80 mmol) was dissolved in anhydrous toluene (100 mL) under argon atmosphere in a 250 mL two-necked round-bottomed flask equipped with a refluxing condenser. A solution of Pt complex (2 mL, 0.54 ppm) was then injected into the solution using a syringe, and the mixture was stirred at room temperature for 5 min. The corresponding stoichiometric amount of phenyltris(dimethylsiloxy)silane (PTDS) (9.3 g, 26.7 mmol) was added, and the solution was warmed to 65 °C and stirred at this temperature for 2 h. After cooling, toluene was evaporated under reduced pressure, and the crude mixture was dissolved in CH_2Cl_2 and passed through a silica gel column to remove the Pt catalyst. Finally, the solvent was evaporated under vacuum, and the resulting product, PTDS-UDM, was obtained as viscous oil (22.5 g, 91%).

¹H NMR (CDCl_3/TMS , δ (ppm)): 7.58–7.27 (m, H_{Ar} , 5H), 3.68 (s, $-\text{OCH}_3$, 9H), 2.32 (t, $-\text{CH}_2-\text{CO}$, 6H), 1.61 (m, $\text{CH}_2\text{CH}_2\text{CO}$, 6H), 1.24 (m, $-\text{CH}_2-$, 42H), 0.53 (t, CH_2-Si , 6H), 0.08 (s, $\text{Si}-\text{CH}_3$, 18H). ¹³C NMR (CDCl_3/TMS , δ (ppm)): 174.55 (s), 135.71 (s), 134.02 (d), 129.58 (d), 127.63 (d), 51.64 (q), 34.32 (t), 33.73 (t), 29.77 (t), 29.73 (t), 29.59 (t), 29.49 (t), 29.39 (t), 25.18 (t), 23.38 (t), 18.45 (t), 0.37 (q).

Reduction of PTDS-UDM

Lithium aluminum hydride (8.3 g, 219 mmol) was dispersed in 500 mL of anhydrous tetrahydrofuran (THF) in a 1-L, two-necked, round-bottomed flask under argon atmosphere. PTDS-UDM (22.5 g, 24.3 mmol), dissolved in anhydrous THF (50 mL), was added dropwise with stirring over a period of 30 min. After addition was complete, the mixture was stirred vigorously at room temperature for 1 h. After this, the excess LiAlH_4 was decomposed by adding 50 mL of ethyl acetate dropwise. Then, 10% H_2SO_4 aqueous solution was added, and the aqueous layer was extracted with ethyl acetate. The combined organic phase was washed with saturated sodium bicarbonate solution (NaHCO_3) until the pH was neutral and brine. The organic phase was dried over anhydrous magnesium sulfate, filtered, and the solvent was evaporated off yielding a viscous liquid (20.0 g, 98%). The titrimetrically determined hydroxyl value of the product was 194 mg of KOH per gram.

^1H NMR (CDCl_3/TMS , δ (ppm)): 7.58-7.27(s, H_{Ar} , 5H), 3.61 (t, $-\text{CH}_2\text{OH}$, 6H), 1.55 (m, $\text{CH}_2-\text{CH}_2\text{OH}$, 6H), 1.23 (m, CH_2- , 48H), 0.54 (t, $\text{Si}-\text{CH}_2-$, 6H), 0.07 (t, $\text{Si}-\text{CH}_3$, 18H). ^{13}C NMR (CDCl_3/TMS , δ (ppm)): 135.73 (s), 133.93 (d), 129.50 (d), 127.54 (d), 62.83 (t), 33.71 (t), 32.84 (t), 29.86 (t), 29.84 (t), 29.80 (t), 29.72 (t), 29.67 (t), 29.60 (t), 25.96 (t), 23.34 (t), 18.41 (t), 0.29 (q).

Synthesis of Polyurethanes

Polyurethanes were synthesized by reacting the appropriate amount of

polyether polyol (P184), silicon polyol (PSi194), and MDI. The NCO/OH ratio was kept constant at 1.02. Polyols and MDI were mixed at 60 °C, and the mixture was poured into a preheated open mold at 60 °C and cured for 2 h at 60 °C and postcured at 110 °C overnight.

Characterization

The NMR spectra of the oil samples were recorded on a Varian Gemini 400 MHz spectrometer (400 MHz for ^1H and 100.57 for ^{13}C). The samples were dissolved in deuterated chloroform, and ^1H NMR and ^{13}C NMR spectra were obtained at room temperature using TMS as the internal standard. The IR spectra were recorded on a Bomem Michelson MB 100 FTIR spectrophotometer with a resolution of 4 cm^{-1} in the absorbance mode. An attenuated-total-reflection (ATR) accessory with thermal control and a diamond crystal (Golden Gate heated single-reflection diamond ATR, Specac-Teknokroma) was used to determine FTIR spectra.

Size-exclusion chromatography (SEC) analysis was carried out using a Waters 510 pump system equipped with a refractive index Shimadzu RID-6A. THF was used as eluent at a flow rate of 1.0 mL/min. The calibration curves for SEC analysis were obtained using polystyrene standards.

Calorimetric studies were carried out on a Mettler DSC822e thermal analyzer with N_2 as the purge gas. The heating rate was 20 °C/min. Thermal stability studies were carried out on a Mettler TGA/SDTA851e/LF/1100 with N_2 as the

purge gas at scanning rates of 10 °C/min.

Powder X-ray diffraction measurements were performed at room temperature on a Bruker AXS D8 Advance diffractometer. Cu anode, $K\alpha$ radiation was used, and graphite was the secondary monochromator. In all experiments, the exit slit window was 0.5 °, the anti-scattering slit was 1.0 mm, and the divergence slit was 0.2 mm. The Bragg angle step was 0.05 °, and the time per step was 5 s.

Mechanical properties were measured with a dynamic mechanical thermal analyzer (DMTA) (TA DMA 2928). Specimens 1.2 mm thick, 5 mm wide, and 10 mm long were tested in a three point bending configuration. The various thermal transitions were studied between -100 and 140 °C at a heating rate of 5 °C/min and a fixed frequency of 1 Hz.

LOI values were measured on a Stanton Redcroft instrument, provided with an oxygen analyser, on 100 x 6 x 4 mm³ polymer plaques prepared by molding.

Scanning electron microscopy (SEM) was performed on a JEOL JSM 6400 scanning electron microscope, at an activation voltage of 15 kV. For the atomic mapping, an Oxford INCA Energy Dispersive X-Ray Micro Analyzer was used. The polymeric samples were mounted on a sample holder and were

sputter-coated under vacuum with graphite.

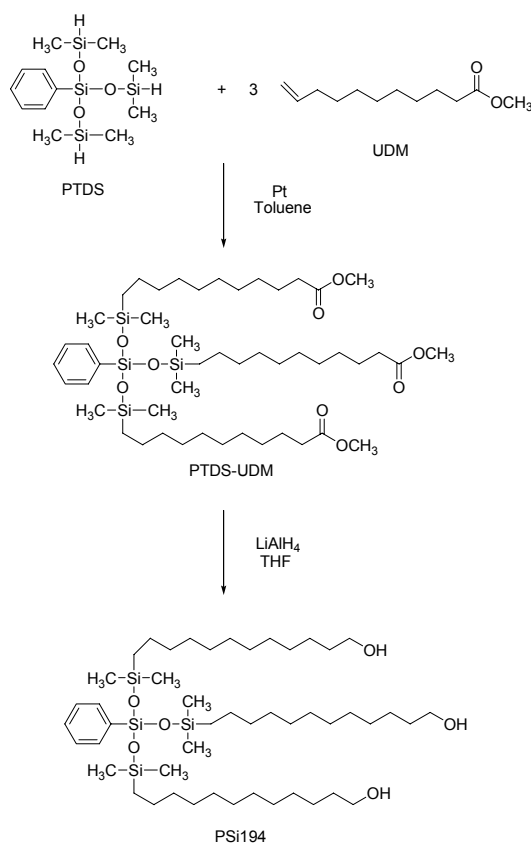
General Procedure for Unilever-Method Hydroxyl Value Determination²⁴

To the amount of weighed sample in a round-bottom flask was added an accurately measured volume of acetic anhydride. After mixing, the flask was placed in an oil bath at 95-100 °C. After 1 h, the flask was cooled, and 1 ml of distilled water was added. After shaking, heating was continued for 10 min to convert the anhydride into acid. After cooling again, 5 ml of 95 % ethanol was added, and the contents were titrated with ethanolic potassium hydroxide solution using phenolphthalein as indicator. A blank determination was carried out with a similar procedure.

RESULTS AND DISCUSSION

Synthesis and Characterization of Polyols

Silicon-containing polyol was synthesized in two steps: hydrosilylation of methyl 10-undecenoate (UDM) with phenyl tris(dimethylsiloxy)silane (PTDS) to obtain PTDS-UDM followed by a reduction of carboxylate groups to give primary hydroxyl groups in PSi194 (Scheme 1).



Scheme 1. Synthesis of Silicon Polyol PSi194.

The chemistry of the hydrosilylation of olefins has been extensively studied,²⁵ but only a few studies on fatty compounds have been published.^{23,26-28} The reaction proceeds when, after the hydrosilane has been activated, it undergoes addition across the carbon-carbon multiple bond. This reaction usually needs a catalyst; the most commonly used are transition metal complexes.

According to our previous results,²³ the hydrosilylation of UDM with PTDS was carried out using Karstedt's catalyst (catalyst/C=C mol ratio $3,5 \times 10^{-5}/1$) at 65 °C. FTIR spectroscopy was used to

follow the reaction's progress, monitoring the disappearance of the characteristic stretching vibration peaks of $-\text{CH}=\text{CH}_2$ and Si-H groups at 1640 and 2168 cm^{-1} , respectively. ^1H and ^{13}C NMR analysis of the obtained product showed the characteristic signals at 0.5 and 18.4 ppm, respectively, which confirms the covalent $-\text{CH}_2-\text{Si}$ linkage between the fatty acid chain and the silicon core. Double-bond isomerization to internal positions (signal at 5.4 ppm) was hardly observed. Since Si-H coupling side reactions have been described for the hydrosilylation reaction,^{29,30} SEC analysis of the product

was carried out to confirm the absence of undesired compounds. The molecular weight determination showed a monomodal molecular weight distribution that implies the absence of these coupling products.

PTDS-UDM was used as the starting material for the reduction of the carboxylate groups to synthesize a triol with primary hydroxyl groups. The reduction was carried out using lithium aluminum hydride (LiAlH_4) as reducing agent in THF solution, and the expected product was characterized by spectroscopic techniques. The FTIR spectrum showed that the ester carbonyl band at 1750 cm^{-1} had disappeared. Figure 1 shows the ^1H and ^{13}C NMR spectra of PSi194 with the signal assignments. The hydroxyl content value (HV) of the PSi194 was determined with the Unilever Method.²⁴ The result (194 mg KOH/g) was very close to the theoretical value of 200. The characteristics of PSi194 are listed in Table 1. The DSC plots for PSi194 exhibit a main peak at $-20\text{ }^\circ\text{C}$ and smaller ones at -12 and $-31\text{ }^\circ\text{C}$. Multi-

ple peaks in PSi194 can be ascribed to different crystalline forms.

Synthesis and Characterization of Polyurethanes

In this study, novel biobased polyurethanes were prepared from epoxidized methyl oleate-based polyether polyol (P184) with OH number of 184 mg KOH/g, silicon-containing triol (PSi194) and 4,4'-methylenebis(phenyl isocyanate) (MDI) as a crosslinking agent. As has been previously described,¹⁰ P184 was obtained from methyl oleate by the epoxidation of carbon double bonds, cationic oligomerization of the resulting epoxy fatty acid ester, and partial reduction of the ester groups. The characteristics of this polyether polyol are summarized in Table 1.

A series of five different polyurethanes with silicon content between 1.7% and 9.0% was prepared from the above-mentioned polyols and MDI by varying the P184/PSi194 molar ratio: PU-0, PU-1.7, PU-3.8, PU-6.2, and PU-9 (see Table 2).

Table 1. General Properties of the Polyols

Polyol	HV ^a (mg KOH/g)	EW ^b (g/equivalent)	M_n (SEC) (g/mol)	M_w/M_n (SEC)	functionality ^c
P184	184	305	1187	1.59	3.8
PSi194	194	295	870	1.12	2.9

^a Hydroxyl content values.

^b Equivalent weight calculated from the HV.

^c Functionality was obtained by dividing the experimental molecular weight (M_n) by the EW.

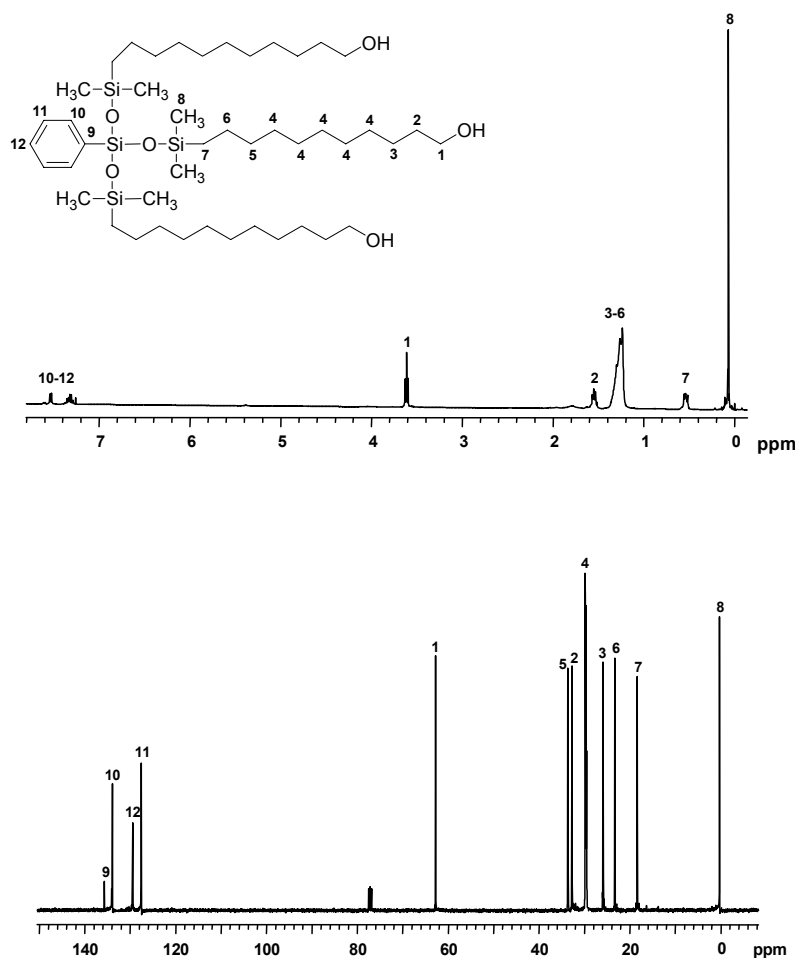


Figure 1. ^1H and ^{13}C NMR spectra of silicon containing polyol PSi194 (CDCl_3 , 400 MHz).

The NCO/OH molar ratio was kept constant at 1.02 and reactants were mixed at 60 °C and cured at this temperature for 2 h and postcured at 110 °C overnight to give the polyurethanes. The conversion of the reaction was monitored by FTIR spectroscopy. The disappearance of the absorption band at 2240 cm^{-1} assigned to the isocyanate group indicated that the reaction was complete. The materials containing P184 remained flexible, while polyurethane PU-9, which does not contain

this polyol, behaved like a rigid material. All the polyurethanes synthesized were characterized by FTIR. Their urethane structure was demonstrated by absorption bands at around 3412 cm^{-1} (N-H stretching), 1530 cm^{-1} (N-H deformation), and 1725 cm^{-1} (C=O). Other peaks at 1270 (Si-CH_3) and 1060 cm^{-1} (Si-O-Si) confirmed the siloxane structure of PSi194-based polyurethanes.

Table 2. Melting Points (T_m), Melting Enthalpies (ΔH_m), and Glass-Transition Temperatures (T_g) of Polyurethanes from DSC and DMTA

	Molar ratio ^a	Si (%)	DSC		DMTA	
			T_m (°C)	ΔH_m (J/g)	T_g (°C) ^b	$\tan \delta_{max}$ ^c
PU-0	1/0	0	-	-	39	63
PU-1.7	0.75/0.25	1.7	-	-	25	50
PU-3.8	0.49/0.51	3.8	54	1.0	20	43
PU-6.2	0.24/0.76	6.2	58	5.4	16	41
PU-9	0/1	9.0	93	22.4	9	31

^a Molar ratio of P184/PSi194.

^b From the second heating of DSC measurements with a heating rate of 20 °C/min.

^c Maximum value of the $\tan \delta$ -temperature curve from DMTA.

The thermal behavior of the materials obtained was investigated with DSC (Figure 2). PU-0 exhibited a T_g at 39 °C. The most notable result of incorporating PSi194 is the appearance of melting endotherms of variable enthalpy and position and a downward shift in the T_g . The samples with no

crystallinity are transparent, while those semicrystalline are white. The rather low melting points seem to be indicative of small domains. The lower T_g values of the silicon-containing polyurethanes can be related by the presence of Si-O and Si-C units in the backbone.

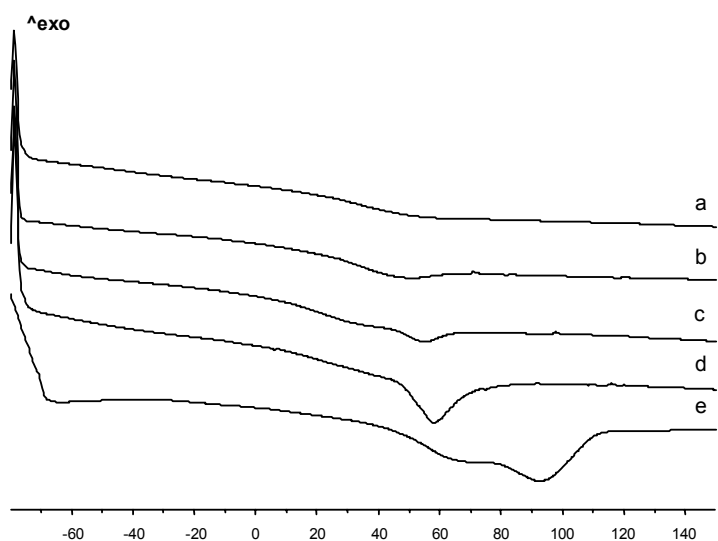


Figure 2. DSC thermograms (20 °C/min) of polyurethanes PU-0 (a), PU-1.7 (b), PU-3.8 (c), PU-6.2 (d), and PU-9 (e).

When samples were run a second time after melting, no melting peaks were observed. This is probably the result of the miscibility of the P184 and PSi194 fragments above the melting point. High viscosity and low mobility due to crosslinking makes crystallization upon cooling difficult. Sample PU-6.2 was annealed at 50 °C for several hours and left to cool slowly to room temperature to promote phase separation and crystallization. Figure 3 illustrates

the DSC thermograms of the PU-6.2 samples after annealing at 50 °C for different periods of time. We found that a small endotherm appearing in the vicinity of the annealing temperature shifted to a higher temperature and increased in enthalpy as the annealing time increased. Therefore, better miscibility of PSi194 segments with the P184 phase raises T_g , and the sample displays higher crystallinity.

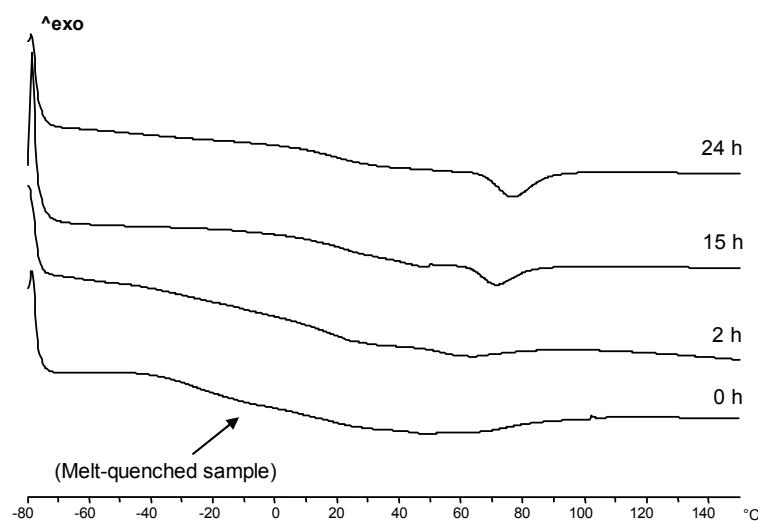


Figure 3. DSC thermograms (20 °C/min) of the melt-quenched PU-6.2 samples, which were annealed at 50 °C for different periods of time.

Wide-angle X-ray diffraction experiments confirmed calorimetric findings. The WAXD pattern of the PU-0 sample shows a broad halo characteristic of amorphous substances with the maximum at about $2\theta = 20^\circ$ (Figure 4 a). As the PSi194 content increases, the WAXD curve essentially shows the same pattern, but the peak becomes narrower, and a crystalline peak can be observed at $2\theta = 18^\circ$ (marked with * in Figure 4) for PU-3.8 and PU-6.2,

suggesting a slight increase in crystallinity. Scattering profiles at small angles is used for checking phase-separated structures. If a maximum appears at small angles, this would be the conclusion of the coexistence of two separated phases, an amorphous-rich phase and a crystalline-rich phase. Figure 4 b) shows the scattering profiles at small angles of the synthesized polyurethanes. As can be seen, PU-0 does not show an appreciable

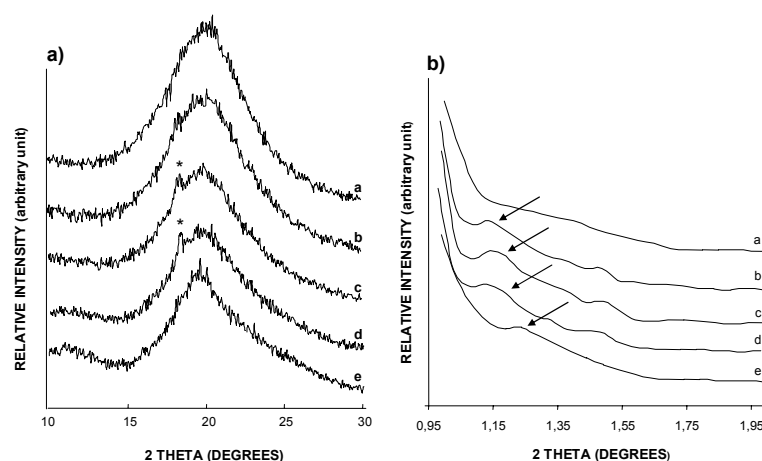


Figure 4. WAXS diffractograms (a) and zoom-in plot of scattering profiles at small angles (b) of polyurethanes PU-0 (a), PU-1.7 (b), PU-3.8 (c), PU-6.2 (d), and PU-9 (e).

scattering on the detector indicating the presence of homogeneous phase. However, samples which contain PSi194 show peaks at small angles (marked with arrows in Figure 4 b) that may be evidence of microphase formation.³¹

The dynamomechanical behaviour of the polyurethanes has been investigated. Figure 5 a) shows the elastic modulus as a function of the temperature. As can be seen, materials containing P184 behave like cross-linked polymeric networks with respect to E' curves. At low temperatures there is a glass state with E' at a high modulus plateau, and at higher temperatures, there is a rubbery state with a lower E' . Figure 5 b) shows the dissipation factor $\tan \delta$ curves as a function of temperature. The location of the $\tan \delta$ peak is dependent on silicon content and shifts to low temperature when the PSi194 content increases. The glass transition temperatures determined from the peaks of $\tan \delta$ curves are higher than those deter-

mined by DSC (see Table 2), which can be related to the heat transporting hysteresis for large-scale samples in DMTA. The magnitude of $\tan \delta$ is also affected by the PSi194 content, and as can be seen, it increases for the silicon-free PU-0 and the lower silicon content of PU-1.7 and PU-3.8. This suggests that the PSi194 incorporation makes the PU more viscous. However, the peak value of $\tan \delta$ for PU-6.2 is lower even though its Si content is higher. This can be explained by the presence of microcrystalline domains in the polymer, as has been observed by DSC, which restricts the chain mobility. Moreover, a β transition can be observed, more clearly for the PU-1.7. The origin of this peak is not known, but it may be related to the rotational motions of the short units in the fatty acid chain.⁹ PU-9 shows a different dynamo-mechanical behavior. As a semicrystalline material, α relaxation peak is associated to the melting of the crystalline phase.

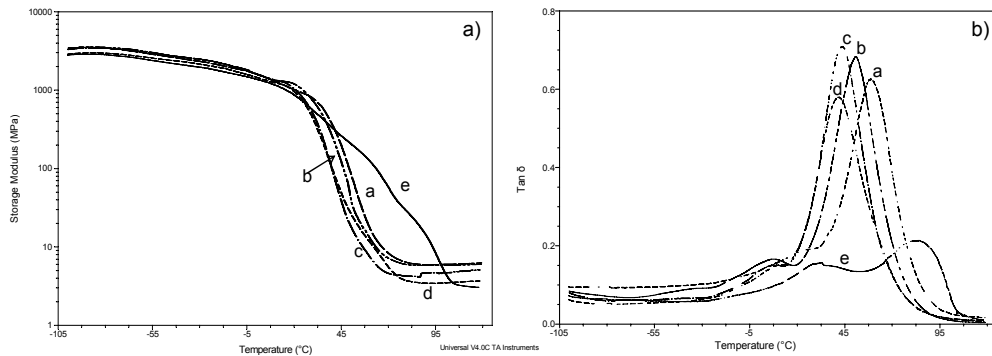


Figure 5. Storage modulus (E') and loss factor ($\tan \delta$) of polyurethanes PU-0 (a), PU-1.7 (b), PU-3.8 (c), PU-6.2 (d), and PU-9 (e) as a function of temperature.

Moreover, a β relaxation, related to the glass transition, can be observed. The magnitude of $\tan \delta$ for this relaxation is much lower than the ones previously described, according to a lower mobility and a higher degree of crystallinity.

The reported thermogravimetric analysis of polyurethanes based on petroleum-based polyols suggests that thermal stability is poor.^{16,32,33} The onset of

urethane bond dissociation is somewhere between 150 and 220 °C, depending upon the type of the isocyanate or polyol. Thermal decomposition of the polyurethanes obtained was investigated by TGA under nitrogen and air atmospheres. Figures 6 and 7 show the TGA and the corresponding derivative curves under both atmospheres, and Table 3 summarizes the thermogravimetric data.

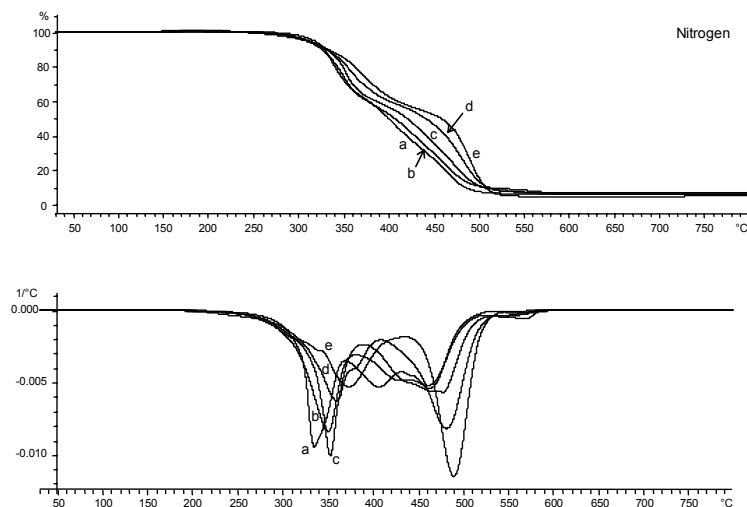


Figure 6. TGA plots (10 °C/min) and first derivative curves of polyurethanes PU-0 (a), PU-1.7 (b), PU-3.8 (c), PU-6.2 (d), and PU-9 (e) under nitrogen atmosphere.

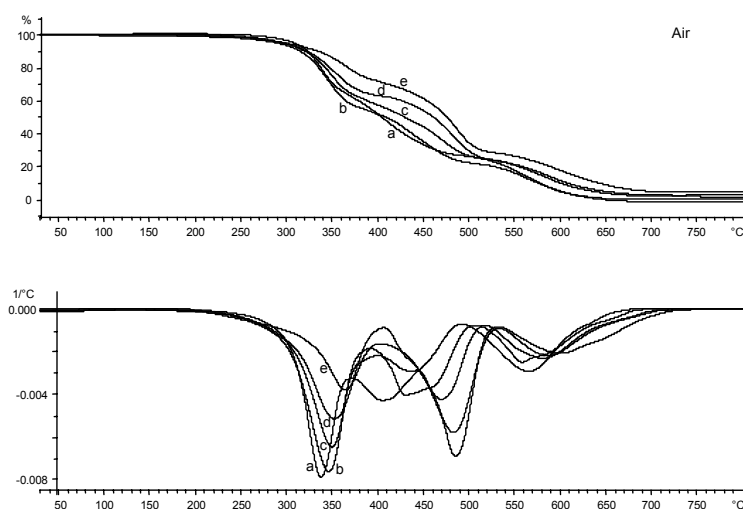


Figure 7. TGA plots (10 °C/min) and first derivative curves of polyurethanes PU-0 (a), PU-1.7 (b), PU-3.8 (c), PU-6.2 (d), and PU-9 (e) under air atmosphere.

As can be seen, onset decomposition temperatures do not show significant differences among the samples, suggesting that the incorporation of silicon does not change the thermal stability under air or nitrogen. From the derivative curves, it can be seen that in both nitrogen and air more than one process

occurs during thermal degradation. Petrovic et al.¹⁶ observed a similar behaviour in the case of vegetable oil-based polyurethanes. They showed that poly(oxypropylene) (PPO)-based polyurethanes degrade in a single step, whereas vegetable oil-based polyurethane show a two-step decomposition.

Table 3. Thermogravimetric Data and Limiting Oxygen Indices (LOI) of Polyurethanes

	Si (%)	TGA (N ₂ Atmosphere)			TGA (Air Atmosphere)			LOI
		T _{10% loss} ^a (°C)	T _{max} ^b (°C)	Yield _{800°C} ^c (%)	T _{10% loss} ^a (°C)	T _{max} ^b (°C)	Yield _{800°C} ^c (%)	
PU-0	0	329	332/404/460	3	322	337/403/565	0	18.2
PU-1.7	1.7	325	349/420/460	7	314	346/432/569	0	19.0
PU-3.8	3.8	330	351/470	6	320	349/469/580	2	20.4
PU-6.2	6.2	330	359/481	7	322	350/482/585	2	22.1
PU-9	9.0	331	371/487	5	333	363/485/600	5	23.6

^a Temperature of 10% of weight loss.

^b Temperature of the maximum weight loss rate.

^c Char yield at 800 °C.

The derivative curves in our study revealed that the temperature corresponding to the maximum weight loss rate increases and the maximum weight loss rate decreases as the silicon content increases. This degradation step, which takes place at temperatures between 330 and 370 °C, can be associated to the decomposition of urethane bonds, which takes place through the dissociation to isocyanate and alcohol, the formation of primary amines and olefins, or the formation of secondary amines.¹⁸ Two more degradation steps can be observed for the silicon-free PU-0 or the lower silicon content PU-1.7, which can be attributed to the polyether polyol decomposition. PU-3.8, PU-6.2 and PU-9 show only one degradation process at higher temperatures that has to be ascribed to the decomposition of silicon units which produced volatile cyclic oligomers.³⁴

In air, the thermooxidative degradation takes place at temperatures higher than 550 °C. Again, the silicon content influences the temperature of the maximum weight loss rate and the maximum weight loss rate. Char yields under nitrogen do not show significant differences among the polymers, while in air, silicon-containing polymers show a slight increase in the char yield.

Silicon has proven to be one of the first choices as a flame retardant element. The silicon dependence of the limiting oxygen index (LOI) has been investigated in several families of silicon-containing polymers.³⁵ LOI measures the ease at which materials can be extinguished and is the minimum percent of oxygen in an oxygen/nitrogen

atmosphere that will just sustain combustion in a candle-like configuration of a top-ignited vertical test specimen. The LOI values obtained for our polyurethanes are listed in Table 3. As soon as a silicon-containing polyol was introduced (from 1.7% wt Si), the LOI improved slightly and reached an index of 19. LOI increased with the PSi194 ratio and was maximum for neat PSi194 polyurethane. The significance of this result is that polyurethanes PU-6.2 and PU-9 (whose LOI values are higher than 21) no longer burn in ambient air if there is no supplementary oxygen and are therefore very interesting materials for applications that require fire resistance.

To understand the role of silicon in the enhancement of flammability, scanning electronic microscopy (SEM) and energy-dispersive X-ray spectroscopy (EDX) images were made of samples before and after the burning test. Figure 8 a,c) are the surface SEM image of the PU-9 sample before and after the LOI test, respectively. The Si-mapping profile before the combustion test (Figure 8b) showed a homogeneous distribution of silicon, while the mapping after combustion (Figure 8d) showed that the burned surface was covered with char layers containing silicon atoms in very high densities. The relatively high oxygen density and low carbon density in the top burned surface (O and C mapping profiles are not shown) demonstrated that the residue contained a certain amount of silica (SiO₂). These observations are in accordance with the mechanism of improved fire performance via silicon modification. Incorporating silicon into the polymers enhanced flame retardancy because it

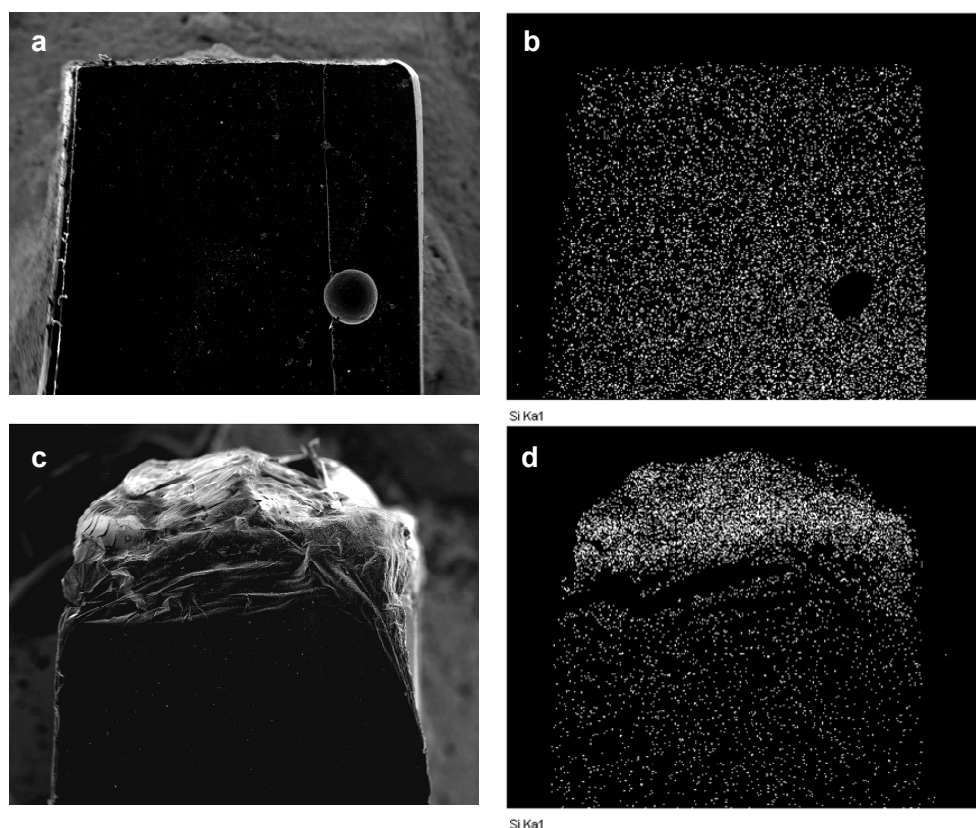


Figure 7. SEM and SEM-EDX Si mapping micrographs of sample PU-9 before (a,b) and after (c,d) burning LOI test: (left) SEM, and (right) SEM-EDX micrographs.

produced continuous layers of silica that retarded the oxidation of the char.³⁶

CONCLUSIONS

A novel silicon polyol (PSi194), based on methyl 10-undecenoate (UDM) and phenyl tris(dimethylsiloxy) silane (PTDS), was synthesized. A series of five different polyurethanes with a silicon content between 1.7% and 9.0% was prepared from the above-mentioned polyol, epoxidized methyl oleate-based polyether polyol (P184), and MDI by varying the molar ratio of the polyols.

The most notable change from the incorporation of PSi194 is the appearance of melting endotherms of variable enthalpy and position and a downward shift in the T_g . These polyurethanes have T_g 's ranging from 9 to 39 °C. As the PSi194 content increases, partial crystallinity and phase separation were detected using WAXD data. The samples with no crystallinity are transparent, while those with crystallinity are white. Polyurethanes containing P184 exhibit a dynamomechanical behaviour typical of crosslinked polymeric networks, while PU-9 behaves like a semicrystalline material; there is a soft rubbery

phase with a glass transition temperature of 31 °C and a hard crystalline phase with a melting transition of 90 °C. All polyurethanes are thermally stable over 250 °C. Char yields under nitrogen do not show significant differences among the polymers, but in air, the char yield for silicon-containing polymers increases slightly. The limiting oxygen index (LOI) increases with the PSi194 ratio and reaches values higher than the atmospheric oxygen index for PU-6.2 and PU-9. From the SEM-EDX analysis before and after burning tests, the improved fire performance can be explained by the production of continuous layers of silica that retarded the oxidation of the char. These novel biobased polyurethanes were prepared using 49-70 wt % of biorenewable materials, which shows that it is possible to exploit renewable resources to manufacture original and useful materials.

Acknowledgements

The authors gratefully acknowledge the CICYT (Comisión Interministerial de Ciencia y Tecnología) (MAT2005-01593) for financial support for this work and the DURSI (Departament d'Universitats, Recerca i Societat de la Informació) and Fons Social Europeu for G. Lligadas' predoctoral (2003FI00765) grant. We thank P. Castell for WAXD measurements and M. Moncusí for SEM analysis.

REFERENCES AND NOTES

1. Feedstocks for the Future: Renewables for the Production of Chemicals and Materials; Bozell, J. J., Patel, M., Eds.; ACS Symposium Series 921; American Chemical Society: Washington, DC, 2006.
2. (a) Soderqvist Lindblad, M.; Liu, Y.; Albertsson, A.-C.; Ranucci, E.; Karlsson, S. *Adv Polym Sci* 2002, 157, 139; (b) Natural Fibers, Biopolymers, and Biocomposites; Mohanty, A. K., Misra, M., Drzal, L. T., Eds.; CRC Press Taylor & Francis Group: Boca Raton, FL, 2005.
3. (a) Baumann, H.; Bühler, M.; Fochem, H.; Hirsinger, F.; Zoblein, H.; Falbe, J. *Angew Chem Int Ed Engl* 1988, 27, 41; (b) Biermann, U.; Friedt, W.; Lang, S.; Lühs, W.; Machmüller, G.; Metzger, J. O.; Klaas, M. R.; Schäfer, H. J.; Schneiderüs, M. P. *Angew Chem Int Ed Engl* 2000, 39, 2206.
4. (a) Andjelkovic, D. D.; Larock, R. C. *Biomacromolecules* 2006, 7, 927; (b) Tsujimoto, T.; Uyama, H.; Kobayashi, S. *Macromolecules* 2004, 37, 177; (c) Eren, T.; Küseföglu, S. H. *J Appl Polym Sci* 2004, 91, 2700; (d) Khot, S. N.; LaScala, J. J.; Can, E.; Morye, S. S.; Williams, G. I.; Palmese, G. R.; Küseföglu, S. H.; Wool, R. P. *J Appl Polym Sci* 2001, 82, 703.
5. Guo, A.; Cho, Y.-J.; Petrovic, Z. S. *J Polym Sci Part A: Polym Chem* 2000, 38, 3900.
6. Zlatanovic, A.; Petrovic, Z. S.; Dusek, K. *Biomacromolecules* 2002, 3, 1048.
7. Zlatanovic, A.; Lava, C.; Zhang, W.; Petrovic, Z. S. *J Polym Sci Part B: Polym Phys* 2004, 42, 809.
8. Guo, A.; Demydov, D.; Zhang, W.; Petrovic, Z. S. *J Polym Environ* 2002, 10, 49.
9. Petrovic, Z.; Zhang, W.; Javni, I. *Biomacromolecules* 2005, 6, 713.
10. Lligadas, G.; Ronda, J. C.; Galià, M.; Biermann, U.; Metzger, J. O. *J Polym Sci Part A: Polym Chem* 2006, 44, 634.

11. Oertel, G. *Polyurethane Handbook*; 2nd ed.; Hanser Publishers: Munich, 1993.
12. Petrovic, Z. S.; Guo, A.; Javni, I. U.S. Patent 6,107,433, 2000.
13. Kluth, H.; Gruber, B.; Meffert, B.; Huebner, W. U.S. Patent 4,742,087, 1988.
14. Hoefler, R.; Gruber, B.; Meffert, A.; Gruetzmacher, R. U.S. Patent 4,826,944, 1989.
15. Suresh, K. I.; Kishanprasad, V. S. *Ind Eng Chem Res* 2005, 44, 4504.
16. Javni, I.; Petrovic, Z. S.; Guo, A.; Fuller, R. *J Appl Polym Sci* 2000, 77, 1723.
17. Guo, A.; Javni, I.; Petrovic, Z. S. *J Appl Polym Sci* 2000, 77, 467.
18. Levchik, S. V.; Weil, E. D. *Polym Int* 2004, 53, 1585.
19. Adhikari, R.; Gunatillake, P. A.; McCarthy, S. J.; Meijs, G. F. *J Appl Polym Sci* 2002, 83, 736.
20. Turri, S.; Levi, M. *Macromolecules* 2005, 38, 5569.
21. Oaten, M.; Choidhury, N. R. *Macromolecules* 2005, 38, 6392.
22. Liu, H.; Zheng, S. *Macromol Rapid Commun* 2005, 26, 196.
23. Lligadas, G.; Callau, L.; Ronda, J. C.; Galià, M.; Càdiz, V. *J Polym Sci Part A: Polym Chem* 2005, 43, 6295.
24. *Handbuch der Lebensmittelchemie*; Springer-Verlag: Berlin, 1965; Vol. IV.
25. Marcinec, B. *Comprehensive Handbook on Hydrosilylation*; Pergamon: London, 1992.
26. Saghian, N.; Gertner, D. *J Am Oil Chem Soc* 1974, 51, 363.
27. Berh, A.; Toslu, N. *Chem Eng Technol* 2000, 23, 122.
28. Delpech, F.; Saadia, A.; Castel, A.; Rivière, P.; Rivière-Baudet, M.; Amin-Alami, A.; Manriquez, J. *Appl Organometal Chem* 2001, 15, 626.
29. Chalk, A. J.; Harrod, J. F. *J Am Chem Soc* 1965, 87, 16.
30. Chalk, A. J.; Harrod, J. F. *J Am Chem Soc* 1965, 87, 1183.
31. Petrovic, Z.; Cevallos, M. J.; Javni, I.; Schaefer, D. W.; Justice, R. *J Polym Sci Part B: Polym Phys* 2005, 43, 3178.
32. Yang, W. P.; Macosko, C. N.; Wellinghoff, S. T. *Polymer* 1986, 27, 1235.
33. Grasiee, N.; Mendoza, G. A. *Polym Degrad Stab* 1985, 10, 267.
34. Moronkov, M. G. *J. Organometallic Chem* 1998, 557, 143.
35. (a) Levchik, S. V.; Weil, E. D. *Polym Int* 2005, 54, 981; (b) Hsiue, G. H.; Wang, W. J.; Chang, F. C. *J Appl Polym Sci* 1999, 73, 1231; (c) Iji, M.; Serizawa, S. *Polym Adv Technol* 1998, 9, 593.
36. Kambour, R. P.; Lignon, W. V.; Russell, R. R. *J Polym Sci Polym Lett* 1978, 16, 327.

4.4.3 Poly(ether urethane) Networks
from Renewable Resources as
Candidate Biomaterials. Synthesis
and Characterization

POLY(ETHER URETHANE) NETWORKS FROM RENEWABLE RESOURCES AS CANDIDATE BIOMATERIALS. SYNTHESIS AND CHARACTERIZATION

G. Lligadas, J.C. Ronda, M. Galià, V. Cádiz

Departament de Química Analítica i Química Orgànica, Universitat Rovira i Virgili, Campus Sescelades, Marcel·lí Domingo s/n, 43007 Tarragona, Spain.

ABSTRACT: A series of poly(ether urethane) networks were synthesized from epoxidized methyl oleate-based polyether polyol and 1,3-propanediol using L-lysine diisocyanate as a non-toxic coupling agent. Polyurethanes with different hard segment contents were prepared in order to tune the final properties of the materials. The polyurethanes were fully chemically and physically characterized, including water uptake and in vitro hydrolytic degradation measurements. The weight loss of the polyurethanes was traced, and the changes in the surface morphology with the degradation time were examined by scanning electron microscopy. The experimental results revealed that the hard segment content is the main factor that controls the physical, mechanical, and degradation properties of these polymers. The observed diversity in material properties suggests that these polyurethanes may be useful for a wide range of biomedical polymer applications.

Keywords: biopolymers; renewable resources; segmented polyurethanes; vegetable oils

INTRODUCTION

Biodegradable polymers are receiving more and more attention due to their wide application in biomedical uses.¹ They may act as a temporary scaffolds to facilitate tissue regeneration or replacement and may also be used for temporary therapeutic purposes, eliminating the need for subsequent removal.^{2,3} The majority of the biodegradable polymers developed in the

last two decades were aimed at either drug delivery systems¹ or fracture fixation devices and are typically hard, rigid materials.⁴ In contrast, few biodegradable elastomers have been synthesized and new materials are required to meet the need for an increasingly diverse range of physical properties. Biodegradable elastomers are expected to be suitable for any application requiring the use of flexible, elastic

material, such as soft tissue engineering.

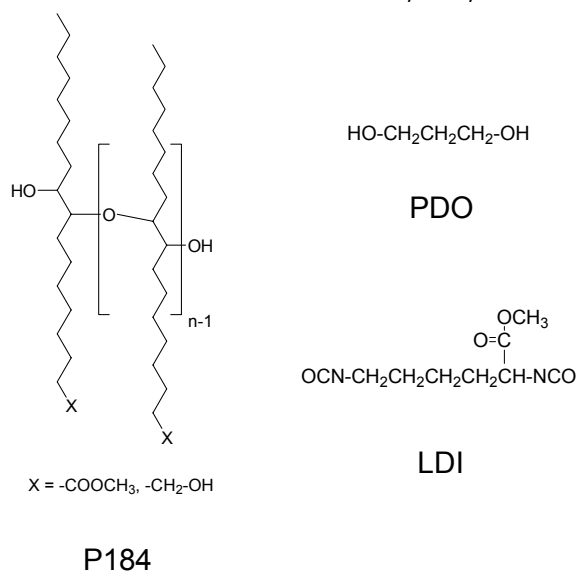
Segmented polyurethane elastomers have been used as biomaterials for several decades in the fabrication of medical implants such as cardiac pace makers and vascular grafts because of their unique physical properties and relatively good biocompatibility.⁵ Segmented polyurethanes are elastomeric block copolymers that generally exhibit a phase-segregated morphology made up of soft rubbery segments and hard glassy or semicrystalline segments.⁶ The soft segment usually consists of polyether or polyester diols whereas the hard segment consists of the diisocyanate component and a low molecular weight chain extender. The advantage of segmented polyurethanes is that their segmental and domain structure can be controlled over a considerable range through the selection of the materials, their relative proportions and the processing conditions.

Segmented polyurethanes can also be designed to have chemical linkages that are degradable in the biological environment and there has been some interest in developing degradable polyurethanes for medical applications such as scaffolds for tissue engineering.⁷⁻⁹ In addition to the physical properties, great care has to be taken in the choice of building blocks. Their degradation products have to be biocompatible, non-toxic and metabolized or eliminated by the living organism. Convenient long chain diols are polyethers such as polyethylene oxide diols or polyesters such as polycaprolactone, due to its good biocompatibility and biodegradability. However, a major prob-

lem has been the toxicity of degradation products, particularly those derived from the aromatic diisocyanate component as carcinogenic and mutagenic aromatic diamines that have been reported as potential degradation products.⁵ Accordingly, in designing degradable polyurethanes, diisocyanates such as L-lysine diisocyanate (LDI) have been used.^{7,10-12} Bruin et al.¹⁰ reported that if the hydrolysis of the urethane bonds of the polymer takes place during degradation, the product would be a lysine derivative, an essentially non-toxic product.

The design of polymers from renewable resources is currently receiving increasing attention and interest has focused on the use of cheap, biodegradable and annually renewable starting materials to reduce petroleum dependence and the negative impact on the environment.¹³ Vegetable oils and fatty acids are one of the cheapest and most abundant biological sources available in large quantities and their use as starting materials has numerous advantages, including low toxicity and inherent biodegradability.¹⁴ In recent years, extensive work has been done to develop polymers from triglycerides or fatty acids as the main component.¹⁵

Polyols derived from vegetable oils are raw materials from renewable resources and are essential in the preparation of any polyurethane product. For natural oils to be used as raw materials for polyol production multiple hydroxyl functionality is required. Different ways of preparing vegetable oil-based polyols have been successfully developed: epoxidation and further oxirane ring-opening,¹⁶ hydroformylation¹⁷, ozonoly-

Chart 1. Chemical Structure of P184, PDO, and LDI

sis¹⁸ or reaction at the double bonds and subsequent reduction of the carboxyl groups.¹⁹

To further extend the applications of these renewable resources, our group has focused on converting vegetable oils into useful biopolymers. In a previous study, we described the synthesis of polyether polyols through the combination of cationic polymerization of epoxidized methyl oleate (EMO) and the reduction of carboxylate groups to hydroxyl moieties. Polyols with different hydroxyl contents were obtained and reacted with MDI to yield polyurethanes that behave like hard rubbers or rigid plastics.¹⁹ We have also developed novel biobased silicon-containing polyurethanes from these polyols and silicon-containing polyol with terminal primary hydroxyl groups.²⁰

On the basis of these premises, in this study we synthesized a series of poly-

urethane elastomer networks with various hard segment contents based on EMO polyether-polyol (P184) with OH number = 184 mg KOH/g, L-lysine diisocyanate (LDI) and 1,3-propanediol (PDO) as a chain extender which can be obtained from rapeseed oil production in the presence of *clostridium butyricum*²¹ or from corn²² (Chart 1). Their chemical structures, molecular characteristics and thermal properties were studied using ¹³C NMR, FTIR, wide-angle X-ray diffraction (WAXD), differential scanning calorimetry (DSC), dynamic mechanical thermal analysis (DMTA), and thermogravimetric analysis (TGA). In view of the future application of the synthesized polyurethanes in the biomedical field, water uptake and in vitro degradation studies were carried out and the morphologies of the degraded polyurethanes were observed by scanning electronic microscopy (SEM).

EXPERIMENTAL

Materials

Epoxidized methyl oleate-based polyether polyol (P184) with OH number = 184 mg KOH/g was synthesized in our laboratory using the procedure described earlier.¹⁹ This OH number corresponds to the equivalent weight of the polyol, 305, functionality, 3.8, and molecular weight, 1187. The diisocyanate chosen was 2,6-diisocyanato methyl caproate (L-lysine diisocyanate, LDI) (Kyowa Hakko Kogyo Co.). Stannous 2-ethylhexanoate (95%) was purchased from Aldrich and was used as received. Chain extender 1,3-propanediol (>98%) was purchased from Aldrich and was distilled and stored at ambient temperature in a desiccator until used.

Synthesis of Polyurethanes

Polyurethanes were prepared using a single-stage process. After 5 min mixing the appropriate amount of EMO-based polyether polyol (P184), chain extender (PDO) and diisocyanate (LDI) under nitrogen at room temperature, a small amount of the catalyst (0.001 wt % of stannous 2-ethylhexanoate) was added and then additional mixing for 0.5 min was conducted. About 1 wt % of excess LDI (NCO/OH ratio = 1.02) was used for the completion of the reaction. The mixture was poured into a preheated open mold and cured for 2 h at 60 °C and then postcured at 110 °C overnight. Chemical composition and hard segment content of the polyurethanes are shown in Table 1. From the sample code in Table 1, the number denotes the hard segment percentage of the polyurethanes.

Characterization

The NMR spectra of the oil samples were recorded on a Varian Gemini 400 MHz spectrometer (400 MHz for ¹H and 100.57 for ¹³C). The samples were dissolved in deuterated chloroform, and ¹H NMR and ¹³C NMR spectra were obtained at room temperature using TMS as the internal standard. The IR spectra were recorded on a Bomem Michelson MB 100 FTIR spectrophotometer with a resolution of 4 cm⁻¹ in absorbance mode. An attenuated-total-reflection (ATR) accessory with thermal control and a diamond crystal (Golden Gate heated single-reflection diamond ATR, Specac-Teknokroma) was used to determine FTIR spectra.

Calorimetric studies were carried out on a Mettler DSC822e thermal analyzer with N₂ as the purge gas. The heating rate was 20 °C/min. T_g was determined from the second heating scan of DSC measurements as the temperature of the halfway point of the jump in the heat capacity. Thermal stability studies were carried out on a Mettler TGA/SDTA851e/LF/1100 with N₂ as the purge gas at scanning rates of 10 °C/min.

WAXD measurements were made using a Siemens D5000 diffractometer (Bragg-Brentano parafocusing geometry and vertical θ - θ goniometer) fitted with a curved graphite diffracted-beam monochromator, incident and diffracted-beam Soller slits, a 0.06 ° receiving slit and scintillation counter as a detector. The angular 2 θ diffraction range was between 1 and 40 °. Samples were dusted onto a low background Si(510) sample holder. The data were collected with an angular step of 0.05 ° at 3 s per step.

CuK_α radiation was obtained from a copper X-ray tube operated at 40 kV and 30 mA.

Mechanical properties were measured with a dynamic mechanical thermal analyzer (DMTA) (TA DMA 2928). Specimens 1.2 mm thick, 5 mm wide, and 5 mm long were tested in a three point bending configuration. The various thermal transitions were studied between -100 and 100 °C at a heating rate of 2.5 °C/min and a fixed frequency of 1 Hz.

Scanning electron microscopy (SEM) was performed on a JEOL JSM 6400 scanning electron microscope, at an activation voltage of 15 kV. The polymeric samples were mounted on a sample holder and were sputter coated under vacuum with graphite.

Hydrophilicity of Polyurethanes

The hydrophilicity of the polyurethanes was quantified by the measurement of the amount of water that each polymer absorbed at 37 °C. The samples were immersed in distilled water and were kept at 37 °C. The samples were removed from water at predetermined time intervals, wiped gently with filter paper and weighted with an analytical balance. After the samples were dried under vacuum at 60 °C, the weight of the dry samples was determined. The water uptake was defined as follows: water uptake (wt %) = $100(W_w - W_d)/W_d$, where W_w represents the weight of the wet sample after immersing and W_d represents the weight of the sample after drying.

In Vitro Degradation of Polyurethanes

Each sample was placed in an individual test bottle and kept at 37 °C in phosphate buffer solution (PBS, 0.1 M, pH 7.4). PBS was changed at each analysis point. The degradation rate was determined by the weight loss over predetermined time intervals. Weight loss was defined as follows: weight loss (%) = $(W_0 - W_t)/W_0 \times 100$, where W_0 represents the weight of the dry sample before degradation and W_t represents the weight of the dry sample after degradation at different time intervals.

RESULTS AND DISCUSSION

Synthesis of Polyurethanes

One of the most widely-used techniques to obtain polyurethanes is the one-shot technique, which consists of the very efficient mixing, in one step only, in a short time, of all the raw materials involved in polyurethane preparation: polyol, chain extender and isocyanate.⁶

In this study, novel segmented biobased polyurethanes were prepared using the one-shot technique from epoxidized methyl oleate-based polyether polyol (P184) with OH number = 184 mg KOH/g, L-lysine diisocyanate (LDI), and 1,3-propanediol (PDO) as a chain extender. As has been previously described, P184 was obtained from methyl oleate by the epoxidation of carbon double bonds, cationic oligomerization of the resulting epoxy fatty acid ester and partial reduction of the ester

Table 1. Chemical Composition of Polyurethane Networks

Sample Code ^a	P184 (g)	PDO (g)	LDI (g)	Molar Composition ^b	%HS ^c
PU	5	0	1.73	1.0/0.0/1.02	-
PU-31	5	0.15	2.14	1.0/0.24/1.26	31.4
PU-42	5	0.5	3.11	1.0/0.8/1.82	41.9
PU-52	5	1.0	4.48	1.0/1.6/2.62	52.3

^a Number in the sample code denotes the hard segment weight percent of the PU.

^b P184:PDO:LDI.

^c % Hard segment calculated as weight percentage of PDO and LDI per total material weight.

groups.¹⁹ The chemical structure and the characteristics of the materials are shown in Chart 1. When synthesizing polyurethanes, aliphatic diisocyanates have lower reactivity than aromatic ones and a catalyst is necessary to speed up the reaction with polyols. However, catalysts such as amines or organometallic compounds may be highly toxic. Among them, stannous 2-ethylhexanoate (commonly referred as stannous octoate) is a good choice on the basis of its acceptance by FDA as a catalyst in the formulation of polymeric coatings in contact with food.²³

The chemical composition and hard segment content of the synthesized polyurethanes are shown in Table 1. The molar composition of the P184 was set at 1.0, and then the molar ratio of the PDO and LDI were varied to obtain polyurethanes with different hard segments content. The NCO/OH molar ratio was kept constant at 1.02 to compensate for isocyanates that are consumed in side reactions during the urethane synthesis, and reactants were mixed at 60 °C and cured at this temperature for 2 h before being postcured at 110 °C overnight to give the poly-

urethanes. ¹³C NMR and FTIR spectroscopies were used to monitor the isocyanate to urethane conversion. The ¹³C NMR spectra for P184, LDI and the swollen PU-52 with the all assignments are shown in Figure 1. The isocyanate peaks essentially disappear upon conversion to the urethane and new resonances assigned to the carbonyls of the newly formed carbamates appear at 156 ppm. FTIR analysis also demonstrated the urethane formation reaction during polymer synthesis. The disappearance of the absorption band at 2240 cm⁻¹ assigned to the isocyanate group indicated that the reaction was complete and their urethane structure was demonstrated by absorption bands at around 3412 cm⁻¹ (N-H stretching), 1530 cm⁻¹ (C-N stretching, combined with N-H out-of-plane bending) and 1725 cm⁻¹ (C=O stretching). A small absorption band at around 1663 cm⁻¹ was due to the formation of urea linkages, which may be the reaction of some of the unreacted isocyanates with the atmospheric moisture while curing as a side reaction.

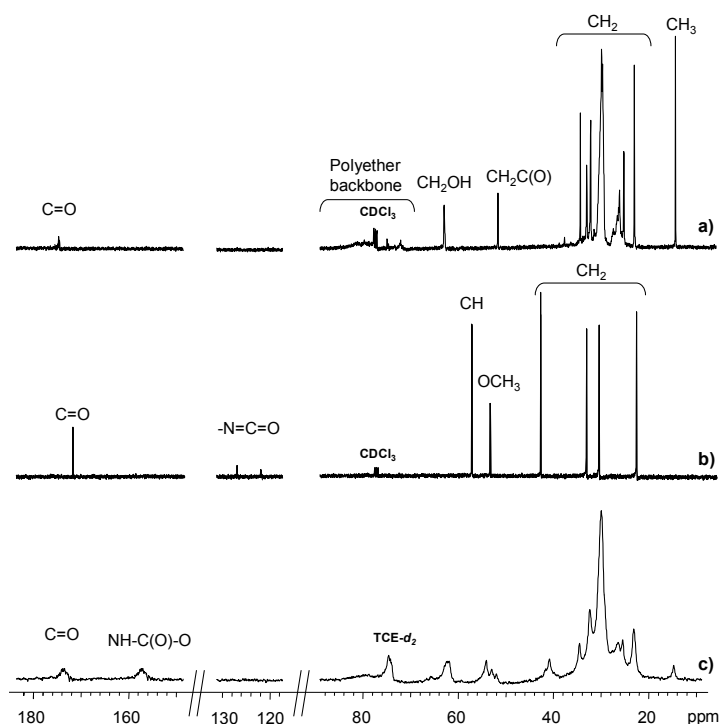


Figure 1. ^{13}C NMR spectra (100.57 MHz) of (a) P184 (CDCl_3), (b) LDI (CDCl_3), and (c) swollen PU-52 ($\text{TCE-}d_2$).

Structural Analysis of Polyurethanes

To investigate the molecular structure of polyurethanes, wide-angle X-ray diffraction (WAXD) and Fourier transform infrared spectroscopy (FTIR) were employed. All samples show similar WAXD curves with a large wide diffraction halo at around 20° , which is typical for amorphous polymeric materials. It seems that the non-symmetrical diisocyanate LDI that also contains a methyl ester side chain produces hard segments that were unable to pack efficiently to form a crystalline hard segment domain. FTIR spectroscopy was used to investigate the structural difference in hard and soft segments of synthesized

polyurethanes with various PDO fractions. Almost all the infrared research on polyurethanes has focused on two principal vibrational regions: the N-H stretching vibration ($3200\text{--}3500\text{ cm}^{-1}$), and the carbonyl C=O stretching vibration amide-I region ($1700\text{--}1730\text{ cm}^{-1}$).^{24,25} Polyurethanes are capable of forming several kinds of hydrogen bonds due to the presence of donor N-H group and C=O acceptor group in the urethane linkage. The oxygen atom of the ester or ether linkage when polyester or a polyether soft segment is present may also act as a proton acceptor. Therefore, hydrogen bonding between hard segment-hard segment or hard segment-soft segment can exist. These bands have been widely

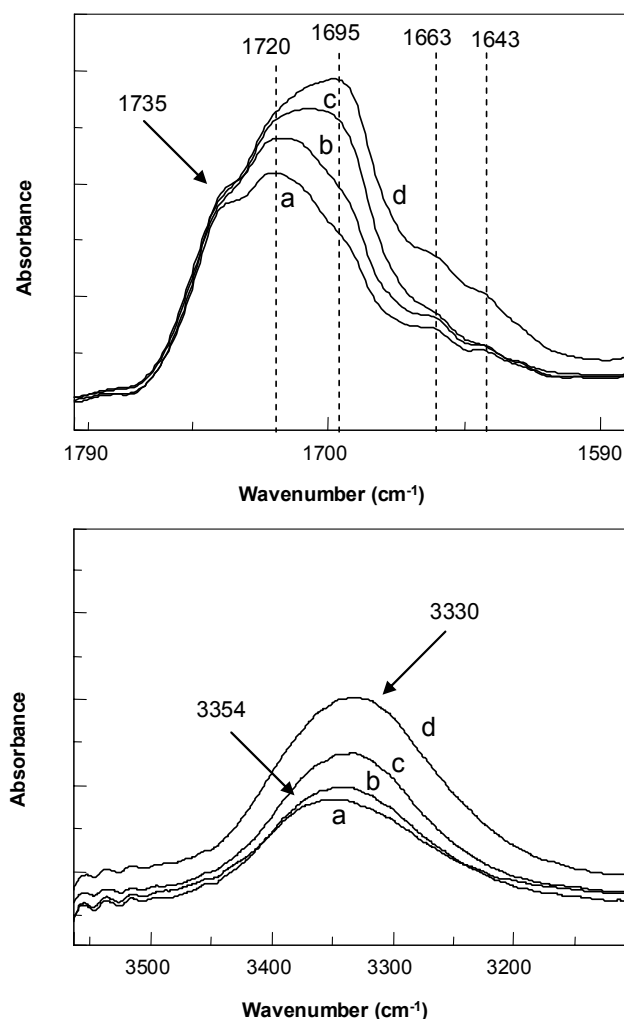


Figure 2. FTIR spectra of carbonyl (up) and amine (down) regions of polyurethane networks: (a) PU, (b) PU-31, (c) PU-42, and (d) PU-52.

used to characterize, at least semi-quantitatively, the hydrogen bonding state of the polymer, and to correlate this to the phase separation in the system. It is well known that in H-bonded urethane N-H and C=O bands appear at lower wavenumbers than that in free ones.²⁶ Figure 2 shows the FTIR spectra of C=O and N-H stretching vibration regions for synthesized

polyurethanes. The band at 1735 cm⁻¹ is ascribed to C=O stretching of the LDI and the remaining methyl ester groups of the polyether polyol, the broad band between 1730-1672 cm⁻¹ is attributable to associated and non-associated C=O urethane groups and the small shoulders at 1663 and 1643 cm⁻¹ are ascribed to associated and non-associated urea linkages.

Analysis of amide-I stretching vibration for PU sample indicates that there is a band at approximately 1720 cm^{-1} , attributable to free C=O urethane groups, and a shoulder at about 1695 cm^{-1} which is due to the H-bonded urethane. The intensity of the bands attributed to free and H-bonded urethane carbonyls increases with increasing PDO fraction, as could be expected, because increasing PDO fraction leads to increase urethane content. The intensity of the band attributed to H-bonded urethane, relative to the band attributed to the non-bonded urethane groups, increases with an increase in the hard segment content. This suggests that the PU-42 and PU-52 C=O urethane groups are hydrogen-bonded to a greater degree than the PU and PU-31 samples. In the amine region (Figure 2, down), the broad band ascribed to N-H stretching grows with the increase in urethane group concentra-

tion and shifts slightly to a lower wavenumber with increasing hard segment content, indicating an increase in the degree of association. The difference in state of molecular aggregation of polyurethanes was further confirmed by DSC and DMTA.

Thermal Properties of Polyurethanes

Thermal analysis of the polyurethanes obtained was performed to provide insights into the morphological structure of the material. Figure 3 shows the second-heat DSC thermogram for the polyurethanes, while thermal transitions are listed in Table 2. No melting or crystallization peaks were found by DSC, which is in full agreement with the WAXD observation. The glass transition temperature of the reference sample measured by DSC was $-17\text{ }^{\circ}\text{C}$.

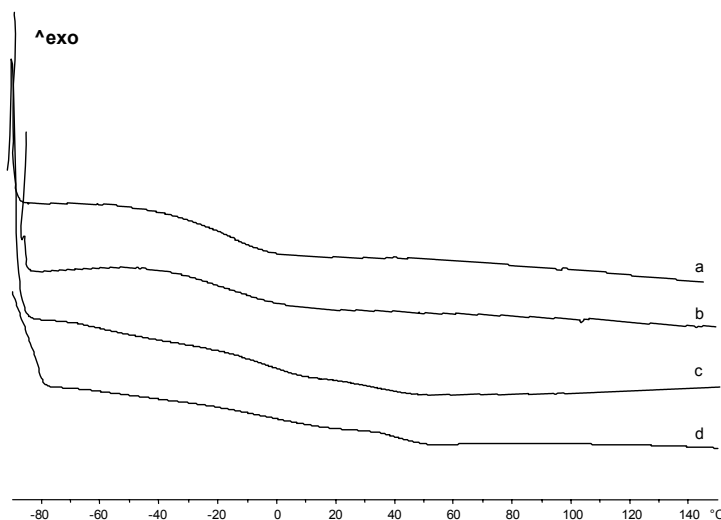


Figure 3. DSC thermograms ($20\text{ }^{\circ}\text{C}/\text{min}$) of polyurethane networks: (a) PU, (b) PU-31, (c) PU-42, and (d) PU-52.

Table 2. Thermal Characterization of Polyurethane Networks from DSC, DMTA, and TGA

Sample Code ^a	%HS ^b	DSC (°C)		DMTA (°C)		TGA (°C)	
		Soft Segment Transition (T _{g1})	Hard Segment Transition (T _{g2})	Soft Segment Transition (T _{g1})	Hard Segment Transition (T _{g2})	T _{5% loss} ^c	T _{max} ^d
PU	-	-17	-	9	-	297	429
PU-31	31.4	-12	-	14	-	282	284/438
PU-42	41.9	0	35	22	45	273	273/432
PU-52	52.3	1	44	21	58	255	260/434

^a Number in the sample code denotes the hard segment weight percent of the PU.

^b %Hard segment content calculated as weight percentage of PDO and LDI per total material weight.

^c Temperature of 5% of weight loss.

^d Temperature of the maximum weight loss rate.

DSC thermograms of all polyurethanes extended with PDO showed a low temperature glass transition, indicated by an endothermic step in the heat flow. Such transitions appeared in the region of -15 to 5 °C, and were attributed to the P184 soft-segment glass transition temperature (T_{g1}). T_{g1} value is a measure of relative purity of the soft-segment regions; when there are hard segments dispersed in the soft domains, the T_{g1} is raised. The degree of hard segment mixing into the soft-segment domain will depend on the overall hard segment content and the affinity of one segment toward the other. In our polyurethanes, hard segment content is high enough to achieve phase separation, but hard segment has a highly irregular aliphatic structure, meaning that phase mixing is more likely than phase separation. As indicated in Figure 3 and Table 2, the T_{g1} increased with the hard segment content. Thus, the experimental results revealed that the dispersion of hard segments in the

soft domain increased with the hard segment content. Apart from this, samples with higher hard segment content (PU-42 and PU-52) revealed a second transition (T_{g2}). This second T_g with a midpoint at approximately 35 and 44 °C, respectively was assigned to the PDO-LDI hard block of the polyurethane and supports the development of a phase-separated morphology. Glass transition temperatures for the hard segment depend strongly on its molecular weight; it can therefore be stated that the lower T_{g2} value in the PU-42 sample could be a consequence of shorter PDO-LDI segments such as could be expected from hard segment content. The enhanced phase separation noted for PU-42 and PU-52 by DSC would indicate that the higher degree of hydrogen bonding observed by FTIR (Figure 2) must be attributed to inter-chain interactions in the hard segments. The phase mixing noted for PU-31 by DSC would indicate that the hydrogen bonding observed by FTIR for the ure-

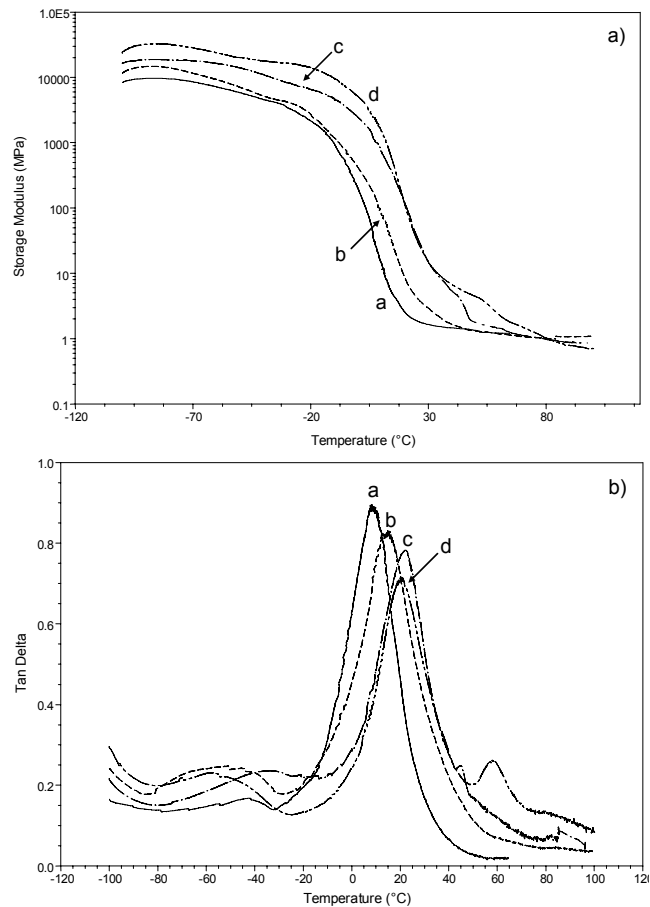


Figure 4. Storage modulus (E') and loss factor ($\tan \delta$) of polyurethanes: (a) PU, (b) PU-31, (c) PU-42, and (d) PU-52.

thane C=O groups is largely between hard segment-soft segment or soft segment-soft segment.

The dynamomechanical behavior of polyurethanes was investigated by DMTA to obtain further evidence on morphology since this technique is more sensitive for detecting glass transitions than DSC. Figure 4 a) shows the elastic modulus (E') as a function of the temperature. As can be seen polyurethanes PU and PU-31 behave like homogene-

ous polymeric networks with respect to E' curves while PU-42 and PU-52 samples show E' curves typical of phase-separated structure. In the glassy region, the storage moduli follow the expected trends. The storage moduli E' is higher when the hard segment content is higher due to the increased number of urethane connections and the increase in interchain interactions caused by the hydrogen bonds. At around 30 °C the storage moduli for PU-42 and PU-52 samples are higher than those for PU

and PU-31 samples. It appears that the hard segments play the role of physical crosslinks and fillers. Figure 4 b) shows the dissipation factor $\tan \delta$ curves as a function of temperature. Reference sample shows a $\tan \delta$ peak at 9 °C assigned to the glass transition of the amorphous soft segment. The glass transition temperature determined from the peak of $\tan \delta$ curve is higher than the one determined by DSC (see Table 2), which can be related to the heat transporting hysteresis for large scale samples in DMTA. Consistent with DSC results, this peak shows a shift of maxima and decreasing height as the hard segment content increases (curves b, c, and d). This suggests greater limitations on freedom of chain mobility in the soft segment which may be explained by the phase mixing between hard and soft segments. The $\tan \delta$ curve of PU-42 and PU-52 samples display a smaller but distinct transition at 45 and 58 °C, respectively. This

transition is attributed to the T_g of the phase-separated LDI-PDO hard block segments of the polymer (T_{g2}). This transition becomes much more prominent in PU-52 due to its more phase separated morphology. Moreover, all $\tan \delta$ curves show a low temperature transition (below -20 °C). The origin of this peak is not known, but it is generally attributed to rotation of smaller groups in the main chain.¹⁸ This peak is larger and is at lower temperature in segmented polyurethanes than in the reference sample. This relaxation at similar temperature was observed in other polyurethanes from vegetable-oil based polyols.¹⁹ DMTA results corroborated the DSC results, indicating that P184 soft segment phase exists in a relatively more phase-mixed state as the hard segment content increases. These results indicate that these materials would be useful in low-temperature applications from around -20 °C up to around body-temperature.

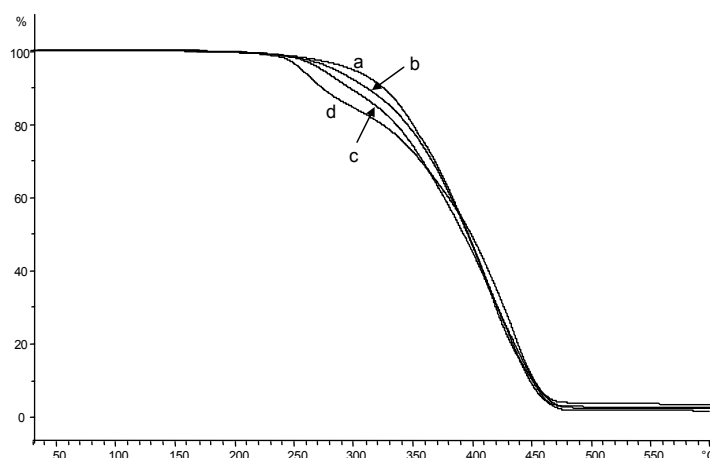


Figure 5. TGA plots (10 °C/min) of polyurethane networks: (a) PU, (b) PU-31, (c) PU-42, and (d) PU-52.

The thermogravimetric analysis was performed on the polyurethanes under nitrogen atmosphere. The reported thermogravimetric analysis of petroleum and vegetable oil-based polyols suggest that thermal stability is poor.²⁰ The TGA thermograms of polyurethanes are shown in Figure 5 and TGA data are listed in Table 2. The thermal decomposition of these polyurethanes involves at least two overlapping steps: a small drop below 300 °C is followed by the main loss weight above 300 °C. The first weight loss is related to the

decomposition of urethane bonds, which takes place through the dissociation to isocyanate and alcohol, the formation of primary amines and olefins, or the formation of secondary amines.²⁷ The main decomposition process is attributed to the polyether polyol chain scission, and occurs at about 430 °C. The weight loss in the first step increases as the hard segment content increases, which is in accordance to the existence of a higher amount of weaker urethane bonds.

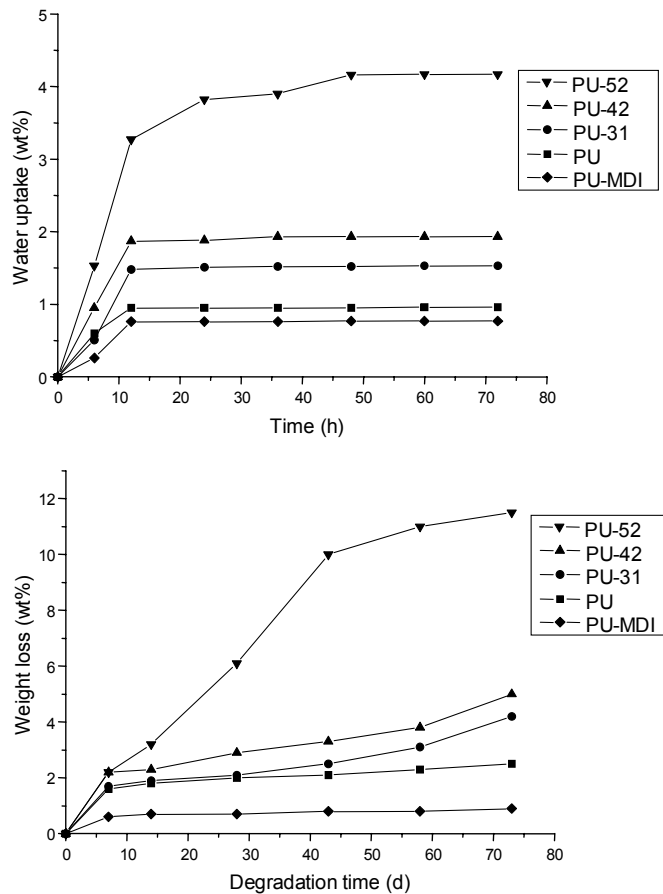


Figure 6. Water uptake (up) and in vitro degradation (PBS, 0.1 M, pH 7.4; 37 °C) (down) of polyurethane networks.

Water Absorption and In Vitro Degradation

Water absorption was measured to determine the polyurethane bulk hydrophilicity because this parameter was expected to have a substantial impact on hydrolytic degradation. The water uptake as a function of the time for all the samples is shown in Figure 6. Water uptake of the polyurethane obtained from P184 and MDI (PU-MDI)¹⁹ was also measured for comparison. The water uptake increased with immersion time and reached a plateau after approximately 25 h. The hard segment content is the main factor that controls the amount of absorbed water. As the hard segment content increases, a more hydrophilic character in the final network due to the presence of higher amount of urethane groups can be expected, thus increasing the water uptake. According to this, similar water uptakes can be observed for PU and PU-MDI, which contains similar amounts of urethane links.

The in vitro degradation experiments of the synthesized polyurethanes were carried out by immersion of the samples in PBS (pH 7.4, 0.1 M) at 37 °C, and the results are plotted in Figure 6. The degradation rate was evaluated by the weight loss of the polymers over predetermined time intervals. After 72 days of degradation, the weight losses of polyurethanes are all below 12 %. As shown in Figure 6, the hard segment content has some influence on the hydrolytic degradation rate. With the increase of the hard segment content, the degradation rate increased, which is in agreement with the hydrophilicity of the polymers. The reason may be

that the resulting polyurethanes containing higher hard segment content have more hydrophilicity and water diffusion is relatively easy. However, sample PU-MDI show lower degradation rate than PU in spite of their similar hydrophilicity, what can be expected from the aromatic character of the MDI.

The visual examination of the surface of the degraded polyurethanes was carried out using SEM. Figure 8 shows the photographs of PU-52 at different degradation stages. For all samples, surface appeared spotted with round pits where material had been removed and showed more extensive cracks and numerous pores in progressive weeks, indicating a larger extent of degradation with time. Moreover, with the increase of the hard segment content, the erosion was more serious. The spotted surface is due to the presence of areas with marked differences in hydrolytic stability. The hydrophobic character of soft-segments prevented the entry of water molecules, resulting in greater hydrolytic stability of the polyurethane. Hard-segments increase the hydrophilicity and promote the susceptibility of urethane bonds to hydrolysis, leading to the formation of significant amounts of water soluble products leaching into the solution, and to a higher degradation rate.

CONCLUSIONS

A variety of novel poly(ether urethane) networks were synthesized from EMO-based polyether polyol, PDO, and LDI as a non-toxic coupling agent with hard segment content between 31.4 and

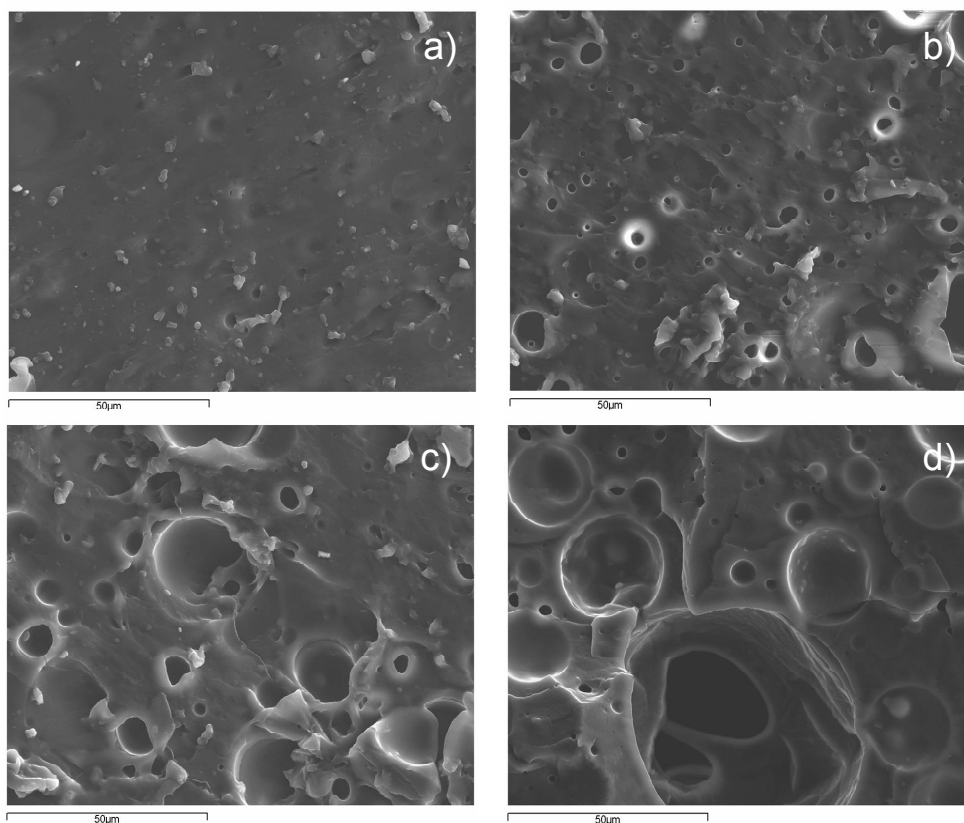


Figure 7. SEM images of degraded polyurethane PU-52 at different degradation stages: (a) 14, (b) 28, (c) 43, and (d) 73 days.

52.3%. The synthesized materials were exhaustively characterized by spectroscopic techniques, WAXD, DSC, and DMTA. WAXD and DSC results showed that the use of non-symmetric and methyl ester side chain containing LDI inhibits any hard segment crystallinity. However, the significant H-bonding of the urethane groups noted by FTIR as well as T_g values obtained by DSC and DMTA indicate that the polyurethanes were phase segregated to varying degrees. Degradation behaviors were found to depend strongly on the hard segment content as the hydrophilicity

promote the susceptibility to hydrolysis and leads to a higher degradation rate. The wide range of material properties that were achieved, as well as the use of a potentially non-toxic diisocyanate, makes these degradable polymers useful for a variety of biomaterials applications. Moreover, these biobased polyurethanes were prepared using 100 wt % of biorenewable materials, which shows that is possible to exploit renewable resources to manufacture original and useful materials.

Acknowledgements

The authors gratefully acknowledge the Comisión Interministerial de Ciencia y Tecnología (MAT2005-01593) for financial support for this work and the Departament d'Universitats, Recerca i Societat de la Informació and Fons Social Europeu for G. Lligadas' predoctoral (2003FI00765) grant. We thank F. Guirado for WAXD measurements and M. Moncusí for SEM analysis. The donation of LDI by A. Marcos is gratefully acknowledged.

REFERENCES AND NOTES

- Uhrich, K.E.; Cannizzaro, S.M.; Langer, R.S.; Shakesheff, K.M. *Chem Rev* 1999, 99, 3181.
- Wald, H. L.; Sarakinos, G.; Lyman, M. D.; Mikos, A. G.; Vacanti, J. P.; Langer, R. *Biomaterials* 1993, 14, 270.
- Sittinger, M.; Bujia, J.; Rotter, N.; Reitzel, D.; Minuth, W. W.; Burmester, G. R. *Biomaterials* 1996, 17, 237.
- Engelberg, I.; Kohn, J. *Biomaterials* 1991, 12, 292.
- Lamba, N. M. K.; Woodhouse, K. A.; Cooper, S. L. *Polyurethanes in Biomedical Applications*; CRC: Boca Raton, FL, 1998.
- Wirpsza, Z. *Polyurethanes, Chemistry, Technology and Applications*; Kemp, T. J., Ed.; Ellis Horwood PTR Prentice Hall: New York, 1993.
- Storey, R. F.; Wiggins, J. S.; Puckett, A. D. *J Polym Sci Part A: Polym Chem* 1994, 32, 2345.
- Kylma, J.; Sépala, J. V. *Macromolecules* 1997, 30, 2876.
- Zdrahala, R. J.; Zdrahala, I. J. *J Biomater Appl* 1999, 14, 67.
- Bruin, P.; Venstra, G. J.; Nijenhuis, A. J.; Pennings, A. J. *Makromol Chem Rapid Commun* 1988, 9, 589.
- Marcos-Fernández, A.; Abraham, G. A.; Valentín, J. L.; San Román, J. *Polymer* 2006, 47, 785.
- Hassan, M. K.; Mauritz, K. A.; Dtorey, R. S.; Wiggins, J. S. *J Polym Sci Part A: Polym Chem* 2006, 44, 2990.
- Kaplan, D. L. *Biopolymers from Renewable Resources*, Springer, Berlin 1998, p. 267.
- Baumann, H.; Bühler, M.; Fochem, H.; Hirsinger, F.; Zoeblein, H.; Falbe, J. *Angew Chem Int Ed Engl* 1988, 27, 41; Biermann, U.; Friedt, W.; Lang, S.; Lühs, W.; Machmüller, G.; Metzger, J. O.; Klaas, M. R.; Schäfer, H. J.; Schneiderüs, M. P. *Angew Chem Int Ed Engl* 2000, 39, 2206; Eissen, M.; Metzger, J.O.; Schmidt, E. Schneidewind, U. *Angew Chem Int Ed Engl* 2002, 41, 414
- Lligadas, G.; Ronda, J. C.; Galià, M.; Cádiz, V. *J Polym Sci Part A: Polym Chem* 2006, 44, 5630; Lligadas, G.; Callau, L.; Ronda, J. C.; Galià, M.; Cádiz, V. *J Polym Sci Part A: Polym Chem* 2005, 43, 6295; Pelletier, H.; Belgacem, N.; Gandini, A. *J Appl Polym Sci* 2006, 99, 3218; Uyama, H.; Kuwabara, M.; Tsujimoto, T.; Kobayashi, S. *Biomacromolecules* 2003, 4, 211; Esen, H.; Kusefoglu, S. H. *J Appl Polym Sci* 2003, 89, 3882; Bunker, S. P.; Wool, R. P. *J Polym Sci Part A: Polym Chem* 2002, 40, 451; Petrovic, Z.; Guo, A.; Zhang, W. *J Polym Sci Part A: Polym Chem* 2000, 38, 4062; Petrovic, Z.; Guo, A.; Javni, I. U.S. Patent 6, 107, 433, 2000.
- Guo, A.; Cho, Y.-J.; Petrovic, Z. S. *J Polym Sci Part A: Polym Chem* 2000, 38, 3900; Zlatanovic, A.; Petrovic, Z. S.; Dusek, K. *Biomacromolecules* 2002, 3, 1048; Zlatanovic, A.; Lava, C.; Zhang, W.; Petrovic, Z. S. *J Polym Sci Part B: Polym Phys* 2004, 42, 809.
- Guo, A.; Demydov, D.; Zhang, W.; Petrovic, Z. S. *J Polym Environ* 2002, 10, 49.

18. Petrovic, Z.; Zhang, W.; Javni, I. *Biomacromolecules* 2005, 6, 713.
19. Lligadas, G.; Ronda, J. C.; Galià, M.; Biermann, U.; Metzger, J. O. *J Polym Sci Part A: Polym Chem* 2006, 44, 634.
20. Lligadas, G.; Ronda, J. C.; Galià, M.; Cádiz, V. *Biomacromolecules* 2006, 7, 2420.
21. Biebl, H.; Menzel, K.; Zeng, A.P. Deckwer, W.D. *Appl Microbiol Biotechnol* 1999, 52, 289.
22. Kurian, J. J. *Polym Environ* 2005, 13, 159.
23. FDA (Food and Drugs Administration). Resinous and polymeric coatings. In: Title 21, Chapter I, Part 175, Subpart C, Sec. 175.300. USA; 2002.
24. Skrovanek, D. J.; Howe, S. E.; Painter, P. C.; Coleman, M. M. *Macromolecules* 1985, 18, 1676.
25. Papadimtrakopoulos, F.; Sawa, E.; MacKnight, W. J. *Macromolecules* 1992, 25, 4682.
26. Seymour, R. W.; Estes, G. M.; Cooper, S. L. *Macromolecules* 1970, 3, 579.
27. Levchik, S.V.; Weil, E.D. *Polym Int* 2004, 53, 1585.

5

Conclusions

In the course of this thesis, new biobased thermosets have been developed from vegetable oils, which show that it is possible to exploit renewable resources to manufacture original and useful materials. These results in more detail are stated below:

- Organic-inorganic hybrid networks were developed from alkenyl-terminated fatty acid derivatives [10-undecenoyl triglyceride and methyl 3,4,5-tris(10-undecenoyloxy)benzoate] by hydrosilylation as a crosslinking reaction. Transparent elastomeric hybrid networks were obtained according to a good miscibility of the organic and inorganic components.
- Epoxy nanocomposites were developed by crosslinking of epoxidized linseed oil and 3-glycidylpropylheptaisobutyl- T_8 -polyhedral oligomeric silsesquioxane. A nanoreinforcement effect of the polyhedral oligomeric silsesquioxane cages on the crosslinked matrix was achieved.
- Epoxy resins were developed from a new phosphorus-containing fatty acid derivative [10-(2',5'-bis(9-oxiranyl-nonanoyloxy)-phenyl)-9,10-dihydro-9-oxa-10-phosphaphenanthrene-10-oxide], epoxidized 10-undecenoyl triglyceride, epoxidized methyl 3,4,5-tris(10-undecenoyloxy)benzoate, and amine hardeners. The presence of phosphorus led to polymers with enhanced flammability.

- Polyether polyols were synthesized by the cationic oxirane ring-opening oligomerization of epoxidized methyl oleate followed by partial reduction of the ester groups to primary alcohols. Polyurethane networks were prepared by the reaction of these polyols with 4,4'-methylenebis(phenyl isocyanate).
- Silicon-containing polyurethanes were developed from a novel Si-based polyol, epoxidized methyl oleate-based polyether polyol and 4,4'-methylenebis(phenyl isocyanate). The incorporation of silicon led to flame retardant polyurethanes.
- Segmented poly(ether urethane) networks were synthesized from an epoxidized methyl oleate-based polyether polyol, 1,3-propanediol, and L-lysine diisocyanate. Hydrolytic degradation behavior was found to depend strongly on the hard segment content of the polyurethane.

Appendix A: List of Abbreviations

AESO	Acrylated epoxidized soybean oil
BA	Bisphenol-A
BAMA	Bisphenol-A maleates
BAMPO	Bis(<i>m</i> -amino-phenyl)methylphosphine oxide
BF ₃ :MEA	Boron trifluoride-ethylamine complex
BPH	N-benzylpyrazinium hexafluoroantimoniate
C _p	Heat capacity
DDM	4,4'-Diaminodiphenylmethane
DMSB	1,4-Bis(dimethylsilyl)benzene
DMTA	Dynamic mechanical thermal analysis
DOPO	9,10-Dihydro-9-oxa-10-phosphaphenanthrene-10-oxide
DOPO-I	10-(2',5'-Dihydroxyphenyl)-9,10-dihydro-9-oxa-10-phosphaphenanthrene-10-oxide
DOPO-II	10-(2',5'-Bis(10-undecenoyloxy)phenyl)-9,10-dihydro-9-oxa-10-phosphaphenanthrene-10-oxide
DOPO-III	10-[2',5'-Bis(9-oxiranyl-nonanoyloxy)phenyl]-9,10-dihydro-9-oxa-10-phosphaphenanthrene-10-oxide
DSC	Differential scanning calorimetry
E'	Storage modulus
E''	Loss modulus
EDX	Energy-dispersive X-ray spectroscopy
ELO	Epoxidized linseed oil
EMO	Epoxidized methyl oleate
EW	Equivalent weight
f	Functionality
FTIR	Fourier transform infrared spectroscopy
GC/MS	Gas chromatography/mass spectrometry

gCOSY	Gradient-selected correlation spectroscopy
gHSQC	Gradient-selected heteronuclear single quantum correlation
gHMBC	Gradient-selected heteronuclear multiple bond correlation
G-POSS	3-Glycidylpropylheptaisobutyl-T ₈ -polyhedral oligomeric silsesquioxane
ΔH_m	Melting enthalpy
HV	Hydroxyl value
LDI	L-lysine diisocyanate
LOI	Limiting oxygen index
MALDI-TOF MS	Matrix-assisted laser desorption/ionization time-of-flight mass spectrometry
MAS NMR	Magic-angle-spinning nuclear magnetic resonance spectrometry
MCPBA	<i>m</i> -Chloroperbenzoic acid
MDI	4,4'-Methylenebis(phenylisocyanate)
M_n	Number average molecular weight
M_w	Weight average molecular weight
M_w/M_n	Polydispersity index
NMR	Nuclear magnetic resonance spectrometry
NPG	Neopentyl glycol
NPGMA	Neopentyl glycol maleates
PBS	Phosphate buffer solution
PDO	1,3-Propandiol
POSS	Polyhedral oligomeric silsesquioxane
PTDS	Phenyl tris(dimethylsiloxy)silane
SEC	Size-exclusion chromatography
SEM	Scanning electron microscopy
SOMGMA	Soybean oil monoglycerides maleates
Tan δ	Loss factor
TCE- d_2	Tetrachloroethane- d_2
T_g	Glass-transition temperature

TGA	Thermogravimetric analysis
T _m	Melting point
TMS	Tetramethylsilane
TKDS	Tetrakis(dimethylsilyloxy)silane
TMCTS	2,4,6,8-Tetramethylcyclotetrasiloxane
UDBM	Methyl 3,4,5-tris(10-undecenoyloxy) benzoate
UDBME	Epoxidized methyl 3,4,5-tris(10-undecenoyloxy) benzoate
UDM	Methyl 10-undecenoate
UDTG	10-Undecenoyl triglyceride
UDTGE	Epoxidized 10-undecenoyl triglyceride
WAXD	Wide-angle X-ray diffraction
XRD	X-Ray diffraction

Appendix B: List of Papers

This thesis is based on the following papers. They are listed together with the author's contribution to each of them.

- I. Novel Organic-Inorganic Hybrid Materials from Renewable Resources: Hydrosilylation of Fatty Acid Derivatives.
Lligadas, G.; Callau, L.; Ronda, J. C.; Galià, M.; Cádiz, V.
J Polym Sci Part: A Polym Chem 2005, 43, 6295.
- II. Synthesis and Characterization of Polyurethanes from Epoxidized Methyl Oleate Based Polyether Polyols as Renewable Resources.
Lligadas, G.; Ronda, J. C.; Galià, M.; Biermann, U.; Metzger, J. O.
J Polym Sci Part: A Polym Chem 2006, 44, 634.
- III. Novel Silicon-Containing Polyurethanes from Vegetable Oils as Renewable Resources. Synthesis and Properties.
Lligadas, G.; Ronda, J. C.; Galià, M.; Cádiz, V.
Biomacromolecules 2006, 7, 2420.
- IV. Synthesis and Properties of Thermosetting Polymers from a Phosphorous-Containing Fatty Acid Derivative.
Lligadas, G.; Ronda, J. C.; Galià, M.; Cádiz, V.
J Polym Sci Part: A Polym Chem 2006, 44, 5630.

- V. Development of Novel Phosphorus-Containing Epoxy Resins from Renewable Resources.
Lligadas, G.; Ronda, J. C.; Galià, M.; Cádiz, V.
J Polym Sci Part: A Polym Chem 2006, in press.
- VI. Bionanocomposites from Renewable Resources: Epoxidized Linseed Oil – Polyhedral Oligomeric Silsesquioxanes (POSS) Hybrid Materials.
Lligadas, G.; Ronda, J. C.; Galià, M.; Cádiz, V.
Biomacromolecules 2006, in press.
- VII. Poly(ether urethane) Networks from Renewable Resources as Candidate Biomaterials. Synthesis and Characterization.
Lligadas, G.; Ronda, J. C.; Galià, M.; Cádiz, V.
Biomacromolecules, submitted for publication.

